Cotutelle thesis

submitted as partial requirement towards the degree of

Doctor of philosophy in science and technology of water, energy and environment of Institut 2iE

Specialty: Material

&

Doctor of philosophy in engineering science and technology (civil engineering, architecture, geology) of
Université de Liège

by

Philbert NSHIMIYIMANA

presented on August 31, 2020

Effect of the type of clay earthen materials and substitution materials on the physico-mechanical properties and durability of compressed earth blocks

« Influence de la nature de matériaux argileux et matériaux de substitutions sur les propriétés physico-mécaniques et durabilité des briques en terre crues/comprimées »

Members of Committee

Frédéric COLLIN	Professor at ULiege (UEE)	President
Shady ATTIA	Professor at ULiege (UEE-SBD)	Member
Gilles ESCADEILLAS	Professor at UToulouse (LMDC)	Member
Nathalie FAGEL	Professor at ULiege (AGEs)	Member
Abdou LAWANE	Professor at Institut 2iE (LEMHaD)	Member
Geoffrey VAN MOESEKE	Professor at UCLouvain (LOCI)	Member
Luc COURARD	Professor at ULiege (UEE-GeMMe)	Co-Director
Adamah MESSAN	Professor at Institut 2iE (LEMHaD)	Co-Director

Laboratoire Eco-Matériaux et Habitats Durables (LEMHaD), Institut 2iE
GeMMe - Building Materials, Urban and Environmental Engineering (UEE), ULiege

"If it takes you a couple months of preparation of earth building materials, remember, it's worth it. If you do your job right, your grandchildren will also have a good house to live in"

Peace Corps, 1981

The correspondence can be addressed to

philbertn@gmail.com

Acknowledgements

This thesis presents the research works carried out in Cotutelle between the Institut 2iE (Burkina Faso) at the Laboratoire Eco-Matériaux et Habitat Durables (LEMHaD) and Université de Liège (Belgium) at GeMMe - Building Materials. It is part of a research and development project: amélioration de la qualité de l'habitat en terre crue au Burkina Faso - *improving the quality of earth-based habitat in Burkina Faso* (PRD2016-2021). I am very thankful for the full fund provided by the Academie de Recherche et de l'Enseignement Supérieur – Commission de la Coopération au Développement (ARES-CCD), Belgium.

I am proud to express my heartfelt gratitude to my Professors, **Adamah Messan** at 2iE and **Luc Courard** at ULiege, whose endless effort made this project see the light. Thank you so much for entrusting me with the responsibility to contribute to something so big, for co-directing this thesis in harmony and with patience, and for guiding me to grow my intellect and humanity.

I would like to address special acknowledgment to **Prof. Nathalie Fagel** at ULiege and **Dr. Dominique O. Wetshondo** at Université de Kinshasa (D.R. Congo) for the assistance throughout the field works and lab analyses.

I appreciate the efforts of the **members of the committee** who followed up the progress of this research from the very beginning, commented and made suggestions for the betterment of the work reported in this thesis. I would like to thank **Prof. Fréderic Collin** (ULiege) for the honor to preside this committee

I would also like to acknowledge the insightful reviews provided by various anonymous **reviewers**. Your contributions largely improved the quality of this manuscripts and related publications.

I address my thankful appreciation to the **research, teaching and administrative staffs** at 2iE and ULiege, **Généviève Yaméogo, Ariane M Ouedraogo, Leila Lang, Lidia Jurin**, who made my stay and research as smooth as it could be.

I appreciate the effort and the spirit of the work teams at 2iE and ULiege throughout laboratory characterizations and data analyses. I would like to mention **Frédéric Michel, Zengfeng Zhao, Grigoletto Sophie, Salif Kabore**, **Amaury Daras, Monique Denotte, Szepetiuk Véronique, Libioulle Fabienne, Joel Otten, François Fontaine, Nicolas Delmelle, Hassan Bouzahzah**.

Your support was far beyond professional; the warm welcome and everyday interactions made me not feel far from home.

My sincere appreciations go to my fellow colleagues and friends, **Ousmane, Césaire, Arnaud, Marie, Roland, Christian, Serge, Charlotte, Adèle, Morino, Mostafa, Salomon, Apolline, Youcef (both), Fabrice** for sharing the "expérience thésard!". I also address my appreciations to the former Ph.D. candidates at 2iE and ULiege, **Sore, Decroly, Karim, Yasmine, Nafissatou,** for being there for me from the very beginning. Thank you all for the humor, and the coffee; it kept my world turn. Cheers for the happy ending!

To the former Masters' students at ULiege and 2iE, **Romain, David, Camie, Hassan, Andy, Serge, Simon,** thank you for the collaborations. Your various contributions were remarkable for the completion of this thesis.

I want also to mention a number of partners, **Burkina Industrial Gas (BIG), UCLouvain, UniKin** and **AutreTerre**. Thank you for your fruitful collaborations.

I owe the gratitude to my family for the support and patience, thank you very much for bearing with me throughout many years away. I hope that you find satisfaction in this thesis.

To my friends in Rwanda, Burkina Faso, Belgium, Nigeria, Ghana, Cote d'Ivoire, Botswana, Tanzania, South Africa, USA, Canada, Cameroon.

I say thank you to you all!

Glossary

a	Thermal diffusivity	m^2/s
Cap	Thermal capacity	J/kg.K
CCR	Calcium carbide residue	
CEBs	Compressed earth blocks	
CEM	Cement	
DE	Depth of erosion	mm
E	Thermal effusivity	$J/m^2.K.s^{1/2}$
EA	Eroded area	%
HL	Hydrated (industrial) lime	
LL	Liquidity limit	
OMC	Optimum moisture content	
PI	Plasticity index	
PL	Plasticity limit	
PSD	Particle size distribution	
RH	Rice husk	
RHA	Rice husk ash	
Rc	Compressive strength	MPa
λ	Thermal conductivity	W/m.K
δp	Depth of penetration of thermal flux	m

Abstract

Clay earthen materials are the most common building materials used all over the world for sustainable constructions. Today, the drastic increase of population and urbanization, especially in developing world, calls for better knowledge of earthen materials in the contemporary construction. The present thesis aimed to characterize the suitability of clay materials from four sites in the vicinity of Ouagadougou, Burkina Faso: Kamboinse, Pabre, Kossodo and Saaba for the production of stabilized compressed earth blocks (CEBs). The study also characterized by-products of industry: calcium carbide residue (CCR) from Kossodo and agriculture: rice husk ash (RHA) from Bagré and Okra plant fibers from Kaya for the stabilization of CEBs. The characterizations were carried out on physico-textural and chemico-mineral properties. The study additionally tested the physico-mechanical, hygro-thermal and durability performances of CEBs stabilized with the by-products for applications in building construction, specifically for applications in the Sahelian climatic context. Mixtures were produced by addition of 0-25 wt% CCR, 10-25 wt% CCR:RHA (various ratios) and 0.2-1.2 wt% fibers to the earthen materials. The mixtures were used to produce the mix solutions and mold stabilized CEBs (295x140x95 mm^3) by static compression (~35 bars), and cured in various conditions for 0 to 90 days. The results show that the clay materials from Pabre and Kossodo respectively contain the highest fraction of clay particles (20-30%) and gravel (40%). Saaba and Pabre respectively contain the highest fraction of kaolinite clay mineral (60-80%) and quartz (40-60%). Kamboinse contains the highest amount of exploitable deposit (700 000 m^3), 10-25% clay particles and 40-75% kaolinite, while Kossodo contains medium fraction of kaolinite (35-50%). The CCR mainly contains portlandite (40-50 % hydrated lime: $Ca(OH)_2$). The RHA is mainly amorphous, with pozzolanic reactivity. Saaba and Kossodo recorded the highest rate of pozzolanic reactivity with CCR, related to the high content and degree of poorly ordered kaolinite. Pabre and Kamboinse recorded the lowest rate of reactivity. With respect to unstabilized CEBs (0 % CCR), the compressive strength of CEBs stabilized with 20% CCR cured at 40±2°C for 45 days produced with the clay material from Saaba improved tenfold (0.8 to 8.3 MPa) compared to Kamboinse (1.1 to 4.7 MPa), Pabre (2 to 7.1 MPa) and Kossodo (1.4 to 6.4 MPa). All clay materials are suitable for the production of stabilized CEBs with compressive strength of 4 MPa. Furthermore, the stabilization of the earthen material from Kamboinse using novel binders improved the structural efficiency of CEBs cured in ambient conditions of the lab (35±5°C): increase of compressive strength and decrease of bulk density. It also improved the hygro-thermal efficiency: decrease of thermal effusivity, conductivity and diffusivity and increase of thermal specific capacity and water vapor sorption. The CEBs stabilized with at least 10 % CCR or 18-2 to 16:4 % CCR:RHA satisfy engineering requirements and durability for the construction of two or three storey buildings. Therefore, the selection of earthen materials should take into account the reactivity with the stabilizer.

Keywords: *calcium carbide residue; compressed earth block; durability; kaolinite clay; microstructure; pozzolanic reactivity; physico-mechanical property, rice husk ash.*

Résume détaillé

La terre argileuse reste le matériau de construction le plus couramment utilisé dans le monde entier pour une construction respectueuse de l'environnement. De nos jours, on constate une augmentation spectaculaire de la population et de l'urbanisation, spécifiquement dans les pays en développement comme le Burkina Faso. Ainsi, une meilleure connaissance du comportement des matériaux de construction en terre serait une réponse adéquate enfin de promouvoir son utilisation dans la construction contemporaine par les populations urbaines et/ou rurales.

La présente thèse est le fruit d'une cotutelle, et a été préparée au Laboratoire Eco-Matériaux et Habitats Durables (LEMHaD) de l'Institut 2iE au Burkina Faso et GeMMe - matériaux de construction, unité de recherche *Urban and Environmental Engineering (UEE)* de l'Université de Liège en Belgique. Les travaux présentés dans cette thèse, **matériaux/produits,** sont menés dans le cadre d'un projet de recherche et développement: amélioration de la qualité de l'habitat en terre crue au Burkina Faso et financé par l'Académie de Recherche et de l'Enseignement Supérieur – Commission de la Coopération au Développement (ARES-CCD: PRD2016-2021) du royaume de la Belgique.

Cette thèse visait à caractériser la convenance de la terre argileuse de quatre sites aux alentours de Ouagadougou, Burkina Faso: Kamboinsé, Pabré, Kossodo et Saaba, pour la production des blocs en terre comprimées stabilisés (BTCs). L'étude a consisté également à caractériser un sous-produit industriel: le résidu de carbure de calcium (CCR) issu de la fabrication de l'acétylène à Kossodo et deux sous-produits agricoles: la cendre de balle du riz (RHA) de Bagré et les fibres végétales de gombo de Kaya pour la stabilisation des BTCs. Les caractérisations ont été menées sur les propriétés physico-texturales et chimico-minérales de ces matières premières.

Ensuite, l'étude a consisté à tester les propriétés physico-mécaniques, hygro-thermiques et de durabilité des BTCs stabilisés avec les sous-produits pour des applications dans la construction de bâtiments, adaptés spécifiquement au contexte climatique Sahélien. Les mélanges ont été produits par addition de 0-25% CCR, 10-25% CCR:RHA (divers ratios) et 0,2-1,2% fibre par rapport à la masse de la terre (plus CCR). Les mélanges ont été utilisés pour produire les solutions et confectionner les BTCs stabilisés (295x140x95 mm^3) par compression statique à l'aide d'une presse manuelle de Terstaram (pression de ~35 bars), et maturés dans diverses conditions pendant 0 à 90 jours.

Les résultats montrent que la terre argileuse des sites de Pabré et Kossodo contient respectivement la plus forte fraction de particules argileuses (20-30%) et gravier (40%). La composition minérale est dominée par la kaolinite, le quartz et la goethite. Saaba et Pabré contiennent respectivement la plus forte fraction d'argile kaolinite (60-80%) et quartz (40-60%). Kamboinsé contient la plus grande quantité de gisement exploitable (700 000 m^3), 10-25% des particules argileuses et 40-75% de kaolinite, tandis que Kossodo contient une moyenne fraction de kaolinite (35-50%). Le CCR contient principalement de la

portlandite (40-50% de chaux hydratée: $Ca(OH)_2$). La RHA est principalement siliceuse et amorphe, avec une réactivité pouzzolanique.

Saaba et Kossodo ont une réactivité pouzzolanique avec le CCR la plus élevée, liée à la teneur et au taux mal cristallisée élevé de kaolinite. Pabré et Kamboinsé ont une réactivité la plus faible. Par rapport aux BTCs non-stabilisés (0 % CCR), la résistance à la compression des BTCs stabilisés avec 20 % CCR, maturées à 40 ± 2 °C pendant 45 jours, produit avec le matériau argileux de Saaba est améliorée dix-fois (0,8 à 8,3 MPa) comparé à Kamboinsé (1,1 à 4,7 MPa), Pabre (2 à 7,1 MPa) et Kossodo (1,4 à 6,4 MPa). Cette amélioration de la résistance des BTCs stabilisés est expliquée par la réactivité de la terre avec le CCR. Tous ces matériaux argileux conviennent pour la production des BTCs stabilisés et atteignant une résistance à la compression requise de 4 MPa. Cette thèse a parvenu à montrer que la sélection du matériau en terre pour la production des BTCs stabilisés doit tenir en compte de son comportement réactionnel, sur base de la composition chimique et minéralogique, en plus du comportement textural et plasticité couramment considéré.

En plus, la stabilisation de la terre de Kamboinsé en utilisant les sous-produits (CCR, CCR:RHA, fibres) a amélioré l'efficacité structurelle des BTCs maturées dans les conditions ambiantes du labo (35±5 °C): augmentation de la résistance à la compression et diminution de la densité apparente. Elle a également amélioré l'efficacité hygro-thermique: diminution de l'effusivité thermique, de la conductivité et diffusivité et augmentation de la capacité thermique et de la sorption de vapeur d'eau. Les BTCs stabilisés avec au moins 10 % CCR ou 18-2 à 16:4 % CCR:RHA répondent aux diverses exigences techniques et ont des excellents indicateurs de la durabilité pour la construction de bâtiments à un ou deux étages. La thèse a également démontré que les sous-produits (CCR:RHA), autrement considérés comme déchets, constituent des liants innovants et efficace pour la stabilisation des BTCs et atteindre les performances comparables, voir même meilleur en terme hygro-thermique, à celles des BTCs stabilisés au ciment Portland.

Dans le même cadre de ce PRD, deux autres thèses se sont particulièrement penchées sur les aspects **architecture** et **socio-économique,** visant à promouvoir l'acceptabilité et l'adoption des BTCs dans la construction de maçonnerie enfin d'améliorer la qualité et le confort thermique de l'habitat.

Mots-clés*: argile kaolinite; bloc en terre comprimé ; carbure de calcium résiduel; cendre de balle du riz; durabilité; microstructure; propriété physico-mécanique; réactivité pouzzolanique.*

List of contents

List of figures

List of tables

BACKGROUND AND LITERATURE

CONTEXTUAL INTRODUCTION

Contextual introduction

"*While geographically united, African countries have considerable differences in urbanization patterns. For instance, since 1995 the urban population in Burkina Faso has consistently grown by more than 6.14 per cent per annum"* (UN-Habitat 2011).

Indeed, the demographic boom in most developing country, including Burkina Faso, stresses the need for sustainable[1] and decent habitats to accommodate this population, among other urban infrastructures. While the urban population of the rest of the globe evolved quasi-constantly in 1950-2010 and projection up to 2050, that of the African continent evolves quasi-exponentially (Figure 0.1). Today[2], the African continent is home for more than 1.3 billion people, among whom 43 % live in urban areas. The share of urban population is expected to exceed 60 % by 2050, equivalent to more than 1.2 billion people (UN-Habitat 2011). This may position Africa as the *"global powerhouse of the future"*[3], but it also constitutes a challenge for the socio-economic and infrastructure development of the continent.

Burkina Faso is similarly experiencing drastic demographic increase. The current population and urbanization rate of Burkina Faso are respectively estimated to exceed 20 million and 30 %, among whom more than 2 million live in the capital city of Ouagadougou (INSD, 2018, 2015).

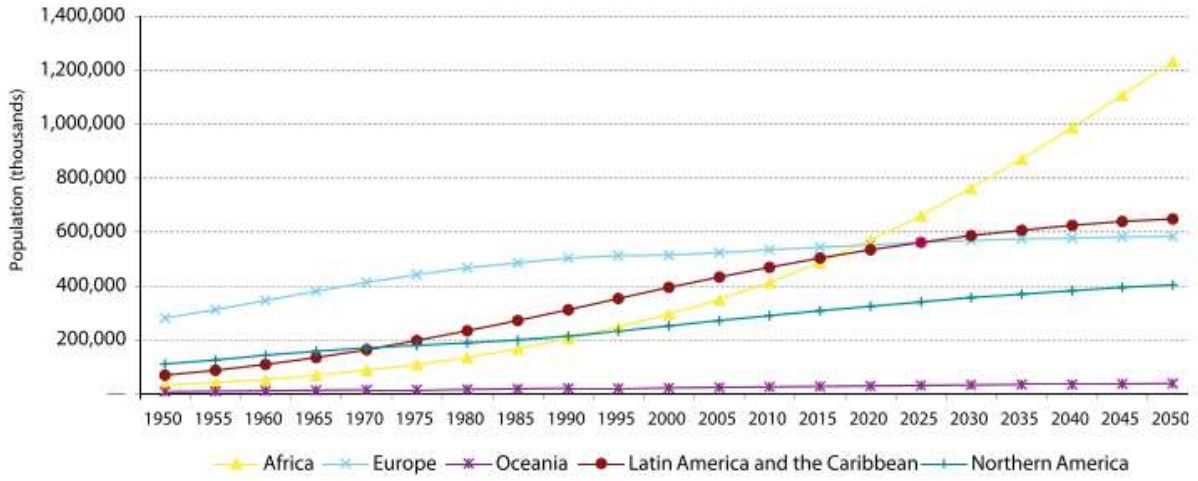

Figure 0.1. Urban population growth in selected regions 1950-2010, and projections for 2010-2050 (UN-Habitat 2011)

[1] *"Make cities and human settlements inclusive, safe, resilient and sustainable*", the 11th goal of the UN sustainable development goal: *The 2030 Agenda for Sustainable Development*. https://sustainabledevelopment.un.org/?menu=1300, 2020 March 19

[2] *Africa Population (LIVE),* https://www.worldometers.info/world-population/africa-population/, 2020 May 27

[3] "*Agenda 2063: The Africa We Want*". https://au.int/en/agenda2063/overview, 2020 March 19

The valorization of local and non-conventional materials in modern building construction is one of the attempts which can potentially contribute to catering the shelter to this population. Historically, the city of Ouagadougou is known to have been constructed using adobe "bancoville" and other techniques based on unfired clay materials (Figure 0.2). Clay materials lost much of the interest and acceptance with the arrival of the so called "modern and durable" materials such as cement, concrete and metal (Wyss, 2005). Clay earthen materials from this region are basically used for road pavement and in some cases for artisanal production of adobe.

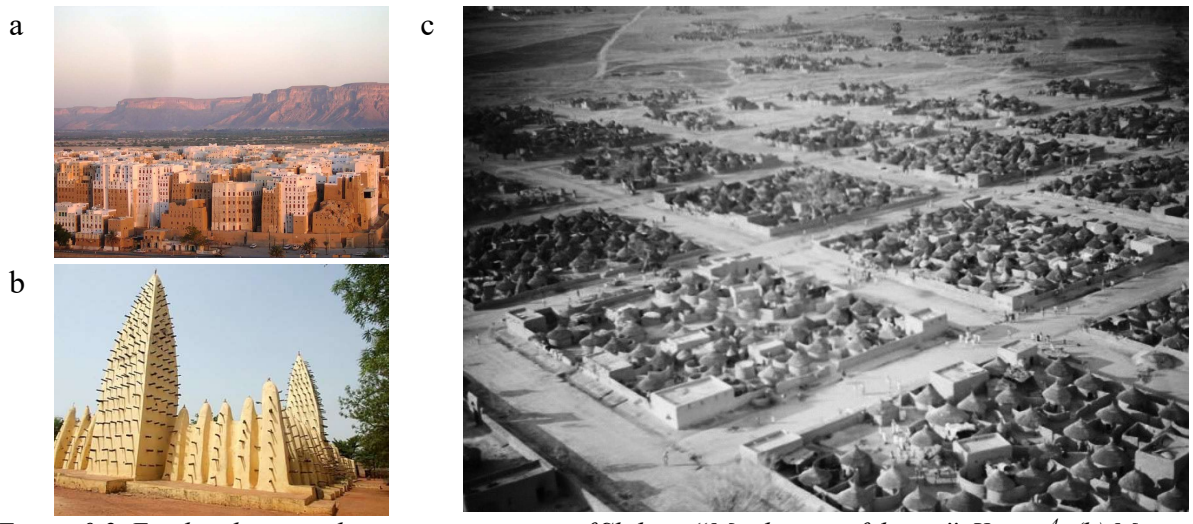

Figure 0.2. Earth in historical constructions: city of Shibām "Manhattan of desert", Yemen[4], (b) Mosque of Bobo Dioulasso (1890)[5], and city of Ouagadougou "bancoville" (1931)[6], Burkina Faso

Today, it is scientifically proven that the usage of earthen and secondary materials in building construction can provide several socio-economic, healthy, environmental and architectural benefits (UNESCO and Craterre 2012, Houben and Guillaud 2006). Lately, many researchers, at the regional or global scale, have been working on different approaches aiming at reviving the usage of such materials in modern building construction (Ouedraogo et al. 2019, Sore et al. 2018, Masuka et al. 2018, Hema et al. 2017, Bruno et al. 2017).

On the one hand, the earthen materials are available and easily accessible on the entire globe. In fact, the share of global population living in earth-based habitats exceeds 30 %, and 50 % in developing countries including Burkina Faso. The usage of earth requires low energy for transport and transformation, and thus low CO_2 footprint. Earth is not only easily accessible and low embodied energy and CO_2, but also earth-based construction provides comfortably

[4] https://www.pinterest.es/joanbartomeu/shibam-yemen 2020 May 21
[5] http://www.burkinatourism.com/La-vielle-mosquee-de-Dioulassoba-a-Bobo-Dioulasso.html, 2020 May 21
[6] Folkers AS, van Buiten BAC (2019) Popular Housing in Ouagadougou. In: Modern Architecture in Africa: Practical Encounters with Intricate African Modernity. Springer International Publishing, Cham, pp 82–116

livable indoor environment. On the other hand, the reuse/recycle of secondary materials allows to limit their hazardous impacts on environment in terms of disposal. This also allows to achieve the circularity and sustainability in building sector by limiting the stress on natural non-renewable resources. Therefore, the awareness of the global warming and necessity for energy saving, and the ability of improving indoor comfort give the unfired clay earthen material the potential for construction of sustainable buildings (Bogas et al. 2018, Murmu and Patel 2018, Hema et al. 2017, Delgado and Guerrero 2007, Reeves et al. 2006).

Figure 0.3. Earth in contemporary constructions, in the vicinity of Ouagadougou: low quality of adobe (a) construction site, (b) Wemtenga village versus improved quality of CEBs (c) construction site of a health center in Ouaga2000, (d) inside the Wemtenga primary school, (e) production of cement-stabilized CEBs at local enterprise, (f) erodability of a house in Kamboinse

For centuries, unfired clay materials have been used in building construction, in various forms such as adobe (sun dried brick), rammed earth, and recently compressed earth block (CEBs), and proved promising to provide affordable, decent and comfortable housing (Bogas et al. 2018, Delgado and Guerrero 2007). The CEBs are the most accepted form of unfired earth masonry for the construction of modern building (Van Damme and Houben 2018, Bogas et al. 2018). This is basically related to their curing which requires low (ambient) temperature and other advantages such as improved mechanical performances and durability, regular shape and size of the brick which allow to achieve various aesthetics of architectural designs, contrary to the adobe (Figure 0.3).

In this context, a research and development project: "Amélioration de la qualité de l'habitat en terre crue au Burkina Faso - *Improving the quality of earth-based habitats in Burkina Faso PRD2016-2021*" was established between the Institut 2iE and ULiege to carry out collaborative research on earth-based materials from Burkina Faso for applications in construction of decent habitats.

One approach of this project consists in developing the **material/product**: CEBs based on clay earth and substitution materials available in the vicinity of Ouagadougou. The results from this approach are presented in the present thesis. Other approaches look at the **architectural and socio-economic** aspects: applications in wall masonry and improvement of thermal comfort of housing, socio-economic acceptability and promotion for the adoption of CEBs (Hema 2020, Zoungrana 2020).

The recent interests for earthen materials: motivations and scopes

Earthen materials for application in construction, in their natural form, are not mostly strong enough to bear load in wall masonry of storey buildings. This requires the construction of thick walls which results in very heavy structures, which compromises their structural efficiency (Bogas et al. 2018). Additionally, earth-based materials are mostly not stable vis-à-vis environmental (water driven) attacks, resulting in immediate or gradual degradation of their mechanical performances and durability (Fabbri et al. 2018). These issues are generally remedied by the stabilization of CEBs

The stabilization of CEBs aims to improve the structural performances of earthen materials over the lifespan of the structure (Giada et al. 2019). In fact, the dry compressive strength of CEBs must reach at least 4 MPa for the construction of load bearing walls (CDI and CRATerre

1998). The mechanical performances of CEBs stabilized with cement and/or lime have been well investigated (Bogas et al. 2018, Nagaraj et al. 2014). Nevertheless, their hygro-thermal behavior, durability and onsite performances in wall masonry are still subjects for further investigations (Giada et al. 2019, Laborel-Préneron et al. 2016).

Additionally, the stabilization using the industrial binder (cement) is criticized for tempering with the natural advantages of earth, i.e. low energy and carbon footprint, recyclability, moisture exchange capacity and other environmental advantages (Saidi et al. 2018, Tiskatine et al. 2018). Moreover, it was repetitively recommended for further studies to investigate the feasibility of incorporating recycled aggregates and/or fibers or secondary materials in earthen materials (Arrigoni et al. 2019, Noolu, Mudavath, et al. 2019, Noolu, Lal, et al. 2019, Liu, Su, et al. 2019, Liu, Chang, et al. 2019, Siddiqua and Barreto 2018, Noolu et al. 2018, Latifi et al. 2018, Saldanha et al. 2018, Bogas et al. 2018). This can potentially enhance the environmental sustainability and socio-economic acceptances of stabilized CEBs in contemporary construction (Beckett et al. 2020, Van Der Linden et al. 2019, Morel and Charef 2019).

Recent decades have recorded a boom in number of research and review publications on the applications of earth-based materials and other non-conventional alternative materials for sustainable green building constructions (Beckett et al. 2020). Among many other studies, the most relevant are: *weathering the storm: a framework to assess the resistance of earthen structures to water damage* (Beckett et al. 2020); *durability of stabilized earthen constructions: a review* (Medvey and Dobszay 2020)*; improvement of lifetime of compressed earth blocks by adding limestone, sandstone and porphyry aggregates* (Mango-Itulamya et al. 2020)*; is stabilization of earth bricks using low cement or lime contents relevant?* (Ouedraogo et al. 2020)*; hygrothermal properties of raw earth materials: a literature review* (Giada et al. 2019); *future of clay-based construction materials - a review* (Shubbar et al. 2019); *assessing the performance of earth building materials: a review of recent developments* (Fabbri et al. 2018); *overview of sustainable future production of bricks incorporating wastes* (Murmu and Patel 2018); s*tabilization of compressed earth blocks (CEBs) by geopolymer binder based on local materials from Burkina Faso* (Sore et al. 2018).

One can also mention the establishment of research and technical institutions such as RILEM technical committee: testing and characterization of earth-based building materials and elements (TCE274), for *"... defining dedicated testing procedure for stabilized and unstabilized earth as a building construction material…and performance oriented tests…*"

based on the specificities of earthen material and envisaged applications (RILEM 2019). These point out the current interest for earth-based materials, and particularly CEBs.

However, in some instances, the literatures report contradictory results about the performances of CEBs stabilized with chemical industrial binders, which also are not environmentally-friendly. In fact, the previous literatures were mostly limited to the physico-textural and plasticity behaviors of earthen materials for the production of stabilized CEBs. They lack a particular attention to the chemico-mineral composition and reactivity of clay materials. This, and specifically in the context of Burkina Faso, is further elaborated in the chapter dedicated to the review of literature (Chapter I), before the justification of research question.

"How to reach the performances required for CEBs using clay earthen materials stabilized with by-products, instead of industrial binders, for load-bearing in building wall construction?"

This is the main research question addressed in the present study, aiming to answer to some of the scopes mentioned above. The study goes all the way from the identification of suitable clay earthen materials and by-product stabilizers available in the vicinity of Ouagadougou, to the production and testing of performances of CEBs stabilized with by-product binders and fibers.

The present thesis: specific objectives

The present thesis specifically aims to:

1. Identify and characterize the physico-chemical and mineral properties of by-products and clay materials available in the vicinity of Ouagadougou and suitable for the production of stabilized CEB.
2. Investigate the effects of by-products - calcium carbide residue (CCR), rice husk ask (RHA) and okra plant (A. Esculentus) fibers - on the microstructural, physico-mechanical and hygro-thermal properties of stabilized CEBs.
3. Study the durability performances of the stabilized CEBs, and specifically for structural applications in the Sahelian climatic context.

This thesis is structured in **five (05) chapters**:

Chapter I reviews the literature about the applications of clay earthen materials, common stabilization techniques and reusable secondary (by-product) materials for the production of stabilized CEBs. The chapter concludes by summarizing the current gaps towards the production of stabilized CEBs.

Chapter II presents the materials and experimental methods used in this thesis.

Chapter III presents the results obtained from the **first specific objective**:

Activities

- Sampling (field work) of clay materials from Kamboinse, Pabre, Kossodo, and Saaba, and by-products from Kossodo, Kaya and Bagre.
- Characterizing (laboratory work), processing and selecting the most suitable materials for the production of stabilized CEBs.

Publication:

- **Nshimiyimana** P, Fagel N, Messan A, Wetshondo, D O, Courard, L (2020) *Physico-chemical and mineralogical characterization of clay materials suitable for production of stabilized compressed earth blocks.* Constr Build Mater 241:1–13. https://orbi.uliege.be/handle/2268/245246

Chapter IV presents the results from the **second specific objective**:

Activities

- Designing the mixtures of earth-CCR-RHA and preparing mix solutions and stabilized CEBs.
- Monitoring the curing process in mix solutions.
- Testing the effect of by-products, CCR, RHA and fibers, on physico-mechanical and hygrothermal properties of CEBs.

Publications:

- Hema C, Soro D, **Nshimiyimana P**, Messan A, Van Moeseke G, (in review), *Improving the thermal comfort in hot region through the design of walls made of compressed earth blocks: an experimental investigation*
- **Nshimiyimana** P, Hema C, Zoungrana O, Messan A, Courard L (in review) *Thermophysical and mechanical properties of compressed earth blocks containing fibres: by product of okra plant & polymer waste*. WIT press
- Hema C, **Nshimiyimana P**, Zoungrana O, Lawane A, Messan A, Van Moeseke G, (in review), *Impact of the design of walls made of compressed earth blocks on the thermal comfort of housing in hot climate*
- Zoungrana O, Bologo/Traore M, Hema C, **Nshimiyimana P**, Pirotte, G Messan A, (in review), *Sustainable habitat in burkina faso: social trajectories, logics and motivations for the use of compressed earth block for housing construction in Ouagadougou*. WIT press
- **Nshimiyimana** P., Messan A., Courard L. (2020) *Physico-mechanical and hygrothermal properties of compressed earth blocks stabilized with industrial and agro by-products: Calcium carbide residue and rice husk ash.* Materials 13(17). 3769. https://orbi.uliege.be/handle/2268/250345
- **Nshimiyimana** P, Moussa HS, Messan A, Courard L (2020) *Effect of production and curing conditions on the performance of stabilized compressed earth blocks: Kaolinite vs quartz-rich earthen material.* MRS Adv 1–7. http://hdl.handle.net/2268/242442

- **Nshimiyimana** P, Messan A, Zhao Z, Courard L. (2019) *Chemico-microstructural changes in earthen building materials containing calcium carbide residue and rice husk ash*. Constr Buil Mat. 216C:622–631. http://hdl.handle.net/2268/235456
- Moussa HS, **Nshimiyimana** P, Hema C, Zoungrana O, Messan A, Courard L (2019) *Comparative Study of Thermal Comfort Induced from Masonry Made of Stabilized Compressed Earth Block vs Conventional Cementitious Material*. J Miner Mater Charact Eng 07:385–403. http://hdl.handle.net/2268/240543
- **Nshimiyimana** P., Miraucourt D., Messan A., Courard L. (2018) "*Calcium Carbide Residue and Rice Husk Ash for improving the Compressive Strength of Compressed Earth Blocks"*, MRS Adv. 3(34-35)2009-2014. http://hdl.handle.net/2268/226552

Chapter V presents the results from the **third specific objective**:

Activities
- Testing the durability performances of stabilized CEBs.
- Testing the weight loss and residual strength of stabilized CEBs after 12 cycles of wetting-drying.
- Testing the resistance to abrasion and erodibility (spray test) of stabilized CEBs.

Publication:
- **Nshimiyimana** P., Messan A., Courard L. (in review) *Hydric and durability performances of compressed earth blocks stabilized by industrial and agro by-product binders*

At the end, the thesis presents a summary discussing the major findings and the main contributions, as well their limitations. The recommendations, as well as technical implications, are also presented for appropriate applications of stabilized CEBs in building construction.

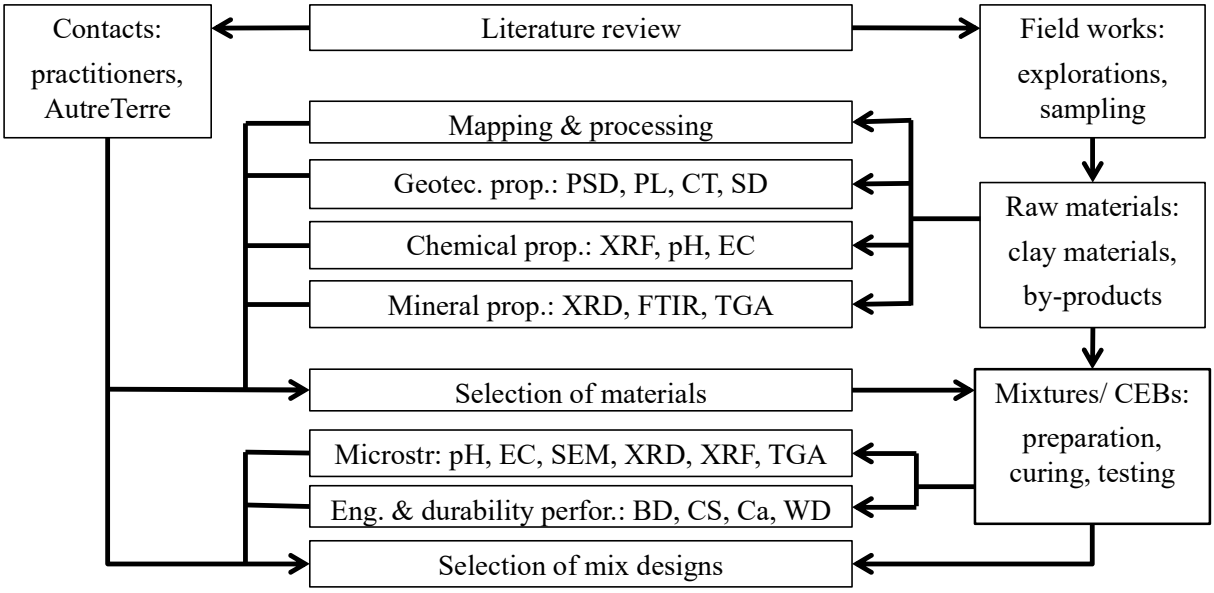

Figure 0.4. Research organization scheme, adapted from (Wetshondo 2012)

CHAPTER:

I. REVIEW OF LITERATURE

1.0. Clay materials and compressed earth blocks: characteristics and treatments, production and performances

1.1. Introduction

This chapter briefly reviews the types and classes of clay minerals and materials. It further presents common stabilization techniques for improving the performances of clay earthen materials, particularly CEBs, for applications in building constructions. It also reviews by-products potentially useful as alternative stabilizers of clay materials. Furthermore, it briefly reviews the effect of the stabilization on the characteristics of clay materials and particularly focuses on the physico-mechanical, hygro-thermal and durability performances of CEBs.

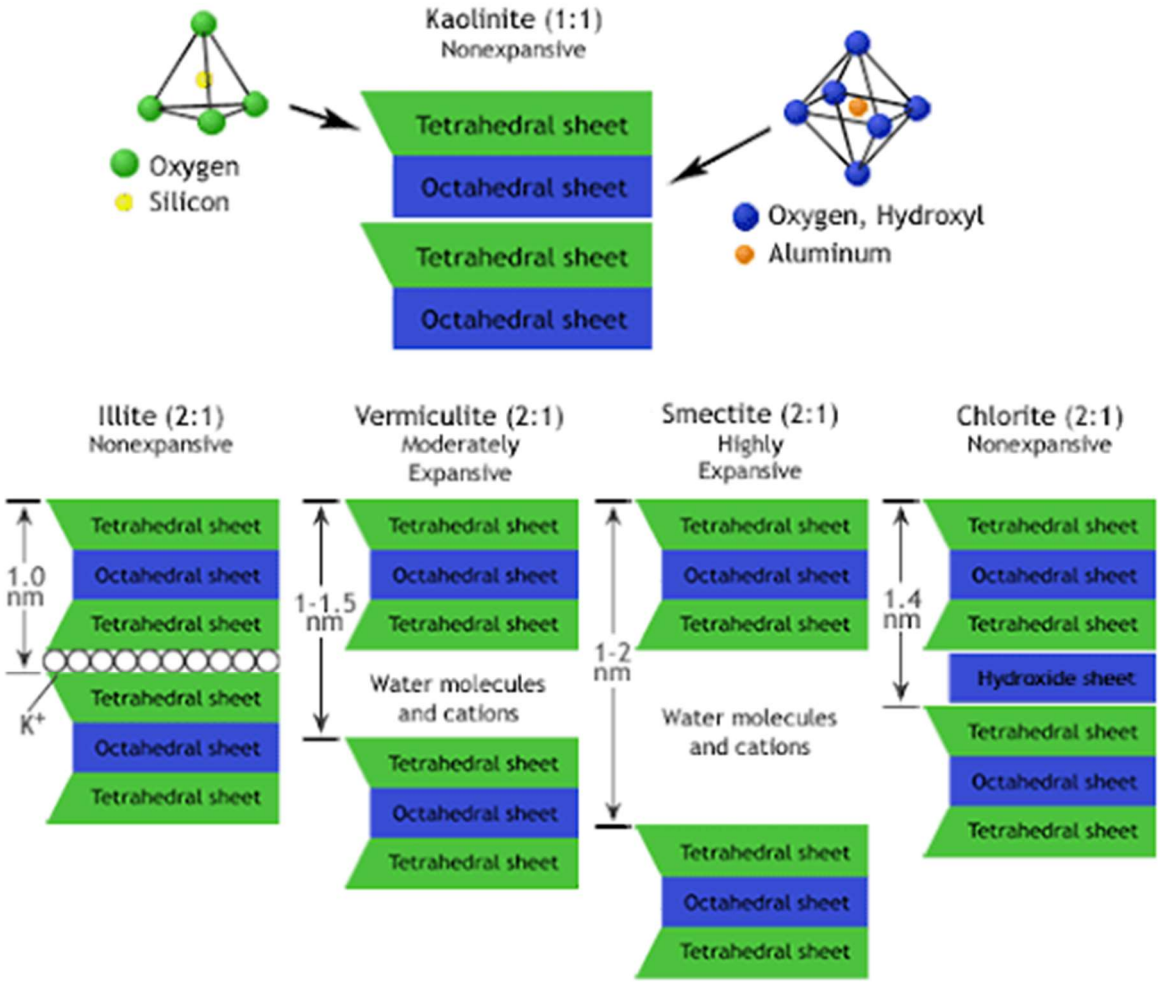

Figure 1.1. Schematic illustration of the lamellar structure of some clay minerals: elementary tetrahedron and octahedron sheets, type 1:1, type 2:1 and type 2:1:1 minerals. *http://soilnews.feedsynews.com/clay-mineralogy/?doing_wp_cron=1594990207.8967978954315185546875; 17 July 17, 2020*

1.2. Clay minerals: type, structure and classification

Clay minerals are mainly pyllosilicates whose structure is formed by layered stacks made of tetrahedral and octahedral sheets respectively centered around silicate (SiO_4^{4-}) or aluminate (AlO_4^{5-}) and Al^{3+} (aluminate), Fe^{3+}, Fe^{2+}, or Mg^{2+}. At the scale of unit cell, the pyllosilicates are considered to have the *a* and *b* dimensions oriented along the x-y plane (the largest face) and the *c* dimension along the z-axis (the thickness) (Meunier 2005). Figure 1.1 presents the schematic lamellar structures of some common clay minerals.

The so called basal planes (x-y plane) are separated by interlamellar space which can contain cations, water, hydrated cations, organic matters or other sheets. Therefore, the thickness of a layer plus the interlamellar space constitute the basal distance. The clay minerals are classified into different types according to the number of tetrahedra and octahedra constituting an elementary layer, the basal distance, and the elements occupying the interlamellar space. The main types of clay mineral are mineral type 1:1, mineral type 2:1, and mineral type 2:1:1, as well as the interstratified minerals (Meunier 2005).

Minerals type 1:1, also symbolized as T-O, having a basal distance of approximatively 7 Å (7.1-7.3 Å), has layers formed of one tetrahedron: T and one octahedron: O. Kaolinite (Figure 1.1) is an example representing the kaolinite group (Table 1.1). Being electrically neutral, these minerals take their cohesion from the hydrogen bonding between the oxygen (of silica) and hydrogen from the hydroxyl groups (of alumina) of the touching layers. Their small basal distance (<10 Å: 1 nm) generally prevents the absorption of water molecules. The minerals type 1:1 are also represented by other species such as halloysite, nacrite (Table 1.1).

Minerals type 2:1, also represented as T-O-T, are constituted with layers composed of an octahedron stacked in middle of two tetrahedra. Their basal distance averages around 10 Å (9.1-15 Å) depending on the content of interlamellar space. *Talc, smectite, mica, vermiculite* representing the main groups (Table 1.1). They are usually negatively charged, except *talc*, resulting from the interstitial substitution of Si^{4+} by Al^{3+} and Fe^{3+} in the tetrahedra and/or the substitution of Al^{3+} by Fe^{2+}, Mg^{2+} and Mn^{2+} or Fe^{2+} and Mg^{2+} by Li^{+} in the octahedra. When not charged, *talc,* their basal distance can be as small as 9.1-9.4 Å. However, when charged, their basal distance is even bigger due to the incorporation of cations (K^{+}, Na^{+}, Ca^{2+} and Mg^{2+}) or cations attached to water to balance the charge.

Table 1.1. Principle simple (non-interstratified) clay species (Meunier 2005)

Types	Crystalline features	Groups	
		Dioctahedral[1]	Trioctahedral[2]
1:1 minerals	E.C. of layer: 0 1T+1O+Int.Sp.=7 Å	Kaolinite Kaolinite, nacrite, halloysite (7 or 10 Å)	Serpentine Amesite, berthierine, antigorite, lizardite
2:1 minerals	E.C. of layer: 0 1T+1O+1T+Int.Sp. = 9 Å	Pyrophyllite	Talc
	E.C. of layer: -0.2 to -0.6 1T+1O+1T+Int.Sp.= 10 →18 Å Int.Sp: cations ±hydrated (Ca, Na) (Ch:10 Å; $2H_2O$: 14 Å; EG: 17 Å)	Smectites Al: montmorillonite, beidellite Fe: nontronite	Smectites Mg: saponite, stevensite, hectorite
	E.C. of layer: -0.6 to -0.9 1T+1O+1T+Int.Sp.=10→15 Å Int.Sp.: cations ±hydrated (Ca, Na) (Ch:10 Å; $2H_2O$:14 Å; EG: 14 Å)	Vermiculites	Vermiculites
	E.C. of layer: -0.9 to -0.75 1T+1O+1T+Int.Sp.=10 Å Int.Sp.: not hydrated cations (K)	Illite, glauconite	
	E.C. of layer: -1 1T+1O+1T+ Int.Sp.=10 Å Int.Sp.: not hydrated cations (K,Na)	Micas Al: muscovite, phengite, Fe: celadonite	Micas Mg-Fe: phlogopite, biotite, lepidolite
	E.C. of layer: -2 1T+1O+1T+ Int.Sp.=10 Å Int.Sp: not hydrated cations (Ca)	Brittle micas	
2:1:1 minerals	1T+1O+1T+1O (Int.Sp.)=14 Å Variable layer E.C. Int.Sp.: brucite- or gibbsite-like layers	Dioctahedral chlorites Donbassite Di-trioctahedral chlorites Cookeite, Sudoite	Trioctahedral chlorites Diabantite, penninite, brunsvigite, ripidolite, sheridanite
2:1 minerals	(fibrous structure)		Palygorskite, Sepiolite

E.C.: electric charge, Int. Sp.: interlamellar space, E.G. ethylene glycol

Illite (Figure 1.1) represents the group of non-expansive minerals type 2:1 with the charge of 0.9-0.75 and basal distance of 9.6-10.1 Å (Table 1.1). The presence of K^+ not only balance the charge, but also contribute to the stability of illite by tightly binding its layers through electrostatic forces. Smectite (Figure 1.1) represents the group of expansive minerals type 2:1 with charge of 0.2-0.6 and average basal distance of 15.5 Å (Table 1.1). This mineral group is able to adsorb large amounts of water, forming a water-tight barrier in the interlayers. The *high-swelling* or *low swelling* minerals are distinguished, respectively when the elements

[1] In the dioctahedral sheet silicates, each O or OH ion is surrounded by 2 trivalent cations, usually Al^{+3}
[2] In the trioctahedral sheet silicates, each O or OH ion is surrounded by 3 divalent cations, like Mg^{+2} or Fe^{+2}
https://www.tulane.edu/~sanelson/eens211/phyllosilicates.htm June 11, 2020

compensating the interlayer charge is sodium (*sodium smectite*) or calcium (*calcium smectite*). The *high-swelling* smectite can adsorb up to 18 layers of water molecules while the *low-swelling* smectite adsorbs smaller amount of water.

Montmorillonite clay, represents the group of smectite characterized with greater than 50 % octahedral charge due to isomorphous substitution in the octahedra. This leaves the nearby oxygen atom with a net negative charge that can attract cations through cation exchange, thus imparting very high cation exchange capacity (CEC) to the montmorillonite: 80-150 meq/100 g (Reeves et al. 2006). The montmorillonite clay has individual crystals which are not tightly bound. Therefore, this clay can swell and greatly increase in volume in the presence of variable quantity of water and loses the swelling capacity in the presence of NaCl and $CaCl_2$.

Minerals type 2:1:1, also represented as T-O-T-O, are constituted with layers composed of an octahedron stacked in middle of two tetrahedra and an interlamellar constituted with an octahedron. Their basal distance averages around 14 Å which corresponds to the chlorite group (Figure 1.1), where the interlamellar is occupied by brucite (aluminum hydroxide) or gibbsite (magnesium hydroxide)-like sheet (Table 1.1). This group is constituted with stable and swelling chlorites, depending on the type 2:1 layer.

Additionally, mixed-layer minerals also occur from the interstratification of layers of clay minerals of different nature, on a regular or random sequence. Some example of interstratified minerals include illite/smectite, kaolinite/smectite, etc (Meunier 2005). Minerals type 2:1 also occur in fibrous structures such as in palygorskite, sepiolite (Table 1.1). Furthermore, clay minerals are usually associated with non-clay minerals such as quartz, hydroxides (goethite, gibbsite), carbonates, etc and organic matters, thus forming clay materials.

The "*clay materials are composed of solid, liquid and vapor phases, with the clay minerals usually the most abundant minerals phase"* (Reeves et al. 2006). The *association international pour l'étude des argiles (AIPEA)* and the clay minerals society (CMQ) nomenclature committees jointly elaborated the definition of clay and clay minerals. *The term "clay" refers to the naturally occurring material composed primary by fine-grained minerals, which is usually plastic at appropriate water contents and will harden when dried or fired* (Reeves et al. 2006). This plasticity is the one, among other properties (§1.3), considered for the applications of clay materials in building constructions.

1.3. Clay materials in building construction: stabilization and production of CEBs

Clay materials are generally composed of heterogeneous mixtures of minerals and mainly clay minerals. The bulk mineral analysis reported the modal composition constituted with clay minerals (60 %), quartz (30 %) feldspar (5 %), carbonates (4 %), organic matter and iron oxide (Reeves et al. 2006). The clay materials, herein also referred to as "earthen materials" are used in building wall construction based on various techniques, namely adobe bricks, fired bricks, rammed earth (RE), and particularly compressed earth blocks (CEBs).

The choice is commonly dependent on their physical and geotechnical properties, and conditions of applications. The texture and particle size distribution (PSD), plasticity and cohesion, and compressibility are regarded as the fundamental properties necessary for a better application of earthen materials in building construction (Houben & Guillaud 2006). Table 1.2 classifies earthen materials into different fractions (clay<0.002 µm, silt: 0.002-0.06 mm, sand: 0.06-2 mm, gravel>2 mm) based on their PSD.

Table 1.2. Properties of earthen materials used for the production of unstabilized and stabilized CEBs (Maïni 2010, Houben & Guillaud 2006, CDI&CRATerre 1998)

Properties of earthen material		Unstabilized	Stabilized (ideal values)	
			Cement	Lime
Particle size distribution (%)	Gravel (20-2 mm)	< 40	0-30 (15)	0-30 (15)
	Sand (2-0.06 mm)	25-80	30-60 (50)	20-40 (30)
	Silt (0.06-0.002 mm)	10-25	10-25 (15)	15-30 (20)
	Clay (<0.002 mm)	8-30	10-30 (20)	30-50 (35)
Plasticity (%)	Liquid limit (WL)		20-30	25-50
	Plasticity index (PI)		10-20	20-30
Sulphate content based on SO_4^{2-} (%)			< 2	< 0.5
Chlorate content based on Cl^- (%)			< 1	< 0.5
Organic matter based on humus (%)			< 1	< 2
Energy and cost effectiveness of CEBs				
*Initial embodied energy: CEBs stabilized with 5 % cement consumes (548.32 MJ/m^3) 11 times lesser energy than fired blocks (6122.54 MJ/m^3)				
*Carbon emission: CEBs stabilized with 5 % cement pollutes (49.37 kg of CO_2/m^3) 13 times lesser than fired blocks (642.87 kg of CO_2/m^3)				
*Stabilized CEBs are mostly cheaper than fired bricks and concrete blocks: finished cubed meter of stabilized CEBs masonry is 15-20 % cheaper than fired bricks (April 2009).				
*Cost breakup for 5% CEM stabilized CEBs: 45 % for labor, 27 % for raw materials, 25 % for cement, 3 % for equipment				

*Auroville earth institute: http://www.earth-auroville.com/compressed_stabilised_earth_block_en.php, retrieved 2019 Oct 29

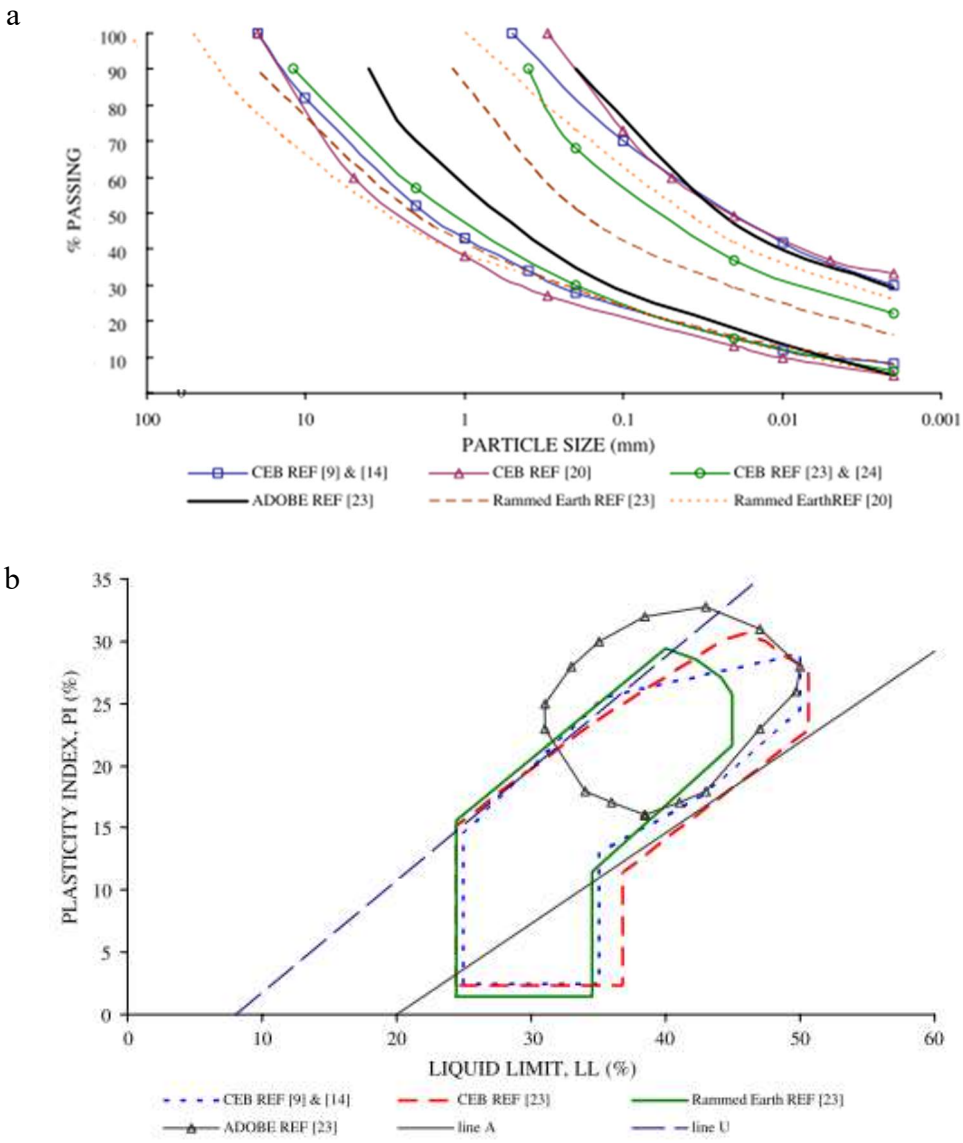

Figure 1.2. Recommended boundaries: (a) PSD, (b) plasticity for different construction techniques with unstabilized earthen material, adapted from (Delgado & Guerrero 2007)

The traditional sun dried (adobe) bricks and fired bricks, which are produced by molding wet material, respectively followed by drying and eventually firing at about 850 °C, require fine, very high plastic and cohesive material. The RE and CEBs, produced by dynamic/static compaction/compression of slightly humid material, require cohesive and coarser materials.

The particle size and cohesion are very important parameters for selecting the earthen materials for the production of CEBs. While gravel and sand constitute the inert fraction and act as skeleton in the CEB structure, silt and clay constitute the active fraction which binds the structure together (Houben & Guillaud 2006). Therefore, criteria and boundary for the PSD and plasticity have been tentatively defined to guide the selection of appropriate earthen materials for building construction, particularly CEBs (Table 1.2). An extensive normative review was

eventually carried out on the selection, mostly based on the texture and plasticity, of soil for unstabilized earth for construction (Delgado & Guerrero 2007). Figure 1.2 presents boundaries of PSD and plasticity recommended for selection of unstabilized earthen materials for CEBs compared with other techniques.

The CEBs, regarded as an evolutive and innovative version of adobe bricks, are produced by compressing the earthen material in a mold using either manual, mechanical or hydraulic machine controlled in static or dynamic mode (Pacheco-Torgal & Jalali 2012). It results in "modern" earth bricks which have regular shapes (prismatic, cylindrical), various forms (plain, perforated, interlocking) and sizes (295x140x90/95 mm, 245x245x90/95 mm) (Maïni 2010, Houben & Guillaud 2006, CDI&CRATerre 1998). This allows to achieve various architectural and aesthetical shapes and textures. Though CEBs may reach better mechanical stability than adobes, they may also be instable vis-a-vis water. Therefore, they need the stabilization using chemical binders (cement or lime) in order to improve their stability, just like firing the bricks (fired bricks), except that the latter is more energy consuming and air polluting.

The stabilization of earthen materials using small amount of chemical binders, generally lesser than 10 wt % (eventually 15 %) results in lower consummation of energy, lower emissions of CO_2, contrary to firing (Shubbar et al. 2019). Table 1.2 shows that CEBs stabilized with 5 % cement contain and emit respectively about 10 times lesser initial embodied energy and CO_2 than fired bricks. Table 1.2 also shows that a finished cubed meter of stabilized CEBs is 15-20 % cheaper than fired bricks. Nevertheless, the stabilization for the production of CEBs would depend on the quality of earthen materials, the quality and quantity of the stabilizers, and level of compaction, among other factors.

1.3.1. Aim and techniques of stabilization

The quality of clay earthen material is improved/altered by treating/stabilizing its structure and/or texture (Houben & Guillaud 2006). The ultimate objective of stabilization is to improve the most useful properties of earthen materials such as the mechanical (§1.6), hygroscopic (§0) and weathering (§1.8) resistance and dimensional stability. The stabilization of earth specifically aims to enhance the strength and durability on contact with water, by:

- reducing the swelling-shrinkage and surface abrasion and increasing waterproofing;
- cementing the particles and increasing the mechanical strength and cohesion;
- reducing the interstitial voids and/or blocking the pores that cannot be eliminated.

To achieve these objectives, it is advised to proceed with one or more of the following techniques:

- physical treatment of the texture of earthen material by mixing different grain fractions, drying (adobe bricks), firing (fired bricks), or adding fibers (synthetic or natural);
- chemical treatment of the microstructure by adding cementitious materials such as cement; lime, geopolymer and/or other additives or exploiting the natural binding cohesion of clay;
- mechanical treatment of the structure of the earthen material by improving the density, compressibility or resistance, and permeability or porosity by mean of compaction.

The mechanical treatment can be carried out on earthen material which previously underwent physical or chemical treatment. This is the case for stabilized CEBs or rammed earth. The chemical stabilization particularly aims to reduce the plasticity, improve the workability and resistance to erosion of earthen material (Pacheco-Torgal & Jalali 2012). At least 50 % of clay lumps should be ground to diameter lesser than 5 mm for effective chemical stabilization (Houben & Guillaud 2006). Moreover, other factors can guide the choice of chemical stabilizer, such as:

- the part of the building where the earth is going to be applied and its orientation;
- the inner properties of earth such as strength, water erosion, abrasion resistance, etc;
- the required level of improvement of earth, depending on applications;
- and most importantly, the cost and availability of, local or imported, stabilizer, as well as substitution materials such as agro-industrial by-products (§1.4).

The following paragraphs focus on the main common techniques of chemical stabilization, i.e. cement, lime, and other additives, as well as reinforcement with fibers.

1.3.2. Stabilization with cement

Stabilization with cement is reputed to be most effective with sandy earthen material, illustrated by the fact that plasticity index should be in the range of 10-20 % and the fraction of clay particles in the range of 10-30 % (Table 1.2). Additionally, stabilization with cement is recommended for earthen materials containing low swelling minerals such as kaolinite, illite, and quartz (Houben & Guillaud 2006). Moreover, lateritic soil containing iron oxide, as in goethite and hematite, achieves efficient stabilization with cement given the possibility of pozzolanic reaction or hardening effects. Organic matters, salts and sulfates should be avoided.

Moisture content should be slightly drier than the optimum moisture content for sandy soil alone.

The stabilization with cement (3-10 %) significantly improves the mechanical properties and durability (§1.6-1.8). This is essentially due to the hydration reaction of cement, taking place for 28 days at 20 °C, for the formation of cementitious products (eq.1.1a). Increasing the clay content in earthen materials may result in detrimental effect, thus requiring to increase the content of cement to counteract this effect (Boffoue et al. 2015, Raheem et al. 2010)

eq.1.1

$$\text{Earth} + \text{cement} + H_2O \rightarrow \text{calcium silicate hydrates} + \text{calcium aluminate hydrates} \quad \text{a}$$

$$\text{Earth} + \text{lime} + H_2O \rightarrow \text{calcium silicates hydrates} + \text{calcium aluminates hydrates} \quad \text{b}$$

1.3.3. Stabilization with lime: interactions in lime-clay and admixtures

Stabilization with lime, also referred to as earth treatment, is reputed to be more effective with clay-sand soil, especially with very clayey soils containing 30-50 % eventually 70 % of clay particles. This justifies the requirement for material with higher plasticity index (20-30 % eventually 35 %), liquidity limit (35-50 %) than in the case of cement stabilization (Table 1.2). Lime reacts with clay through the pozzolanic reaction (eq.1.1b), thus requiring more water as the amount of lime increase (Harichane et al. 2012, Oti et al. 2009a, 2009b). Additionally, lime has better interactions with swelling minerals such as montmorillonite/smectite (Al-Mukhtar et al. 2010a, 2010b). Some components such as sulfates, phosphate and organic matters are harmful for the stabilization and hence can result in erroneous results (ASTM 1999).

Test methods were developed to assess the amount of lime required for the stabilization of clayey soil. One of the tests determines the fraction of lime for addition to the soil to reach the pH of 12.4 for the mixture solution of soil-lime, as a result of the dissolution of lime and dissociation of $Ca(OH)_2$ into Ca^{2+} and OH^-. This pH (12.4) is considered as the minimum requirement for the pozzolanic reaction to take place (Al-Mukhtar et al. 2010a). The lime interacts with clay materials in two main phases: modification and stabilization.

The modification phase constitutes the short term interactions that occur immediately after addition of small fraction of lime (2-6 %) to the clay. It satisfies the affinity (to water) of clays, also referred to as lime fixation point (LFP). This results in the modification of the texture by coagulation of particles and decrease of the plasticity and shrinkage of clay material through cation exchange, of mainly calcium ion (Ca^{2+}), between the lime and clay.

The stabilization phase mainly occurs through the reaction of clay with lime, pozzolanic reaction (eq. 1.1b), resulting in the formation of cementitious products (§1.5). Beyond the LFP (pH >12.4), the aluminosilicates in the clay material dissolve in solution and combine with Ca^{2+} to form hydrates of calcium silicate, calcium aluminate and eventually calcium alumino-silicate (C-S-H, C-A-H, C-A-S-H), which increases the mechanical and durability performances (Di Sante et al. 2014, Al-Mukhtar et al. 2010a). Moreover, some studies reported that fine particles of quartz can possibly react with lime or at least serve as nucleation sites for the formation of CSH products (El-Mahllawy & Kandeel 2014, Millogo et al. 2008).

In addition to enough amount of lime and water, the pozzolanic reaction between clay material and lime requires enough curing time (eventually beyond 28 days) and higher temperature (>20 °C) (Nagaraj et al. 2014, Al-Mukhtar et al. 2010a, Oti et al. 2009a). The tests than can be used to follow up this pozzolanic reaction is the lime consumption extent through measurement of electrical conductivity (EC) and concentration of calcium ions [Ca^{2+}] in clay-lime solution over time (Al-Mukhtar et al. 2010a, 2010b).

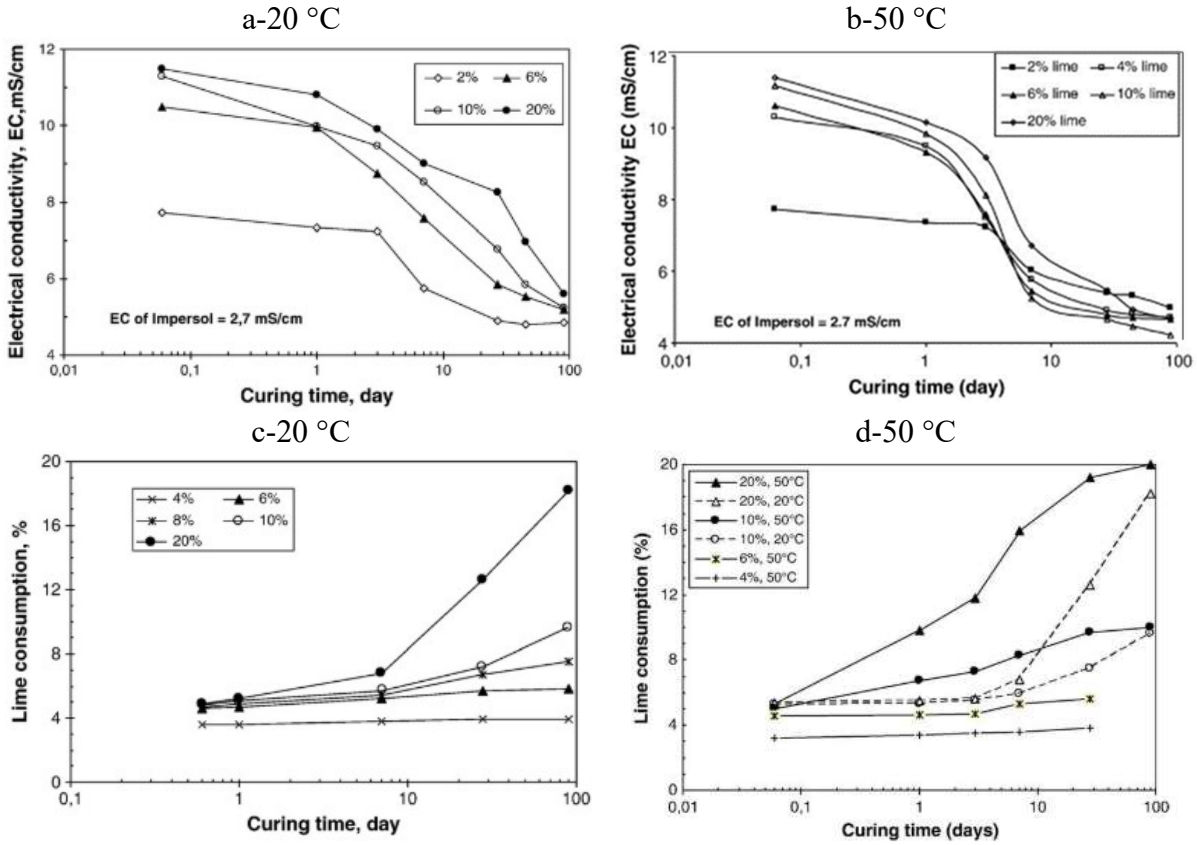

Figure 1.3. Evolution of (a-b) EC and (c-d) lime consumption in mix solution of smectite rich clay and 2-20 % lime cured at 20 and 50 °C (Al-Mukhtar et al. 2010a, 2010b)

Figure 1.3 presents the evolution of EC and lime consumption of smectite rich clay material at 20 °C and 50 °C, over the curing time. The mixtures cured at 50 °C (Figure 1.3b) recorded more rapid decrease of the EC, related to the rapid decrease of the concentration of Ca^{2+}, than those cured at 20 °C (Figure 1.3a). It was accompanied by the increase of the pozzolanic reaction by a factor of 6, in terms of rapid rate of consumption of lime at 50 °C than at 20 °C (Figure 1.3). This points out the interest for stabilization of earthen materials with lime in warm regions.

The earthen material containing very high fraction of clay particle and/or high swelling minerals, can be pretreated with lime before stabilization with cement for achieving better results (Nagaraj et al. 2014, Houben & Guillaud 2006). Small fraction of lime (2-4 %) allows to satisfy the affinity of the clay materials, while the supplement content of cement contribute to the rapid improvement of engineering performances.

Additionally, lime/cement is sometimes combined with other (secondary) cementitious materials (SCM) such as natural pozzolan (NP), fly ash (FA), ground granulated blast furnace ash (GGBS), or metakaolin (MK) to activate their pozzolanic activity useful for soil stabilization (Van Damme & Houben 2018, Kampala et al. 2013, Horpibulsuk et al. 2013, Horpibulsuk et al. 2012). The stabilization with lime and pozzolan results in double effects: the pozzolanic reaction between the clay material and lime and between lime and pozzolan, responsible for the microstructural changes (§1.5) and achieve better performances (§1.6).

1.3.4. Reinforcement with fibers

The matrix of earthen materials, unstabilized or stabilized with chemical binders, can further be reinforced with fibers, natural or synthetic/manmade (§1.4.3). The addition of fibers/granulates (1-4 % eventually up to 12 % by weight) allows to reduce the shrinkages (unstabilized materials), increase the mechanical strength (mainly tensile) through the improvement of the ductility and mainly impart the thermal properties (Toguyeni et al. 2018, Laborel-Préneron et al. 2016, Guettala et al. 2016, Ashour et al. 2015, Danso et al. 2015a). The content of fibers to incorporate in the earthen matrix matters as much as the length or aspect ratio; the length ranges in 5-100 mm, and eventually up to 500 mm (Danso et al. 2015b).

Shorter fibers allow to achieve homogeneous mixing but lower mechanical performances. In fact, it was reported that the embedded length of fiber of 25 mm was insufficient to develop full tensile capacity of CEBs (Mostafa & Uddin 2015). By contrast, longer fibers are not easily dispersed in the mixture, thus, at high content, can lower the mechanical performances given

the risk of high deformation and creep governed by the softness of fibers. The typical fiber content in earth blocks range below 1 %, with the optimum mostly occurring around 0.35-0.4 % for mechanical performances and beyond 0.5 % for improving the ductility and thermal properties. Moreover, the inclusion of hydrophilic natural/plant fibers in earth blocks increases the water absorption more than hydrophobic polymeric fibers (Elenga et al. 2011).

1.4. By-product binders and fibers: alternative stabilizers of earthen materials

1.4.1. Calcium carbide residue

Calcium carbide residue (CCR) is a white greyish industrial by-product formed by the hydrolysis of calcium carbide during the production of acetylene gas (eq. 1.2). Figure 1.5a presents the XRD of CCR, compared to that of industrial hydrated lime (HL), showing the diagnostic peaks of portlandite (CH: $Ca(OH)_2$) at 2.62 Å. Table 1.3 shows that the CCR can contain up to 70 % CaO, similarly to HL. Furthermore, Table 1.3 reports the specific density of 2.21 g/m^3 for the ground CCR which is lower than 2.35g/m^3 for the HL and specific surface area of 11.3 m²/g versus 18 m²/g, respectively. These differences were related to their mineral composition, shape, porosity and PSD; the CCR was coarser (medium particle size: D_{50} of 20 µm) than HL (D_{50} of 10 µm) (Cardoso et al. 2009).

$$CaC_2{}^{(s)} + 2H_2O{}^{(l)} \rightarrow C_2H_2{}^{(g)} + Ca(OH)_2{}^{(aq)} + 64\ \text{kcal} \qquad \textit{eq. 1.2}$$

Table 1.3. Physical properties and chemical composition of CCR and RHA versus HL and FA

Physical properties	CCR [a]	HL [a]	RHA [b]	RHA [c]	FA[d]
Mean particle size (µm)	20 (D_{50})	10 (D_{50})	0.15	5	3.5 (D_{50})
Specific gravity (-)	2.21	2.35	-	2.19	2.39
Fineness: passing 45 µm (%)	-	-	-	99.5	-
Specific surface area, BET (m²/g)	11.3	18	77.4	50.2	-
Chemical composition (%)	CCR [a]	HL [a]	RHA[b]	RHA[c]	FA[d]
CaO	71.2	70.9	0.9	2.7	12.1
SiO_2	-	-	91.7	89.5	45.7
Al_2O_3	0.7 (Al_2O_3+Fe_2O_3)	0.7 (Al_2O_3+Fe_2O_3)	0.4	-	24.6
Fe_2O_3			0.9	0.6	11.3
MgO	0.1	0.3	0.3	1.2	2.9
SO_3	0.1	0.2	-	0.9	1.6
K_2O	-	-	1.7	0.8	2.7
LOI	26.4	26.9	3.1	2.3	1.2

CCR: calcium carbide residue, HL: hydrated lime, RHA: rice husk ash, FA: fly ash, D_{50}: median size.

[a] (Cardoso et al. 2009), [b] (Xu et al. 2012) calcination at 600 °C, [c] Muthadhi & Kothandaraman 2010 at 500 °C-2h, [d] (Horpibulsuk et al. 2013)

The usefulness of CCR was mostly assessed for stabilization of soil for foundation and pavement applications. The amount of CCR used for stabilization of soil is 2-25 % of the mass of soil depending on the reactivity of the materials and curing time of 7, 28 days (Saldanha et al. 2018, Horpibulsuk et al. 2013). Saldanha et al. (2018) showed that CCR by-product is an environmentally-friendly chemical additive through physical, mineralogical, and chemical characterization. This was based on the concentration of heavy metal present in CCR, such as arsenic, barium or so, which were very low compared to the limits of hazardous waste and leachable metals recommended by USEPA[3] and WHO[4].

In the same sense, the CCR can potentially be useful for the stabilization of CEBs. Further assessments of environmental impacts of CCR can be carried in terms of the end of life and CO_2 footprint of stabilized CEBs, which is out of the scopes of the present study.

1.4.2. Rice husk ash

Rice husk ash (RHA) is a microporous and cellular structured powder produced from the combustion/calcination of rice husk (RH). The RH is an agricultural by-product from the rice paddy. Its production is estimated at 20-22 % of total mass of the rice paddy (Muthadhi & Kothandaraman 2010). The combustion of RH generally produces heat and ash (RHA); about 20 % of the initial mass of RH (Deshmukh et al. 2012). The calcination of RH at controlled temperature and in oxidizing atmosphere particularly yields whitish RHA which can contain more than 90 % of silica (SiO_2), compared to 45 % for FA (Table 1.3).

Figure 1.4a presents the range of temperature (400-700 °C) and soaking time (5-1 hours) for the controlled calcination of RH to yield microporous and cellular structured, and thus reactive RHA. In fact, the RHA can contain up to 90 % of amorphous SiO_2 and potentially reactive in alkaline conditions such as NaOH, KOH, $Ca(OH)_2$ (Hwang & Huynh 2015, Muthadhi & Kothandaraman 2010, Deshmukh et al. 2012). Figure 1.4b shows that the energy consumption for the calcination of RH is relatively low, up to 600 °C for <150 minutes (3 h). This is was related to the contribution of inner-energy of the RH (Muthadhi & Kothandaraman 2010).

Figure 1.4c additionally shows color change during the controlled calcination of RHA, from dark-blackish through white-greyish to lilac-pink, related to the degree of calcination and phase

[3] USEPA: United States Environmental Protection Agency. 2009. Waste characteristics, materials recovery and waste management division in the office of resource conservation and recovery. Washington, DC).
[4] WHO: World Health Organization. 2011. Guidelines for drinking-water quality, 4th Ed., Geneva).

transformations. The dark blackish color indicates the incomplete calcination of RHA, containing unburnt carbon; the white-grey color indicates the formation of amorphous silica; while the lilac pink color reveals the crystallization of RHA (Figure 1.4a). In fact, the calcination beyond 700 °C tends to crystallize the previously formed amorphous silica into cristobalite and tridymite, which results in the loss of reactivity (Xu et al. 2012).

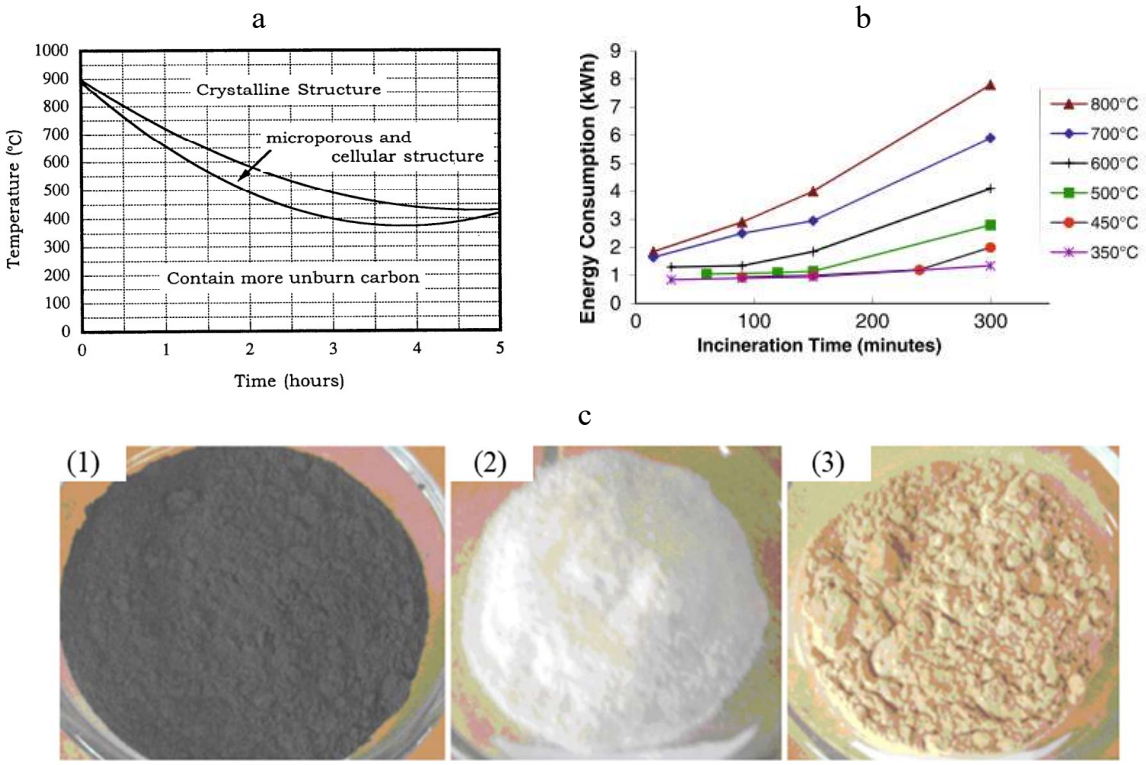

Figure 1.4. Controlled calcination of RH to produce RHA (a) optimum conditions and (b) energy consumption (1.5 kg of RH), (c) color transitions: calcined at 400°C (1), 500°C (2), 900°C (3) for 12 h (Hwang & Chandra 1996, Muthadhi & Kothandaraman 2010, Deshmukh et al. 2012)

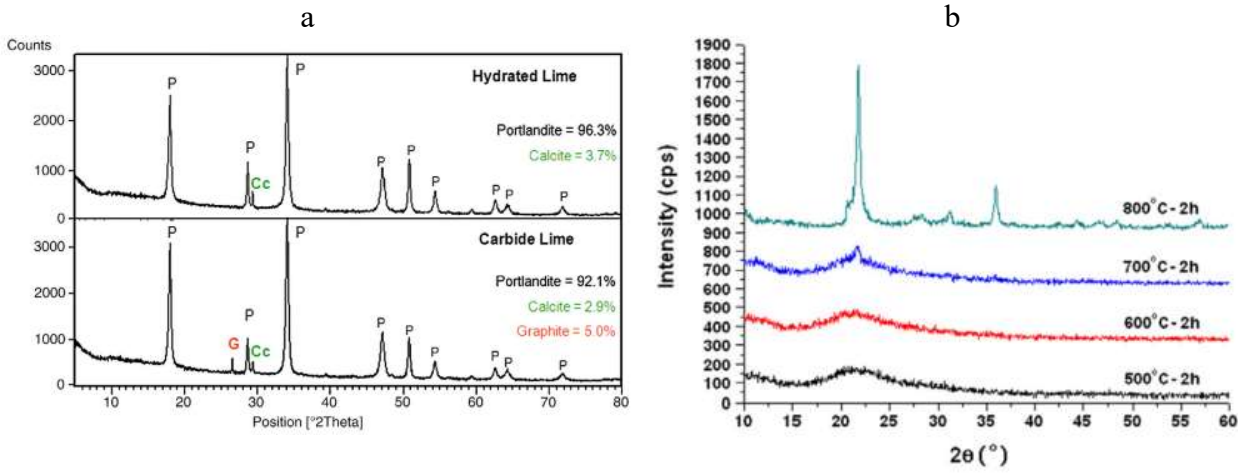

Figure 1.5. XRD spectra of (a) hydrated lime (industrial) & carbide lime (CCR) and (b) RHA calcined at different temperature (Cardoso et al. 2009, Xu et al. 2012)

Figure 1.5b shows the XRD of amorphous silica in the RHA calcined below 600 °C (broad peak around 22° 2θ), which crystallizes at 800 °C into cristobalite (2θ~22°) and tridymite (2θ~21°). Additionally, the fine particles may sinter/coalesce at higher temperature, which reduces the specific surface area (SSA) and reactivity of RHA. Electron microscopy of RHA revealed three layered structure: inner, outer and interfacial layer having honeycombed and interstitial pores (Xu et al. 2012).

The porous structure and amorphousness of the RHA are the main reason for the high SSA and chemical activity (Xu et al. 2012, Muthadhi & Kothandaraman 2010). In fact, the SSA can reach 77-50 m^2/g for the RHA of mean particle size of 0.15-5 μm and specific density of 2.12 respectively compared to 20-28 m^2/g, 3.5 μm and 2.39 for FA (Table 1.3). Therefore, it can be advised to calcine below 600 °C for less than 3 hours to produce reactive RHA and use less energy.

It is clear that the higher the calcination temperature, the greater the percentage of silica in the RHA, and the least the content of oxides of K, S, Ca, Mg and volatile components. As of the ASTM C618 (ASTM 1994) specification, the RHA should contain at least a combined 70 % of SiO_2, Al_2O_3 and Fe_2O_3 to be qualified as a pozzolan and not more than 10-12 % of unburnt carbon, determined as loss on ignition at 1000 °C. Therefore, there is necessity to find the optimum conditions of calcination that would yield lower content of volatile constituents and high fraction of amorphous reactive silica at minimized energy consumption.

In addition to the XRD, number of techniques were devised to evaluate the reactivity of the RHA based on analytical method, electrical conductimetry, or mechanical activity index (Walker & Pavía 2011, Muthadhi & Kothandaraman 2010, Payá et al. 2001, Mehta 1978). As early as 1973, Mehta patented a technique to evaluate the silica activity index (SAI) of RHA as the fraction of silica which is amorphous. It is determined as the percentage of RHA passing the 44 μm sieve which dissolves in excess of boiling solution of 0.5 M NaOH during an extraction period of 3 minutes (Mehta 1978).

Payá et al. (2001) adapted two methods on the RHA: one previously applied on clay and another applied on pozzolans. In application of first methods (glycerol method), free amorphous silica (FAS_{Gly}) in RHA was evaluated by treating the RHA by glycerol and forming glycerosilicate solution. The solution was titrated with glycerol solution of barium hydroxide ($Ba(OH)_2$), using phenolphthalein or alizarin yellow as indicator, in order to determine the $FAS_{Gly,}$ and taking between 35-50 minutes. In the second method (KOH method), the FAS_{KOH} was evaluated by

attacking the RHA with boiling solution of 4 M KOH to yield results in only 3 minutes. There was good agreement between the two methods.

Walker & Pavía (Walker & Pavía 2011) evaluated the chemical activity index by measuring the evolution of the electrical conductivity (EC) of saturated solution of $Ca(OH)_2$ added with 4 g of RHA and other pozzolans over 125 hours. The rapid diminution of the EC of the solution containing RHA is related to its ability to fix easily the dissolved $Ca(OH)_2$ and form hydration products, compared to other pozzolans (Figure 1.6a). Moreover, the RHA calcined at 500 °C for 2 h contains the highest amount of amorphous and soluble silica, with respect to the analytical method using glycerol (Figure 1.6b) and conductimetry in HF solution (Figure 1.6c).

While most studies focused on the application of the RHA in cement and concrete, some studies showed that RHA decreases the plasticity of soil for pavement, similarly to cement and lime, and maximum dry density and increases the OMC and Californian bearing ratio (Choobbasti et al. 2010, Basha et al. 2005). Basha et al. (2005) recommended the addition of 6-8 % cement and 10-15 % RHA as the optimum regarding the plasticity, compaction, strength, resistance to immersion and economy. Moreover, adding lime (4-6 %) and RHA (5 %) to the soil decreases the deformability, producing a brittle material (Choobbasti et al. 2010).

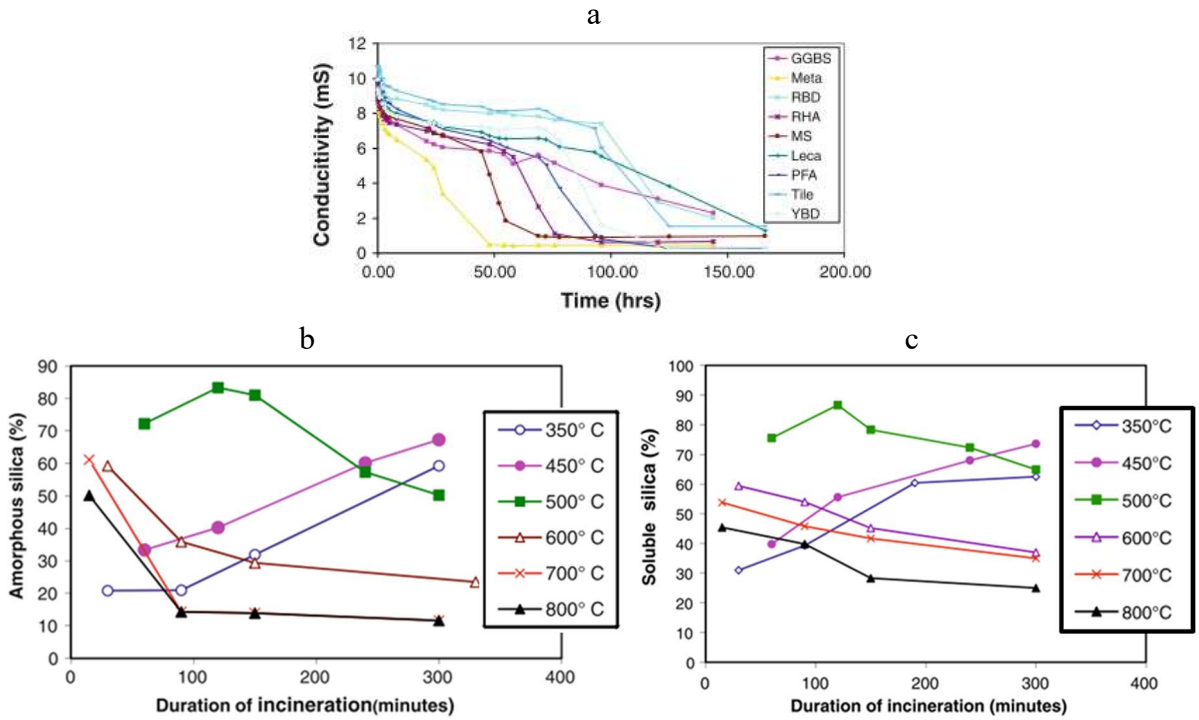

Figure 1.6. Pozzolanic activity of RHA (a) decrease of electrical conductivity (EC) in saturated solution of $Ca(OH)_2$ over time, (b) amorphous and (c) soluble silica with respect to the calcination time, adapted from (Walker & Pavía 2011, Muthadhi & Kothandaraman 2010)

Therefore, the stabilization using a combination of RHA and CCR (§1.4.1) as binders can potentially improve the properties of CEBs, instead of cement or industrial lime (§1.6-1.8). However, similarly to CCR, the assessment of environmental impacts (out of scopes) from the calcination and utilization of RHA would potentially allow to achieve a complete comparison with industrial binders. Furthermore, the incorporation of fibers, such as Okra fiber (§1.4.3.), would reduce the brittleness, among other properties (§1.6-1.7), of stabilized CEBs.

1.4.3. Okra fiber

Okra fibers are extracted from the skin of okra plant. Okra plant, also known as Gombo or Ladies Fingers (Malvaceae family, Abelmoschus Esculentus L. specie), is a 2-4 m tall plant and mostly grown in warm region (West Africa, India) for its dietary values (leaves, fruits). Its applications as a plant fiber has been previously investigated on the chemical composition, physico-mechanical properties and effects of different treatment on its properties (De Rosa et al. 2011, Khan et al. 2009, Alam & Khan 2007).

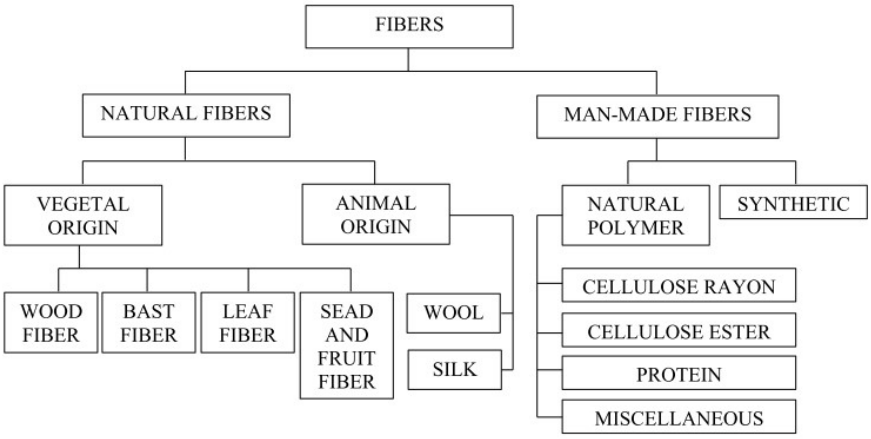

Figure 1.7. Classification of fibers based on their origin, adapted from (Mustapha 2015)

Figure 1.7 presents the classification of fibers based on their origin: natural and manmade fibers. Okra fibers are classified among fiber from vegetable origin. Vegetable fibers constitute the category of natural fibers, from plant, which have attracted the attentions of many researchers for different applications given their sustainable exploitability. The vegetable fibers are cellulosic fibers and exist in various forms according to the part of the plant where they are extracted. This includes bast and skin fibers, leaves fibers, seed fiber, etc.

Bast fibers such as okra, flax, kenaf, etc are collected from the skin or bast around the stem of the plant. Given their high content of cellulose (up to 75 %), bast fibers have higher tensile strength than other plant fibers, and are therefore used for yarn, fabric, packaging. They also

contains non-cellulosic constituents such as hemicellulose (10-20 %), lignin (0.5-20 %), pectin (0.2-5 %), wax (0.3-5 %) and moisture (5-20 %) (De Rosa et al. 2010, Alam & Khan 2007). The XRD diffractogram of Okra bast fibers presents three main peaks of cellulose at 15.6°, 22.5° and 34° Å (Khan et al. 2017). Table 1.4 presents some properties of different bast fibers such as the specific density (1.1-1.6 g/cm^3), water absorption capacity (120-150 wt. %), tensile strength (200-1500 MPa). Indeed, these properties are very scattered for different types of bast fibers, and even for one type of fiber.

Table 1.4. Chemical composition, physical and mechanical properties of bast fibers

Fibers	Cellulose (%) [a]	Density (g/cm^3) [b]	Water absorption (wt.%) [c]	Diameter (µm) [b]	Tensile strength (MPa) [b]	Elongation to failure (%) [b]
Flax	64.1-71.9	1.5	120	40-600	345-1500	2.7-3.2
Hemp	70.2-74.4	1.47	133	25-250	550-900	1.6-4
Jute	61-71.5	1.3-1.49	151	25-250	393-800	1.16-1.5
Kenaf	31-57	1.5-1.6	149	2.6-4	350-930	1.6
Ramie	68.6-76.2	1.5-1.6		34-49	400-938	1.2-3.8
Okra	60-70	1.15-1.45		40-180	234-380	2.5-8.6

t al. 2018, [c] Symington et al. 2009.

The processing of okra bast into fibers is achieved mainly by water retting or field retting, mechanical separation, chemical extraction. Through these processes, Okra fibers, constituting about 15-20 % of total dry weight of the skin, are separated from the pectin. Water retting consists of leaving the bast of plant in tap water for 3-4 weeks for the non-cellulosic matter to spoil. After this period, the bast fibers are washed in water many times to remove all impurities and dried before any further treatment (Khan et al. 2017).

Figure 1.8 presents the schematic and microstructural images of bast fiber at different scales. The single or technical bast fiber (bundle: Φ 50-100 µm), extracted from the stem of the plant, is made of a bunch of multiple elementary or ultimate fibers (cells: Φ 10-20 µm) structured in two main layers (cell walls) around the lumen (cylindrical cavity). These layers are distinguished as the primary outer cell wall and the secondary inner cell wall. The secondary cell wall is made of three microfibrillar (4-10 µm) layers: the inner S1 and the outer S3 transversally oriented layers and the middle S2 longitudinal layer. The microfibrils are the one made up of cellulose (mainly ordered structure) alternatively connected to the hemicellulose (disordered), hence controlling the strength of the fiber (Figure 1.8a). Figure 1.8b additionally shows the cross section and longitudinal shapes of okra bast fiber, with the polygonal shape and the thickness varying along the length.

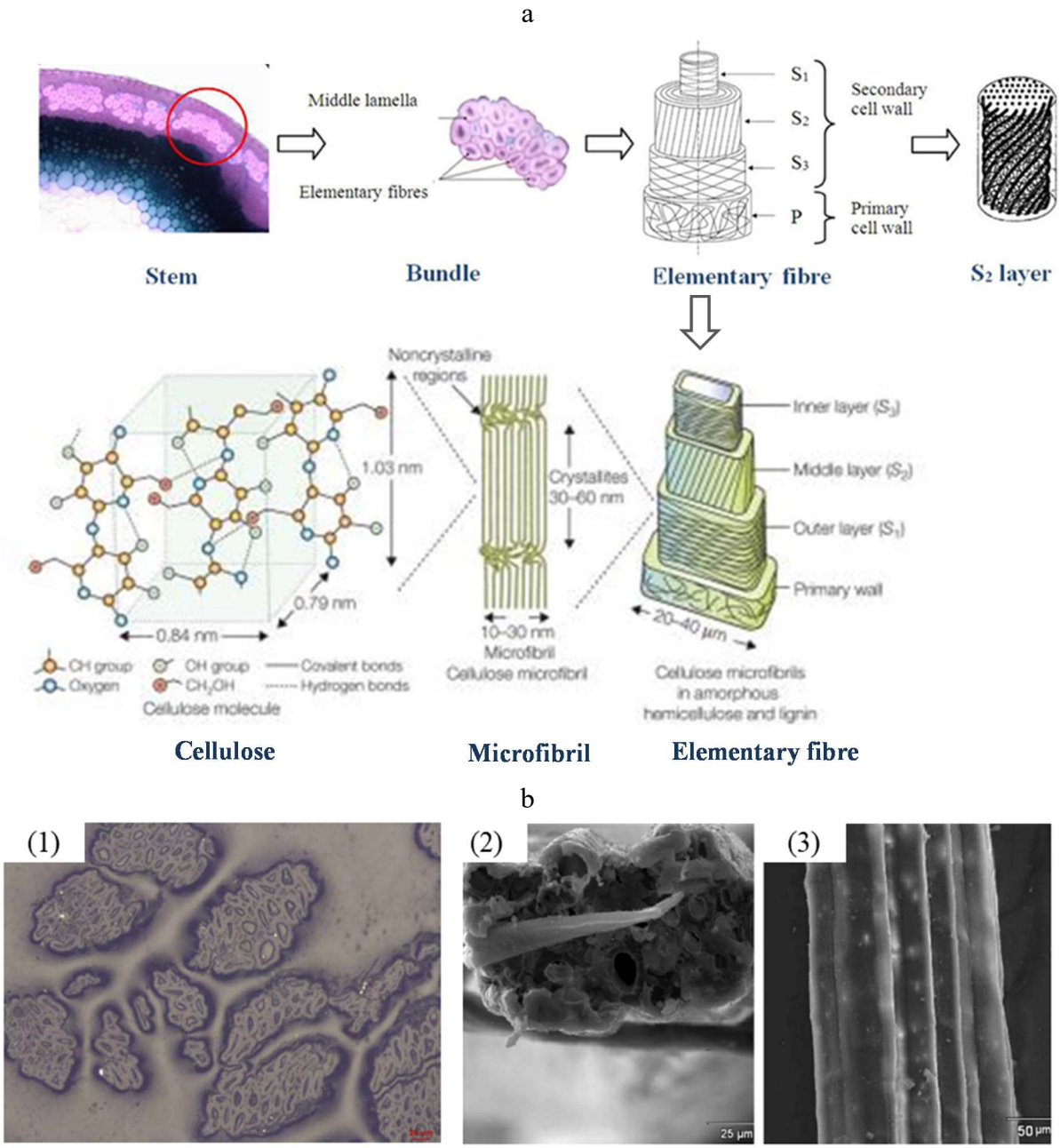

Figure 1.8. (a) schematic structure of bast fibers, (b) micrographs: optical of cross section (1) and SEM (2-3) of cross section and longitudinal views, adapted from (De Rosa et al. 2010)

The large variability of the tensile strength and Young's modulus of bast fibers and other types of plant fibers is usually influenced by the defects, pores in their structures, conditions of cultivation, extraction, treatment and testing, among others. In fact, the strength of ultimate fiber is much greater than that of the single fiber and the shorter the testing gauge length, the higher the strength of fibers. Generally, for a particular plant fiber, the strength can vary from 7000 MPa at a molecule scale to 480 MPa for microfibrils (cellulose) and 140 MPa for elementary fiber (cell). This assumes that thinner and shorter fibers have lesser defects.

The studies on carbon and glass fibers evidenced that the tensile strength and extension at failure generally decreases with increasing the gauge length (Pardin et al. 2002). This implies that thicker and longer fiber bundle contains more defects than ultimate fiber. Though bast fibers present acceptable performances for structural application, they are very sensitive to thermal decomposition, decomposing around 300-400 °C for okra bast fibers (De Rosa et al. 2010). Therefore, okra bast fibers can have better applications in conditions where they are not subjected to any heat degradation (room temperature), like for the reinforcement of CEBs.

Different standards were referred to test the tensile strength of plant fibers considering various gauge length and different loading rate, for instance 10 mm at 1 mm/min as of ASTM D 3379-75 (ASTM 1989a) in (De Rosa et al. 2011) and 70 mm at 10 mm/min as of ASTM D 3822-01 (ASTM 2001) in (Symington et al. 2009). The ASTM D 3379-75 is applied to the single filament of high modulus fiber (>21 GPa) such as carbon and glass fiber, with gauge length 2000 times the diameter. The ASTM D 3822-01 is applied on natural and man-made single textile fibers. The long gauge length (70 mm) might have been considering because this fibers are supposed to be used in long shapes (textile).

By contrast, the ASTM C 1557-03 (ASTM 2003), which is generally applied on single fiber, recommends the gauge length equivalent to several fiber diameter, usually 25 mm. It also suggests that other practical gauge length can be used provided that they are reported. Therefore, the length of fibers to be used for the reinforcement of CEBs can be considered as the gauge for testing the tensile strength (Chapter II).

1.5. Microstructural characteristics of earthen materials

The treatment/stabilization effect on the improvement of performances of clay earthen materials is related to the formation of new cementitious products from the reaction between the clay materials and stabilizing agents. In fact, the reaction between different type of clay and lime under various conditions resulted in the formation of calcium silicate hydrates (CSH) and/or calcium aluminate hydrates (CAH), and eventually CASH (Al-Mukhtar et al. 2010a, 2010b).

Al-Mukhtar et al. (2010a, 2010b) studied the mineral change in mixtures of impersol (kaolinite+smectite clay) treated with lime (20 %) and cured at 20 and 50 °C. The authors showed that the intensity of new XRD reflection formed at 7.6 and 3.67 Å (11.6 and 23.6 2θ) increased with the curing time, while that of lime, kaolinite and smectite decreased (Figure 1.9). New peaks were also detected at 2.86 and 1.66 Å (31.3 and 55.3 2θ) which were relatively weak

in samples cured at 20 °C compared to 50 °C (Figure 1.9a-b). This demonstrated the progress of the pozzolanic reaction between clay and lime resulting in the consumption of lime and formation of CAH ($Ca_3Al_2O_6$ xH_2O). Furthermore, Figure 1.9b shows new peaks at 3.08 and 2.79 Å (29.0 and 32.1 2θ), represented as poorly defined CSH ($Ca_3Si_2O_7$ xH_2O). Therefore, increasing the curing temperature results in quicker and better formation of pozzolanic products in clay earthen materials stabilized with lime.

The thermogravimetric analysis/derivative thermogravimetric (TGA-DTG) was also used to follow the formation of CSH and CAH gel in stabilized earthen materials (Figure 1.10). The TGA-DTG shows the loss of gel water at around 100-150 °C and 200-300 (260) °C related to the dehydration of CSH and CAH (Arrigoni, Pelosato et al. 2017).

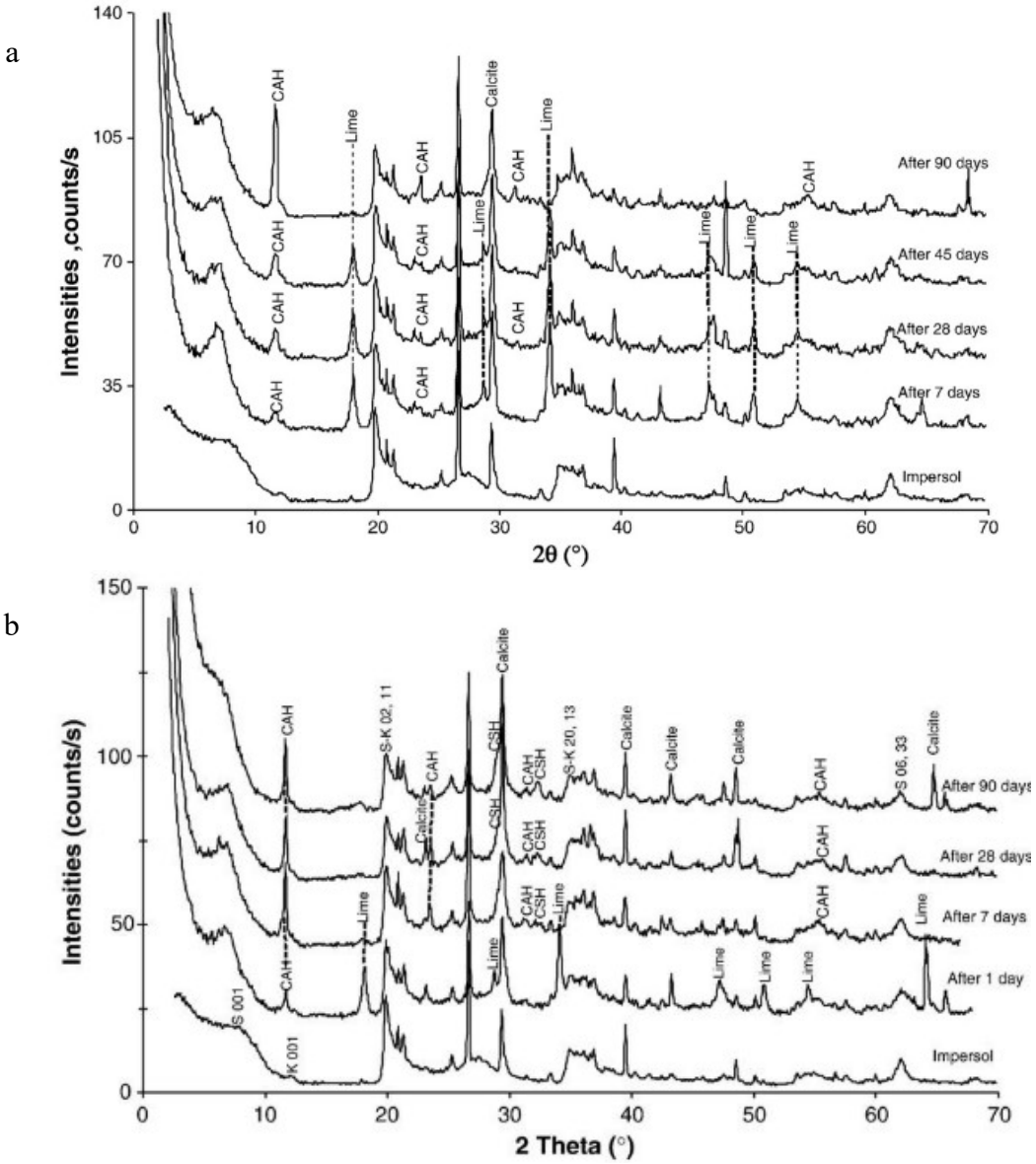

Figure 1.9. XRD diffractograms of impersol treated with 20 % lime cured at (a) 20 °C and (b) 50 °C, adapted from (Al-Mukhtar et al. 2010a, 2010b)

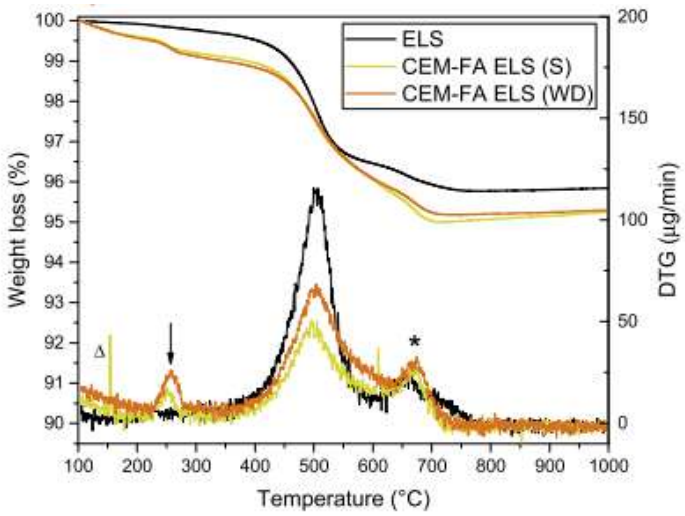

Figure 1.10. TGA-DTG of samples cured in standard conditions (S) showing the dehydration of CSH (Δ), CAH (➔), and decomposition of carbonates (*): ELS= Engineered Local Soil, CEM: Cement, FA= Fly Ash, CCR= Calcium Carbide Residue (Arrigoni, Pelosato et al. 2017)

Additionally, the scanning electron microscopy (SEM) was used to analyze the microstructural changes induced by the stabilization of earthen materials. Di Sante et al. (2014) studied the time of reaction in a lime treated clayey soil cured at 20-25 °C and the influence of curing conditions on its microstructure and behavior. Firstly, the untreated clayey soil showed the usual laminated morphology of clay minerals (Figure 1.11a), whereas the treated soil revealed flock-like structure after 24 hours of curing (Figure 1.11b). The formation of these flocks corresponds to the modification/flocculation in the steps of soil treatment (§1.3.3).

After 7 days of curing in saturated conditions, the microstructure of treated soil showed very fully developed uniformly distributed features (Figure 1.11c). In these micrographs, two important microstructures were identifiable, the coat-like gel around the soil particles transformed into aggregates of spongy appearance and the needle-like crystals, both related to silicate hydrates. The development of needles (10 µm) starts to form crumbs of aggregates and act as bridges connecting pores (Di Sante et al. 2014). These new products were confirmed through EDS on the needle features, revealing mainly calcium, silicon and alumina.

The needle-like morphology was related to CSAH and CSH phases (Chindaprasirt & Pimraksa 2008) and the floc-like morphology to CSH ($Ca_{1.5}SiO3.5.xH_2O$) after confirmation with XRD peaks at 3.04, 2.79, 1.82 Å (Yu et al. 1999). The curing of lime treated soil in saturated conditions or at least in humid conditions is necessary to form fully developed (crystalline) reaction products. The development of the microstructure was related to the consumption of lime, which resulted in the increase of the compressive strength of the composite (§1.3.3 and §1.6.2).

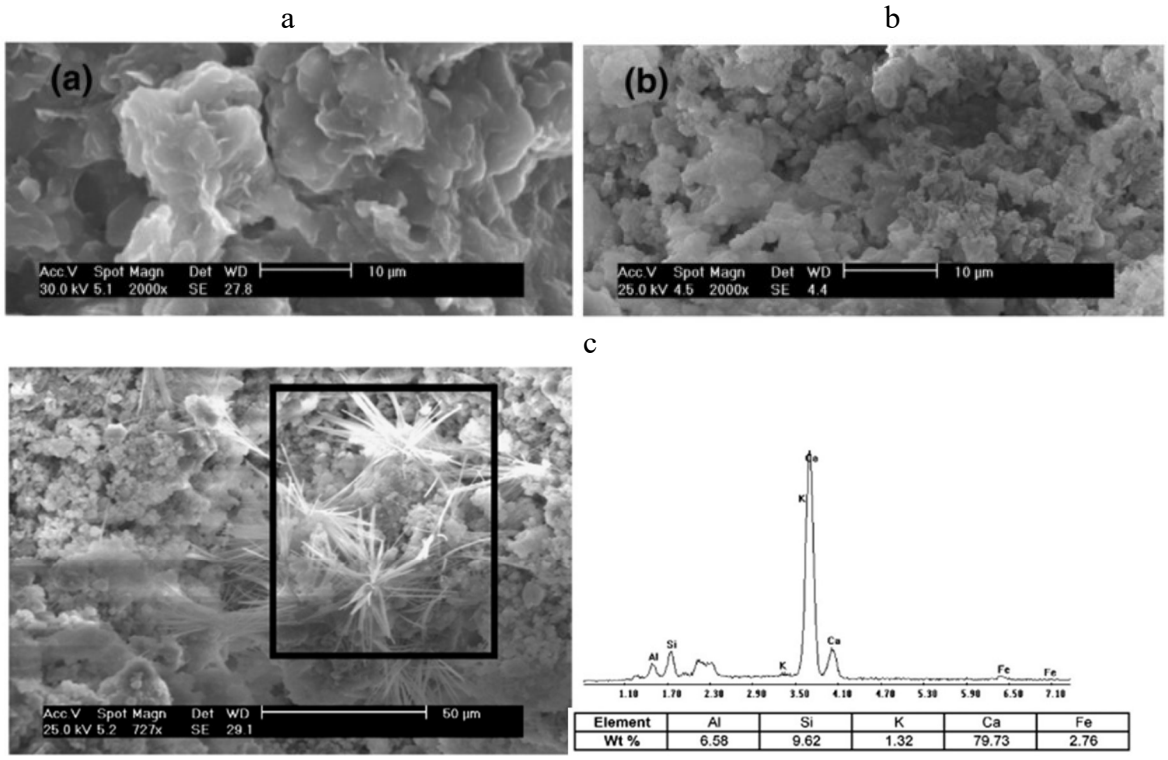

Figure 1.11. SEM micrographs of compacted (a) untreated soil, (b) lime treated soil after 24 h, (c) samples cured for 7 days in saturated conditions, adapted from (Di Sante et al. 2014)

1.6. Physical and mechanical properties of CEBs

1.6.1. Bulk density and porosity

The bulk density of CEBs is affected by the composition of the earthen material and type and content of stabilizer and/or fiber, as well as the rate of compaction. The bulk density of cement stabilized CEBs evolves in the range of 1500-2200 kg/m^3, with the porosity in the range of 42-22 %, produced with very low to high compaction pressure of 1-10 MPa (Zhang et al. 2018, Zhang et al. 2017, Mansour et al. 2016, Danso et al. 2015a, Kerali 2001).

More specifically, the bulk density (porosity) evolved in the range of 1600-2200 kg/m^3 (42-22 %) for unstabilized CEBs produced at compaction pressure of 0.4-3 MPa (Mansour et al. 2016). The bulk density of CEBs stabilized with 5-20 % geopolymer evolved in the range 1730-1840 kg/m^3, with the water accessible porosity evolving in the range of 33-38 % (Sore et al. 2018). Figure 1.12a presents the evolution of the bulk density with the compaction pressure. It shows that the bulk density of unstabilized CEBs can barely reach 2300 kg/m^3, even after hypercompaction (Bruno et al. 2015). This can be related to the compressibility and water demand of the material among other parameters.

The stabilization with cement (3-11 %), at compaction pressure of 6 MPa, increased the bulk density in the range of 2075-2125 kg/m^3, while lime-rich stabilizer would tend to decrease the bulk density (Zhu et al. 2019, Kerali 2001). By contrast, the addition of CCR with FA was reported to increase the bulk density of silty clay, compared to the addition of CCR alone, but still lower than that of compacted clay alone. This was related to the specific density of both the CCR (2.32) and FA (2.39) which is lower than that of clay (2.76) and the decrease of the OMC with the addition of FA. It was also related to the ability of spherical FA particles to slide clay and CCR particles into densely packed structure (Horpibulsuk et al. 2013).

On the contrary, the incorporation of fibers has an opposite effect. The bulk density of CEBs compacted with a pressure of 10 MPa, incorporated with 0 to 1 % of bagasse, coconut and oil palm fibers respectively evolved from 1950 kg/m^3 to 1810, 1800, and 1820 kg/m^3 (Danso et al. 2015a). This is basically related to the increase of the bulk porosity in the CEBs from the incorporation of fibers (Danso et al. 2015a). Figure 1.12b shows that the bulk density of CEBs decreases quasi-linearly with fibers content, depending of the type of earthen material and fiber.

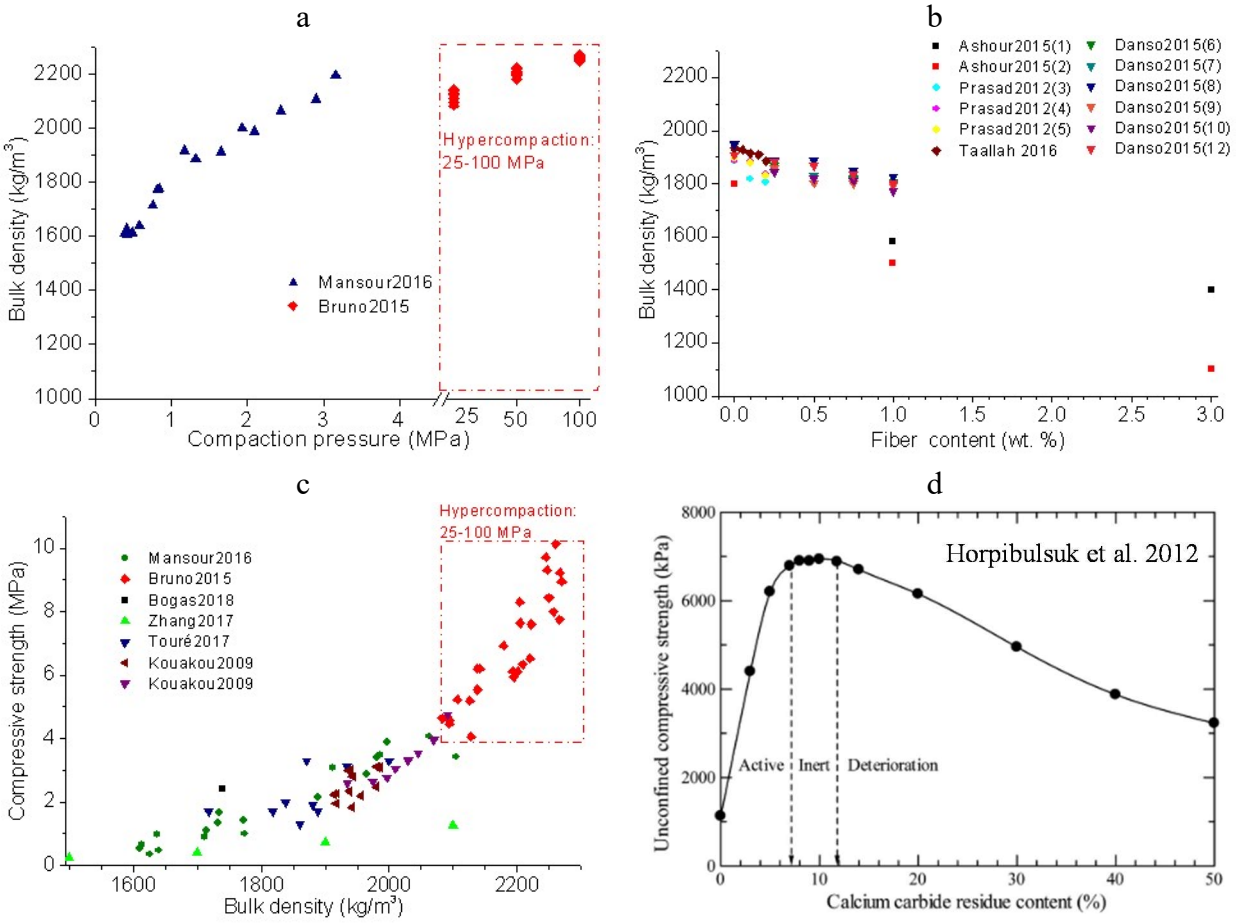

Figure 1.12. Evolution of the bulk density of CEBs with (a) compaction pressure, (b) fibers content, (c) evolution of the compressive strength with bulk density of CEBs, and (d) improvement zones of the compressive strength in CCR-stabilized clay, cured for 28 days

1.6.2. Compressive strength

The improvement of the compressive strength is one of the most sought out property throughout the stabilization of CEBs. This improvement can be divided into time independent physico-mechanical component resulting from the effect of compaction, packing and the time dependent chemico-mineral component from the binding in the earthen material and/or chemical binders (Kampala et al. 2013). The compaction and packing effects depend on the production conditions (packing density of the mixture, compaction pressure, and type and content of the earthen material and stabilizer, and production moisture). The binding effects rather depends on the type and content of materials (clay material and stabilizer) and curing conditions (curing age, temperature, etc) (Mansour et al. 2016, Horpibulsuk et al. 2013, Kampala et al. 2013, Al-Mukhtar et al. 2010a, 2010b).

Figure 1.12c shows that the dry compressive strength of unstabilized CEBs increases quasi-exponentially with respect to the bulk density in the range of 1500-2300 kg/m^3. The compressive strength increased in the range of 0.5 to 4 MPa (0.5 to 1.25 MPa in some instance) for the bulk density in the range of 1500-2100 kg/m^3, and 4-10 MPa for the bulk density of 2100-2300 kg/m^3 from the hypercompaction. However, the hypercompaction would require high end equipment and energy to reach such compaction pressure and does not fully assure the stability of CEBs in liquid water (Bruno et al. 2017). Therefore, there is still need for chemical stabilization.

Figure 1.12d therefore shows the three zones of improvement of the unconfined compressive strength of soil stabilized with CCR (0-50 %). The active zone is represented by significant increase of the strength (up to 7 MPa with 7 % CCR), the inert zone by quasi-constant strength and the deterioration zone by quick decreased of the strength (down to 6 MPa with 20 % CCR) due to the presence of excess unreacted CCR (Horpibulsuk et al. 2012). It should be noted that the extent of these improvement zones can vary depending on the characteristic of materials, such as the plasticity, PSD, mineralogy and type of stabilizer, among other parameters.

Table 1.5. Structural categories of CEBs: physico-mechanical, hygrometric and durability properties of facing CEBs (CEB F) for applications in wall masonry, according to standards ARS 671:1996, ARS 675:1996 (CDI&CRATerre 1998) and XP P13-901 (2001)

Designation	Constraint category*		Compressive strength, Rc **		Water absorption ***		Abrasion ****	
	Environmental	Mechanical	Dry Rc (MPa)	Wet Rc (MPa)	Capillary (%) [a] [Coefficient (g/cm².s$^{1/2}$)] [b]	Total (%) [c]	Loss of mater (%)	Coefficient (cm²/g)
CEB F 1D	Dry	1	≥2	NA	NA		≤10	≥2
CEB F 2D	environment	2	≥4	NA	NA		≤5	≥5
CEB F 3D	(D)	3	≥6	NA	NA		≤2	≥7
CEB F 1R	Effect of water	1	≥2	≥1	NA		≤10	≥2
CEB F 2R	by lateral	2	≥4	≥2	NA	15-25	≤5	≥5
CEB F 3R	spraying (R)	3	≥6	≥3	NA		≤2	≥7
CEB F 1C	Effect of water	1	≥2	≥1	≤15 [40]		≤10	≥2
CEB F 2C	by vertical	2	≥4	≥2	≤10 [20]	15-25	≤5	≥5
CEB F 3C	penetration (C)	3	≥6	≥3	≤5		≤2	≥7

NA: Not applicable

* The use of CEBs in R and C category environments requires using a stabilizer if the protection provided is not guaranteed. If the protection provided against water damage is guaranteed, the environmental can be regarded as category D.

** The values given are average values obtained from tests carried out on a set of samples, according to [a](CDI&CRATerre 1998).

*** If tests to establish water absorption or abrasion are not feasible, or if the results are not available, this deficiency can be compensated by increasing the required dry and/or wet compressive strength by one category.

*** [a] Water absorption at saturation by capillary immersion, according to [a](CDI&CRATerre 1998).

*** [b] [Coefficient of capillary absorption ≤ 20 g/cm².s$^{1/2}$ for very low capillary CEBs and ≤ 40 g/cm².s$^{1/2}$ for low capillary CEBs, according to [b]XP P13-901 (2001)].

*** [c] Total water absorption by total immersion: 15-25 % in [c](Bogas et al. 2018, Masuka et al. 2018, Guettala et al. 2006, Kerali 2000).

****[b] Loss of mater after abrasion, coefficient of abrasion of CEBs subjected to the risk of abrasion due to the human activity according to [b]XP P13-901 (2001).

Additionally, the wet (soaked) compressive strength of CEBs is usually tested after 2 hours of immersion in water, referring to standard XP P13-901 (2001). It is usually required to record half the value of the compressive strength tested in dry conditions, referring to the same standard (XP P13-901 2001). The dry compressive strength of CEBs for construction of wall masonry should reach 2, 4 and 6 MPa respectively for usage in non-load-bearing (single storey) and load-bearing (two-storey and three-storey) buildings in dry state, according to standards XP P13-901 (2001) and ARS 675:1996 (CDI&CRATerre 1998). Table 1.5 further summarizes the requirements for CEBs for applications in facing masonry, depending on the mechanical and environmental constraints. Among other requirements, they include water absorption, the resistance to abrasion, and are briefly discussed in the following sections.

1.7. Hygroscopic and thermophysical properties of CEBs

1.7.1. Water vapor sorption

There are still limited number of studies on the behavior of earth blocks, particularly CEBs, in interaction with water vapor. This can be assessed through the test of vapor sorption/desorption which is carried out following the mass change of material when exposed to increasing/decreasing relative humidity (RH) at constant temperature, referring to EN ISO 12571 (CEN 2000). The literature reported that stabilized CEBs can absorb between 2 to 8 % of moisture after equilibrium on exposure to the RH up to 95 % (Kabre et al. 2019, Zhang et al. 2018, El Fgaier et al. 2016, McGregor et al. 2014, Cagnon et al. 2014).

Figure 1.13 shows that the sorption capacity of stabilized CEBs slightly decreases with cement and lime and increases with geopolymer stabilization, with respect to unstabilized CEBs. Furthermore, earth that contains plant fibers such as barley straw have been shown to absorb more (6.5 %) than the earth alone (1.7 %) (Laborel-Préneron et al. 2016). The sorption depends on the type of earthen maternal and stabilizer, among others (Zhang et al. 2018, El Fgaier et al. 2016). Earthen material containing high content of active clay minerals such as smectite (montmorillonite) would absorb more moisture than less active minerals (kaolinite) (§1.2).

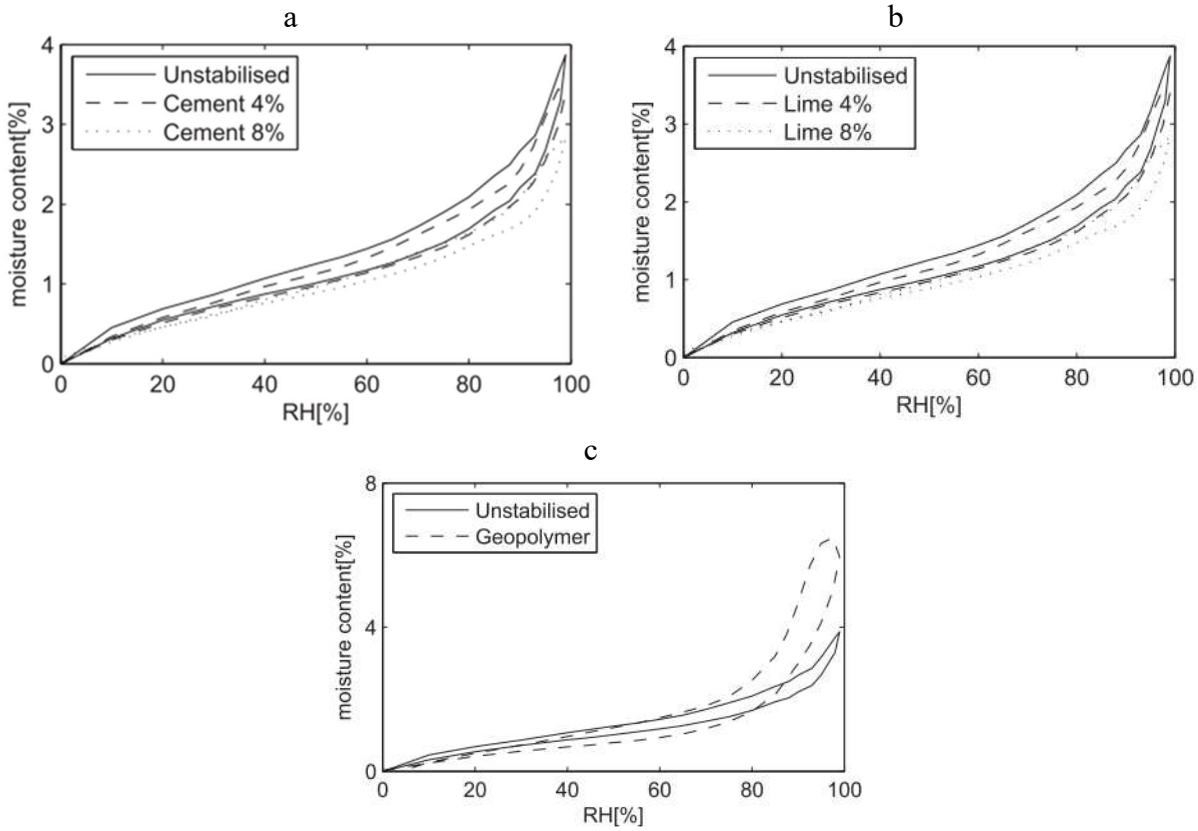

Figure 1.13. Evolution of sorption-desorption of CEBs stabilized with (a) cement, (b) lime, (c) geopolymer (McGregor et al. 2014)

1.7.2. Liquid water absorption and water accessible porosity

The improvement of water absorption of CEBs, another most sought out property, is assessed based on the absorption capacity through capillary and/or total immersion. It was observed to depend on the type and content of clay and stabilizer, the age and bulk density of the specimens. The water absorption increases with lime and decreasing with cement and pozzolan in substitution of lime (microsilica), while the water accessible porosity reversely decrease with increasing the bulk density, similarly to the total porosity (Guettala et al. 2006, Kerali 2001).

The capillary water absorption (CWA) of CEBs, tested referring to the standard XP P13-901 (2001), assesses the action of surface tension on the capillaries that allows the transport of liquid water in porous solids. The CWA of CEBs is basically expressed as the coefficient of capillary absorption (Cb_{10min}) equivalent to the percentage rate of absorption in 10 min. The Cb_{10min} should record value lesser than 20 and 40 g/cm².min$^{1/2}$ respectively for the CEB to be classified as very low and low capillary (XP P13-901 2001).

The CWA can additionally be expressed as the percentage ratio of the mass of water absorbed after saturation by capillary immersion, with respect to the mass of dry sample. The Uniform

Building Code in (Guettala et al. 2006), specified that the CWA should be less than 2.5 %, while the ARS 674:1996 & ARS 675:1669 (CDI&CRATerre 1998) prescribed values less than 5-15 % depending on the structural category of CEBs (Table 1.5).

The total water absorption (TWA) assesses the percentage ratio of the mass of water absorbed after saturation by total immersion with respect to the mass of dry sample, according to XP P13-901 (2001). It was suggested to be less than 15 % according to (Guettala et al. 2006) and 20 % according to NBR 1986 standard in (Bogas et al. 2018). Table 1.5 summarizes the absorption capacity of CEBs considered acceptable depending on the test standards and structural category.

Remarkable decrease of the TWA were recorded on cement:lime (4:4 %) stabilized CEBs from 15 to 7 % after 6 months of curing (Nagaraj et al. 2014). Bogas et al. (2018) recorded the values of TWA of 13 and 17 % respectively for CEBs stabilized with 8 % cement and cement:lime produced using 9-10 % of moisture, which the authors considered suitable for use in wet environment. Guettala et al. (2006) reported the TWA in the range of 8-7 % and 10-9 % respectively for CEBs stabilized with for 5-8 % cement and 8-12 % lime and compacted with a pressure of 15 MPa. By contrast, Sore (2017) reported the TWA increasing in the range of 15-18 % for CEBs stabilized with 10-20 % geopolymer, compared to 13 % for CEBs stabilized with 8 % cement.

The water absorption of unstabilized soil blocks incorporated with 0-1 % fibers increased in the range of 8-17 % (Danso et al. 2015a). The TWA of CEBs stabilized with 8 % cement and 0-0.2 % fibers also increased in the range 9-10.5 % (Taallah et al. 2014). Therefore, the parameters of absorption cannot only be related to the characteristics of the raw materials (type and content of clay and stabilizers), but also the conditions of production and curing of stabilized CEBs (water demand for production, compaction pressure, temperature and time). The lower water absorption generally corresponds to the greater durability[5] (Hwang & Huynh 2015). The durability indicators are further elaborated in section 1.8.

[5] The durability *is the ability to last a long time without significant deterioration*. Durable concrete *resists weathering action, chemical attack, and abrasion while maintaining its desired engineering properties*. (https://www.cement.org/learn/concrete-technology/durability; retrieved July 17, 2020).
Durable material would maintain the engineering performances in deteriorating conditions.

1.7.3. Thermophysical properties: influence of water content and other parameters

The thermal properties (conductivity, effusivity, diffusivity and specific capacity) of CEBs, determined using hot plate or hot wire methods either in steady or transient mode, are also affected by the stabilization (Fabbri et al. 2018, Asadi et al. 2018, Mansour et al. 2016, Cagnon et al. 2014, Félix 2011). The thermal conductivity, being the most studied thermal property of building materials, and particularly CEBs, is generally considered to increase with cement stabilization. By contrast, the addition of fibers have an opposite effect (Bogas et al. 2018, Tiskatine et al. 2018, Saidi et al. 2018, Taallah 2014). Besides, the thermal conductivity tends to increase with increasing bulk density of CEBs, regardless the type or content of stabilizers (Bogas et al. 2018, Mansour et al. 2016, Laborel-Préneron et al. 2016, Cagnon et al. 2014).

Bogas et al. (2018) reported the values of the thermal conductivity of 0.58 and 0.64 W/m.K respectively for unstabilized CEBs and stabilized CEBs (4:4 % lime:cement or 8 % cement). Additionally, Mansour et al. (2016) reported the values in the range of 0.6-1.5 W/m.K, which linearly correlated with the bulk density in the range of 1600-2200 kg/m^3 for unstabilized CEBs. Figure 1.14a presents the evolution of the thermal conductivity (0.5-1.6 W/m.K) reported for CEBs of bulk density in the range of 1400-2200 kg/m^3, compared to the trend for concrete. Although, CEBs do not show a particular trend of the thermal conductivity (Fabbri et al. 2018), they reach lower values than the concrete in the similar range of bulk density. The lack of particular trend of the thermal conductivity can be related to the difference in the behavior of different earthen materials, and methods of production and testing of CEBs.

Figure 1.14b shows that the thermal conductivity of unstabilized (0 % stabilized) CEBs produced from different materials ranges in 0.5-1 W/m.K. It additionally shows that the thermal conductivity of CEBs ranges in 0.5-1.2 W/m.K with respect to chemical stabilizer (cement, lime, or geopolymer) in the content of 0-20 %. This is comparatively lower than 0.5-1.6 W/m.K with respect to the bulk density of CEBs in the ranges of 1400-2200 kg/m^3 (Figure 1.14a). It basically suggests that the thermal conductivity of stabilized CEBs is not only influenced by the stabilizer (type or content), but also the characteristics of earthen material itself, the compaction energy, and the measurement methods, among others.

In fact, it was reported that the thermal conductivity is less influenced by the composition of CEBs and lacks obvious trend (increase or decrease) with small addition (≤10 %) of cement (Bogas et al. 2018, Zhang et al. 2017). The thermal conductivity ranges around 0.15-1.8 W/m.K for clay, 0.3 W/m.K for Portland cement, 0.4-0.7 W/m.K for cement paste (1900-2100 kg/m^3),

and 0.4-1.5 W/m.K for cement concrete (1200-2100 kg/m^3) (ETB 2019, Asadi et al. 2018, Xu & Chung 2000). Therefore, this suggests that cement may not be the main factor affecting the thermal conductivity of stabilized CEBs. It can be mentioned that the thermal properties of CEBs are possibly influenced by the stabilization through the evolution of the resulting bulk density: the denser is the stabilized CEBs, the higher would be the thermal conductivity (§1.6.1).

Furthermore, the thermal effusivity, diffusivity and capacity similarly seem to be related to the bulk density of CEBs. For the unstabilized CEBs of bulk density in the range of 1600 to 2200 kg/m^3, the thermal effusivity and diffusivity, measured using hot wire method, respectively increased in the ranges of 650 to 1300 J/m².K.s$^{1/2}$ and 7E-7 to 15E-7 m²/s, while their thermal capacity remained quasi-constant around 520 J/kg.K (Mansour et al. 2016). The thermal capacity, measured using desprotherm (hot plate), evolved in the range of 950 to 1020 J/kg.K for extruded earth bricks with bulk density in the range of 1900 to 2100 kg/m^3 (Cagnon et al. 2014).

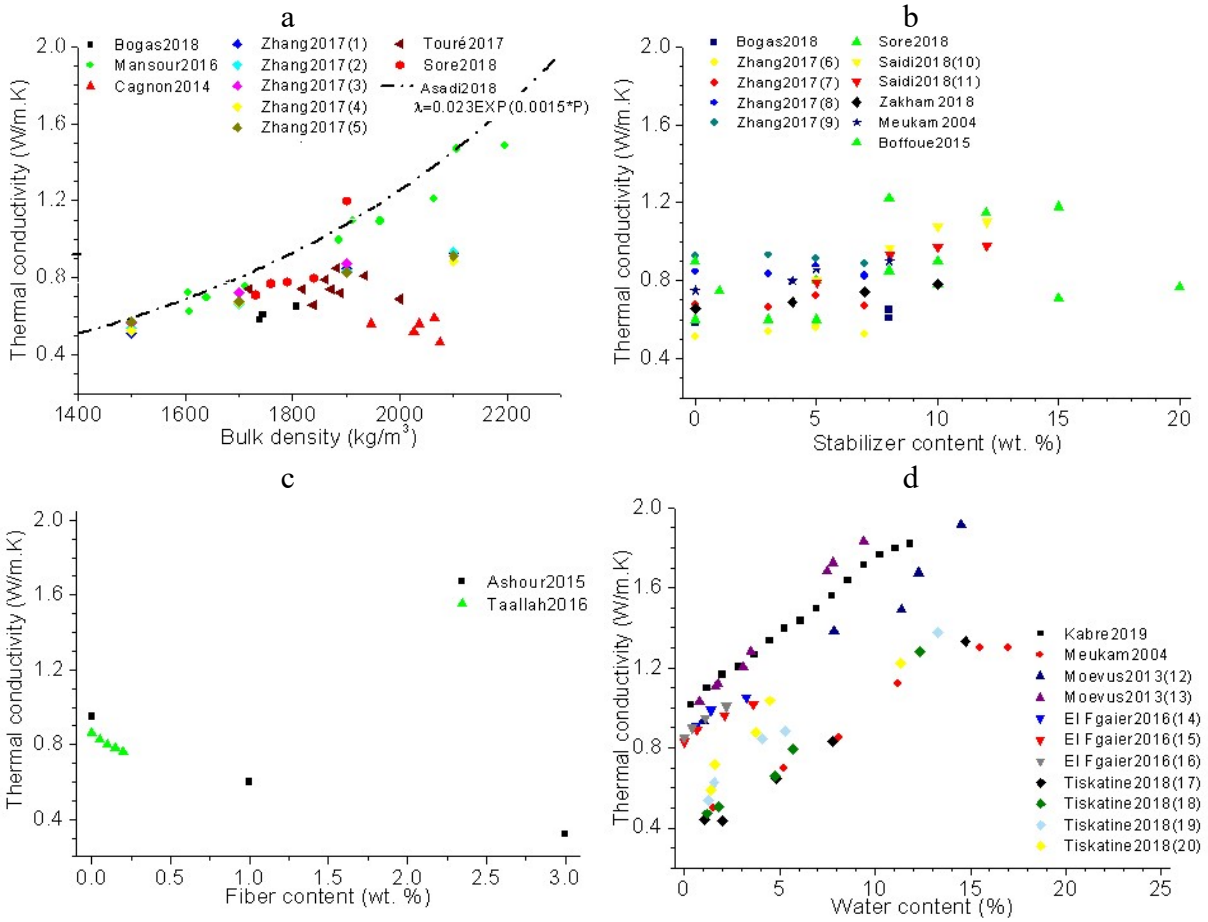

Figure 1.14. Thermal conductivity, λ, of CEBs: effects of (a) bulk density, ρ, compared to concrete (exponential law), (b) binder content, (c) fiber content, and (d) water content

Sore et al. (2018) reported the values of thermal effusivity, diffusivity and capacity respectively in the ranges of 1070 to 1200 J/m².K.s$^{1/2}$, 3.2E-7 to 4.6E-7 m²/s and 920 to 1040 J/kg.K for CEBs stabilized with 0 to 20 % geopolymer and bulk density of 1700 to 1850 kg/m^3. These properties were respectively 1598 J/m².K.s$^{1/2}$, 5.8E-7 m²/s and 1107 J/kg.K for CEBs produced from the same earthen material and stabilized with 8 % cement of bulk density of 1900 kg/m^3 (Sore et al. 2018). More specifically, CEBs have values of thermal diffusivity lower than 12E10-7 m²/s for concrete, thus better thermal inertia (Laborel-Préneron et al. 2016). This points out the possibility of engineering CEBs during production to control the thermal properties.

The incorporation of natural fibers and granulates in CEBs drastically decreases the thermal conductivity (Figure 1.14c), following the decrease of bulk density (Figure 1.12a). Although, only limited data were reported on the effect of fibers on the thermal properties of CEBs, the thermal conductivity of earth-based materials incorporated with fibers can decrease by 30 % (eventually 70 %) depending on the content, type and size of fibers (Toguyeni et al. 2018, Ashour et al. 2015, Taallah 2014). Specifically, the incorporation of 0 to 1.4 % fibers (H. Sabdariffa) in CEBs stabilized with lime (7 %) decreased the thermal conductivity from 1 to 0.8 W/m.K (Toguyeni et al. 2018).

The decrease of the thermal conductivity of earthen materials incorporating fibers or granulates can be essentially explained by the increase of porosity (air) and/or lower values of the thermal conductivity of fibers than earthen materials. In fact, the thermal conductivity of air (0.02 W/m.K) and fibers/granulates (0.03-0.06 W/m.K) are respectively 50 and 10 times lower than that of earth blocks (0.4-1.5 W/m) (ETB 2019, Tiskatine et al. 2018, Guettala et al. 2016, Ashour et al. 2015). Moreover, the thermal conductivity of CEBs was reported to evolve in the range of 1.5-0.5 W/m.K for porosity in the range of 15-40 % (Zhang et al. 2017, Mansour et al. 2016).

A limited number of studies reported the effect of water content on the thermal property of CEBs. Bogas et al. (2018) reported that the thermal conductivity (1.5 W/m.K) of CEB in saturated conditions (14-17 % water content) is more than 2 times higher than in dry conditions (0.6 W/m.K). Tiskatine et al. (2018) observed that the thermal conductivity reached about 75 % increase for the average water content of 1 to 13 %. Figure 1.14d presents the evolution of the thermal conductivity of earth blocks with respect to water content. It shows a linear trend, $\lambda=axwc+b$, with the coefficient, a, varying around 0.06 W/m.K.%. This can allow to estimate

the thermal conductivity, λ (W/m.K), in function of the water content, wc (%), and thermal conductivity of dry sample, b (W/m.K).

The increase of the thermal conductivity with water content was related to creation of conduction bridges by replacing the air porosity by liquid water, whose thermal conductivity (λ=0.6 W/m.K) is 30 times higher than that of air (λ=0.02 W/m.K). This facilitates the conduction through solid-solid and solid-liquid interfaces, as well as through the movement (diffusion) of liquid water (Tiskatine et al. 2018, Laborel-Préneron et al. 2016, Raheem et al. 2010). Additionally, the thermal conductivity of materials containing lower content of fine/clay particles seems to be more sensitive to the humidity. This was related to the possible occurrence of free, non-adsorbed, water which creates consistent hydric bridge (Moevus et al. 2013). Furthermore, the thermal effusivity and diffusivity were also affected by the water content in the sample, also showing a quasi-linear increase with water content in the range of 0-10 % (Kabre et al. 2019, Meukam 2004).

1.8. Durability and weatherability of CEBs

The durability of earthen materials is illustrated by the longevity of earth based-structures, which can last for hundreds or even thousands of years (Fabbri et al. 2018, Pacheco-Torgal & Jalali 2012). The durability of earthen materials and structures is generally regarded to be controlled by the actions of water which can be driven by various force such as capillary suction, wind pressure and differential vapor pressure. Moreover, ice, wind, fire, solar radiation and chemical agents are among other actions that impart the degradation and deterioration in service of earthen material depending on the environment of applications, thus affecting their durability (Beckett et al. 2020, Fabbri et al. 2018, Morel et al. 2012). In addition, the materials and processing technology and the resulting engineering properties, as well as the appropriateness and care given to the structure are considered as other relavant factors affecting the durability of earthen masonry (Kinuthia 2015). This section review some of the common tests for assessing the durability indicators of earthen materials, particularly CEBs.

Heathcote (2002) reviewed and classified number of durability tests of earthen wall units into indirect and direct tests. Indirect tests assess the parameters such as the compressive strength which has little or no relation with the degradation mechanism, but considered as reliable predictors of the in-service performances based on past experiences. Accelerated tests tentatively model and assess the degradation mechanisms with increased factors of degradation in order to compensate for the reduced testing time. Simulation tests attempt to exactly model

the in-service conditions (Heathcote 2002). The following subsections briefly review the most common indicators and testing approaches of the durability of CEBs.

1.8.1. Resistance to water erodability

The resistance to water erodability of CEBs simulates the action of wind driven rain (Elenga et al. 2011). The erodability of earthen materials is simulated by measuring the depth of erosion after exposure to a jet of water, based on two main tests: drip or spray test, which allow to determine the erodability index and classify the CEB.

In the drip test (Figure 1.15a), mainly applied on less strong materials such as adobe, the surface of the sample is inclined by 27 ° and exposed to series of water drops (total volume of 100 ml) from a height of 400 mm. After the test, the pitting depth should not exceed 15 mm for the sample to pass the erodability test (Table 1.6). The drawbacks of this test are related to the high risk of testing the weak spot, given that it is a localized test, and the inability to test stronger materials. Moreover, the pitting depth from this test was criticized to be more related to the runoff rather than water drop (Heathcote 2002).

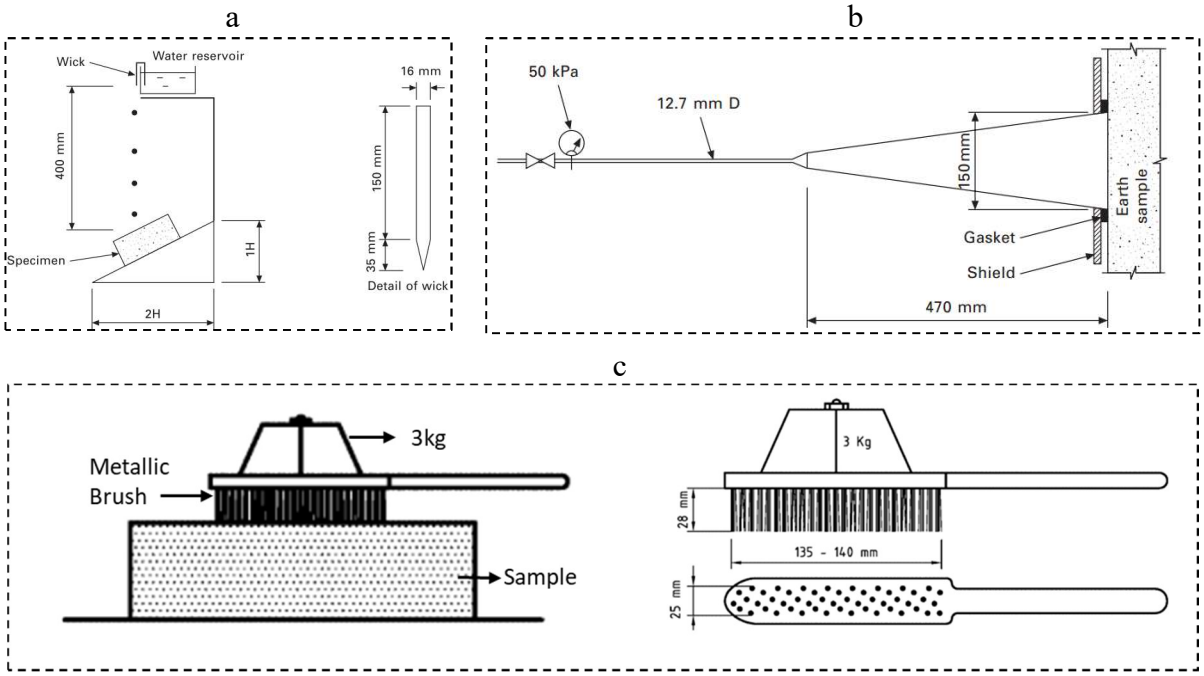

Figure 1.15. Schematic setup of durability tests: (a) drip erodability, (b) spray erodability, (c) CRATerre's setup for abrasion test, adapted from (Morel et al. 2012, XP P13-901 2001)

Table 1.6. Erodability category with respect to the depth and rate of erosion respectively from the drip and spray test, adapted from (NZS 1998) *in (Bogas et al. 2018)*

Drip test: Depth of erosion (DE in mm)	Spray test: Erosion rate (DE/hour in mm/hour)	Erodability index	Erosion category
-	0≤DE<20	1	Non erodable
0≤DE<5	20≤DE<50	2	Slightly erodable
5≤DE<10	50≤DE<90	3	Erodable
10≤DE<15	90≤DE<120	4	Very erodable
15<DE	120<DE	5	Reject

The spray test (Figure 1.15b), mainly applied on stronger materials such as stabilized CEBs, is carried out based on the Bulletin 5 spray test of the New Zealand Code of Practice on earth wall buildings (NZS 1998) or its modified versions. In its original version, the surface of the sample (diameter of 150 mm) is exposed to a continuous and horizontal jet of water at a pressure of 50 kPa, from a distance of 470 mm, for a period of 60 minutes. After the test, the depth of erosion (DE per hour in mm/hour) is measured and should be lesser than 120 mm/h for the sample to pass the test (Table 1.6). Table 1.6 presents the erodability categories, allowing to classify the material as 1: non erodable, 2: slightly erodable, 3: erodable, 4: very erodable.

The spray test seems more appropriate than drip test for simulating the action of rain on stabilized CEBs given that it allows to relatively test the surface, by homogeneously distributing the water fall, thus reducing the risk to test the "weak spot". It can also allow to simulate various rain intensities through the adjustment of erosion pressure and time (Heathcote 2002). In fact, various studies attempted to assess the erodability of CEBs at erosion pressure in the range of 50-4130 kPa (Bogas et al. 2018, Cid-Falceto et al. 2012, Obonyo et al. 2010). Therefore, the erodability test can allow to estimate the life span of construction made of earthen material based on the rate of erosion and rain fall in the region.

1.8.2. Resistance to abrasion

The resistance to abrasion of earthen material allows to assess the hardness of the materials to resist the field abrasion from the weathering conditions in arid region or human activities (Izemmouren et al. 2015). The abrasion test, referred to as "CRATerre abrasion test" is carried out using metallic wire brush loaded with 3 kg (Figure 1.15c). The resistance to abrasion is evaluated based the coefficient of abrasion, Ca (cm^2/g), consisting of the ratio between the brushed surface and weight loss after 60 cycles of abrasion.

Figure 1.16a shows the coefficient of abrasion in the range of 5-25 cm²/g for steam cured CEBs stabilized with lime (6-8 %) partially substituted with natural pozzolan (0-40 %) (Izemmouren et al. 2015). This shows that the stabilization with lime and pozzolan can potentially improve the durability of the CEBs. The coefficient of abrasion should attain values of 2, 5 or 7 cm²/g for classification of CEBs in the first, second or third categories, respectively (Table 1.5).

1.8.3. Resistance to wetting-drying cycles

The wetting-drying (WD) test, also referred to as "ASTM D559-03 (ASTM 1989b) wire brush test", was developed to determine the minimum amount of cement for achieving the adequate degree of hardness of cement-soil for pavement to resist field weathering (Heathcote 2002, Morel et al. 2012). It consists of exposing the sample to a series of wetting (5-6 hours in tap water at 20 °C) and drying (42 hours in oven at 70 °C) and applying two firm strokes using wire brush (1.3-1.5 kg) on its surface to remove the loosen materials. The W-D cycles are repeated 12 times to calculate the percentage of mass loss (Morel et al. 2012, Heathcote 2002).

The maximum limit of mass loss to achieve acceptable performance was respectively proposed to be 7 % and 14 % for clayey soil and sandy soil for road pavement (Heathcote 2002). Furthermore, the limits for mass loss for cement stabilized CEBs in permanent buildings was recommended to be less than 5 % and 10 % respectively for the regions with annual rain fall less than 500 mm and more than 500 mm (Morel et al. 2012). The mass loss ranged in 6-1% for steam cured CEBs stabilized with lime (6-10 %) partially substituted with natural pozzolana (0-40 %) (Figure 1.16b). This shows that pozzolan improve the resistance to W-D cycles and was considered satisfactory for CEBs for construction in Biskra region (Algeria), where the annual rain fall exceeds 500 mm (Izemmouren et al. 2015).

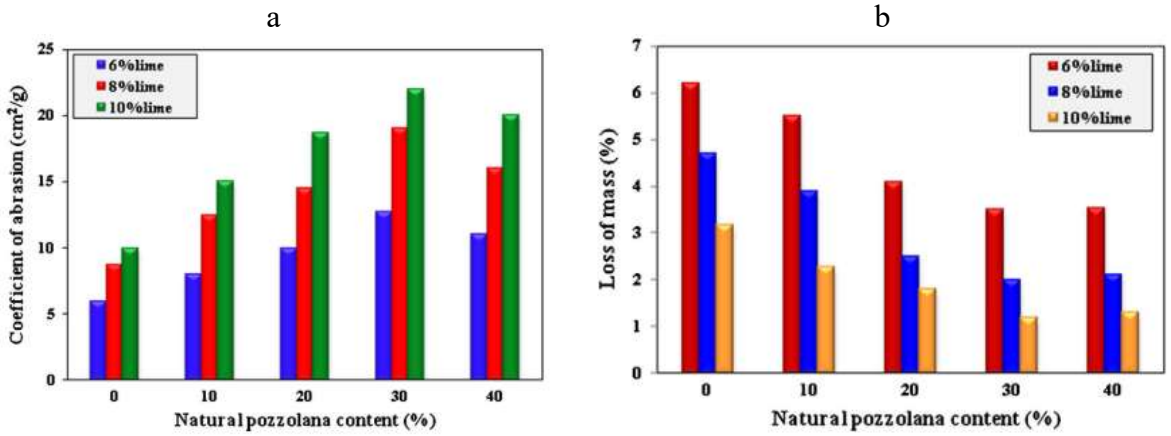

Figure 1.16. (a) Coefficient of abrasion and (b) loss of mass after 12 cycles of wetting-drying of CEBs stabilized with lime and natural pozzolana (Izemmouren et al. 2015)

Furthermore, Arrigoni, Pelosato et al. (2017) showed that the compressive strength of earthen materials stabilized with CEM and FA improves by a factor of only 0.35 after W-D curing compared to the CEBs cured in standard condition of humidity (>95 %). The compressive strength of materials stabilized with CCR and FA improved by 1.6. This was related to better consumption of calcium hydroxide through the pozzolanic reaction with FA after W-D cycles. In addition, Hakimi et al. (1998) showed that the compressive strength of CEBs stabilized with 4 % cement decreased by factor of 0.3 after only 6 cycles of W-D, with respect to the initial strength. This reveals that stabilization of CEBs with CCR (lime-rich stabilizer) may be beneficial than cement on the performances after W-D cycles.

1.8.4. Other indicators of the durability

The stability in static water and water absorption by capillary or total immersion are direct and immediate indicators of durability of earthen materials. According to Minke (2006), the materials suitable for earthen construction should not disintegrated (5 cm depth of pit) before 45 minutes when they are in contact with static water. Additionally, the percentage amount of water absorbed by the samples is directly related to its durability. As indicated in section 1.7.2, earthen materials should absorbed lesser than 5-15 % and 15-20 % respectively after 24 hours of capillary and total immersion.

Water strength coefficient (WSC), expressed as the ratio between the saturated (wet) to the dry compressive strength is also considered as an indicator of the durability of CEBs and masonry walls. The WSC should reach 0.5 for the earthen material of acceptable performances (Bogas et al. 2018, Izemmouren et al. 2015, Morel et al. 2012, Houben & Guillaud 2006). The WSC of commonly stabilized CEBs, produced and cured in normal conditions (compression pressure 1-2 MPa, curing at ambient temperature) ranges in 0.3-0.7, which is still considered acceptable (Bogas et al. 2018, Guettala et al 2006).

1.9. CEBs in Burkina Faso: a brief research interest and applications

In Burkina Faso, only a limited number of studies is found in the literature on earthen materials, particularly CEBs, for building construction. Few studies reported the thermophysical and hygro-mechanical properties, microstructure of CEBs stabilized with common industrial binders, such as cement (Kabre et al. 2019, Ouedraogo et al. 2015) or hydrated lime (Malbila et al. 2020, 2018). Other studies also reported on the incorporation of (natural) fibers in earth blocks (Malbila et al. 2018), sawdust (Boro et al. 2017), and paper/cellulose (Ouedraogo et al. 2015). It is noteworthy that most studies focused mainly on the stabilization of adobes and using classic industrial binders. More recently, a study reported the physico-mechanical and thermal properties of CEBs stabilized with an innovative geopolymer binder (Sore et al. 2018). Some other studies reported on the applications of the hygrothermal performances of earth based walls for improving the thermal comfort and energy performance in buildings (Moussa et al. 2019, Ouédraogo et al. 2018, Compaore et al. 2017, Hema et al. 2017, Zoma et al. 2015, Wyss 2005).

Each of these studies reported on only one type of clay materials and/or using classical industrial binders (cement or lime), and without taking into consideration the variability of local materials. Therefore, this points out the need for more in-deep studies of the suitability of earthen materials, particularly, for the production of CEBs and ways toward improving their performances by stabilization with innovative by-product binders.

1.10. Summary: towards highlighting the current gaps and the research question

This chapter reviewed the literature on the clay materials used in building construction, mainly focusing on their application for the production of stabilized CEBs. The clay materials are mainly constituted with clay minerals such as kaolinite, montmorillonite, illite, and/or their interstratifications, which are usually accompanied with other non-clay minerals such as quartz, goethite and carbonates. The selection of clay materials for applications in building construction has been, and remains, mainly guided by their particle size distribution and plasticity.

However, the contribution of chemical and mineral compositions should not be ignored, mainly for chemical stabilization of earthen materials. It was indeed proven that the common chemical stabilizers, cement and lime, interact and react with the clay materials through hydration and/or pozzolanic reaction. But also, the environmental impacts (out of the scopes of the present study) of the stabilization with cement are questionable.

Therefore, the present study adopted alternative and secondary (by-product) materials such as the calcium carbide residue (CCR: hydrated lime-rich), rice husk ash (RHA: amorphous silica-rich), and eventually (okra) plant fibers were; for their potential for chemical stabilization and eventually reinforcement of clay earthen materials. It was pointed out that lime-rich (CCR) binder is more beneficial for the stabilization/curing of earthen materials in hot regions, like Burkina Faso. It is also advisable to calcine the RH in controlled conditions: below 600 °C, below 3 hours, for the production of amorphous-reactive RHA, with minimum energy consumption. Although, the usage of residual RHA from the combustion of RH for the production of energy would be the ideal scenario, but its quality (reactivity) would be questionable. Additionally, the length of fibers to be used for reinforcement of CEBs can be considered as the gauge length for testing their tensile strength.

The clay earthen materials stabilized with chemical industrial binders (cement or lime) can produce CEBs which have improved performances, through the modification of the microstructure. In fact, the XRD, TG-DTG and SEM analyses of stabilized earthen materials allows to depict the formation of hydrated cementitious products such as C-S-H, C-A-H and C-S-A-H responsible for binding cohesion and improvement of the performances of earthen matrix. The reactive effect, in addition to the compaction effect, affect the bulk density and hydric behaviors, which in turn affect the mechanical resistance (dry and wet conditions), thermophysical properties and durability, among other properties of stabilized CEBs.

However, there is no standard test to assess the reactivity of clay earthen materials for appropriate selection, prior to the chemical stabilization of CEBs. But again, the industrial binders are scrutinized to temper with the natural advantages, moisture exchange and thermal resistance, of earthen materials. Furthermore, cement stabilized earthen materials fails to resist *vis-a-vis* wetting-drying cycles.

It was also shown that the most controlling parameters of the applicability of earthen materials in building construction, such as water absorption, strength, thermal properties and durability, are related to the characteristics of the raw materials (type and content of clay and stabilizers). These parameters are also related to the conditions of production (compaction pressure, curing temperature and time), and conditions of usage (water content).

However, there are only limited data on the influence of production, curing and testing conditions on the engineering properties and durability of earthen materials. This lack particularly occurs on the effect of stabilization with by-products binders, effect of water

content on the thermal properties and durability of CEBs, and more specifically in the Sahelian climatic context of Burkina Faso.

From this review, it turns out that the effect of the type of clay materials should be assessed on the engineering and durability properties of stabilized CEBs in order to better understand their potential as alternative building materials. Moreover, previous studies focused on the stabilization of CEBs using cement or lime, and without taking into consideration the variability of clay materials. Therefore, it is interesting to assess the potentials of different clay and by-product materials for the production of stabilized CEBs. This goes back to justify the research question.

"How to reach the performances required for CEBs using clay earthen materials stabilized with by-products, instead of industrial binders, for load bearing in building wall construction?"

The present study specifically assesses the reactivity of clay materials for the appropriate and suitable production of stabilized CEBs. The study evaluates the contribution of the reactive effect in the mix of clay materials and the CCR alone and featured effects of the CCR and RHA, as well as the contribution of Okra plant fibers towards the development of engineering and durability performances of stabilized CEBs. Moreover, the effect of the conditions of production and curing are assessed by evaluating the effect of production moisture, curing temperature and time on the key properties of stabilized CEBs. The study concludes by proposing the recommendations for the selection of mix designs for efficient structural and thermal applications in building constructions, and particularly in the warm Sahelian climatic context of Burkina Faso.

EXPERIMENTAL STUDIES AND RESULTS

CHAPTER:

II. MATERIALS AND EXPERIMENTAL METHODS

2.0. Identification and processing of raw materials, production and curing of mixtures and characterizations

2.1. Introduction

This chapter presents field and laboratory works carried out and equipment used for sampling, processing/treatment and characterization/testing of the characteristics/properties of raw materials/products. The raw materials were collected from different localities in the vicinity of Ouagadougou, Burkina Faso. The processing and characterization of microstructural, thermophysical and mechanical properties and durability were carried out mainly in the *Laboratoire Eco-Matériaux et Habitats Durables* (LEMHaD) of the Institut 2iE, Burkina Faso, and *Laboratoire Matériaux de Construction-GeMME Matériaux de Construction* (UEE) and *Argile, Geochimie et Environnements sedimentaires* (AGEs) of the Université de Liège, Belgium.

2.2. Identification and processing of raw materials

2.2.1. Calcium carbide residue

The calcium carbide residue (CCR) by-product from the production of acetylene gas through the hydrolysis of calcium carbide. It was collected from local industry (Figure 2.1a), Burkina Industrial Gas (BIG) located in Kossodo, Ouagadougou (N12°25.935', W001°29.374', alt. 301 m). It was ball milled and sieved on 125 µm to obtain fine powder.

BIG generates this by-product (wet CCR) at a rate of 600 l per day of acetylene production. The wet CCR is sun-dried (open air) to form a soft friable by-product of white-greyish color. The currently application of the CCR from BIG is for wall painting by the local population. At the time of sampling, the quantity of CCR available onsite was estimated at 8mx3mx2.5m (Figure 2.1a); that is about 60 m^3.

2.2.2. Rice husk/rice husk ash

The rice husk (RH) was collected form the locality of Bagré in the region of Centre-Est (230 m in the South–East of Ouagadougou) of Burkina Faso (N11°28.43', W002°03.35'). It was calcined to produce the rice husk ash (RHA). The calcination was carried in muffle furnace at a heating rate of 5 °C/min from 30 °C (ambient temperature of the lab) to the soaking temperature (Figure 2.1b). Different soaking temperatures (400, 500, 600 °C) and time

(0.25-6 h) were considered for the calcination (Table 2.1). The choice of such calcination programs aims to produce the RHA with optimum properties at minimum energy consumption, as guided by Muthadhi & Kothandaraman (2010). Different characterizations of the RHA allowed to determine the optimum conditions, before mass calcination for the stabilization of CEBs.

Table 2.1. Proposed temperature and time ranges for the calcination of RH into RHA

Temperature (°C)	Time (h)							
	0.25	0.5	1	2	3	4	5	6
400								
500								
600								

The RH can eventually be collected from other regions, producing the rice, of Burkina Faso whose production increased more than 285 % in the past decade (Gecit 2020, Guissou and Ilboudo 2012, MAHRH. 2009). In 2007, Burkina Faso produced 90 978 tons of rice (80 % of 113 723 tons of rice paddy) (MAHRH 2009), equivalent to 22 745 tons of RH (20 % of 113 723 tons of rice paddy). In 2010, the production of rice increased to 270 658 tons (Guissou and Ilboudo 2012), equivalent to 67 665 tons of RH. In 2018, the rice production was 350 392 tons (Gecit 2020), equivalent to 87 598 tons of RH. This suggests that at least 15 520 tons of RHA (20 % of 87 598 tons of RH) can be produced in Burkina Faso.

2.2.3. Control: Portland cement and lime

Industrial Portland cement, CEM IIA 42.5, produced by CIMBURKINA, Burkina Faso and hydrated lime produced by Carmeuse, Belgium were used as control binders.

2.2.4. Fibers

The Okra plant fibers were extracted from the skin of the stem of Okra (Gombo) plant (*Abelmoschus Esculentus*) collected from the locality of Kaya in the region of Centre-Nord (100 km in the North-East of Ouagadougou). The bast/skin were soaked in tap water for 3-4 weeks in order to enable the decomposition of undesired organic matters (Figure 2.1c-d). They were physically leached and washed multiple time until water turns clean and sun dried.

The current data and status of research did not allow to estimate the quantity of Okra bast fibers that can be potentially produced in Burkina Faso. However, the production of Okra (Gombo) itself in Burkina Faso was estimated at 23 000 tons in 2013 (Ouedraogo, Bougma et al. 2016).

Figure 2.1. (a) collection of CCR, (b) calcination of rice husk, (c)-(d) retting processing of fibers, (e) clay materials in Kamboinse, (f) Pabre, (g) Kossodo, (h) Saaba

2.2.1. Clay materials

The clay earthen materials were collected from 4 different sites in the vicinity of Ouagadougou, i.e. Kamboinse, Pabre, Kossodo and Saaba (Figure 2.1e-h). The number of samples collected from each site depended on its size, exploitability and apparent variability (Table 2.2). The estimation of the available deposits of clay materials is presented in chapter III (Table 2.2).

Kamboinse (K) is located 15 km in the North of Ouagadougou (12°29'24.48" N, 1°32'59.28" W, altitude 326 m). It has an average area of 700mx200m and average thickness of exploitable layer of 6 m. The clay material from Kamboinse has a reddish-brown color, with some whitish irregularities. The apparent texture of particles varies depending on depth: gravelly on surface layer (<2 m of depth), clay in middle (2-6 m) and sandy in depth (>6 m) (Figure 2.1e). The site of Kamboinse is exploited by engineering company for road pavement.

Pabre (P) is located 20 km in the North of Ouagadougou (12°31'23.46" N, 1°34'22.8" W, Alt. 297 m). It has an average area of 600mx100m and thickness of exploitable layer estimated at 2 m. The clay material from Pabre was collected 50 cm under the top layer and has a silty clay texture (Figure 2.1f). This material has grey color and is used for artisanal production of adobe bricks.

Kossodo (Ko) is located 10 km in the North-East of Ouagadougou (12°27'49.32" N, 1°26'34.02" W, Alt. 303 m) and extends on an average area of 350mx150m and an average thickness of exploitable layer of 5 m. The clay material from Kossodo has reddish-brown color, gravel-like texture on top (depth ~3 m) and silty-sandy texture in depth (Figure 2.1g). The clay material from this site is used for the production of cement stabilized CEBs by a local enterprise.

Saaba (S) is located 15 km in the East of Ouagadougou (12°22'48.12" N, 1°24'2.22" W, Alt. 310 m) and extends on an average area of 350x70 m² and thickness of exploitable layer of 4 m. It is characterized by whitish purple-brown clay material, which has sandy silt texture (Figure 2.1h). The clay materials from Saaba are exploited by the local population for artisanal production of construction materials and pottery.

Table 2.2. Location and description of the samples of clay materials from the four (04) sites

Samples	Geographical coordinates on the surface	Depth (m)	Sample description (Rock color chart)
K1-3	12°29'24.48" N, 1°32'59.28" W, 326 m	3.5	Reddish brown (10R 4/6)
K3-1	12°29'32.76" N, 1°32'55.62" W, 315 m	2.5	Reddish brown (10R 4/6)
K3-2		3.5	Reddish brown (10R 4/6)
K3-4		3.5	Whitish orange (10 YR 8/2)
K3-5		5	Yellowish orange (10YR 8/6)
K4-1	12°29'32.4" N , 1°32'52.44" W, 313 m	6.5	Reddish grey (5YR 8/1)
K4-2		6.5	Reddish brown (10R 4/6)
K4-3		5.5	Reddish brown (10R 4/6)
K4-4		7.5	Rose-grey (5YR 8/1)
K5-1	12°29'23.46" N , 1°32'58.8" W, 321 m	5	Reddish brown (10R 4/6)
K5-2		4	Reddish brown (10R 4/6)
K5-3		3.5	Greyish orange (10YR 7/4)
K5-4		6	Greyish orange (10YR 7/4)
K6	12°29'17.88"N, 1°32'59.28"W, 310 m	1	Greyish orange (10YR 7/4)
K8	12°29'15.54" N, 1°33'2.4"W, 318 m	4	Reddish brown (10R 4/6)
K9-1	12°29'23.46" N , 1°33'2.88"W, 328 m	1.5	Reddish brown (10R 4/6)
K9-2		3	Pale brown (5YR 6/4)
K9-3		3.5	Pale brown (5YR 6/4)
K9-4		4.5	Pale brown (5YR 6/4)
K9-5		5.5	Pale brown (5YR 6/4)
K9-6		6.5	Pale brown (5YR 6/4)
K9-7		7.5	Dark red-brown (10R 3/4)
K9-8		8.5	Pale orange (10 YR 8/2)
K9-9		9	Red (5R 5/4)
K9-10		3.5	Pale rose grey (5YR 8/1)
K9-11		5.5	Pale orange (10 YR 8/2)
P1	12°31'35.7" N, 1°34'31.5"W, 299 m	0.5	Yellowish brown (10YR 6/2)
P2	12°31'23.46" N, 1°34'22.8"W, 297 m	0.5	Yellowish brown (10YR 6/2)
P3	12°31'18.36" N, 1°34'18"W, 293 m	0.5	Yellowish brown (10YR 6/2)
Ko1-1	12°27'49.32" N, 1°26'34.02" W, 303 m	2.9	Brown gravel-like
Ko1-2		3.1	Pale brown silty clayey (5YR 5/6)
Ko1-3		3.9	Pale brown silty clayey (5YR 5/6)
Ko1-4		4.9	Dark yellowish orange silty clayey (10YR 6/6)
S1-1	12°22'44.88" N , 1°24'38.1" W, 315 m	2.3	Reddish brown (10R 4/6)
S1-2		3.9	Rose orange (10R 7/4)
S1-3		4	Pale red (5R 6/2)
S1-4		4.5	Rose grey (5YR 8/1)
S1-5		5	Pale red (5R 6/2)
S2-1	12°22'48.12" N, 1°24'2.22"W, 310 m	0.75	Greyish orange (10R 8/2)
S3-1	12°22'44.04" N, 1°24'34.08"W, 312 m	4	Greyish orange (10R 8/2)
S3-2		4.5	Reddish brown (10R 5/4)

2.3. Design, production and curing of mixtures and stabilized CEBs

2.3.1. Design of mixtures

The fraction of representative clay materials from different sites was washed on 400 µm then dried (40±2°C). The bulk clay materials were eventually dry sieved on 5 mm. Some dry mixtures were prepared using the clay material and 0-25 wt% CCR with respect to the dry mass of the clay material (Table 2.3a). Other mixtures were prepared using the clay material and 10-25 wt% CCR:RHA (various ratios), i.e. 10-25 wt% CCR from which 10-40 wt% was

partially substituted by RHA (Table 2.3a). Moreover, 0-1.2 wt % fibers was added to the matrix of CEBs stabilized with 10 wt% CCR (Table 2.3b). Mixtures containing 8 wt% cement were also prepared for control purpose.

Table 2.3. Weight percentage of (a) binder and (b) fiber added to the earthen material

a

Binder	Fraction of binder added to the earthen material (wt %)						
CCR	0	2	4	5	10	20	25
CCR:RHA (ratios)					(9:1)	(18:2)	(22.5:2.5)
					(8:2)	(16:4)	(20:5)
					(7:3)	(14:6)	(17.5:7.5)
					(6:4)	(12:8)	(15:10)
CEM (control)	8						

b

Fiber	Fraction of fiber added to the matrix stabilized with 10 CCR (wt %)				
Vegetable fiber	0	0.2	0.4	0.8	1.2

2.3.2. Production of mix solutions and stabilized CEBs

Firstly, the dry fraction finer than 400 µm was softly crushed and used for the production of mix solutions for testing the reactivity of clay materials given their contribution towards cohesion and reactivity, contrary to the coarser fraction. Mix solutions were also produced using the undersize of 5 mm of clay materials with binders for monitoring the curing process. Dry mixtures were prepared using 5 g of clay material and different weight percentage of binders (Table 2.3a). The dry mixtures were kept in bottles, filled with 100 mL of deionized water and rigorously shaken for preparing mix solutions (Figure 2.3a).

Secondly, dry undersize on 5 mm was manually (with hands) dry mixed with different fractions of binders and eventually fibers (Table 2.3), until apparent homogeneity for the production of stabilized CEBs, as recommended by CRATerre (Houben and Guillaud 2006). The optimum moisture content (OMC) of each mixtures, determined according to static compaction method (CDE 2000), was added to the dry mix and mixed until homogeneous moisture distribution. The OMC for achieving maximum dry density linearly increases with the CCR content, while the estimated maximum dry density decreased with increasing moisture of production (CCR content), similarly to industrial hydrated lime (Figure 2.2). This suppose that the CEBs were produced at different moisture content, but similar consistency.

Furthermore, OMC+2 was used for assessing its effect on the compressive strength of CEBs stabilized with CCR. Humid mixtures were manually compressed in standard prismatic mold,

295x140x95 mm^3 (XP P 13-901 2001), of terastaram machine to produce CEBs (Figure 2.3b). The press was designed to offer a compaction pressure of ~35 bars (Sore 2017). At least, three (03) specimens of CEBs were produced for each mix design in order to account for the variability (average and standard deviation).

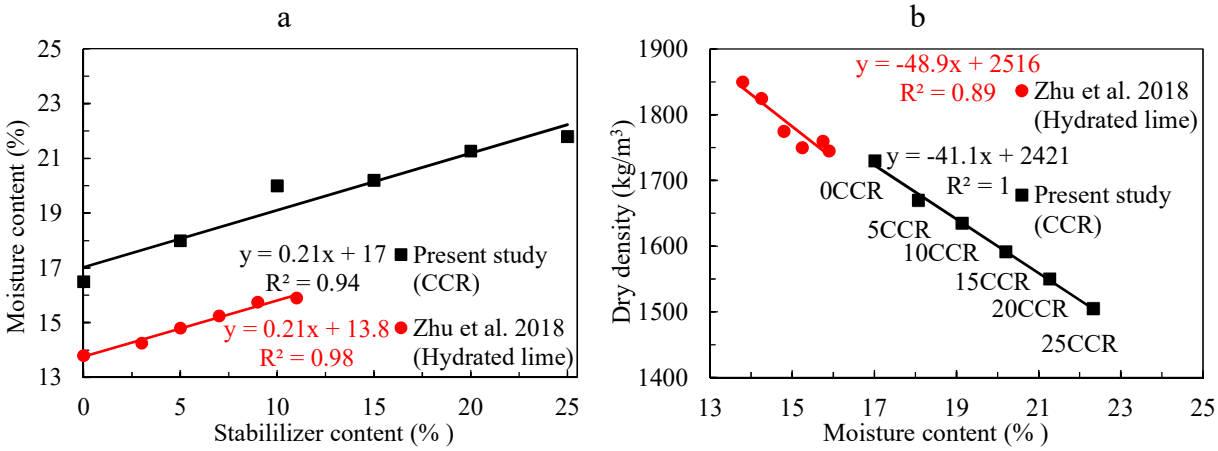

Figure 2.2. Evolution of the (a) optimum moisture content and (b) maximum dry density of clay material from Kamboinse with selected content of CCR, compared with industrial lime

2.3.3. Curing of mix solution and stabilized CEBs

The bottles containing the mix solutions were tightly closed and the CEBs were stored in polyethylene bags to minimize the loss of humidity and eventual carbonation during curing process (Figure 2.3a and Figure 2.3c). The curing was undertaken for 0, 1, 7, 28, 45 and 90 days in the ambient conditions of laboratory (30±5 °C in LEMHaD) and eventually at controlled temperature in oven (20±2 and 40±2 °C). This aimed to assess the effect of curing conditions on the reactivity of materials and compressive strength of stabilized CEBs.

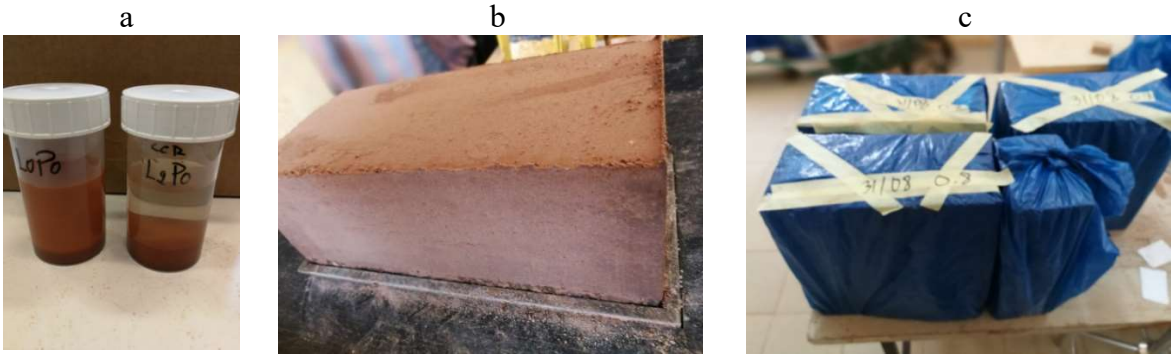

Figure 2.3. (a) mix solutions, stabilized CEBs (b) after production and (c) during curing

2.4. Characterizations of the raw materials, cured mixtures and stabilized CEBs

Various techniques and methods were carried to characterize the properties of raw/processed materials and stabilized cured mixtures and CEBs. These techniques include sieving and laser diffraction, electrical conductivity and titration of calcium ion [Ca^{2+}], X-ray fluorescence, X-ray diffraction, thermogravimetric analysis, scanning electron microscopy, Fourier transform infrared spectroscopy, and compression tests, among many others.

2.4.1. Characterizations of the physical and mechanical properties of materials

This consists of characterizing raw/processed materials before the production of mixtures and eventually stabilized CEBs. The specific surface area of CCR and RHA was determined according to Blain and BET (Brunauer-Emmett-Teller) methods. The BET was performed by Nitrogen adsorption using micrometrics Gemini V1.01 instrument. The specific density, ρ_s, of CCR, RHA, fibers and clay materials was determined using water pycnometer, according to NF EN 1097-6 (2014).

The particle size distribution (PSD) of CCR and RHA was analyzed by laser diffraction using a Mastersizer analyser machine (Michel & Courard 2014). The PSD of clay materials, clay: <0.002 mm, silt: 0.002-0.08 mm, sand: 0.08-2 mm and gravel: >2 mm, was determined by sieving (≥80 µm) and sedimentation (<80 µm), referring to the standard NF EN ISO 17892-4 (2018). The Atterberg's plasticity limits (liquidity and plasticity) and compressibility (optimum moisture content and maximum dry density) of clay materials were determined using Casagrande apparatus and normal Proctor compaction, in accordance with NF P 94 051 (1993) and NF P94-093 (2014)

The water absorption of fibers was determined on 2-3 g of fibers (30 mm long) (LMC, UEE, ULiège). Overall, nine (09) samples were prepared which were soaked in deionized water for 1 h (03 samples), 2 h (03 samples), and 24 h (03 samples). After soaking time, the fibers were removed from the water and kept at 22±1°C, 65±5% RH until the release of gravitational water, then weighted (saturated weight). The saturated fibers were dried at 105 °C for 24 h before weighting (dry weight) and determining the percentage mass of water absorbed. The tensile strength of fibers was determined on more than 50 samples of single fibers selected randomly from different bundles and parts of fiber. The test was carried at Celabor (Chaineux, Belgium) on gauge length of 30 mm, 70-100 µm thick, at loading rate of 1 mm/min, using a tensile testing machine of the Zwick Roell which has cell of maximum load capacity of 10 N.

2.4.2. Characterizations of chemical, mineral and microstructural properties

The chemical composition of CCR, RHA and clay materials was analyzed by means of X-ray fluorescence (XRF) using ARL Perform'X Sequential XRF equipment (Department of geology, PGEP, ULiege). After the determination of loss-on-ignition at 1000°C for 2 hours (LOI 1000), about 340-450 mg (Ms) of the samples wer fused in lithium borate (11xMs) to form pellets. The major chemical elements were determined on the pellets against internal standard of the XRF equipment calibrated from sodium to uranium.

The mineral composition of CCR, RHA and clay materials was analyzed by X-ray diffraction (XRD) performed using Bruker D8-Advance Eco 1.5 kW diffractometer equipped with copper anticathode (Cu Kα λ=1.54060 Å at 40 kV and 25 mA) and Lynxeye xe detector (AGEs, ULiège). The bulk mineralogy was identified by powder diffraction on samples ground to less than 150 µm, while the clay minerals were identified on oriented, <2 µm, aggregates throughout treatments (air-dried, glycolated and heat treatment). The XRD patterns were acquired from 2 to 70° 2θ, at step size of 0.02° 2θ, scan time of 2 s per step for bulk samples and 2 to 30° 2θ, step size of 0.009° 2θ, scan time of 0.5 s per step for oriented aggregates. The acquired patterns were analyzed using Diffrac.Eva V4.11 software of the Bruker.

The mineral composition was further confirmed by thermogravimetric analysis (TGA) and Fourier transform infrared spectroscopy (FTIR). The TGA was carried out using automatic multiple sample thermogravimetric analyzer TGA-2000 of the Las Navas Instruments (AGEs). The analysis was carried out in the range of 25-1000 °C, at heating rate of 5 °C/min in dry air environment. FTIR was recorded using FTIR spectrometer in the range of 4000-400 cm^{-1}, at scan size of 1 cm^{-1} (UEE). The FTIR was carried out on pellets formed using about 2 g of materials (ground to <250 µm) and 148 g of potassium bromide.

The semi-quantitative estimation of the mineral composition was achieved based on the measurement of the intensity of diagnostic peaks of minerals identified by XRD on which corrective factors were applied, i.e. “XRD, Method A” according to (Cook et al. 1975, Boski et al. 1998, Fagel et al. 2003). The content of kaolinite and goethite were confirmed based on the mass loss on the TGA due to their respective dehydroxylation, compared to that of pure kaolinite (13.97 % at 530-590 °C) and pure goethite (10.13 % at 290-330 °C), i.e. “TGA, Method B” (Földvári 2011).

Additionally, the mineral composition was quantified based on chemical analysis by XRF and applying the formula proposed by (Yvon et al. 1982) in (Nkalih Mefire et al. 2015). The so-called "XRF, Method C" allowed to assign different oxides to the minerals identified by the XRD and TGA. The following assignments were made in eq. 2.1: (a) K_2O to illite or K-feldspar, (b) CaO to plagioclase, (c) Al_2O_3 to kaolinite after subtracting the contribution to illite or K-feldspar, (d) SiO_2 to quartz after subtracting the contribution to illite or K-feldspar and kaolinite, (e) Fe_2O_3 to hematite after subtracting the contribution to goethite (determined from TGA). The total mineral and chemical compositions were normalized to 100 %.

eq. 2.1

$$\%\text{illite} = \frac{K_2O}{94}814 \quad \text{or} \quad \%\text{K-feldspar}\frac{K_2O}{94}557 \qquad a$$

$$\%\text{plagioclase} = \frac{CaO}{56}278 \qquad b$$

$$\%\text{kaolinite} = \frac{\%Al_2O_3 - \frac{\%\text{illite x } 102x3}{814} - \frac{\%\text{K-feldspar x}102}{557} - \frac{\%\text{plagioclase x } 102}{278}}{102}258 \qquad c$$

$$\%\text{quartz} = \frac{\%SiO_2 - \frac{\%\text{illite x 60 x6}}{814} - \frac{\%\text{K-feldspar x 60 x 6}}{557} - \frac{\%\text{plagioclase x 60 x 2}}{278} - \frac{\%\text{kaolinite x 60 x 2}}{258}}{60}60 \qquad d$$

$$\%\text{hematite} = \frac{\%Fe_2O_3 - \frac{\%\text{goethite x } 160}{178}}{160}160 \qquad e$$

814= molar mass of illite $(K_2O)(SiO_2)_6(Al_2O_3)_3(H_2O)_3$ in g/mol

94= molar mass of K_2O in g/mol

557= molar mass of K-feldspar $(K_2O)(SiO_2)_6(Al_2O_3)$ in g/mol

56= molar mass of CaO in g/mol

278= molar mass of plagioclase $(CaO)(SiO_2)_2(Al_2O_3)$ in g/mol

102= molar mass of Al_2O_3 in g/mol

258= molar mass of kaolinite $(SiO_2)_2(Al_2O_3)(H_2O)_2$ in g/mol

60= molar mass of SiO_2 in g/mol

60= molar mass of quartz (SiO_2) in g/mol

160= molar mass of Fe_2O_3 in g/mol

178= molar mass of goethite $(Fe_2O_3)(H_2O)$ in g/mol

Furthermore, the microstructure of materials and products was analyzed by scanning electron microscopy (SEM) using the ZEISS GeminiSEM (Sigma 300) equipped with two energy dispersive spectrometers (EDS, Silicon Drift Detector XFlash of Bruker, 30 mm²). The operating conditions of the SEM were set at 20 keV, ~200 µA and at distance of 8.5 mm.

2.4.3. Tests of the suitability of materials for the production of stabilized CEBs

The suitability of materials for the production of stabilized CEBs was evaluated based on the chemical and mineral compositions of CCR, RHA and clay materials. The mineral composition was determined using XRD, TGA techniques as described above (§2.4.2). The amorphicity and reactivity of RHA and clay materials was assessed using different methods such as XRD, TGA,

and FTIR (§2.4.2), reactivity with $Ca(OH)_2$ solution through measurement of the electrical conductivity, and dissolution rate during attack with boiling 0.5 M NaOH solution.

2.4.3.1. Reactivity of RHA with the solution of calcium hydroxide

The reactivity of the RHA with the saturated solution of calcium hydroxide ($Ca(OH)_2$) consists of monitoring the decrease of the electrical conductivity (EC) when RHA is added to the saturated solution of $Ca(OH)_2$ at 40 °C. The decrease of the EC is related to the consumption of Ca^{2+} and OH^- dissolved in the solution from $Ca(OH)_2$ by the RHA, mainly the amorphous silica. The saturated solution of $Ca(OH)_2$ was prepared by dissolving excess $Ca(OH)_2$ analytical grade (94 %) in deionized water and mixing thoroughly to achieve maximum dissolution. The filtered saturated solution had an initial EC of 5.83 mS/cm. It was placed in the oven at 40 °C and left to reach thermal equilibrium. Approximatively 1 g of each types of RHA was added in bottles containing 200 mL of $Ca(OH)_2$ solution, conserved in the oven and shaken vigorously every 10 minutes for 60 minutes (1 h). The measurements were carried out after 1, 6, 12, 24, 48 h.

2.4.3.2. Dissolution of RHA in the solution of sodium hydroxide

This method determines the silica activity index (SAI) of RHA (Mehta 1973), as the fraction of RHA that dissolves in the boiling solution of sodium hydroxide (0.5 M NaOH). It represents the fraction of amorphous, thus reactive, silica in the RHA. Approximatively 1 g of each type of RHA was added to the boiling 0.5 M NaOH solution and left to interact for 3 minutes. The residues of this interaction were filtered, dried in oven (105 °C) and weight to evaluate the percentage fraction of RHA which dissolved.

2.4.3.3. Reactivity of clay materials

The suitability of different clay materials for the production of stabilized CEBs was tested based on the rate of reactivity with the $Ca(OH)_2$ in the CCR and physico-mechanical performances of CEBs stabilized with CCR. The evaluation of the reactivity aims to estimate the initial CCR required by the clay material for the pozzolanic reactivity to take place. It also monitors the rate of consumption of the CCR over the curing time. This was assessed based on the evolution of the pH, electrical conductivity (EC) and concentration of unconsumed calcium ions [Ca^{2+}] in the mix solutions made of clay materials and CCR (§2.3.2).

The pH of the solutions was immediately measured after 1 hour (0 day) of curing to evaluate the change in the basicity as described by Eades and Grim (Eades & Grim 1996). The EC and

unconsumed [Ca^{2+}] were monitored in mix solutions of earth-CCR and eventually earth-CCR:RHA systems. After each curing period: 1, 7, 28, 45 and 90 days (§2.3.2), the mix solutions were shaken and filtered to get 60 mL which were used for the measurements of the EC and [Ca^{2+}]. The pH and EC was measured using pHenomenal MU 6100 L multiparameter lab conductimeter, equipped with pH and CO 3100 conductivity probes. The [Ca^{2+}] was titrated by potentiometric method with 0.05 M EDTA (Ethylenediaminetetraacetic acid), using 905 titrado equipped with polymer-calcium membrane electrode. This method was similarly used by Al-Mukhtar et al. (Al-Mukhtar et al. 2010a, 2010b) for monitoring the behavior and mineralogy changes in lime-treated clayey soils.

2.4.4. Characterization of mechanical and hygro-thermal properties of stabilized CEBs

After curing, the CEBs were dried at 40±2°C until reaching constant mass, change of weigh less than 0.1 % between two consecutive weighing in 24 hours, before any further treatments for testing different properties.

Figure 2.4. (a) testing the compressive strength, measuring the thermal properties in (b) dry and (c) wet conditions using DEsProTherm, (d) measuring the water vapor sorption

2.4.4.1. Compressive strength

The compressive strength of CEBs was tested using hydraulic press equipped with a load cell which has a capacity of 300 kN, at loading rate of 0.2 mm/s, on double-stack of halves of CEBs (Figure 2.4a), according to the standard XP P13-901 (2001). The compressive strength of CEBs, Rc (MPa), was determined using eq. 2.2, where Fr is the maximum load at failure (kN), and S is the applied surface area (cm²). Similarly, the compressive strength of CEBs was tested in wet condition. The dry sample of CEBs was cut into two equal pieces, weighed (Md), and sought in tap water for 2 hours, then weighed (Msat.air) to evaluate the water absorbed, before testing their wet compressive strength.

$$R_c = 10xF_r/S \qquad \textit{eq. 2.2}$$

2.4.4.2. Thermal properties

Thermal properties of CEBs were measured on the basis of hot plate method using DEsProTherm "d*ispositive d'éstimation des propriétés thermiques*" in dry and wet conditions. In dry conditions, the measurements were carried out on samples dried at 40±2 °C (Figure 2.4b). By contrast, in wet conditions, the measurements were carried out on samples containing different amount of water (sook in liquid water after drying), in the range of 0-20 %, for assessing the effect of water content on thermal properties of CEBs. The specimens were wrapped in polymer bag to prevent the change of humidity during measurement (Figure 2.4c)

The thermal effusivity, E (J/m^2.K.s$^{1/2}$), was measured on specimen of size (6x4x3 cm^3) which does not allow the thermal flux to cross through the specimen. The volumetric thermal capacity, Cap (J/m^3.K) was measured on specimen of size (6x4x1 cm^3) which allows the flux to cross through the specimen (Sore 2017, Cagnon et al. 2014) . The specific heat capacity in J/kg.K was determined from the volumetric thermal capacity, Cap (J/m^3.K) and the bulk density, ρ (kg/m^3) of CEBs (§2.4.5).

eq. *2.3*

$$\lambda = E^2/(Cap) \qquad \textit{a}$$

$$a = \lambda/(Cap\ ) \qquad \textit{b}$$

$$\delta_p = \sqrt{(axT/\pi)} \qquad \textit{c}$$

The thermal conductivity, λ (W/m.K), thermal diffusivity, a (m^2/s), and thermal penetration depth, δ_p (m), were respectively determined using eq. 2.3a, eq. 2.3b, and eq. 2.3c; assuming a semi-infinite medium and harmonic variation of the thermal signal over a period, T (s), of

24 hours (86400 s). This suggests that the thermal effusivity should ideally decrease and the thermal capacity increases in order to decrease the thermal conductivity, diffusivity and thermal penetration depth and improve the thermal inertia of CEBs.

2.4.4.1. Water vapor sorption

The sorption capacity was measured on the specimens of CEBs (6x4x1 cm^3) using the method of saturated salt solutions, according to the standard EN ISO 12571 (CEN 2000). The specimens were dried at 40±2 °C, at relative humidity (Ψ of 3 % in presence of silica gel). They were exposed to continuously increasing relative humidity (Ψ: Table 2.4) produced by different saturated salt solutions, in a desiccator conditioned at 20±2 °C (Figure 2.4d).

Table 2.4. Relative humidity produced by saturated salt solutions.

Salt	KOH	$MgCl.6H_2O$	K_2CO_3	KI	NaCl	KCl	$K_2Cr_2O_4$
Relative humidity, Ψ (%)	9	33	43	69	75	83	97

The equilibrium moisture content, EMC (%), adsorbed by the specimens in equilibrium (2-3 weeks) with the relative humidity in the desiccator was determined between the dry mass, Md, and wet mass, Mw, respectively before and after exposure to each Ψ (eq. 2.4a). The isotherms of the EMC were fitted by Guggenheim-Anderson-de Boer (GAB) model, using eq. 2.4b; C, k, Wm are the parameters of the model. This model was previously used for CEBs and other construction materials to cover large interval of Ψ (5-95 %) (Kabre et al. 2019, Labat et al. 2016).

$$EMC = 100x(Mw - Md)/Md \quad \textit{eq. 2.4a}$$

$$EMC = \frac{Cxkxw_m}{(1 - kx\Psi)x(1 - kx\Psi + Cxkx\Psi)} . \Psi \quad \textit{b}$$

2.4.5. Tests of the hydric and durability performances of stabilized CEBs

2.4.5.1. Water absorption, bulk density and porosity

The capillary water absorption was measured on the bottom side (surface, S= 29.5x14 cm^2) of the specimen of CEBs which has a dry mass, Md (g), the immersed in water at a depth of 1±0.5 cm (Figure 2.5a). The mass of wet specimen, Mwi (g), was recorded over time, i.e: 0.17 (10 min), 0.5, 1, 2, 4, 8, 16, and 24 hours of capillary immersion. The mass allowed to determine the coefficient of capillary absorption, Cb_{10min} ($g/cm^2.min^{1/2}$), after 10 min (0.17 h) XP P13-901 (2001) and capillary water absorption, CWA (g/cm^2), over time, respectively using eq. 2.5a and eq. 2.5b.

eq. 2.5

$$Cb_{10min} = 100x(Mw_{10min} - Md)/(Sx\sqrt{10}) \quad a$$

$$CWA = (Mw_i - Md)/(29.5x14) \quad b$$

$$TWA = \frac{100x(Msat.\,air - Md)}{Md} \quad c$$

$$WAP = 100x(Msat.\,air - Md)/(Msat.\,air - Msat.\,wt) \quad d$$

$$\rho_b = Mdx\rho_{wt}/(Msat.\,air - Msat.\,wt) \quad e$$

$$TP = 100x(1 - \rho_b)/\rho_s \quad f$$

The total water absorption was measured, after capillary measurement, on the specimens totally immersed in water (5 cm beneath water surface) for 24 hours, considered enough for water saturation at atmospheric pressure (Figure 2.5b). This allowed to carry out hydrostatic weighing, referring to the standard XP P13-901 (2001). The mass of saturated specimen was weighed in water, Msat.wt (kg), and in air, Msat.air (kg). The total water absorption, TWA (%), of the specimen was determined from eq. 2.5c. Additionally, the percent of water accessible porosity, WAP (%), was determined using eq. *2.5*d. The bulk density, ρ_b (kg/m^3), was determined, after hydraulic weighing (NF P 18-459 2010), using eq. *2.5*d; ρ_{wt} is the density of water (1000 kg/m^3). The total (bulk) porosity, TP (%), was further estimated form the bulk density, ρ_b, of CEBs and equivalent specific density, ρ_s, of constituting particles, using eq. *2.5*f.

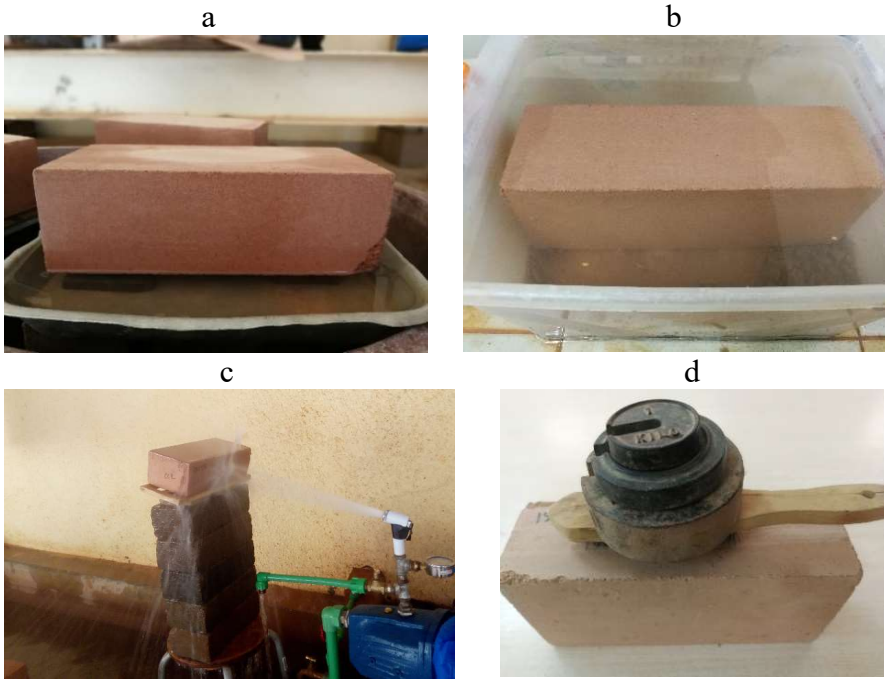

Figure 2.5. Test setups for water absorption (a) capillary and (b) total immersion, resistance to (c) erodability and (d) abrasion

2.4.5.1. Resistance to erodability

The resistance to water erodability of CEBs was tested referring to the Bulletin 5 spray test (NZS 1998). Bulletin 5 prescribes to apply the water pressure of 50 kPa on a diameter of 150 mm of specimen, at a distance of 473 mm for 60 min (1 h). This diameter (150 mm) could not be realized if testing the side external face of the CEBs (height 95 mm). The test was adapted to a diameter of 90 mm. Firstly, the erodability test was carried out in the same conditions as the Bulletin 5 spray test (NZS 1998). Secondly, the water pressure was arbitrary increased to 500 kPa, keeping other parameters the same, to assess the effect of different stabilizers on the erodability of stabilized CEBs (Figure 2.5c).

After the erosion test, the average depth of erosion was measured for each specimen, by means of a needles inserted in each pits on the same specimen. Additionally, the average percentage of eroded area was also estimated on the face of each specimen, with respect to the total exposed area (diameter of 90 mm). This was achieved by subdividing each of the eroded area into a closely related geometric figure. These procedures were repeated on three specimens of the same design, in order to determine the average values of the depth of erosion and percentage of eroded area.

2.4.5.2. Resistance to abrasion

The resistance to abrasion was tested referring to the standard XP P13-901 (2001). The test was carried out by applying 60 cycles of abrasion on the side external face of the dry CEBs, using a metallic brush loaded with 3 kg (Figure 2.5d). After the abrasion test, the weight loss and abraded area of specimen were measured for determining the coefficient of abrasion (Ca) and percentage weight loss (WL), with respect to the total weight of dry specimen. The Ca (cm^2/g) was determined as the ratio between the abraded area (cm^2) and weight loss (g). The higher is the Ca, the better would be the resistance to abrasion of CEBs.

2.4.5.3. Resistance to wetting-drying cycles

The resistance to wetting-drying (W-D) cycles was tested referring to the D559-03 standard (ASTM 1989b). The dry specimens of CEBs were sought in tap water at room temperature (30±5 °C) for 6 hours, then dried in oven at 70 °C for 42 hours. This constitute one cycle of W-D, which was repeated 12 times. After each cycle, the specimens were slightly brushed, using a load of 1.5 kg, to remove any degraded particles, in order to determine the weight loss. Moreover, the compressive strength of CEBs was determined after the 12 cycles of W-D.

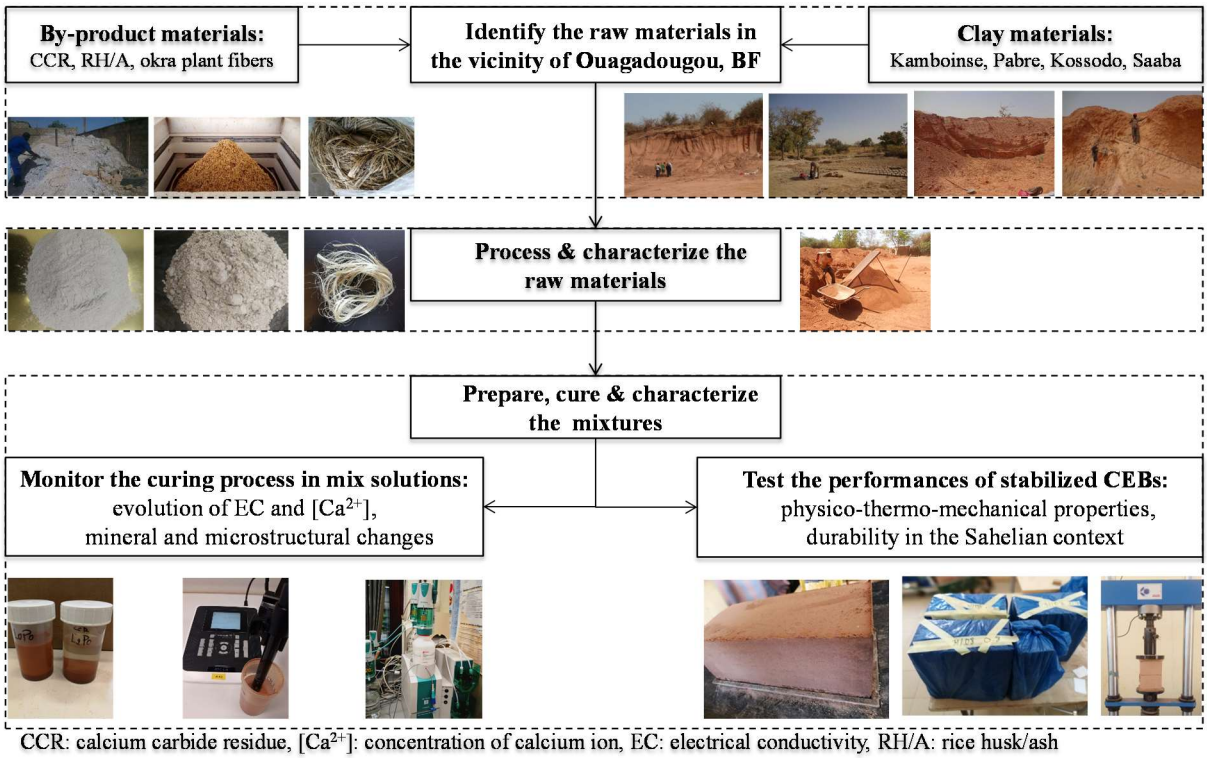

CCR: calcium carbide residue, $[Ca^{2+}]$: concentration of calcium ion, EC: electrical conductivity, RH/A: rice husk/ash

Figure 2.6. Schematic summary of the experimental procedures

2.5. Summary

This chapter detailed different procedures followed to identify samples, and to process and characterize the raw materials. It also presented the mix designs used to produce mix solutions and mold stabilized CEBs for testing the suitability of the materials for the production of stabilized CEBs. Furthermore, stabilized CEBs were produced, cured and characterized for their microstructural, physico-mechanical and hygro-thermal properties and durability. Figure 2.6 schematically summarizes the whole methodological procedures.

Different techniques such as sieving, laser diffraction, XRF, XRD, TGA, FTIR and SEM allowed to characterize the physico-chemical and mineral compositions and the microstructure of materials and stabilized CEBs. The compressive test, (ab)sorption test, hot plate (DEsProTherm) thermal test method, erodability, abrasion and wetting-drying tests allowed to characterize the effects of stabilization using by-products on the engineering and durability performances of stabilized CEBs. The results of these characterizations are discussed in the following chapters (III-V).

CHAPTER:

III. SUITABILITY OF MATERIALS FOR THE PRODUCTION OF STABILIZED CEBs

3.0. Suitability of by-product and clay materials for the production of stabilized CEBs

3.1. Introduction

This chapter presents the results from the characterization of the suitability of by-products and clay materials, from different locations in the vicinity of Ouagadougou for the production of stabilized CEBs. It responds to a specific question "*how do the chemical and mineral compositions of clay earthen materials affect the stabilization of CEBs using by-products*?"

Firstly, the physico-chemical and mineral compositions of materials are presented based on the XRF, XRD, TGA and FTIR. The effect of the physico-chemical and mineral compositions on the reactivity of materials was evaluated based on the rate of consumption of calcium ions throughout the monitoring of the electrical conductivity of their mix solutions over the curing time. The physico-mechanical properties were tested on the bulk density and compressive strength of CEBs produced from four different sites of clay materials and stabilized with CCR in order to select the most appropriate for construction of at least two-storey buildings.

3.2. Characterization of by-product materials for the stabilization of CEBs

3.2.1. Calcium carbide residue

Calcium carbide residue (CCR), after ball milling, is constituted with fine powder (Figure 3.1a). Figure 3.2a presents the particle size distribution (PSD) and Table 3.1 summarizes other physical properties of the CCR. The CCR has plurimodal PSD around 10-100 µm, median diameter (D_{50}) of 20.5 µm and 90 % of particles lesser than 125 µm (D_{90}=100 µm), similarly to the report by Cardoso et al. (2009). The BET specific surface area and specific density of CCR are 14 m^2/g and 2.49 g/cm^3, respectively.

Table 3.1 shows that the chemical composition of CCR is dominated by CaO (67.4%) and total loss on ignition (LOI) of 26.7 %. The XRD spectrum of CCR mainly revealed the presence of diagnostic peaks of portlandite at 2.62 Å (34.1° 2θ) and 4.93 Å (18° 2θ), calcite at 3.03 Å (29.4° 2θ) and other carbonate minerals (Figure 3.3a). This was further confirmed on TGA by the weight loss of 12.8 % at 510 °C (425-550 °C) and 13.6 % at 815 °C (675-875 °C) which respectively corresponds to the dehydration of portlandite and decomposition calcite (Figure 3.3b). It justified the total LOI observed during chemical analysis. Cardoso et al. (2009) reported similar thermal events for the CCR at 400-620 °C and 620-900 °C, respectively.

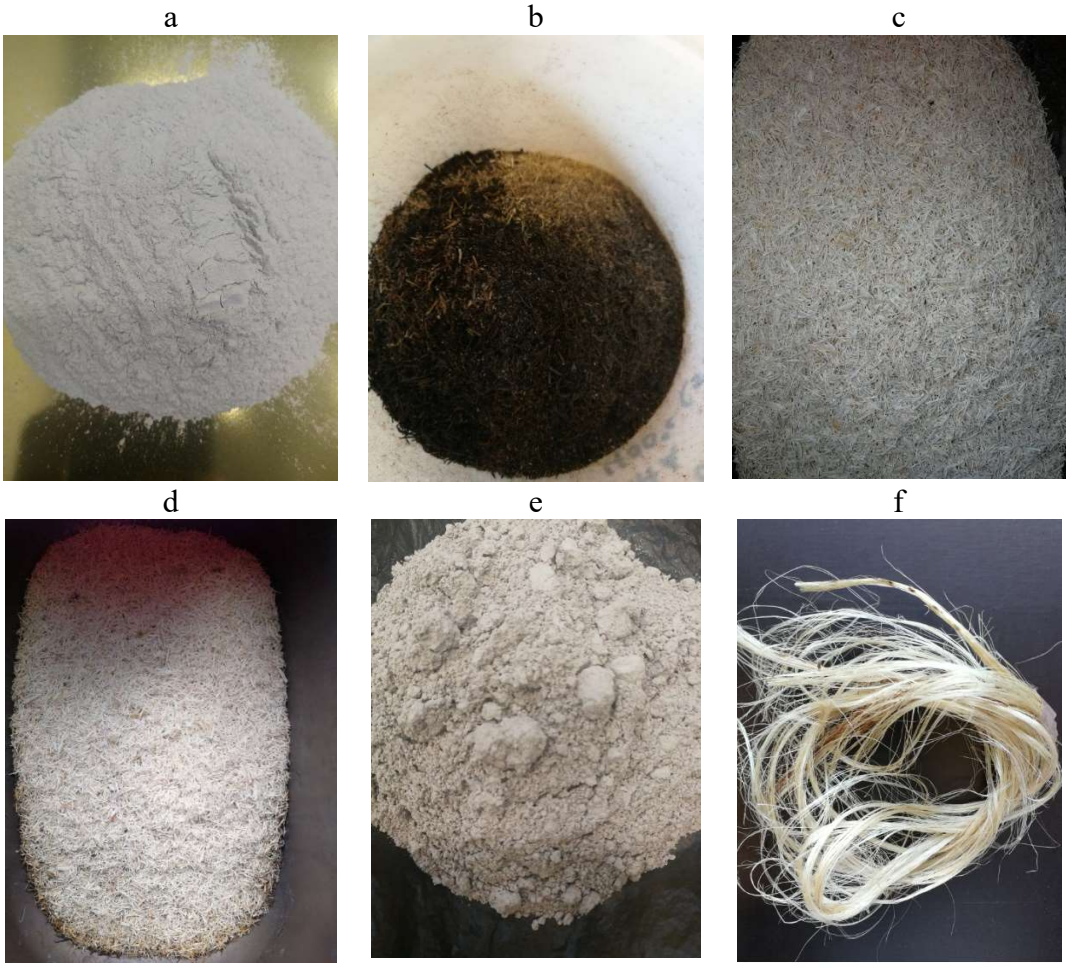

Figure 3.1. Processed materials (a) CCR, (b) calcined RHA (400 °C-4h), (c) RHA (500 °C-2h), (d) RHA (600 °C-1h), (e) ground RHA (500 °C-2h), (f) Okra bast fibers

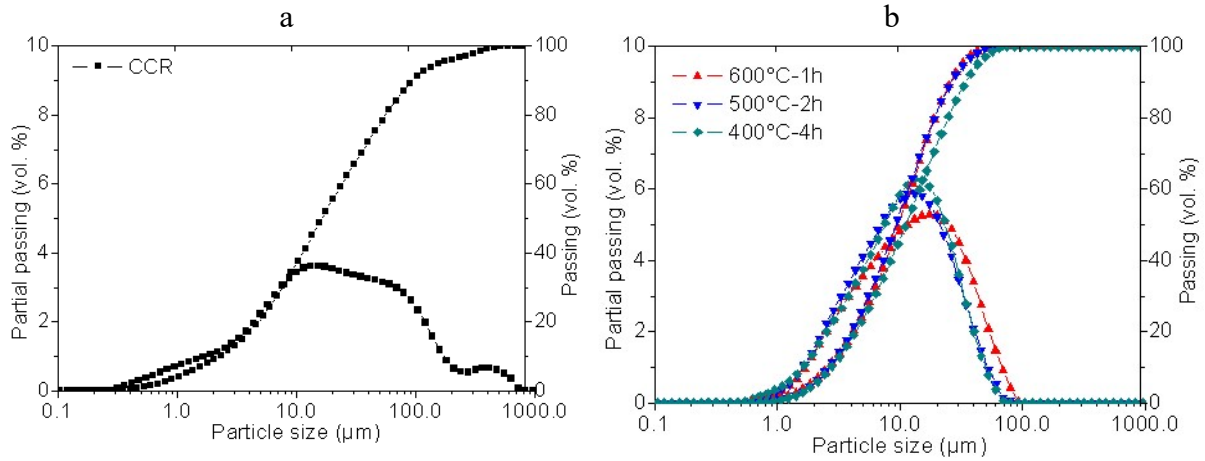

Figure 3.2. Particle size distribution after grinding of (a) CCR and (b) RHA

The semi-quantitative analysis of the mineral composition of CCR mainly estimated the portlandite ($Ca(OH)_2$) at 43 % from the XRD. The content of portlandite was also estimated at 53 % from the TGA, with respect to the weight loss (12.8%) of $Ca(OH)_2$ in CCR and weight loss (24.3 %: Földvári 2011) of pure $Ca(OH)_2$, The CCR also contains calcite (16 %: XRD) and other carbonates such as aragonite (21 %), rapidcreekite (13 %) and traces of quartz and

kaolinite (7 %) (Table 3.1). Note that the portlandite ($Ca(OH)_2$) is the one responsible for the lime treatment of clayey soil (Horpibulsuk et al. 2013, Houben & Guillaud 2006). Additionally, FTIR presents transmittance peaks at 3640 cm^{-1} from the OH-group of portlandite ($Ca(OH)_2$), at 1440 and 870 cm^{-1} from CO_3-groups of carbonates (Figure 3.3c).

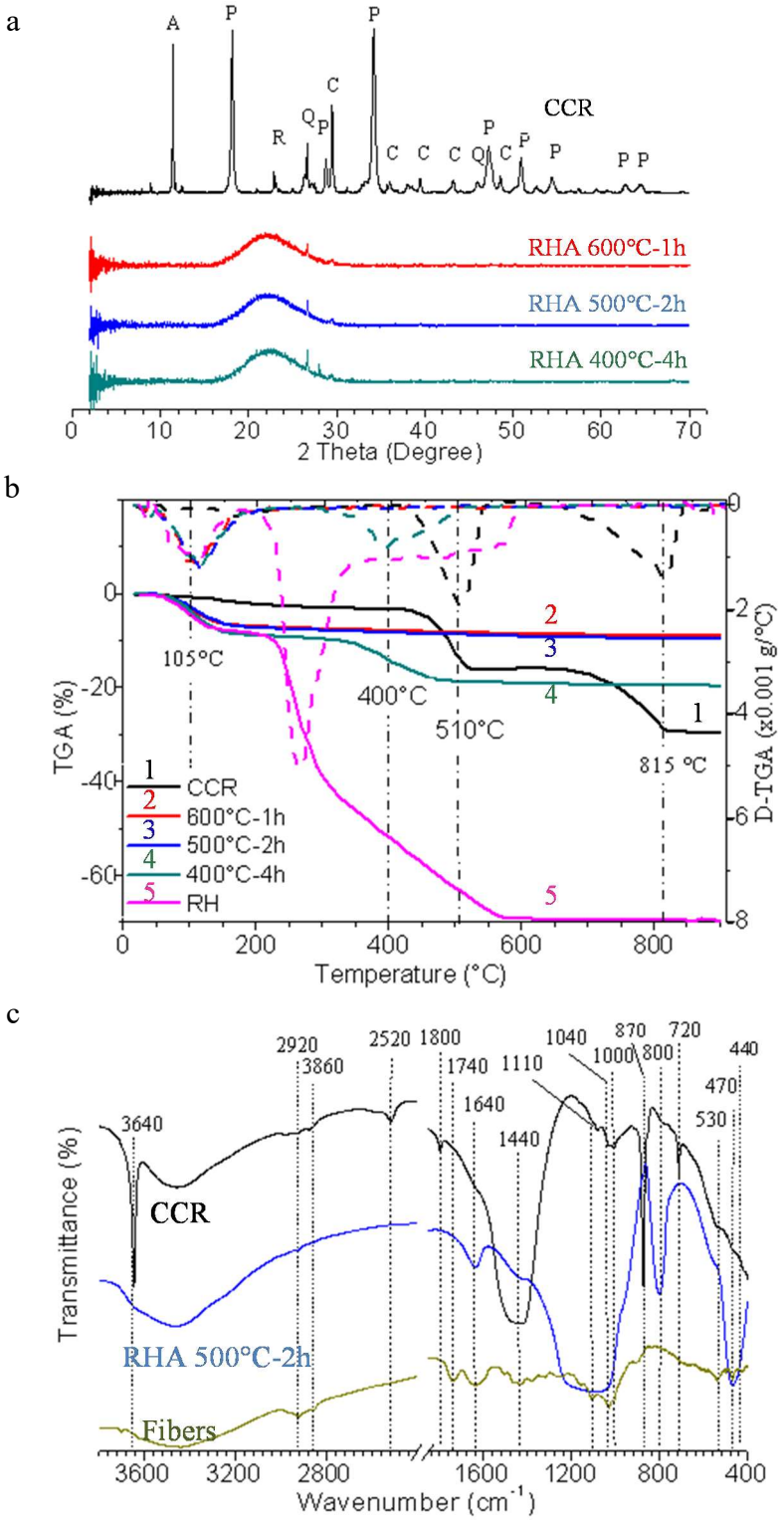

Figure 3.3. (a) XRD, (b) TGA, (c) FTIR of CCR and RH/RHA produced in different conditions, and fiber: Q=quartz, P=portlandite, A=aragonite, C=calcite, R=rapidcreekite

However, the content of $Ca(OH)_2$ is far lower than the 92 % (XRD) and 88 % (TGA) reported for CCR from Brazil (Cardoso et al. 2009). This can be related to the conditions of the production of CCR, which encouraged the carbonation in the present case, as the CCR was immediately exposed to dry in open air (Figure 2.1a).

3.2.2. Rice husk ash

The calcination of rice husk resulted in porous rice hush ash (RHA) of dark to greyish white color, depending on the increasing temperature and time of calcination (Figure 3.1b-d). RHA produced at 400 °C visibly shows residues of unburnt organic matters (dark color) for all soaking time (Figure 3.1b). However, calcination at 500 °C and 600 °C produced very clean RHA (greyish white color) respectively for soaking time of 2 and 1 h, related to the maximum burning of organic matters (Figure 3.1c&d). Grinding and sieving of the RHA on 80 µm resulted in powder (Figure 3.1e), finer than the CCR (Figure 3.2b). It has a D_{50} of 10 µm, with a monomodal PSD concentrated around 10 µm, D_{10}=2 µm and D_{90}=27 µm. The BET specific surface area of RHA of 154 m^2/g is also higher than that of CCR, with the specific density of 2.24 g/cm^3 (Table 3.1).

Table 3.1 shows that the chemical composition of the RHA (500 °C-2 h) is mainly constituted with silica (up to 91 %), which is greater than 70 % for classification as a pozzolan, and LOI at 1000 °C of only 2.6 %. The content of silica is also comparable to 89 % reported for RHA produced at 500 °C for 2h, from India (Muthadhi and Kothandaraman 2010). The XRD spectrum of RHA shows broad peak around 22° 2θ revealing its amorphous nature, with some peaks of impurity from quartz (Figure 3.3a). The TGA curve shows that the loss of weight from the thermal transformation of rice husk (RH) occurred mainly in the range of 200-600 °C (Figure 3.3b). This confirms the appropriateness of the calcination of RH in the temperature range of 400-600 °C. It also shows that the loss of weight of RHA occurred around 105 °C during the evaporation of adsorbed water, except the RHA calcined at 400 °C which presents weight loss around 400 °C from the calcination of residual organic matter. This further confirms the visual observation of dark unburnt organic matter in the RHA (400 °C-4 h) (Figure 3.1b).

The weight loss from 350-1000 °C is 11 % for RHA produced at 400 °C-4h, and 1 % for the RHA 500°C 2h and RHA 600°C-2h (Figure 3.3b). This suggests that the calcination of rice husk resulted in production of amorphous (Figure 3.3a) and well calcined RHA for the calcination temperature of 500 °C and above. FTIR of RHA also presents important broad bands between 1200 and 1000 cm^{-1} depicting the amorphous silica (Figure 3.3c). Therefore, there is

necessity to particularly assess the degree of amorphicity/reactivity of different RHA for a better selection of the most appropriate calcination conditions for the production of reactive RHA for the stabilization of CEBs

Table 3.1. Physical, chemical and mineral (XRD) properties of processed CCR, RHA (500°C-2 h) and fibers

Physical properties				Chemical compositions (%)			Mineral composition (%)		
Parameters	CCR	RHA	Fiber	Oxides	CCR	RHA	Minerals	CCR	RHA
Specific density	2.49	2.25	1.09	SiO_2	4.7	91.2	Kaolinite	4	Mainly amorphous
				Al_2O_3	1.7	1.6	Portlandite	43	
Blaine SSA (cm^2/g)	8 286 ± 218	2 6114 ±305	ND	Fe_2O_3	0.7	0.6	Aragonite	21	
				CaO	66.3	0.8	Calcite	16	
BET SA (m^2/g)	14 ±0.1	154 ±2	ND	TiO_2	0	0.1	Rapidcreekite	13	
				MnO	0	0.2	Quartz	3	
D10 (µm)	3	2	ND	MgO	0.3	0.2			
D50 (µm)	20.5	10	ND	Na_2O	0	0			
D90 (µm)	100	25	ND	K_2O	0.1	1.8			
TWA	ND	ND	364 ±13	P_2O_5	0	0.6			
				LOI	26.2	2.9			
				Total	100	100	Total	100	

ND: not determined, SSA: specific surface area, TWA: total water absorption (24 h), LOI: loss on ignition at 1000 °C

3.2.2.1. Reactivity of RHA in solution of calcium hydroxide

Figure 3.4a shows that the EC of saturated solution of $Ca(OH)_2$ drastically decreased after addition of the RHA, compared to the control solution of $Ca(OH)_2$ alone. The decrease of the EC is related to the consumption of calcium ion (Ca^{2+}), initially dissolved form the $Ca(OH)_2$, throughout the reaction with the RHA. Therefore, the faster is the decrease of the EC and the consumption of Ca^{2+}, the more reactive is the RHA.

Figure 3.4b shows that the RHA calcined at lower temperature for larger soaking time (400 °C for > 4h) would present the fastest decrease of EC (highest initial rate of consumption of Ca^{2+} after 1 h). Nevertheless, all the solutions reached the same minimum EC after 6 hours, related to the end of the consumption of the RHA. From this method, one may argue that 400°C-4h gives the RHA with the highest initial rate of consumption of $Ca(OH)_2$, though all the RHA reach the same final rate. Nevertheless, the choice of RHA 400°C-4h may be misleading in sense that it contains high content unburnt carbon, which may have contributed to the decrease of EC through the adsorption of Ca^{2+}. This needed further confirmation by the test of the dissolution of RHA in solution of sodium hydroxide.

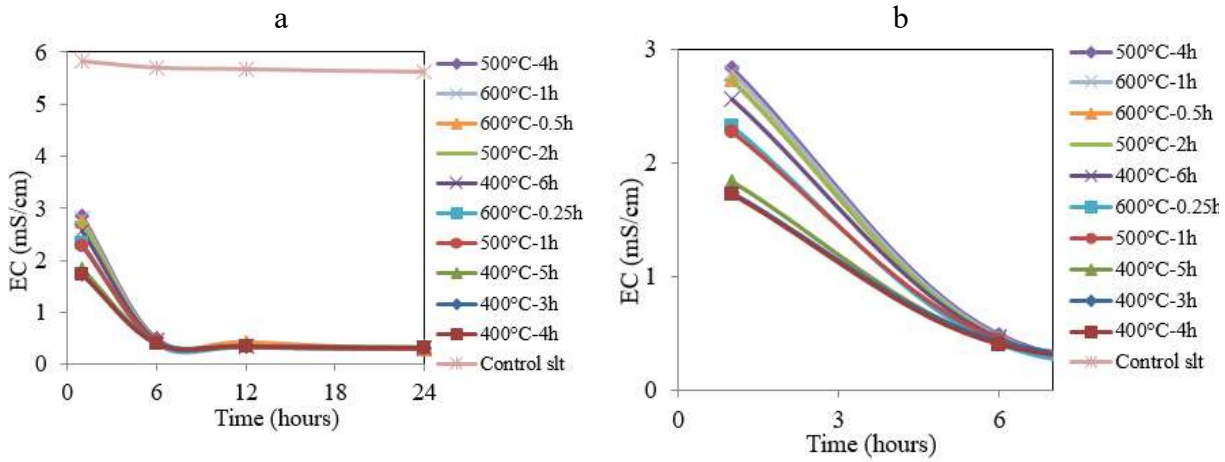

Figure 3.4. Evolution of the electrical conductivity (EC) of saturated $Ca(OH)_2$ solution after addition of RHA calcined in different conditions

3.2.2.2. Dissolution of RHA in solution of sodium hydroxide

The amount of amorphous RHA was tentatively estimated based on the fraction of silica soluble in boiling solution of 0.5 M NaOH. Table 3.2 presents these fractions for different RHA. It confirms that the RHA 500 °C-2h records the highest fraction (89 %), while the RHA 400°C-4h contains only 68 % of soluble silica. This agrees with the 88 % previously reported for RHA produced at 500 °C for 2 h (Muthadhi & Kothandaraman 2010). Comparing the results from the present study with the literature, the calcination at 500 °C for 2 hours was considered the optimum condition to produce the RHA of good quality (lower content of unburnt organic matter) and reactivity (highest fraction of soluble silica). This is beneficial in sense that 500 °C-2h would relatively consume less energy during calcination than 400 °C-4h, according to Muthadhi & Kothandaraman (2010).

Table 3.2. Fraction of silica of the RHA soluble in boiling solution of 0.5 M NaOH

RHA	Soluble silica (%)	RHA	Soluble silica (%)	RHA	Soluble silica (%)
400°C-3h	64	500°C-1h	64	600°C-0.25h	77
400°C-4h	68	500°C-2h	89	600°C-0.5h	82
400°C-5h	68	500°C-4h	77	600°C-1h	82
400°C-6h	71				

3.2.3. Okra bast fibers

The processing of Okra bast resulted in bundles of fibers of whitish color and average diameters of 70-100 µm (Figure 3.1f). The fibers have average specific density of 1.09, water absorption capacity of 326 % (after 1 hour) and 364 % (after 24 hours) (Table 3.1). Figure 3.3c presents the FTIR of fibers, showing broad band at 3400-3300 cm^{-1} from O-H groups of adsorbed water.

It presents also weak bands at 2920 and 1110 cm^{-1} from C-H stretching, 1740 and 1640 cm^{-1} from the C=O bonds, and 1040 cm^{-1} from C-O bonds (Khan et al. 2017, De Rosa et al. 2011).

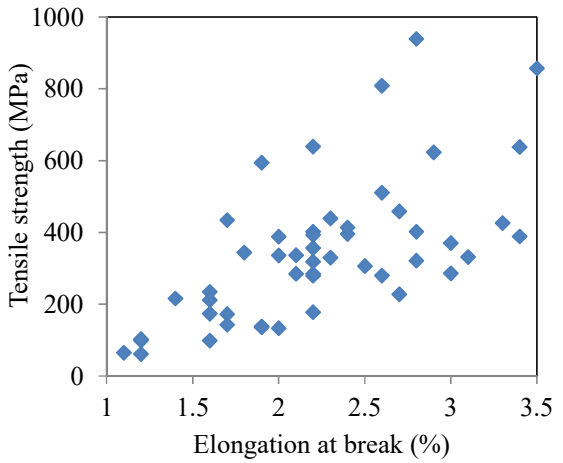

Descriptive statistic	
No. of observations	50
Minimum	62
Maximum	938
1st Quartile	213
Median	331
3rd Quartile	411
Mean	346
Standard deviation	197
Variation coefficient (%)	56
Skewness (Pearson)	1.03

Figure 3.5. Tensile strength of Okra bast fibers

Figure 3.5 presents the mechanical behavior of fibers, showing the dispersion of tensile strength with respect to the strain at failure. The values of the tensile strength of fibers ranged in 60-940 MPa, with the mean value of 346 MPa, standard deviation of 197 MPa and median value of 331 MPa. In addition, the Person skewness (1.03) is positive which shows that the distribution is right-skewed, thus the majority of the values of tensile strength are lower than the mean (346 MPa).

3.3. Characterization of clay materials for the production of stabilized CEBs

Figure 3.6 presents the geographical location and some of the outcrops of studied clay materials. Table 3.3 presents the quantity of exploitable clay materials, given the total volume of the deposit estimated from average dimensions (area and depth) of deposit and volume of material already excavated from the deposit. Kamboinse contains the largest quantity of exploitable clay materials (700 000 m^3), while Saaba contains the smallest quantity (49 000 m^3).

3.3.1. Particle size distribution

The particle size distribution (PSD) curves of different samples of clay materials are presented in Figure 3.7. These curves show continuous PSD for all samples from different sites, basically clay particles (<0.002 mm), silt (0.002-0.06 mm), sand (0.06-2 mm) and gravel (> 2 mm). The shapes of PSD curves vary for different sites and within the same site for Kamboinse. The clay materials from Pabre (Figure 3.7a) and Saaba (Figure 3.7d) have PSD fitting in the boundaries recommended by CRATerre (Houben and Guillaud 2006) for the production of CEBs stabilized with lime. By contrary, Kossodo (Figure 3.7c) does not fit within these boundaries, as well as

some samples from Kamboinse (Figure 3.7b). However, it is noteworthy that these boundaries are just guidelines which do not have to be fully satisfied by the earthen materials.

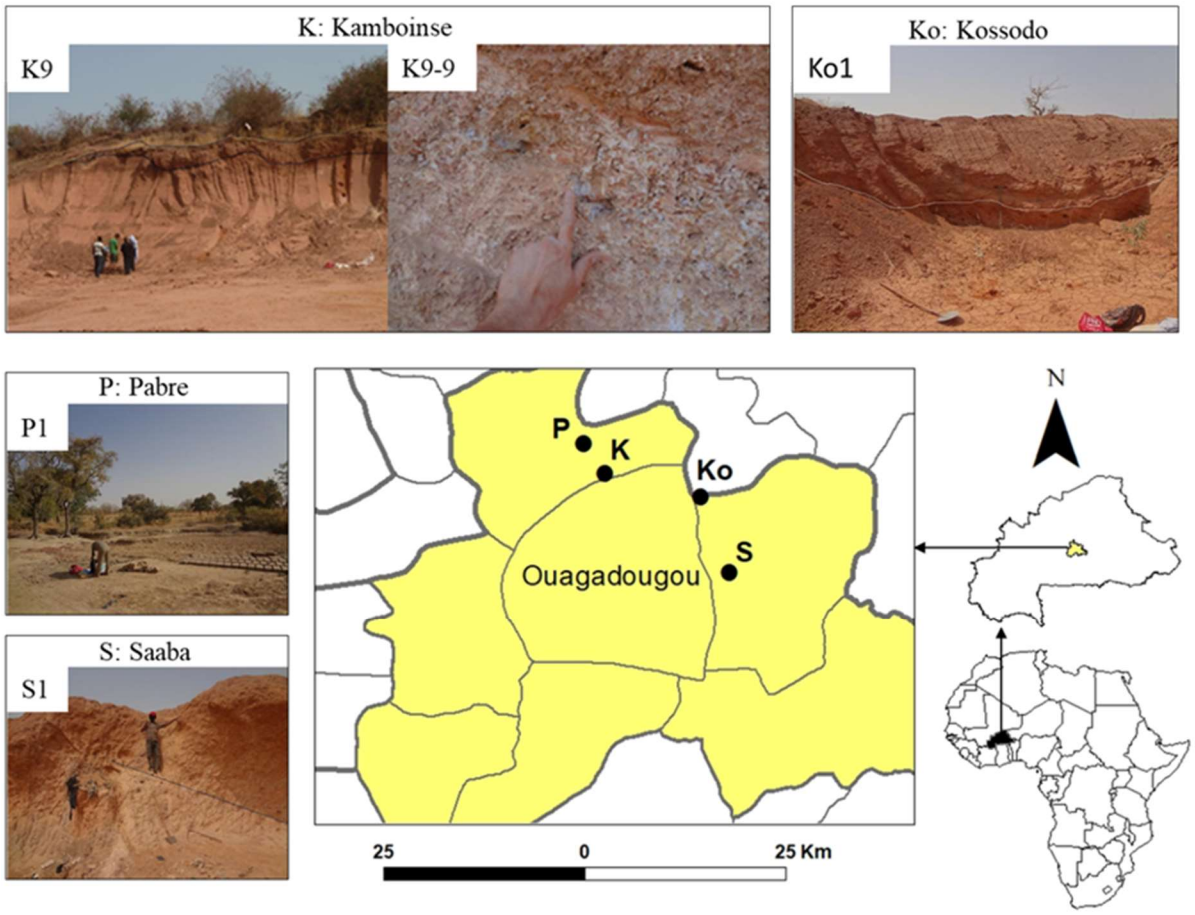

Figure 3.6. Geographical setting of the Centre region of Burkina Faso and some views of the studied outcrops of clay materials

Table 3.3. Average resources of exploitable clay materials from the four studied sites

Site	Length (m)	Width (m)	Depth (m)	Total volume (m^3)	Excavated volume (m^3)	Exploitable volume (m^3)
Kamboinse	700	200	6	840 000	140 000	700 000
Pabre	600	100	2	120 000	-	120 000
Kossodo	350	150	5	262 500	131 250	131 250
Saaba	350	70	4	98 000	49 000	49 000

The variations of PSD of the clay materials from Kamboinse range in 10-25% of clay particles; except K3-1, K8, K11 and K9-1, K9-2 which respectively contain <10% and >25% of clay particles; 30-60% of silt, 15-45% of sand and 0-20% of gravel (Figure 3.8a). The PSD of the clay materials from Pabre is characterized by 20-30% of clay particles, 40-55% of silt, 15-35% sand and 0-5% gravel (Figure 3.8b).The sample analyzed from Kossodo contained less than 10% of clay particles, 15% of silt, 35% of sand and 40% of gravel (Figure 3.8c). The materials from Saaba contained 20-25% of clay, 25-30% of silt, 40-45% of sand and less than 10% of gravel (Figure 3.8d).

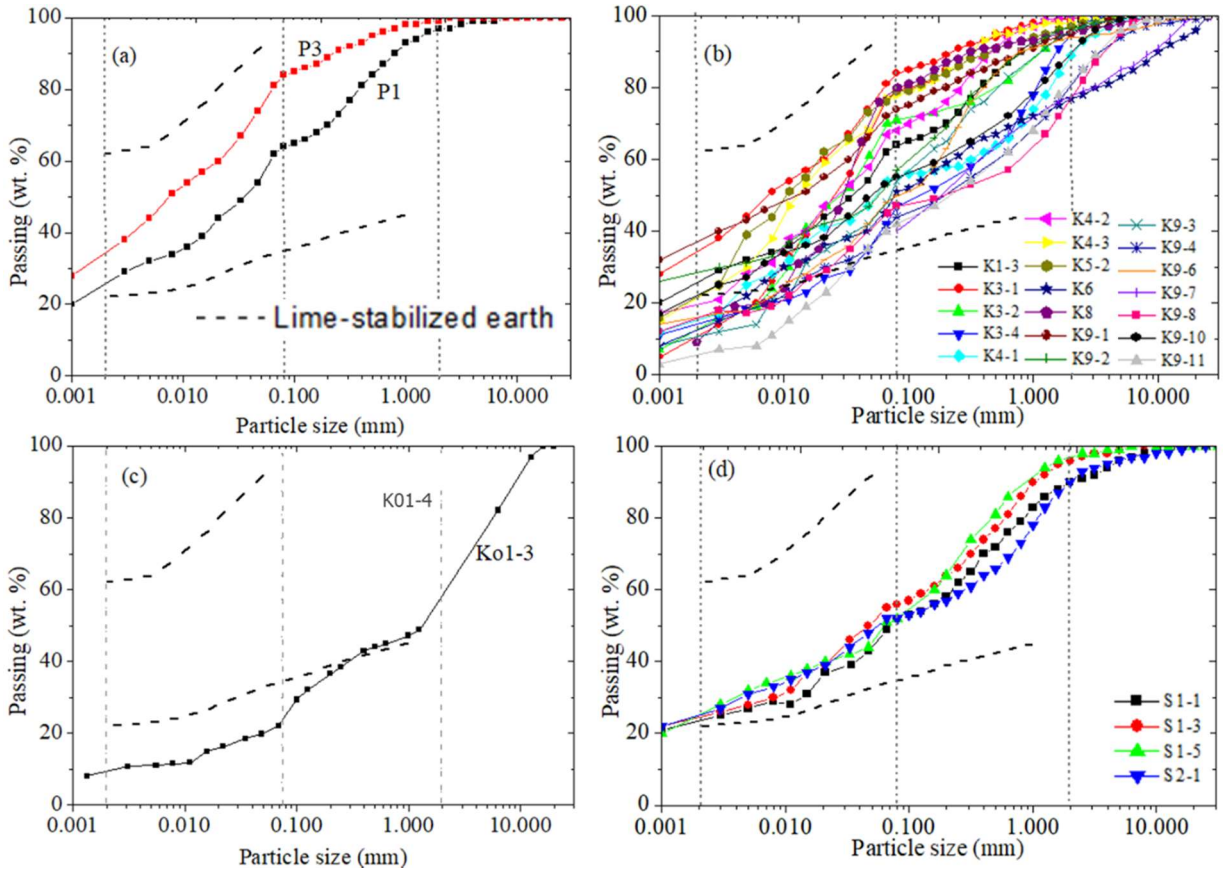

Figure 3.7. Particle size distribution of bulk samples from the four studied sites: (a) P=Pabre, (b) K=Kamboinse, (c) Ko=Kossodo, (d) S=Saaba. Comparison with CRATerre boundaries recommended for lime-stabilization of earthen materials (Houben and Guillaud 2006)

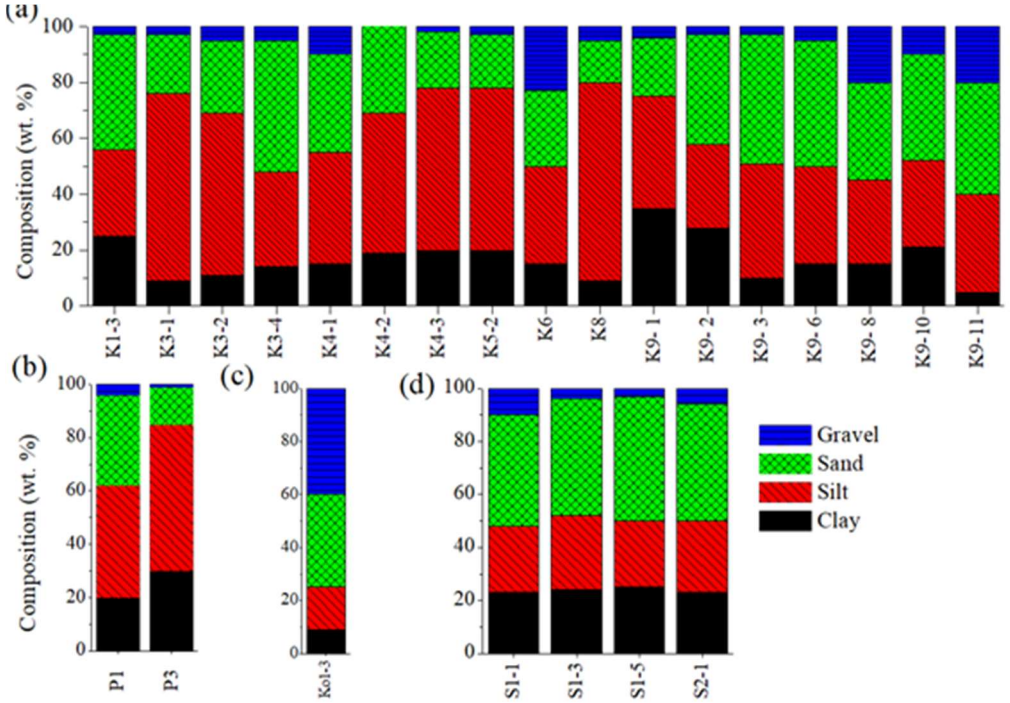

Figure 3.8. Fractions of particle size of the bulk samples from the four studied sites: (a) K=Kamboinse, (b) P=Pabre, (c) Ko=Kossodo, and (d) S=Saaba

Samples from Pabre contain the highest fraction of clay particles, while Kamboinse, Saaba and Kossodo respectively contain the highest fractions of silt, sand and gravel particles. In term of total fraction of fine particles (<0.08 mm), Pabre contains the highest fraction (60-85%), followed by Kamboinse (50-80%), Saaba (~50%) and Kossodo (~25%). It is noteworthy that Saaba has relatively homogeneous PSD, while Kamboinse has the most heterogeneous PSD.

3.3.2. Plasticity limits

Figure 3.9 presents the relationship between plasticity index (PI) and limit of liquidity (LL) for all samples. The plasticity behaviors vary from medium to high plastic silt (under the A-line) and medium to high plastic clay (above the A-line). The clay materials from Pabre are characterized by PI of 20 and LL of 35-40 (Figure 3.9a). The PI and LL of the clay materials from Kamboinse vary between 10-25 and 40-65, respectively, except for K3-1 and K8 (PI: 35, LL: 60) (Figure 3.9b). The sample from Kossodo has PI of 15 and LL of 40 (Figure 3.9c). The clay materials from Saaba have PI of 10-20 and LL of 45-55 (Figure 3.9d). These results suggest that the clay materials from Pabre behave as clay of medium plasticity, the materials from Kamboinse and Saaba as silt-clay and silt of medium to high plasticity, respectively, and Kossodo as silt-clay of medium plasticity.

The clayey behavior of the materials from Pabre ($PI \geq 20$, $LL > 30$) agrees with the high content of fine particles (60-85% of clay and silt) and gives them high cohesion. Similarly, clay materials from Kamboinse have medium to high cohesion given their silt-clay behavior (PI more or less than 20 and $LL > 30$) and high fraction of fine particles (50-80%). Kossodo and Saaba both have $PI < 20$ and small fraction of fine particles (< 50%), thus a medium cohesion (Houben and Guillaud 2006). Moreover, clay materials from Pabre and Kossodo have the plasticity mostly close to that recommended for earth construction (XP P 13-901 2001). Therefore, they would be more suitable for production of unstabilized CEBs. Clay materials with high cohesion and continuous PSD would be suitable for production of CEBs with interesting physical stability and mechanical performances.

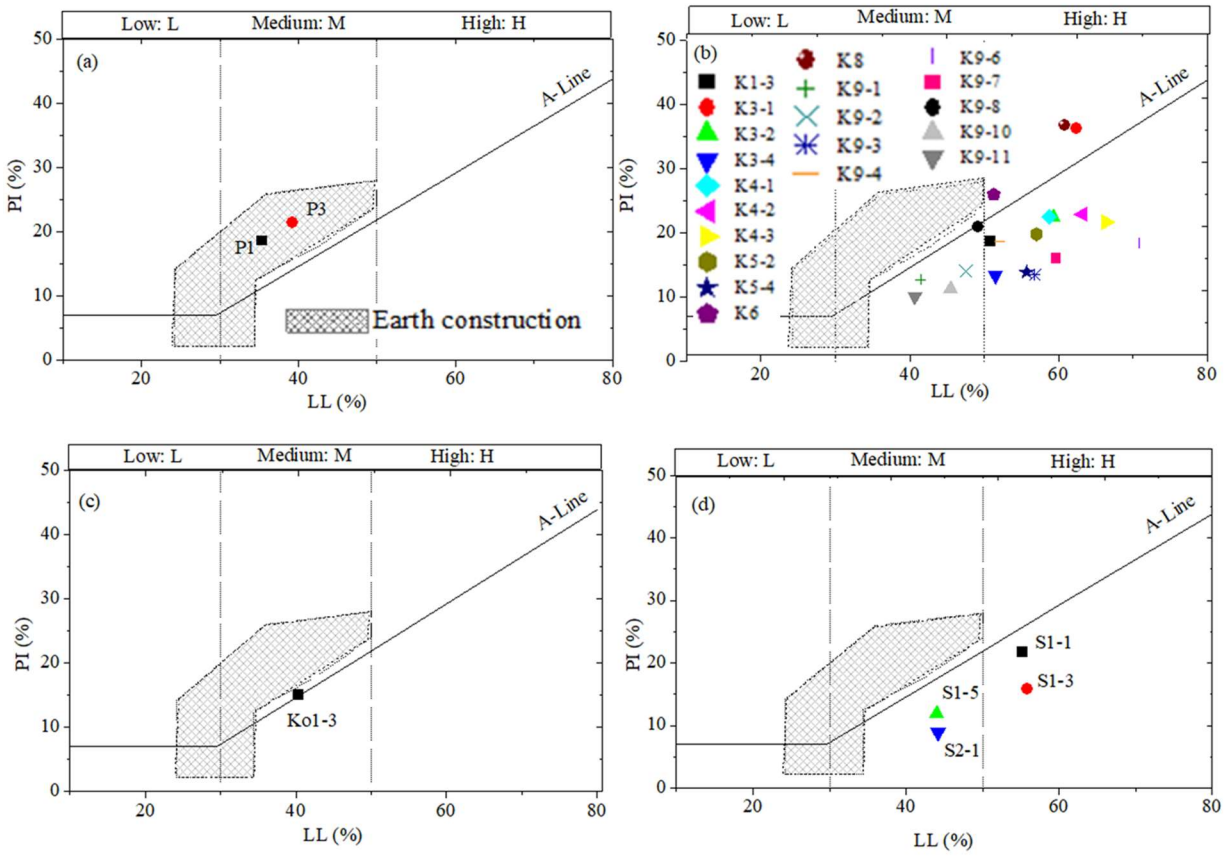

Figure 3.9. Plasticity of bulk samples from the four studied sites: (a) P=Pabre, (b) K=Kamboinse, (c) Ko=Kossodo, and (d) S=Saaba. Comparison with the boundaries recommended for earthen construction (XP P 13-901 2001)

3.3.3. Chemical composition

The chemical composition of selected samples from different sites mainly consists of silica (SiO_2), alumina (Al_2O_3) and iron oxide (Fe_2O_3) and traces of CaO, MgO, Na_2O, K_2O (Table 3.4). The samples from Kamboinse, Kossodo and Saaba basically contain 40-60% of silica, 20-30% of alumina and 0-15% of iron (III) oxide. The sample from Pabre (P1) contains the highest fraction of silica (~75%) and the lowest fraction of alumina (~11%) compared to other sites. The contents of oxides in samples from Kamboinse, Kossodo and Saaba are consistent with the chemical composition of kaolinite-rich clay minerals (Tsozué et al. 2017). The occurrence of CaO, MgO, Na_2O, K_2O in trace reflects the unlikely presence of high swelling clay minerals such as smectite (Lorentz et al. 2018).

The content of iron (III) oxide (0-15%) can be related to the increasing reddish brown color which may suggest the presence of goethite. The ratio of SiO_2/Al_2O_3 generally varied between 2 to 3, apart from exceptional samples such as P1 (6.6), K3-1 (1.6) (Table 3.4). This ratio reveals the difference in mineral content, where the highest ratio can be related to the highest content

of quartz and *vice versa* (Nkalih Mefire et al. 2015). For most samples, the range of variation of LOI 1000 between 8-12% (except P1, LOI 1000°C = 5.5%) reveals the presence of mainly hydrated minerals such as clay and goethite (Nkalih Mefire et al. 2015). High ratio of SiO_2/Al_2O_3 (>3) and low LOI 1000°C (5.5%) in sample from Pabre (P1) rather suggest an important contribution of quartz and low content of clay minerals (Nkalih Mefire et al. 2015, Abdelmalek et al. 2017). Moreover, Table 3.4 shows that the sum of $SiO_2+Al_2O_3+Fe_2O_3$ >75% which agrees with the recommendations for stabilized CEBs (Murmu & Patel 2018).

Table 3.4. Chemical and mineral composition of selected samples from the four studied sites

Chemical composition of selected samples (%)								
Oxides		Kamboinse			Pabre	Kossodo	Saaba	
		K3-1	K5-4	K9-1	P1	Ko-4	S1-1	S2-1
SiO_2		42.9	63.7	49.7	76.9	55.0	53.5	60.9
Al_2O_3		27.3	23.3	24.0	11.7	23.4	24.7	27.6
Fe_2O_3		15.7	2.3	13.0	3.8	8.1	9.7	0.6
CaO		0.1	0.1	0.6	0.2	0.1	0.1	0.1
TiO_2		1.4	0.5	0.9	0.9	1.2	0.9	0.0
MnO		0.1	0.0	0.0	0.1	0.0	0.0	0.0
MgO		0.1	0.0	0.1	0.0	0.0	0.0	0.0
Na_2O		0.0	0.0	0.0	0.0	0.0	0.0	0.0
K_2O		0.1	0.3	0.2	0.8	2.3	0.1	0.1
P_2O_5		0.1	0.0	0.1	0.0	0.1	0.0	0.0
Total LOI (1000°C for 2 hours)		12.1	9.7	11.3	5.7	9.8	10.9	10.6
Total oxides		100	100	100	100	100	100	100
SiO_2/Al_2O_3 ratio		1.6	2.7	2.1	6.6	2.4	2.2	2.2
$SiO_2 + Al_2O_3 + Fe_2O_3$		85.9	89.3	86.8	92.4	86.5	87.9	89.2
TGA mass loss: 200-400°C		-0.8	-0.6	-1.3	-0.8	-1.3	-1.3	-0.4
TGA mass loss: 450-650°C		-9.4	-7.3	-7.9	-3.4	-6.8	-7.9	-8.9
Mineral composition of selected samples (%)								
Methods	Minerals	K3-1	K5-4	K9-1	P1	Ko1-4	S1-1	S2-1
A: XRD (powder & oriented aggregate)	Quartz	11	31	29	61	30	31	14
	Goethite	6	12	12	0	12	9	3
	Hematite	9	0	5	0	0	2	0
	K-feldspar	0	0	0	8	19	0	0
	Plagioclase	0	0	0	0	0	0	0
	Mica	0	3	0	0	2	0	2
	Rutile	0	0	0	0	1	0	0
	Total clay minerals	74	54	54	31	36	58	81
	Clay minerals							
	Kaolinite	69	47	53	29	35	58	78
	Illite	5	7	1	2	1	0	3
	Total: Method A	100	100	100	100	100	100	100
B: TGA (weight loss)	Goethite (200-400°C)	8	6	13	8	12	12	4
	Kaolinite (450-650°C)	67	53	57	24	49	56	64
C: XRF (chemical analysis)	Illite	1	3	2			1	1
	K-feldspar				5	13		
	Plagioclase	1	1	3	1	1		
	Kaolinite	70	55	58	26	52	61	67
	Quartz	11	35	22	60	22	25	28
	Goethite	8	6	13	8	12	12	4
	Hematite	9		2		1	1	
	Total: Method C	100	100	100	100	100	100	100

3.3.4. Mineral composition

The XRD spectra of bulk samples selected from the four studied sites mainly revealed the diagnostic reflection of clay mineral (4.47 Å), kaolinite (7.15 Å), quartz (3.34 Å), goethite (2.44 Å), hematite (2.69 Å) and traces of K-feldspars and illite (Figure 3.10a). The spectra of oriented aggregates confirm the predominance of kaolinite and some traces of illite (Figure 3.10b). The reflection of kaolinite clay appeared at 7.15 Å on air-dried and glycolated samples and disappeared on heat treated samples at 500°C for 4 h, while that of illite appeared at 10 Å and remained throughout all treatments (Bergaya et al. 2006 in Fagel et al. 2003).

a

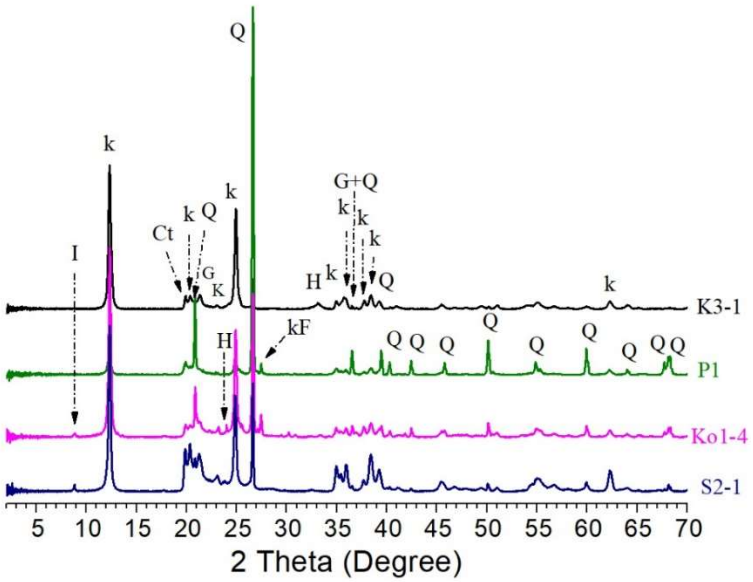

b

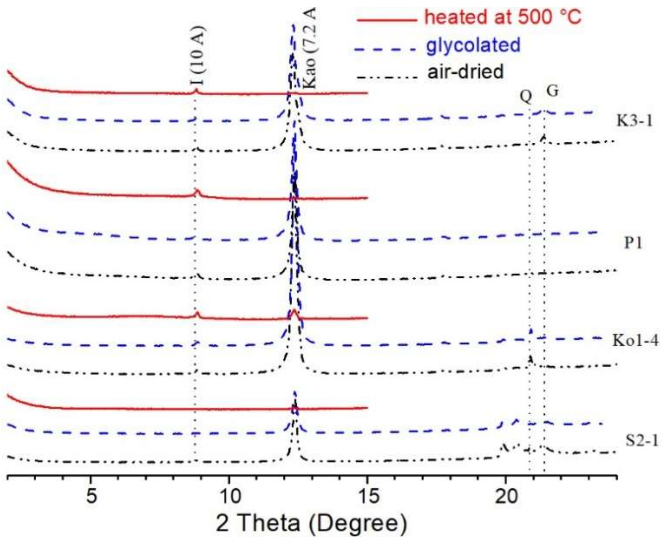

Figure 3.10. XRD patterns of selected (a) bulk samples and (b) oriented aggregates from the studied sites: K=Kamboinse, P=Pabre, Ko=Kossodo, S=Saaba, Ct= total clay, k/kao=kaolinite, I= Illite, Q= quartz, kF=K-feldspar, G= goethite

Figure 3.11 presents the thermogravimetric analysis (TGA) of selected samples from different sites. The samples recorded important loss of mass around 550°C (i.e., between 450 and 650°C) corresponding to the dehydroxylation of kaolinite (Földvári 2011). At this temperature range, sample S2-1 recorded the highest loss of mass (9%), while P1 recorded the lowest loss of mass (3.33%). This confirms that S2-1 and P1 respectively contain the highest and lowest fraction of kaolinite.

The thermal removal of hydroxyl groups in kaolinite was previously reported around 530-590°C, depending on the degree of crystallinity (Földvári 2011, Al-Mukhtar et al. 2012, Nkalih Mefire et al. 2015). The early onset of the dehydroxylation can be related to poorly ordered structure of kaolinite (Lorentz et al. 2018). The TGA/D-TGA displays the peak of dehydroxylation of kaolinite in samples P1 and Ko1-4 at lower temperature (525-535°C) compared to other samples (550°C) (Figure 3.11). This suggests that the sample form Pabre not only contains the lowest content of kaolinite but also, similarly to Kossodo, the kaolinite is poorly ordered relatively to other samples.

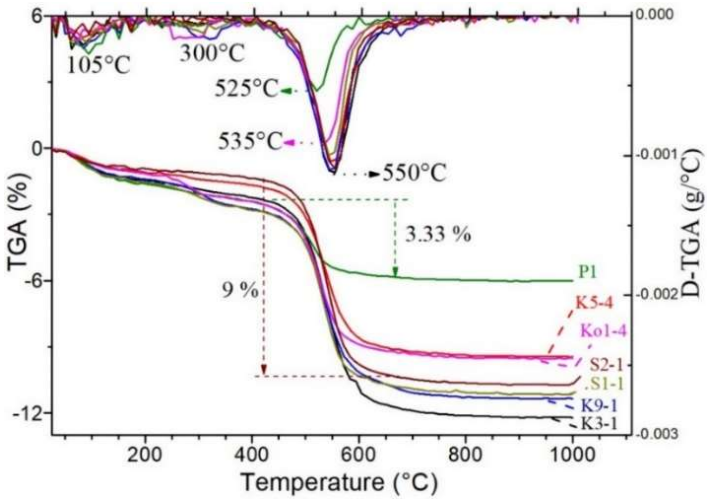

Figure 3.11. Thermogravimetric analysis (TGA) and derivative thermogravimetric analysis (D-TGA) of bulk samples selected from the studied sites: K=Kamboinse, P=Pabre, Ko=Kossodo, S=Saaba

The semi-quantitative estimation (XRD) of the mineral composition of bulk samples confirmed the predominance of clay minerals and quartz, with minor goethite, hematite, K-feldspar and traces of mica, plagioclase and rutile (Figure 3.12). The mineral composition widely varied from one site to another. The clay materials from Kamboinse contain 40-75% of clay minerals, 5-40% of quartz, 0-20% of goethite, <10% of hematite (Figure 3.12a). Pabre contains 30-35% of clay minerals, 40-60% of quartz, < 5% of goethite, <5% of hematite, and <10% of K-feldspar (Figure 3.12b).

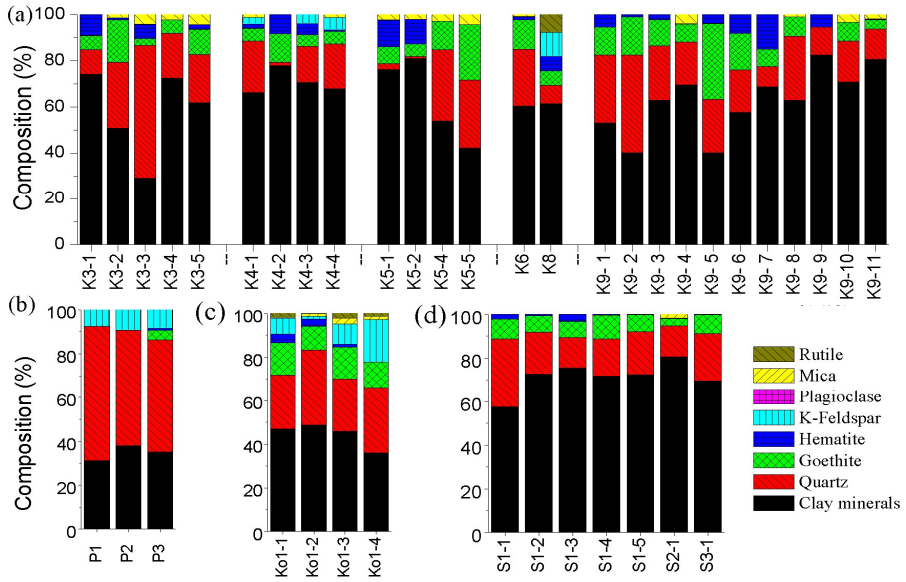

Figure 3.12. Semi-quantitative analysis of bulk samples from the studied sites estimated by XRD powder diffraction (i.e. method A): K=Kamboinse, P=Pabre, Ko=Kossodo, S=Saaba.

Kossodo is characterized by 35-50% of clay minerals, 25-35% of quartz, <15% of goethite, <5% of hematite and <20% of K-feldspar (Figure 3.12c). Saaba contains 60-80% of clay minerals, 15-30% of quartz, <10% of goethite and <5% of hematite (Figure 3.12d). Saaba contains the highest fraction of clay minerals (60-80%) and lowest fraction of quartz (15-30%). By contrast, Pabre contains the lowest fraction of clay minerals (30-35%) and highest fraction of quartz (40-60%). Kamboinse and Kossodo have medium composition of clay minerals. The mineral composition of Kamboinse is the most heterogeneous amongst the studied sites.

Table 3.4 comparatively summarizes the chemical and mineral composition of selected samples from different sites using different methods. It shows that kaolinite is the main clay mineral accompanied by traces of illite (±5%). The kaolinite content determined from TGA (Method B) is in good agreement (within ±5%) with XRF (Method C), while the content estimated by XRD (Method A) differs up to ±10%. As an exception for the sample Ko1-4 from Kossodo, the content of kaolinite significantly differs for XRD (35%) and TGA or XRF methods (49 or 52%). This difference can be related to the possible disorder in the structure of kaolinite from Ko1-4, as suggested by TGA, the fraction of poorly ordered kaolinite is not detected by XRD.

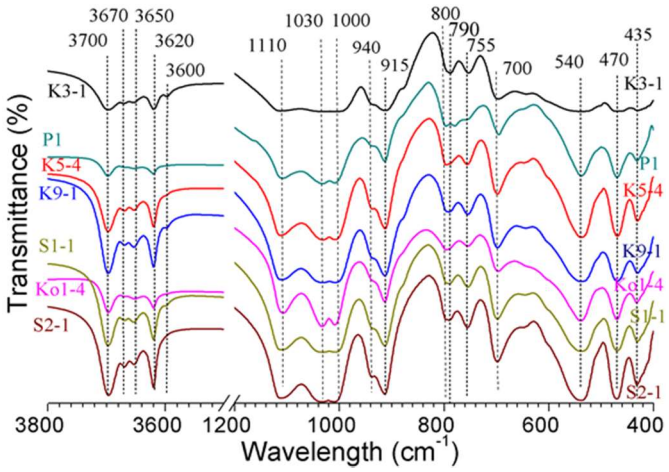

Figure 3.13. FTIR spectra of bulk samples of clay materials selected from the studied sites: K=Kamboinse, P=Pabre, Ko=Kossodo, S=Saaba

The FTIR confirmed the predominance of kaolinite and quartz minerals (Figure 3.13). Intense transmittance bands detected at 3700, 3670, 3652 and 3620 cm^{-1} are related to the stretching of hydroxyl groups in kaolinite, while the mild band at 3600 cm^{-1} is related to illite (Bich et al. 2009). Bands at 1110, 1030 and 1000 cm^{-1} correspond to the vibration of Si-O bonds, at 940 and 915 cm^{-1} to vibration of Al-OH bonds in kaolinite (Bich et al. 2009, Tsozué et al. 2017, Lorentz et al. 2018). The bands at 790 and 755 cm^{-1} correspond to the vibration of Si-O-Al, while bands around 540 cm^{-1} and 470 cm^{-1} respectively correspond to the stretching of Si-O-Al and Si-O bonds of kaolinite (Bich et al. 2009).

The bands in the ranges of 3700-3620 cm^{-1} are useful for qualitative assessment of the structure of kaolinite. This is in a sense that well-defined bands represent well-ordered kaolinite and the disappearance of the band at 3670 cm^{-1} represents poorly ordered kaolinite (Bich et al. 2009, Tironi et al. 2012, Tsozué et al. 2017, Lorentz et al. 2018). Samples K9-1 and K5-4 (from Kamboinse), S1-1 and S2-1 (from Saaba) present intense and well-defined diagnostic bands of kaolinite (3700-3620 cm^{-1}). By contrast, K3-1, P1 and Ko1-4 (from Kamboinse, Pabre and Kossodo, respectively) recorded low intensities. The contents of kaolinite in samples K3-1, P1, and Ko1-4 estimated from TGA are respectively 67%, 24% and 49% (Table 3.4). This suggests that the disappearance of the bands at 3650 and 3670 cm^{-1} cannot only be related to the low content of kaolinite in P1, but also to the poor order of kaolinite in K3-1and Ko1-4. This agrees with the early onset of dehydroxylation of kaolinite in P1 and Ko1-4 observed in TGA/D-TGA.

The mild intensity of vibration band at 940 cm^{-1} for K3-1 and Ko1-4 samples is also consistent with a poorly ordered clay mineral (Tsozué et al. 2017, Lorentz et al. 2018). Additionally, the lack of well resolved bands at 1110-1000 cm^{-1} and 540 cm^{-1} in sample K3-1 suggests the

presence of defects in Si-O and Si-O-Al bonds of kaolinite. The occurrence of poorly ordered kaolinite suggests the suitable for pozzolanic reaction with lime (Al-Mukhtar et al. 2012, Tironi et al. 2012, Nagaraj et al. 2014, Lorentz et al. 2018).

3.4. Suitability of clay materials for the production of stabilized CEBs

3.4.1. Effect of the type of clay materials on the reactivity with CCR

The initial pH of the solutions of clay materials (<400 µm) was 8.5 for Kamboinse, 6.1 for Pabre, 5.2 for Kossodo, and 5.5 for Saaba. After 1 hour of addition of only 2 % CCR, the pH reached the apparent maximum values of 11.7 for Kamboinse, 11.4 for Pabre, 11.3 for Kossodo, and 11.4 for Saaba, compared to the pH of 11.6 for the solution of 2 % CCR alone. It suggests that 2 % CCR is enough to satisfy the short term modification and increase the pH of all clay materials (Eades and Grim 1996). This is related to the predominance of low activity clay mineral, kaolinite, in all clay materials. Therefore, more than 2 % CCR would be necessary for triggering and sustaining the long term pozzolanic reaction in all clay materials (Al-Mukhtar et al. 2010a, 2010b). Moreover, the pH of mix solution of CCR alone remained quasi-constant, while the pH of different mix solution of clay materials and 10 or 20 % CCR slightly decreased, at similarly rate, over the curing time (Figure 3.14).

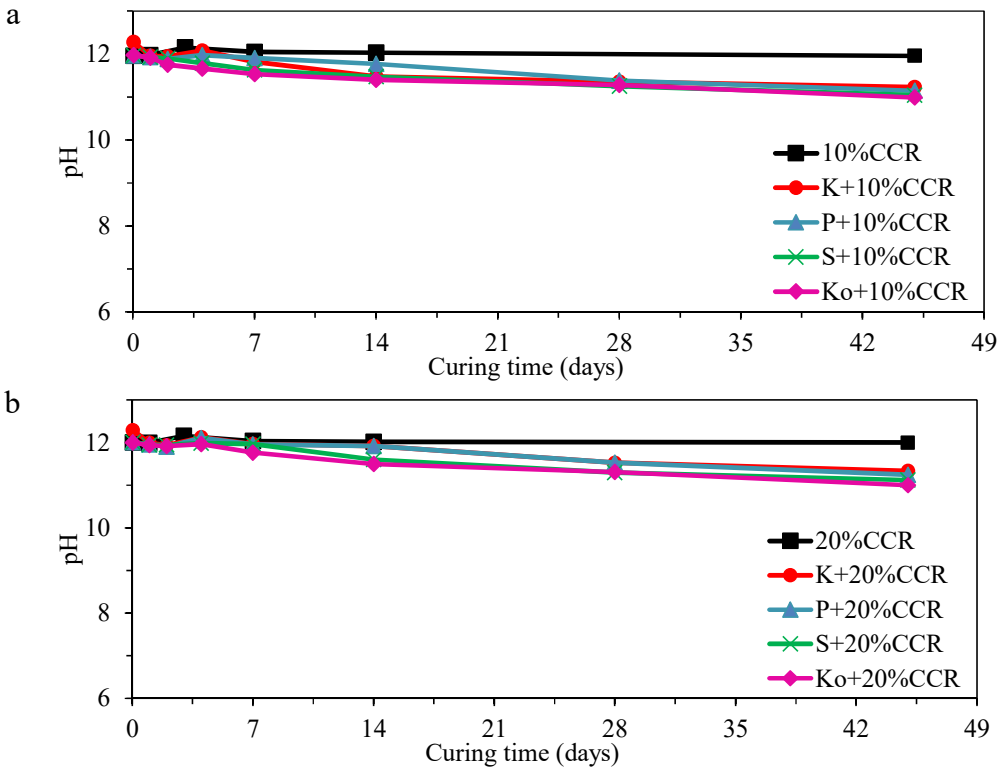

Figure 3.14. Evolution of pH in mix solutions of clay materials (<400 µm) and (a) 10 % CCR, (b) 20 % CCR: K= Kamboinse, P= Pabre, Ko= Kossodo, S= Saaba

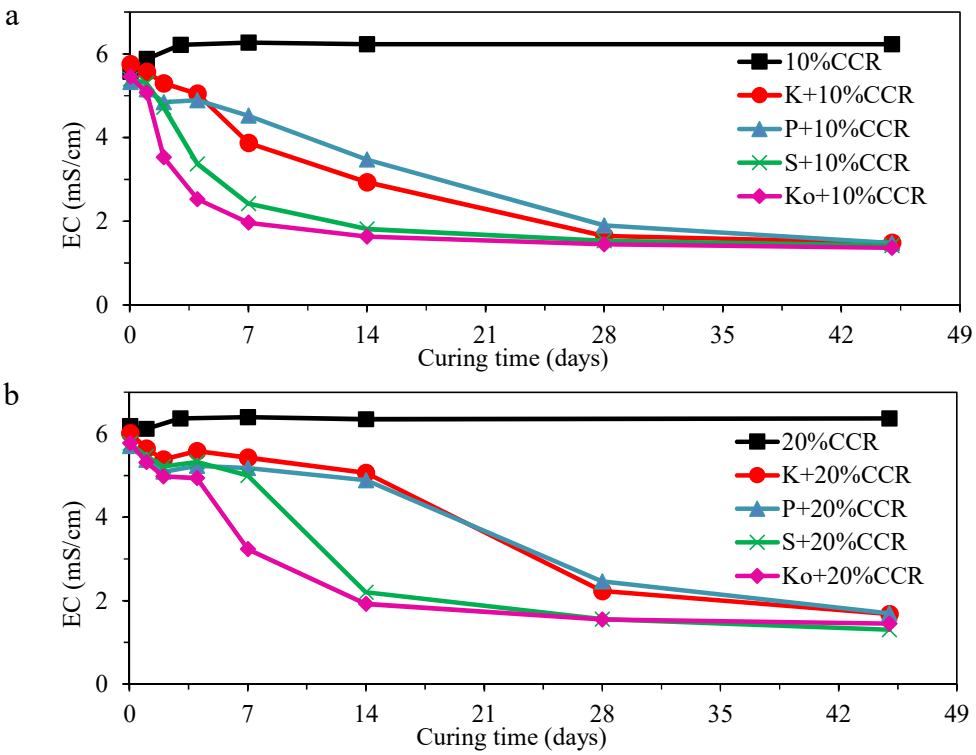

Figure 3.15. Evolution of electrical conductivity (EC) in mix solutions of clay materials (<400 µm) and (a) 10 % CCR, (b) 20 % CCR

Figure 3.15 shows the evolution of the electrical conductivity (EC) of the mix solutions containing the clay materials and 10 or 20 % CCR over the curing time at controlled temperature (40 °C). Note that the EC of the solution of the clay materials alone was less than 0.1 millisiemens/cm (mS/cm) over time, while that of the solutions of CCR alone was greater than 6.3 mS/cm. Figure 3.15a and b show that the initial EC (after 1 hour) of the clay materials mixed with 10 % and 20 % CCR respectively reached at least 5.8 mS/cm and 6.0 mS/cm. The dissolution of portlandite ($Ca(OH)_2$) from CCR into Ca^{2+} and OH^- was responsible for the drastic increase of the initial pH and EC (Al-Mukhtar et al. 2010).

The EC of all mix solutions decreased over the curing time, at similar rate in the first 3 days, after which a clear difference was recorded for different clay materials and CCR contents (Figure 3.15). For mixtures containing 10 % CCR, the clay materials from Saaba (S) and Kossodo (Ko) recorded the highest rate of decrease of EC compared to Kamboinse (K) and Pabre (P) between the 3rd and 14th day. This resulted in reaching the apparent minimum EC (about 2 mS/cm) after 14 days of curing for Kossodo and Saaba and 28 days for Kamboinse and Pabre (Figure 3.15a). For mixtures containing 20 % CCR, similar evolution of the EC was observed, with the EC of Kamboinse and Pabre delaying until the 14th day before starting to decrease and reaching the apparent minimum value of EC after 28 days (Figure 3.15b). For

both CCR contents, the EC reached the minimum value after 28 days for all clay materials, no substantial decrease of EC was recorded between the 28th and 45th day.

The decrease of the EC is explained by the consumption of Ca^{2+} and OH^- during the pozzolanic reaction of CCR with the clay materials (Al-Mukhtar et al. 2010).The minimum EC in mix solutions can be related to the end of consumption of Ca^{2+} and occurrence of optimum maturity of the pozzolanic reaction. Therefore, the clay materials from Kossodo and Saaba have better reactivity, given the early and rapid rate of consumption of the Ca^{2+}, than the materials from Kamboinse and Pabre. The reactivity of clay materials from Saaba and Kossodo can respectively be related to their relatively high content and poorly ordered kaolinite, as shown by XRD, TGA and FTIR (§3.3.4).

In fact, the pozzolanic reaction involves the aluminosilicate minerals such as kaolinite and eventually fine quartz from the clay materials and lime ($Ca(OH)_2$) from the CCR (Mechti et al. 2012, Ciancio et al. 2014). This is highly dependent on the particle fineness and content of reactive constituents and degree of order in their structure, with finer and poorly ordered materials presenting better reactivity (Tironi et al. 2012).

3.4.2. Effect of the type of clay materials on physico-mechanical properties of stabilized CEBs

Figure 3.16 presents the evolution of the average compressive strength of CEBs produced with the clay materials from different sites stabilized with 0, 10, or 20 % CCR, cured at 40 °C for 45 days. It was compared with the compressive strength of 4 MPa and 6 MPa required for the construction of two or three-storey buildings (CDI and CRATerre-EAG 1998). The average compressive strength of CEBs which do not contain CCR (unstabilized/control) was 1.1 MPa for Kamboinse, 2 MPa for Pabre, 1.4 MPa for Kossodo and 0.8 MPa for Saaba (Table 3.4). The compressive strength of unstabilized CEBs is basically related to the cohesion behavior as well as the granular distribution of the clay materials. In fact, Pabre which was characterized as highly cohesive material (§3.3.2) recorded the highest average compressive strength (2 MPa) compared to other sites which have medium cohesion. This suggests that only unstabilized clay material from Pabre are likely to produce ordinary CEBs for construction of single-storey (non-load-bearing) building, according to ARS 674:1996 (CDI and CRATerre-EAG 1998).

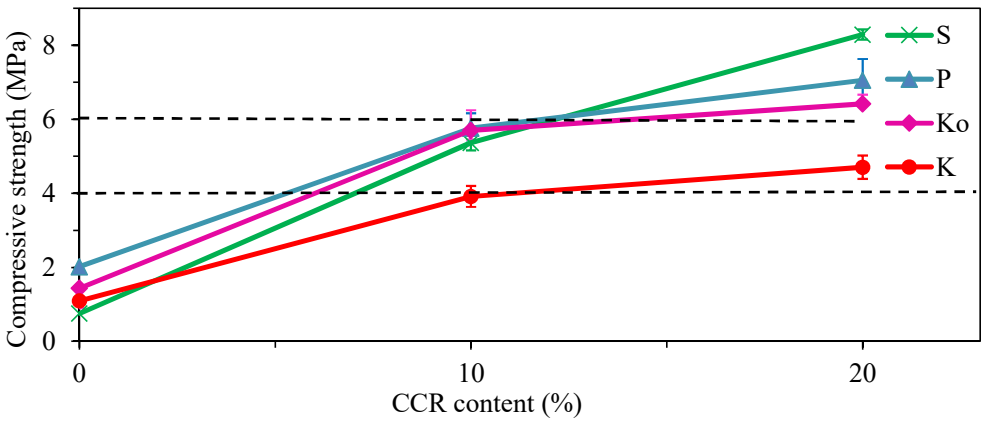

Figure 3.16. Evolution of dry compressive strength of the CEBs made of clay materials from different sites stabilized with CCR cured for 45 days: K= Kamboinse, P= Pabre, Ko= Kossodo, S= Saaba

The average compressive strength of the CEBs was substantially improved by stabilization with 10 % or 20 % CCR (Figure 3.16). The addition of 20 % CCR resulted in increasing the compressive strength, with respect to the control (0 % CCR), more than 3.3 times (1.1 to 4.7 MPa) for Kamboinse, 2.6 times (2 to 7.1 MPa) for Pabre, 3.5 times (1.4 to 6.4 MPa) for Kossodo and 10 times (0.8 to 8.3 MPa) for Saaba (Table 3.4). Saaba not only recorded the highest compressive strength (8.3 MPa) after stabilization with 20 % CCR, but also the similar rate of improvement of the strength in the ranges of 0-10 % and 10-20 % CCR. By contrary other sites presented reduced improvement beyond 10 % CCR (Figure 3.16).

This suggests that the compressive strength of clay material from Saaba can further be improved by addition of more than 20 % CCR, while it would likely tend to the optimum beyond 20 % CCR for other sites. Additionally, the average compressive strength of CEBs from Kossodo, Pabre and Saaba stabilized with 10 % CCR is greater than 4.5 MPa of the CEBs stabilized with 10 % geopolymer (Sore et.al 2018). The compressive strength of CEBs from Saaba stabilized 20 % CCR is comparable to 8.5 MPa of CEBs stabilized 20 % geopolymer or 8-10 % cement (Walker & Stance 1997, Sore et.al 2018).

The improvement of the compressive strength with the addition of CCR is related to the pozzolanic reaction between the clay materials and CCR. This reaction was previously responsible for the formation of cementitious products such as CSH and CAH for binding the matrix of stabilized CEBs (Al-Mukhtar et al. 2012). The reactivity of different clay materials (§3.4.1) is partly responsible for the difference in the improvement of the compressive strength of CEBs. Clay materials which recorded the highest rate of pozzolanic reactivity (Saaba and Kossodo) recorded the highest rate of improvement of compressive strength. Therefore, clay

materials which would not fit for production of unstabilized CEBs can rather be used for production of stabilized CEBs.

Moreover, some physical properties such as bulk density and total void ratio can have impact on the mechanical performance of CEBs. Table 3.4 shows that the bulk density of CEBs stabilized with 0-20 % CCR ranged in 1800-1600 kg/m^3 for the clay materials from other sites than Kossodo which has 2000-1800 kg/m^3. This is related to the high optimum water content (OMC) required for achieving appropriate consistency for the production of stabilized CEBs which evolved between 16-22 %, except for Kossodo (13-17 %), with the addition of 0-20 % CCR. The OMC increases with the plasticity and fraction of the fine particles of clay materials and addition of CCR. , After curing and drying, this resulted in increasing total void ratio in the range of 32-40 % for stabilized CEBs, except for Kossodo (30-34 %) (Table 3.4).

The low OMC required for the material from Kossodo can be explained by its lower content of fine particles (clay and silt) and higher content of gravel compared to other sites (§3.3.1). This is partly responsible for the relatively higher bulk density of CEBs produced from Kossodo. Additionally, the relatively higher bulk density can be related to the relatively higher specific density (2.9) of the clay materials from Kossodo compared to other sites (2.6-2.7). Therefore, the earthen materials that have higher specific density (containing heavier minerals such as goethite and hematite) would produce CEBs of higher bulk density. Similarly, the materials which have lower plasticity would require lower OMC for the production of stabilized CEBs, thus reaching lower porosity (higher bulk density).

Table 3.5. Physico-mechanical properties of stabilized CEBs produced from four studied sites

Clay materials	*CCR content (wt%)	**OMC (wt%)	Dry compressive strength (MPa)	Bulk density (kg/m^3)	Total void ratio (%)
Kamboinse	0	17	1.1 (±0.4)	1800 (±12)	34.5 (±0.5)
	10	19	3.9 (±0.3)	1666 (±11)	38.8 (±0.4)
	20	22	4.7 (±0.3)	1624 (±9)	39.8 (±0.3)
Pabre	0	16	2.0 (±0.5)	1805 (±10)	32.1 (±0.6)
	10	18	5.8 (±0.4)	1729 (±5)	35.4 (±0.4)
	20	20	7.1 (±0.6)	1629 (±8)	38.0 (±0.3)
Kossodo	0	13	1.4 (±0.4)	2036 (±17)	30.0 (±0.8)
	10	15	5.7 (±0.5)	1892 (±15)	34.0 (±0.5)
	20	17	6.4 (±0.2)	1849 (±26)	34.6 (±0.9)
Saaba	0	18	0.8 (±0.3)	1646 (±15)	38.1 (±0.4)
	10	20	5.4 (±0.2)	1617 (±31)	38.8 (±1.2)
	20	22	8.3 (±0.1)	1613 (±9)	38.6 (±0.3)

*CCR : Mass percent of CCR with respect to the dry mass of the clay material

**OMC: Optimum moisture content, with respect to the dry mass of clay material + CCR, required for achieving the maximum dry density

(…) The values in parentheses are standard deviation

The bulk density of CEBs stabilized with 10 % CCR is lesser than 1775 Kg/m^3 of CEBs stabilized with 10 % geopolymer or cement, except for the materials from Kossodo (Sore et. al 2018). This points out the structurally benefit to stabilize the CEBs with CCR which can provide similar or better mechanical performance and lower dead load than cement stabilized CEBs. Furthermore, the decrease of the bulk density of CEBs stabilized with CCR would potentially decrease their thermal conductivity and possibly contribute to the improvement of the thermal comfort in the building (Sore et. al 2018). It is also noteworthy that denser and lesser porous CEBs are more likely to have better durability performances such as resistance to water absorption and erosion (Bogas et al. 2018).

The results from this study suggest that all the clay materials investigated from the four sites stabilized with 20 % CCR, cured for 45 days at 40±2°C, are suitable for the production of ordinary stabilized CEBs for construction of tree-storey building except Kamboinse which is suitable for two-storey building. This is regardless whether the parameters of texture and plasticity of the clay materials fit in the recommended boundaries guidance. Nevertheless, further studies should assess the engineering and long-time durability of stabilized CEBs produced and cured in ambient conditions.

3.5. Summary and conclusions

This chapter discussed the results from the characterization of physico-chemical and mineral compositions of CCR, RHA, and clay materials for their suitability to produce stabilized CEBs. The CCR is constituted with fine particles, <125 µm after grinding, and mainly contains portlandite (43-53 % of $Ca(OH)_2$) essential for its reactivity and carbonates (40 %). The RHA produced by calcination at soaking temperature of 500 °C for 2 hours is finer than the CCR, <80 µm after grinding, and is the most reactive (89 % soluble RHA) among others. The Okra bast fiber presents large variation of tensile strength (346 ±197 MPa).

The characterizations of clay materials showed that Pabre and Kossodo respectively contain the highest (20-30 %) and lowest (<10 %) fraction of clay particles. The material from Kamboinse behaves as medium to high plastic clay-silt, Pabre as medium plastic clay, giving it high cohesion, Kossodo as medium plastic clay-silt and Saaba as medium to high plastic silt.

The material from Saaba contains the highest fraction of clay minerals (60-80 %), mainly kaolinite, followed by Kamboinse (40-75 %), while Pabre contains the highest fraction of quartz (40-60 %). Although Kossodo contains medium fraction of clay minerals (35-50%),

different independent analyses suggested that it contains kaolinite which is poorly ordered than the materials from other sites. Moreover, the clay materials from Kossodo as well as Saaba recorded the earliest and highest rate of pozzolanic reactivity with CCR. This reactivity was assessed on the basis of the evolution of the electrical conductivity and consumption of Ca^{2+} in mix solutions of earth-CCR, reaching the apparent maturity in 28 days of curing at 40±2 °C.

The relatively high cohesion of clay material from Pabre allows to produce unstabilized CEBs which have the highest compressive strength (2 MPa) compared to Kamboinse (1.1 MPa), Kossodo (1.4 MPa) and Saaba (0.8 MPa). Additionally, the compressive strength of CEBs remarkably improved by stabilization with 20 % CCR, cured at 40±2 °C for 45 days, reaching 7.1 MPa for Pabre, 4.7 MPa for Kamboinse, 6.4 MPa for Kossodo and 8.3 MPa for Saaba.

The highest improvement of the compressive strength of stabilized CEBs from Saaba and Kossodo corroborated with the highest rate of pozzolanic reactivity with CCR. This reactivity is related to the highest content and/or poorly ordered structure of kaolinite in the clay materials from Saaba and Kossodo. In addition, the clay material from Kossodo recorded the highest bulk density (2000-1800 kg/m^3) and lowest void ratio (30-34 %) related to the low plasticity and fraction of fine particles and high specific density compared to other sites.

The result shows that, in the above conditions, the clay materials from all studied sites are suitable for the production of stabilized CEBs (10-20 % CCR), which reach the compressive strength of 4 MPa required for bearing load in the walls of two-storey building. This suggests that clay materials which would not be suitable for the production of unstabilized CEBs can be suitable for the production of stabilized CEBs. It also reveals that the selection of clay materials for the production of stabilized CEBs based on only the texture and plasticity may be misleading to leave out the materials which would be suitable considering their reactivity with stabilizers.

Nevertheless, more engineering and durability properties, such as water absorption, compressive strength in dry and wet conditions and thermal properties, erodability, etc should be tested in order to better understand the performances of the stabilized CEBs in conditions of usage. Moreover, the study of technical feasibility should be carried on the viability of exploitation of the largest deposit (Kamboinse), whose volumetric quantity was estimated at 700 000 m^3. Part of these scopes are the subjects of the following chapters (IV & V), which further investigate the engineering and durability performances of stabilized CEBs produced with the clay material form Kamboinse. Hypothetically, the compliance of the clay material

from Kamboinse with the requirements for applications in building construction would suggest the compliance of other studies sites.

CHAPTER:

IV. MICROSTRUCTURAL & ENGINEERING PROPERTIES OF CEBs STABILIZED WITH BY-PRODUCTS

4.0. Microstructural, physico-mechanical and hygro-thermal properties of CEBs stabilized with by-product materials

4.1. Introduction

This chapter presents the results from the investigation of the effects of stabilization using CCR and CCR:RHA and incorporation of Okra fibers on the properties of stabilized CEBs produced from the clay earthen materials from Kamboinse. The aim was to further improve the performances of stabilized CEBs produced from Kamboinse which previously recorded the lowest compressive strength among other sites (Chapter III). It specifically answers to the question "*how does the stabilization using by-products affect the microstructural and engineering properties of CEBs for structural applications, compared to unstabilized and cement-stabilized CEBs?"*

Firstly, the chapter assesses the chemical interactions which take place in the mixtures of earth-CCR-RHA systems to understand the curing process. This was achieved by simply monitoring the evolution of the electrical conductivity and concentration of unconsumed calcium ions in the mix solutions of earth-CCR-RHA. The effects of the interactions on the chemico-microstructural changes in the cured mixtures were analyzed by XRD, TGA and SEM. Secondly, the chemico-microstructural changes and other influencing parameters were related to the physico-mechanical and hygro-thermal properties of stabilized CEBs

4.2. Chemico-microstructural changes in the mixtures of earth, CCR and RHA

4.2.1. Initial pH in mix solutions

The initial pH (before curing) of mix solutions immediately reached the maximum value of 12.4 with the addition of only 2 % CCR (after 1 hour), from a pH of 9.6 for the earthen material (<5 mm) from Kamboinse alone (Figure 4.1). This is explained by the amount of portlandite (43 % of $Ca(OH)_2$) contained in CCR which dissolves into hydroxyl ions (OH^-) and calcium ions (Ca^{2+}); the OH^- is responsible for the increase of the basicity. According to Eades and Grim (1996), the 2 % is the fraction of CCR necessary for affinity saturation of earthen material from Kamboinse.

This is the fraction of CCR responsible for the short term modification of the clay material through cation exchange and flocculation-agglomeration (Al-Mukhtar et al. 2010a, 2010b, 2012). Beyond this fraction, the CCR must contribute in the time dependent pozzolanic

reaction, with the aluminosilicates, responsible for the mineral changes in the mixtures (Al-Mukhtar et al. 2010a, 2010b, 2012). The low cation exchange capacity of kaolinite-rich earthen material, from Kamboinse, was related to the limited occurrence of oxides of alkali and alkaline earth in its chemical composition.

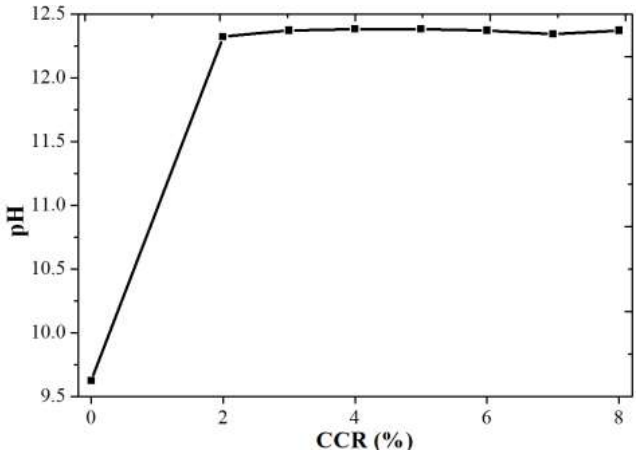

Figure 4.1. Evolution of the initial pH, after 1 hour, in the mix solution of earthen material (<5 mm)-CCR system

4.2.2. Chemical interactions in mix solutions

The chemical interactions in the mix solutions of earth (<5 mm)-CCR-RHA were assessed based on the evolution of electrical conductivity and unconsumed calcium ions. Figure 4.2a shows that the initial electrical conductivity (EC) of mix solutions (at 40 °C) reached ~5.5 mS/cm (millisiemens/cm) and ~6.5 mS/cm (after one day) respectively with addition of 5 % CCR and ≥10 % CCR. The EC was 0.1 mS/cm for the mix solution of earthen material from Kamboinse alone. The elevated EC in solution containing CCR is related to the Ca^{2+} and OH^- from the dissolution of portlandite in CCR. The low EC in the solution of the earthen material (0.1 mS/cm) can also be explained by the limited content of alkali and alkaline earth.

The EC in mix solutions of earthen material and CCR decreased over time, as the curing proceeds, but at different rate depending on the mix composition (Figure 4.2a). Moreover, the concentration of unconsumed calcium ions [Ca^{2+}] in the mix solutions similarly decreased over the curing time (Figure 4.2b). The EC and [Ca^{2+}] reached the apparent minimum values after 45 days of curing in all mix solutions containing earthen material and CCR alone. Nevertheless, the EC and [Ca^{2+}] continuously decreased at the highest rate between the 7^{th} and 45^{th} day for the mix solution containing ≤10 % CCR, while the highest rates were recorded between the 28^{th} and 45^{th} day for the mix containing >10 % CCR (Figure 4.2).

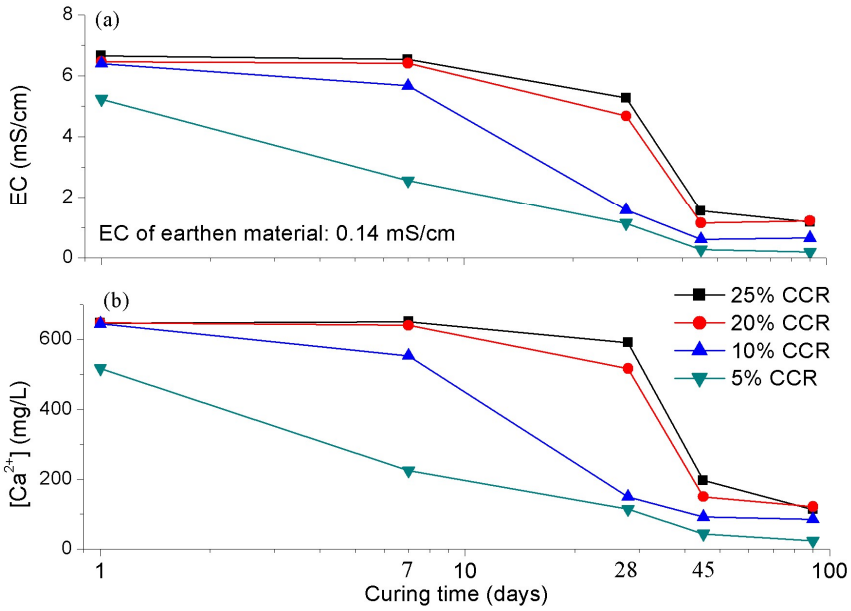

Figure 4.2. Evolution of (a) electrical conductivity (EC) and (b) concentration of unconsumed calcium ions [Ca^{2+}] in the mix solutions of earthen material (<5 mm) and 5-25 % CCR

Figure 4.2 shows that the decrease of the EC is related to the consumption of Ca^{2+} which initially dissolved from the CCR. At early age of curing (1-28 days depending on the mix composition), this consumption is counteracted by more calcium ions dissolving from the excess CCR (>10 %). This partly explains the delayed decrease of the EC and [Ca^{2+}] for the mix solutions containing >10 % CCR, which remained practically constant until the 7th day. Additionally, the delayed decrease of EC and [Ca^{2+}] can be explained by the presence of low affinity kaolinite clay in the earthen material whose low cation exchange capacity results in limited short term consumption of Ca^{2+}. The effect of the pozzolanic reaction, responsible for consumption of Ca^{2+}, as well as OH^-, was essentially noticeable after the 7th day of curing. The consumption of Ca^{2+}, which is eventually accompanied by the consumption of OH^-, resulted from the pozzolanic reaction between $Ca(OH)_2$ in the CCR and aluminosilicates in the earthen material (Al-Mukhtar et al. 2010a, 2010b).

For the mixtures containing ≤10 % CCR, the EC and [Ca^{2+}] immediately started decreasing from the first day of curing given that its fraction (2 % CCR) contributes to the immediate satisfaction of the affinity of the earthen material and the remaining fraction to the beginning of the pozzolanic reaction. This leaves only limited fraction of excess CCR to further dissolve and replenish the mixtures with Ca^{2+} and OH^-. The rate of the evolution of the EC and [Ca^{2+}] can suggest that 10 % is the amount of CCR which initially dissolves to saturation for effective contribution to the pozzolanic reaction with the earthen material from Kamboinse cured at 40 °C. This pozzolanic reaction is not only time dependent, but also temperature dependent.

The mix solutions cured at 20 °C did not undergo pozzolanic reaction, even with 10 % CCR (Nshimiyimana et al. 2020b).

The excess content (>10 % CCR) may result in occurrence of residual CCR in the mixtures which, in addition to not reacting efficiently, may compromise the physico-mechanical stability of the mixtures. In fact, the clay soil for pavement was previously reported to reach the maximum compressive strength after addition of 8-10 % CCR, beyond which the strength either remained constant or decreased (Horpibulsuk et al. 2013, Kampala et al. 2013). Therefore, there was need for effective consumption of the residual CCR, which justifies the partial substitution of the CCR with the RHA, a pozzolanic material locally available in Burkina Faso.

Figure 4.3 shows that the EC and [Ca^{2+}] decreased even faster for mix solutions containing the earthen material and CCR:RHA, thus faster reaction in mixtures containing RHA. Figure 4.3b obviously shows that the consumption of Ca^{2+} is faster in the mix solution containing the earthen material and 10 % CCR:RHA (7:3 ratio), i.e. 7 % CCR and 3 % RHA, than it was in the solution containing the earthen material and only 5 % CCR in Figure 4.2b. This implies that the CCR is simultaneously consumed by the earthen materials and the RHA in mixtures containing the earth and CCR:RHA, while it is only consumed by the earthen material in the mixtures containing earth and CCR alone.

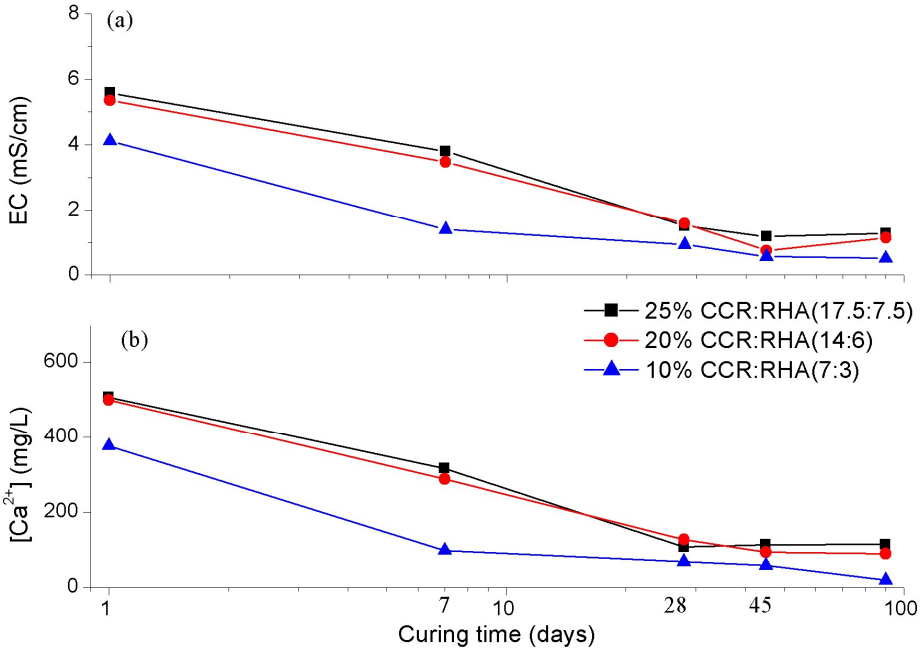

Figure 4.3. Evolution of (a) electrical conductivity (EC) and (b) concentration of unconsumed calcium [Ca^{2+}] in mix solutions of earthen material (<5 mm) and 10-25 % CCR:RHA (7:3 ratio)

Moreover, while the mix solution containing 10 % CCR alone required 45 days to reach the minimum values of EC and [Ca^{2+}] (Figure 4.2), the solution containing 20 % CCR:RHA (14:6 ratio), i.e. 14 % CCR and 6 % RHA, reached the minimum values in only 28 days (Figure 4.3). The minimum EC and [Ca^{2+}] basically correspond to the end of the reaction. Therefore, it can be deduced that RHA accelerated the reaction in earth-CCR-RHA mixtures and considerably reduced the time pending for the reaction to take place and reach the optimum maturity. This implies that curing time of earth-based mixtures can potentially be reduced from 45 to 28 days when they are stabilized with CCR:RHA, instead of CCR alone.

The optimum content of CCR:RHA can effectively act similar to cement for the stabilization of earth-based materials, in term of curing time and possibly improve the mechanical performances of CEBs at early age. Note that this improvement does not only depend on the reactivity of materials, i.e. CCR reacting with earth and RHA, but also on the conditions in which the mixtures were produced and cured. The pozzolanic reactivity improves with the curing temperature (Nshimiyimana et al. 2020b).

The effect of curing temperature was also shown in other previous studies (Al-Mukhtar et al. 2010a, 2010b). Al-Mukhtar et al. (2010) showed the accelerated consumption of lime by a clayey soil at curing temperature of 50 °C compared to 20 °C. In the same studies, the unconfined compressive strength of the soil treated with 10 % lime cured at 50 °C (~4 MPa) improved almost twice compared to the strength recorded at 20 °C (~2 MPa) after 45 days of curing. Therefore, the effect of the improvement of the pozzolanic reaction was investigated on the mechanical performances of CEBs stabilized with CCR and CCR:RHA (§4.3).

Furthermore, Figure 4.4 shows linear correlations between the EC and [Ca^{2+}], with regression coefficients, R^2>0.95. These correlations are presented in Figure 4.4a for mix containing the earthen material and 5-25 % CCR alone, Figure 4.4b for the mix containing the earthen material and 10-25 % CCR:RHA and Figure 4.4c for the compilation of all data. The equation relating the EC and unconsumed [Ca^{2+}] of the mix solution was proposed, $[Ca^{2+}] = k*EC$, with the correlation coefficient (k) varying around 97. This coefficient can reach the values of 101 for CCR-rich mixtures (Figure 4.4a) and 95 for RHA (CCR:RHA)-rich mixtures (Figure 4.4b).

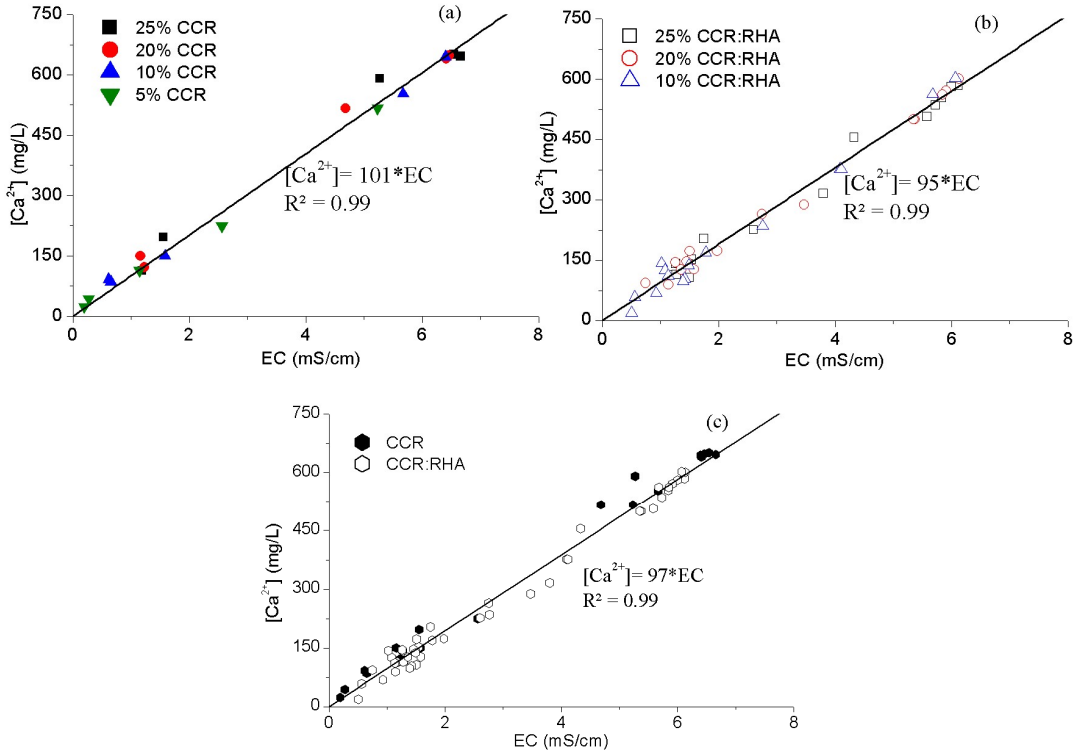

Figure 4.4. Correlation between the EC and unconsumed [Ca^{2+}] in the mix solutions cured for various time (1, 7, 28, 45, 90 days) containing the earthen material and (a) 5-25 % CCR, (b) 10-25 % CCR:RHA in various ratios, (c) combination of all data

This implies that [Ca^{2+}] can simply be deduced from the measurement of the EC in the mix solutions and vice versa, rather than having to carry out series of titrations of calcium ions. Therefore, it is possible to monitor the extent of curing and rate of consumption of calcium in stabilized earth based-materials. The correlation between the EC and [Ca^{2+}] is mostly useful for mixtures where the consumption of Ca^{2+}, through the pozzolanic reaction, is the main phenomena controlling [ca^{2+}] in the solutions, such as in kaolinite-rich earthen material. If other ions such as sodium and potassium existed in the solution, for instance from the exchangeable cations in smectite-rich soil, where EC=2.7 mS/cm (Al-Mukhtar et al. 2010a), the EC and its correlation with [Ca^{2+}] would have to take into account the contribution of these ions.

4.2.3. Mineral changes in cured mixtures

The change of mineralogy, from the raw materials to the cured stabilized mixtures, was characterized using XRD and TGA. Figure 4.5 presents the XRD spectra of selected cured mixtures. It reveals that the specific reflection of portlandite at 2.62 Å in CCR disappears after one day of curing, while that of kaolinite at 7.15 Å significantly reduced over the curing time (Figure 4.5a). This reveals the mineral changes in the cured mixtures resulting from the reaction of the constituent materials. Secondary peaks are also observed at 3.87, 3.67, 3.26, 2.86, 2.28,

1.82, 1.60, and 1.54 Å. These peaks confirm the formation of crystalline products in the cured mixtures, identified as calcium silicate hydrates (CSH) and calcium aluminate hydrates (CAH).

Prior studies similarly reported the formation of CSH and CAH from the reaction between kaolinite clay and $Ca(OH)_2$ (Al-Mukhtar et al. 2012, Reddy & Hubli 2002). Moreover, the XRD spectra of cured mixtures significantly changed between 3.0-1.5 Å (Figure 4.5b). There was appearance of new peaks and increase in the intensity of some peaks existing in the raw earthen material, mainly corresponding to quartz mineral. Although these peaks re not fully identified, they are possibly related to the CSH products of reaction involving silica and $Ca(OH)_2$.

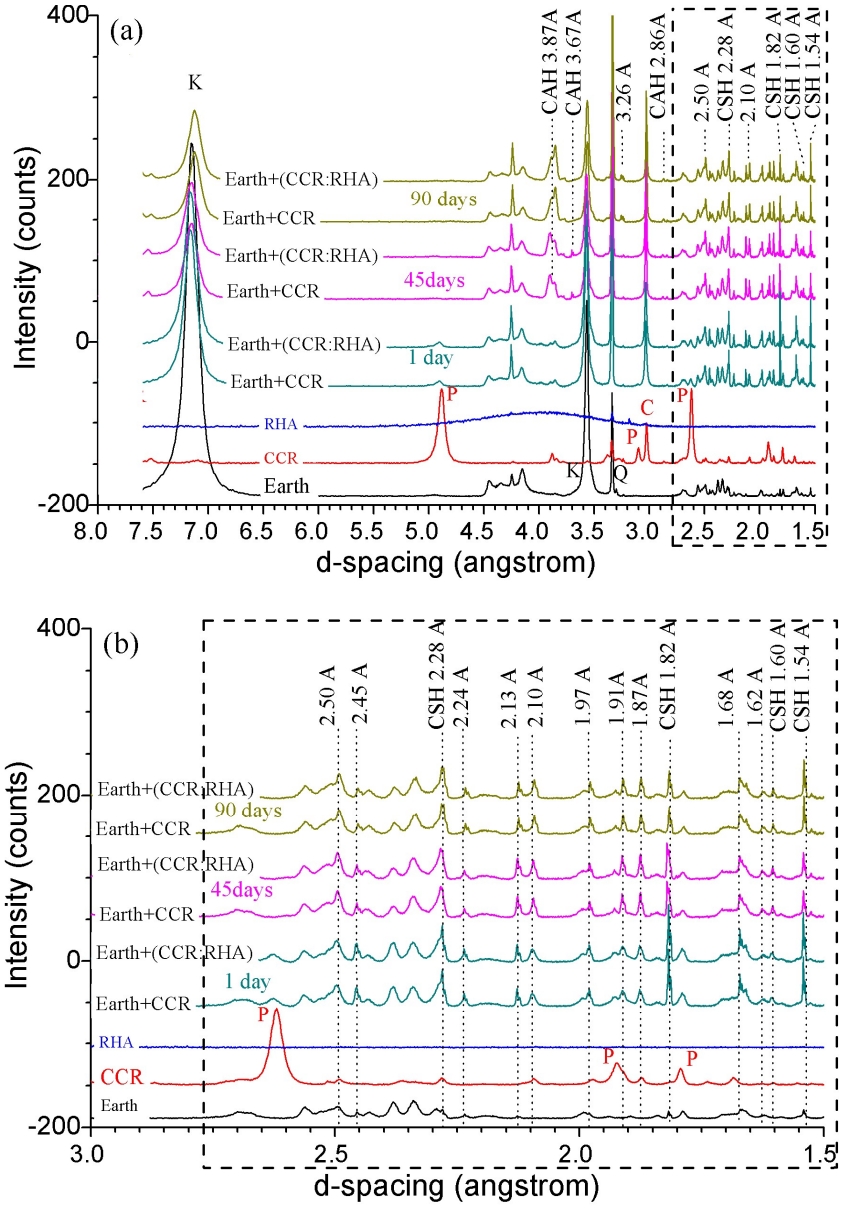

Figure 4.5. XRD spectra of earthen material, CCR, RHA and mixtures cured for 1, 45, 90 days: earth+20 % CCR and earth+20 % CCR:RHA (16:4 ratio), (a) full view, (b) detailed view, k= Kaolinite, P= Portlandite, C= Calcite, Q= Quartz, CSH= Calcium silicate hydrates, CAH= calcium aluminate hydrates

Figure 4.1 showed the increase of the pH in the mix solutions, containing only 2 % CCR, up to the initial value of 12.4 due to the dissociation of the $Ca(OH)_2$ from the CCR into Ca^{2+} and OH^-. The increase of the basicity in the mix solutions was responsible for the dissolution of fine aluminosilicates, kaolinite clay and silica among others (Arabi & Wild 1986). In the presence of Ca^{2+}, this resulted in the precipitation into CSH and CAH products (Al-Mukhtar et al. 2010b).

Figure 4.5a additionally shows that only 50 % of the intensity of the peak of kaolinite (7.15 Å) remained after 45 days of curing compared to 1 day of curing, for mixtures containing either the earthen material and CCR or earthen material and CCR:RHA. The remaining intensity of this peak (7.15 Å) reached 40 % after 90 days of curing which shows that the reaction involving kaolinite substantially took place in 45 days. This agrees with the concentration of unconsumed calcium which reached the apparent minimum after 45 days of curing in mix solution containing the earthen material and CCR alone (Figure 4.2b).

Therefore, the consumption of portlandite from CCR and kaolinite from the earthen material is responsible for the reaction between the earthen material and CCR, which reached the optimum maturity after 45 days of curing. Additionally, this suggests that RHA basically interact with the CCR not the earthen material given that the intensity of the peak of kaolinite remains practically the same for mixtures containing either CCR or CCR:RHA at a given curing time (Figure 4.5a). Besides, the intensity of the reflection of calcite (~3.01 Å) slightly increased in the mixtures cured for 45 and 90 days compared to the mixtures cured for 1 day (Figure 4.5a). This reveals that carbonation have taken place possibly during the monitoring and drying of mixtures, though precautions were taken by carefully covering the samples during the curing.

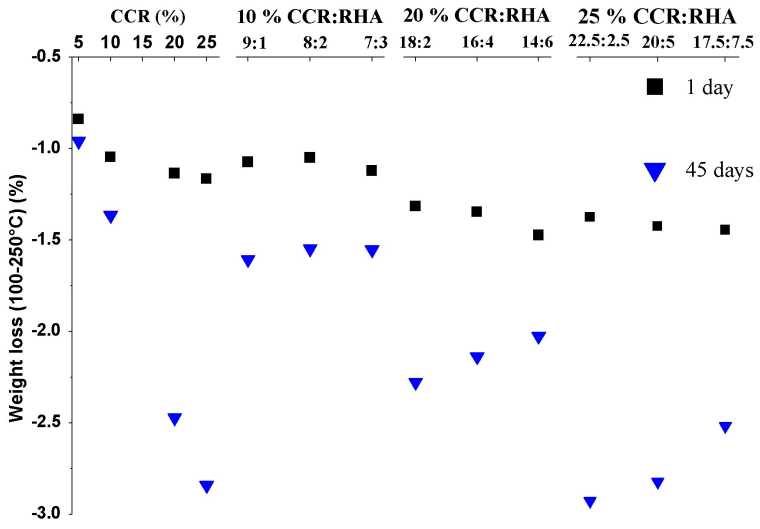

Figure 4.6. Loss of weight in the range of 100-250 °C for various cured mixtures

Furthermore, the loss of weight of cured mixtures was tentatively determined from the TGA between 100 and 250 °C (Figure 4.6). It shows that the loss of weight in this temperature range generally increased with the binder (CCR or CCR:RHA) content from 1 day to 45 days of curing. It agrees with prior report (Arrigoni et al. 2017b) that CSH mainly losses the gel water in this temperature range. This complies with the XRD of cured mixtures (Figure 4.5a) confirming the formation of more CSH products with the curing time and binder content.

4.2.4. Microstructural changes in cured mixtures

Figure 4.7 presents the SEM micrographs to confirm the chemical interactions and microstructural changes which took place in cured mixtures. Figure 4.7a shows portlandite-rich particles in the CCR, which dissolved in the cured mix solution (Figure 4.7b). The curing resulted in the formation of new products rich in calcium-silica, in plate-like shape, which grow into an interlocking network in cured mixtures containing CCR:RHA (Figure 4.7c). The formation of similar products was previously reported in cured soil-lime mixtures, which were identified as CSH phases (Arabi & Wild 1986).

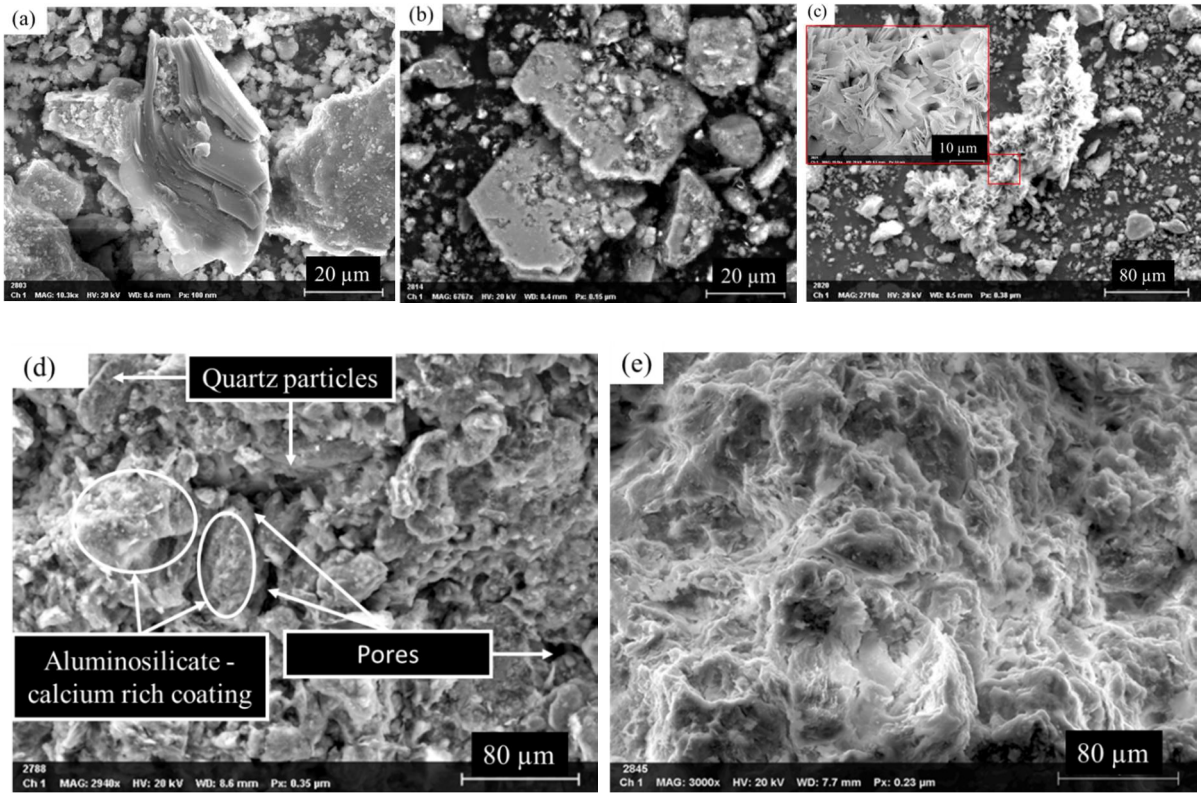

Figure 4.7. SEM micrographs (a) raw CCR, (b) cured mixtures containing 20 % CCR, (c) cured mixtures containing 20 % CCR:RHA (14:6 ratio), (d) CEBs stabilized with 20 % CCR, (e) CEBs stabilized with 20 % CCR:RHA (14:6 ratio)

The SEM micrographs of stabilized CEBs show the formation of "porridge-like" cementing products. The microstructure of CEBs stabilized with 20 % CCR shows the earthen particles coated with aluminosilicate-calcium rich products and appearance of no-cemented pores in the inter-particle zones (Figure 4.7d). By contrary, the microstructure of CEBs stabilized with 20 % CCR:RHA (14:6 ratio) shows cementation of the particles and inter-particle zones (Figure 4.7e). For CEBs containing CCR alone, the cementing products are only limited to the earthen particles, leaving some open inter-particle pores. The RHA, in CEBs containing CCR:RHA, seems to improve the formation of more cementitious products. Nevertheless, it would be interesting to confirm the evolution of the percentage and size of pore in stabilized CEBs using specialized tests, such as mercury intrusion porosimetry or X-ray tomography.

4.3. Physico-mechanical properties of stabilized CEBs

The apparent behavior and the bulk density as well as mechanical resistance of CEBs were also affected by the stabilization of earthen material from Kamboinse with by-product materials. Unstabilized CEBs were friable in dry state (degraded corners) and quickly degraded in contact with liquid water (Figure 4.8a). However, the CEBs stabilized with CCR or CCR:RHA were very stable both in dry and direct contact with liquid water (Figure 4.8b).

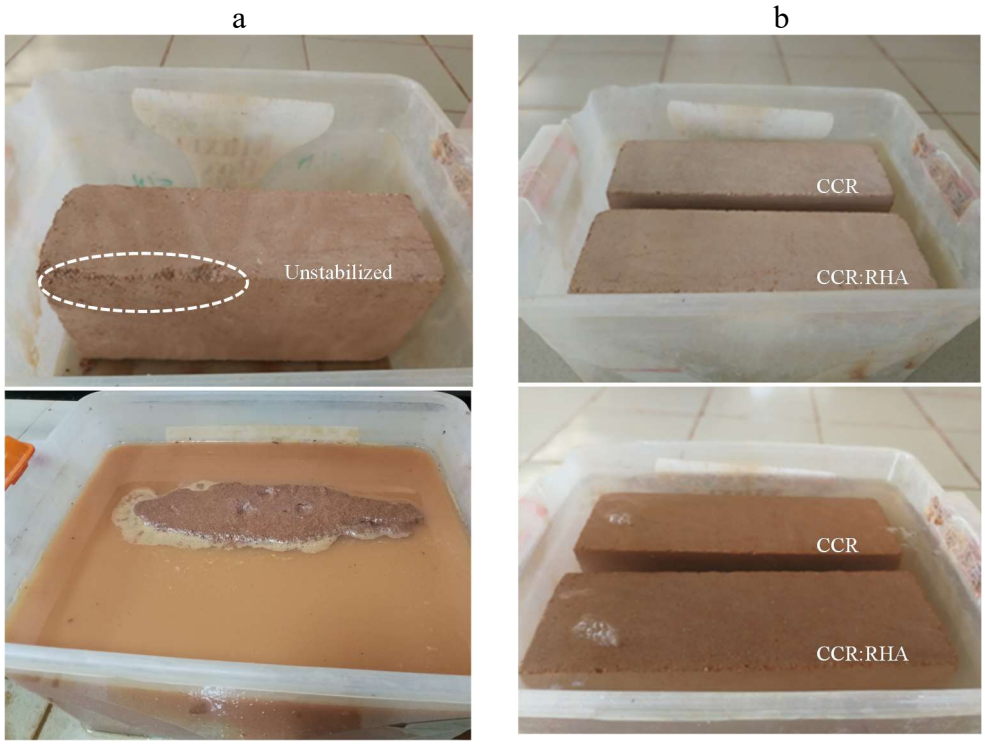

Figure 4.8. Apparent behaviors of CEBs in dry state (top) versus immersed in water for 2 hours (bottom): (a) unstabilized (b) stabilized with the CCR or CCR:RHA

4.3.1. Effects of production and curing conditions

The effects of the production and curing conditions, mainly the production moisture, curing time and temperature, were firstly assessed on the dry compressive strength of CCR-stabilized CEBs for the latter production in optimum conditions. Considering the CEBs cured at room temperature in the lab (30±5 °C) for 45 days, the compressive strength was sensible to the production moisture. This was assessed on stabilized CEBs produced using optimum moisture content (OMC of earth+CCR), determined by static compression, and OMC plus 2 % (OMC+2). The preliminary study had shown that not taking into account the water demand of CCR in earth-CCR mixtures results in the decrease of the compressive strength of CCR-stabilized CEBs at high (≥10 %) CCR content (Nshimiyimana et al. 2018).

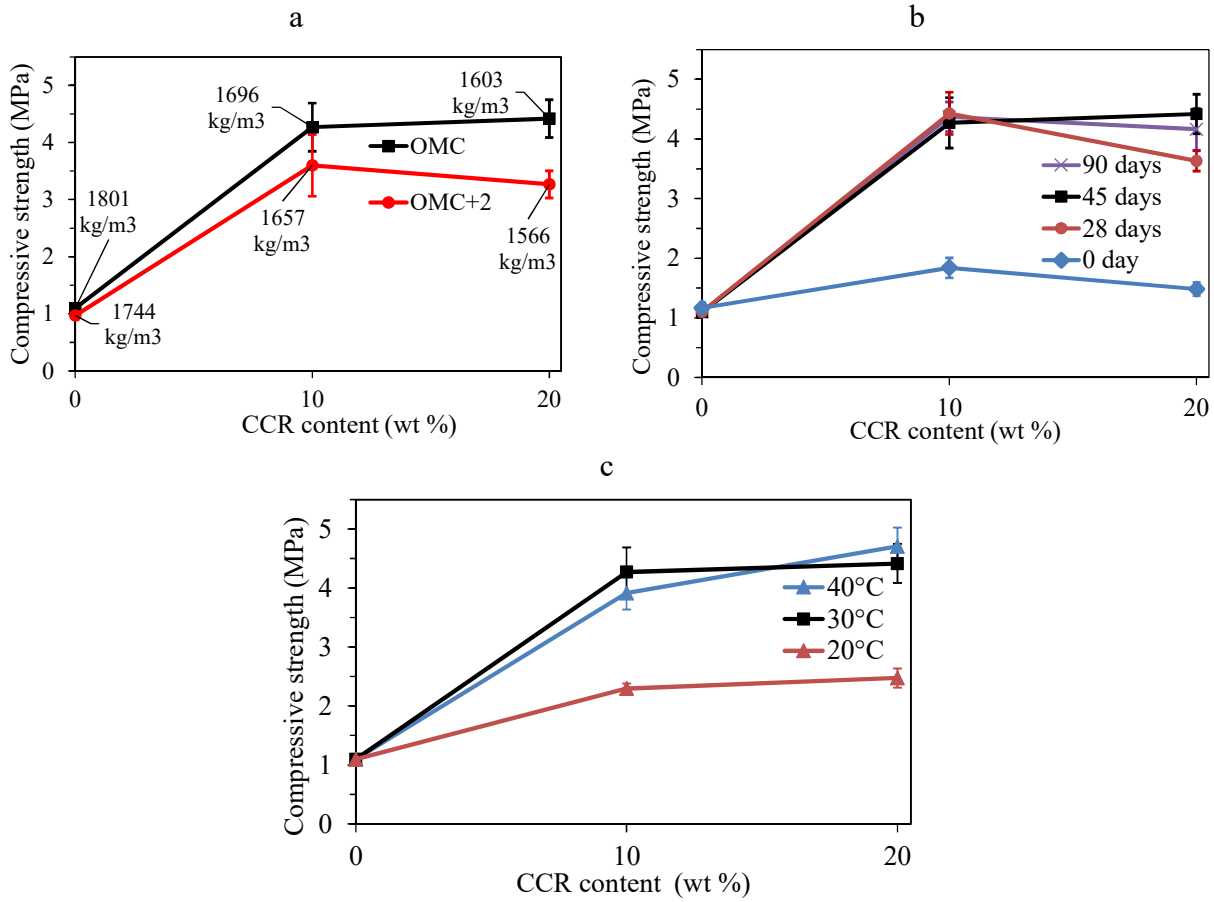

Figure 4.9. Effects of (a) production moisture, (b) curing time and (c) temperature: 20±2 °C, 30±5 °C and 40±2 °C (45 days) on the compressive strength of CCR-stabilized CEBs: (a) indices are apparent density, (a &) curing time of 45 days

The present study shows that the compressive strength keeps increasing up to 20 % CCR, if the OMC of earth+CCR is taken into account (Figure 4.9a). By contrast, increasing the moisture, from OMC to OMC+2, decreases the average compressive strength by 0.2 times (4.3 to 3.6 MPa), i.e. (4.3-3.6)/4.3, and 0.3 times (4.4 to 3.3 MPa) respectively for CEBs stabilized

with 10 % and 20 % CCR This is basically justified by the decrease of the apparent density of CEBs stabilized with the same content of CCR, from OMC to OMC+2 (Figure 4.9a).

Figure 4.9a shows that the higher is the content of the CCR (20 vs 10 % CCR) the more is sensible the compressive strength to the production moisture of CEB. This is in comparison to the compressive strength of unstabilized CEBs (0 % CCR) which was almost the same, around 1.1 MPa, at both OMC and OMC+2. In fact, the more the CCR content added to the earthen material, the more the OMC required to achieve the maximum dry density. Therefore, further increase of the production moisture (from OMC to OMC+2) rapidly affect the compressibility of the mixtures. Therefore, the production moisture equivalent to the OMC was considered for further studies of the properties of CEBs stabilized with CCR.

Figure 4.9b shows that the average compressive strength of stabilized CEBs, produced using OMC and cured at 30±5 °C in plastic bag at production moisture, increased with the curing time (0-90 days). It reached the apparent maximum (4.3 MPa) after 28 days with 10 % CCR and 45 days with 20 % CCR. This respectively corresponds to the increase factors of 1.4 and 1.9 times with respect to the compressive strength at 0 day of curing. In fact, it was previously reported that the lime does not have much influence on the compressive strength of CEBs at early age and/or for low content of clay (XP P 13-901 2001, Nagaraj et al. 2014).

However, the compressive strength did not record further increase beyond 45 days of curing. This shows that higher content of CCR would require more time for curing to reach optimum compressive strength. It suggests that 45 days is the appropriate curing time for reaching optimum performances of CCR-stabilized CEBs cured in the ambient conditions of the lab (30±5 °C). Therefore, the curing time of 45 days was considered for further studies.

Figure 4.9c shows that the average compressive strength of stabilized CEBs cured at ambient temperature (30±5 °C) and controlled temperature (40±2 °C) evolves similarly for all CCR contents. By contrast, reducing the curing temperature to 20±2 °C decreased the average compressive strength 0.5 times (4.3 to 2.3 MPa) and 0.4 times (4.4 to 2.5 MPa) respectively for CEBs stabilized with 10 % and 20 % CCR with respect to the CEBs cured at 30±5 °C. This is related to the limited pozzolanic reactivity of earthen material form Kamboinse with CCR at lower temperature (Nshimiyimana et al. 2020b). It shows the benefits of stabilization with the CCR in warm regions and suggests that CEBs stabilized with lime-rich binders can be properly

cured in ambient conditions of Ouagadougou, where the average annual temperature is 28 °C[1]. Therefore, the curing in further studies was carried out at ambient temperature (30±5 °C).

4.3.2. Compressive strength of stabilized CEBs in dry and wet conditions

Figure 4.10 details the evolution of the compressive strength, in dry and wet conditions (dry strength and wet strength), of CEBs stabilized with by-product binders (CCR and RHA) or containing fibers, produced using the OMC of earth+CCR and cured in ambient conditions of the lab (35±5 °C) at the production moisture. The average dry compressive strength of CEBs remarkably increased (2.8 times) by stabilization with CCR, from 1.2 MPa (unstabilized: 0 % CCR) to the maximum value of 4.6 MPa (10 % CCR); i.e., (4.6-1.2)/1.2. Beyond 10 % CCR, the compressive strength did not record remarkable improvement (Figure 4.10a).

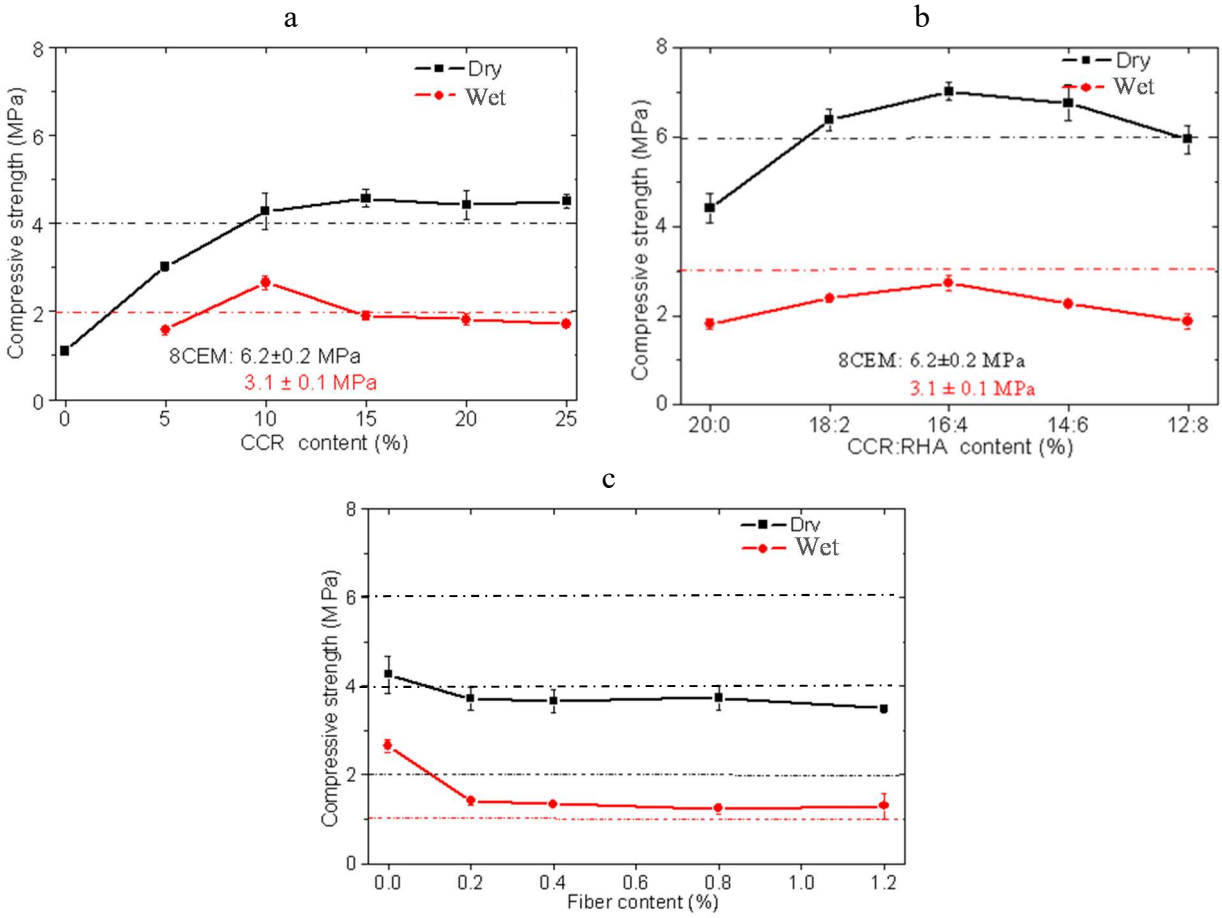

Figure 4.10. Compressive strength of CEBs stabilized with (a) CCR, (b) CCR:RHA and (c) 10 % CCR containing fibers, cured for 45 days at ambient temperature of the lab (35±5 °C) and production moisture. Comparison with the strength required for load-bearing in walls of two and three-storey building

[1] https://en.climate-data.org/africa/burkina-faso/centre/ouagadougou-512/. Accessed February 3, 2020

Additionally, the average wet compressive strength of CEBs slightly improved to reach the maximum value of 2.7 MPa (10 % CCR), beyond which it decreased to <2 MPa (Figure 4.10a). The wet compressive strength of unstabilized (0 % CCR) CEBs could not be determined; they immediately deteriorated in water (Figure 4.8c). The asymptotic evolution of the compressive strength (>10 % CCR) can be explained by the ineffective pozzolanic reaction between the clay earthen material and excess CCR (§4.2). It can be suggested that CEBs should be stabilized with at least 10 % CCR to reach the dry and wet compressive strength respectively of 4 and 2 MPa required for wall construction of two-strorey building (CDI&CRATerre 1998).

For the CCR content in the range of ineffective pozzolanic reaction with the earthen material, the partial substitution of 20 % CCR by RHA (CCR:RHA in various ratios) further improved the compressive strength of stabilized CEBs. The dry compressive strength reached the average maximum value of 7.0 MPa with 16:4 % CCR:RHA (Figure 4.10b); it increased 0.6 times with respect to 4.4 MPa reached with 20:0 % CCR:RHA (20 % CCR alone), i.e. (7.0-4.4)/4.4. This improvement is significant in sense that it allows to produce CEBs suitable for bearing load in walls of three-storey buildings, i.e. dry compressive strength of 6 MPa (CDI&CRATerre 1998).

Nevertheless, the load-bearing capacity of CCR:RHA-stabilized CEBs was compromised in wet conditions; the wet compressive strength reached the maximum value of only 2.7 MPa with 16:4 % CCR:RHA (Figure 4.10b). It failed to reach the required strength of 3 MPa for the application in facing masonry in three-storey building (CDI&CRATerre 1998). However, the CEBs can potentially be used in dry environment or subjected to surface or architectural protection against direct contact with liquid water. CCR:RHA-stabilized CEBs recorded the optimum dry compressive strength which is comparable to that of CEBs stabilized with 8 % cement (8CEM: 6.2 and 3.1 MPa in dry and wet conditions, respectively). The improvement of the compressive strength is mainly related to the rapid pozzolanic reaction and microstructural changes in the mixtures of earthen material and CCR:RHA compared to the mixtures of earth and CCR alone (Nshimiyimana et al. 2019).

By contrast, the compressive strength of CEBs stabilized by the optimum content of the CCR (10 %) decreased by incorporation of 0-1.2 % Okra bast fiber (Figure 4.10c). The dry compressive strength decreased from 4.4 MPa with 0 % fiber to the quasi-constant value of 3.7 MPa with 0.2 % fiber and beyond. Similarly, the wet compressive strength decreased from 2.7 MPa with 0 % fiber to 1.3 MPa with 0.2 % fiber and beyond. Thus, the CEBs containing fibers lost their ability for applications in storey building. Nevertheless, they can be useful for

constructions of non-load bearing walls which require the compressive strength of 2 MPa and 1 MPa in dry and wet conditions (CDI&CRATerre 1998).

Table 4.1 further summarizes the average compressive strength along with the coefficients of variations (CV) of stabilized CEBs, in dry and wet conditions. It shows that the compressive strength records similar degree of variation for CEBs stabilized with CCR and CCR:RHA, as the CV is less than 10 %. By contrast, the CEBs containing fibers have higher variations (CV of 22 % with 1.2 % fiber), related to the complications of achieving homogeneous mixtures with fibers. Appendix I also shows that the effects of stabilization with 15 % CCR or 16:4 % CCR:RHA are the most statistically significant on the compressive strength of CEBs. Stabilization with 10 % CCR has also significant effect with respect to 0 % CCR.

Table 4.1 also presents the coefficient of water strength (CWS), ratio between the wet and dry compressive strength. The CWS evolved in the range of 0.4 and 0.6 for CEBs stabilized with by-products, compared to 0.5 for 8 % cement stabilized CEBs. This is indeed a good indicator of the durability, as it is further discussed latter in chapter V.

The literature reported lower or comparable values of the compressive strength of CEBs stabilized with cement, lime or geopolymer. For instance, Bogas et al. (2018) reported the dry compressive strength of 2.3, 3.3 and 5.5 MPa respectively for unstabilized, CEBs stabilized with 4:4 % cement:lime, and 8 % cement. The authors also recorded drastic decrease of the compressive strength in direct contact with liquid water. Sore et al. (2017) reported comparable dry and wet compressive strength, i.e. 4.4 MPa and 2.2 MPa, for CEBs produced from the earthen material from Kamboinse stabilized with 10 % geopolymer from 1.4 MPa for unstabilized CEBs. The binder type and content clearly affect the strength of CEBs.

4.3.3. Bulk density and total porosity

The addition of 0-25 % CCR decreased the bulk density of CEBs in the range of 1800 to 1477 kg/m^3, following the increase of the total porosity in the range of 35-45 % (Figure 4.11a). The increase of the total porosity with the addition of the CCR can be related to the increase of the OMC (17-23 %) required for the production of CCR-stabilized CEBs at same consistency (Figure 2.2a).

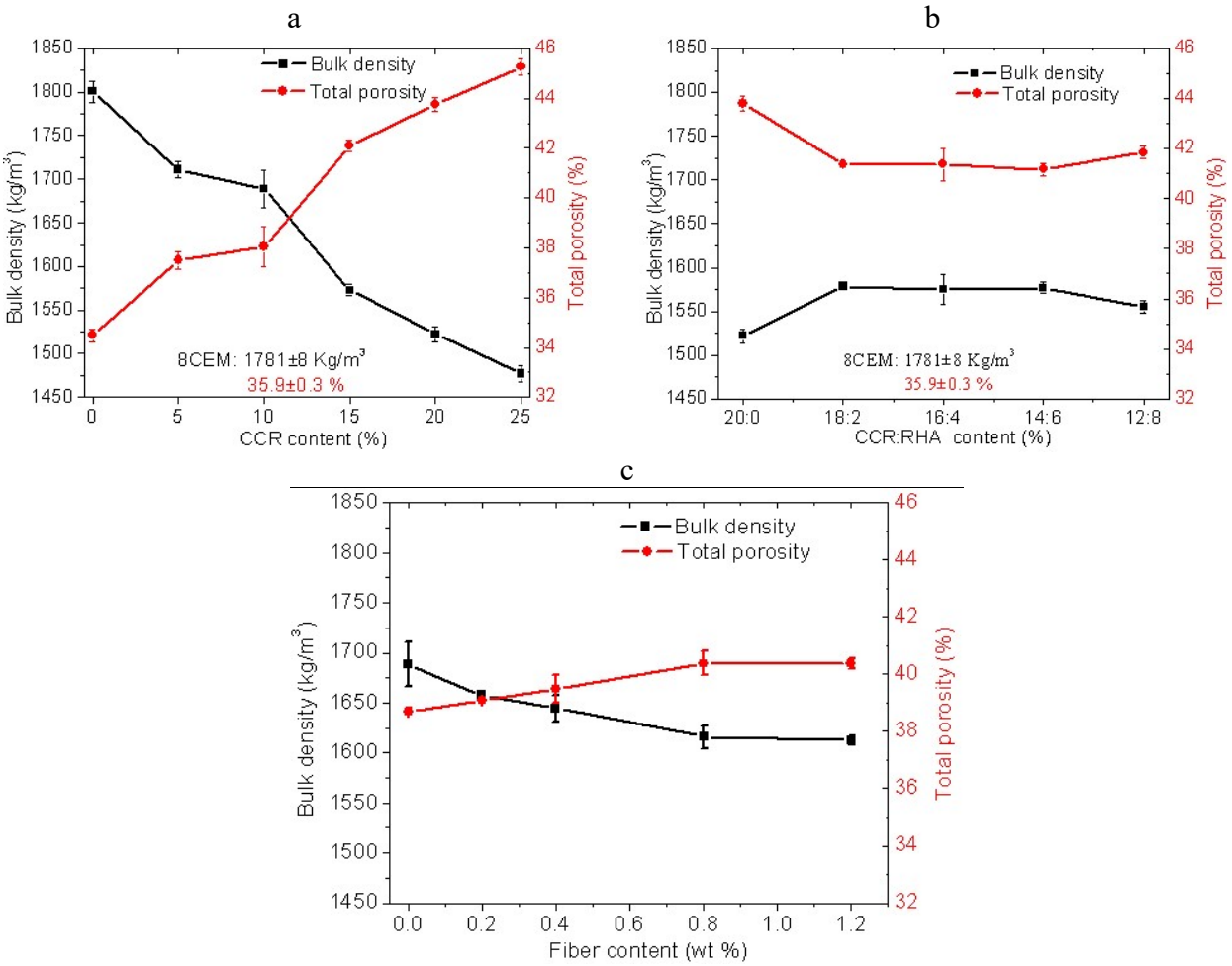

Figure 4.11. Bulk density and total porosity of CEBs stabilized with (a) CCR, (b) CCR:RHA and (c) 10 % CCR containing fibers

By contrast, the partial substitution of 20 % CCR by RHA (CCR:RHA various ratios) slightly increased the bulk density from 1522 kg/m^3 (20:0 % CCR:RHA, i.e. 20 % CCR alone) to 1578 kg/m^3 (18:2 % CCR:RHA). It corresponds to a slight decrease of the total porosity from 44 to 41 %. Beyond 18:2 % CCR:RHA, the bulk density and total porosity tend to be constant (Figure 4.11b). This clearly points out the usefulness of the substitution of the CCR (at high content: 20 %) by the RHA on improving the compressive strength (§4.3.2) without compromising (increasing) the porosity of CEBs.

It is noteworthy to remind that the production moisture (22 %) for CEBs stabilized with CCR:RHA (various ratios) was the same as CEBs stabilized with 20 % CCR alone. The tendency of the bulk density and total porosity to reach the constant values suggests that, at the similar content of production moisture, the CCR:RHA can produce denser and lesser porous CEBs than the CCR alone. This suggests that the bulk density and total porosity can further be improved by optimization of the production moisture of CEBs stabilized with CCR:RHA. The

bulk density of the CEBs stabilized with by-product binders is lower than 1780 kg/m^3 and the porosity is higher than 36 % for CEBs stabilized with 8 % cement.

Moreover, the incorporation of 0-1.2 % fibers in the matrix of CEBs stabilized with 10 % CCR quasi-linearly decreased the bulk density in the range of 1690 to 1610 kg/m^3 (Figure 4.11c). Table 4.1 further summarizes the averages and coefficients of variations of the bulk density and total porosity of CEBs stabilized with CCR, CCR:RHA or containing fibers; it shows similar range of variations (CV<2). Appendix I additionally shows that the bulk density of CEBs was significantly affected by the stabilization with at least 10 % CCR.

In the present study, the bulk density and total porosity of unstabilized CEBs or stabilized with by-products are respectively lower and higher than 2000 kg/m^3 and 25 % reported in the literature for unstabilized CEBs produced using normal compaction pressure (<2 MPa) (Mansour et al. 2016). This can be related to the type of earthen material (from Kamboinse) used in present study which required OMC (≥17 %), higher than 13 % used in the literature (Mansour et al. 2016). Similar observation was made for the CEBs stabilized with 8 % cement in the present study which have bulk density (1780 kg/m^3) and porosity (36 %) respectively slightly lower and higher than their counterparts in the literature, i.e. 1810 kg/m^3 and 30 % (Bogas et al. 2018). The latter were produced using OMC of 9.5 % and compaction pressure of about 3.5 MPa (Bogas et al. 2018). The more is the moisture demand for the production of CEBs, the higher is the evaporation during the drying and creation of porosity.

By contrast, the values bulk density and total porosity of CEBs stabilized with 8 % cement are respectively lower and higher than the values for CEBs stabilized with CCR or CCR:RHA, in the present study. Indeed, it was previously reported that the bulk density decreases with lime (CCR in the present case), while it increases with cement stabilization (Zhu et al. 2019, Kerali 2001, Morel et al. 2013). This cannot only be related to the low demand of production moisture of CEBs stabilized with cement, but also higher specific density of cement (3.1) compared to that of CCR (2.49). Additionally, the total porosity was observed to be mostly affected by the compaction pressure (consolidation) and OMC of production more than the binder (cement, lime) content (Bogas et al. 2018).

This can explain the simultaneous increase of the compressive strength (§4.3.2) and decrease of the bulk density of stabilized CEBs. It is mainly due to the counteracting phenomena: (1) formation of the cementitious hydrates responsible for the binding cohesion and improvement of strength, (2) increase of the total porosity from the increase of OMC which

decreases the cohesion, bulk density and strength. The first phenomenon prevails during the improvement stage of the compressive strength of stabilized CEBs, i.e. 0 to 10-15 % CCR or 20:0 to 16:4 % CCR:RHA, beyond which there is a compromise of the two phenomena.

4.3.4. Structural efficiency

The coefficient of structural efficiency (CSE) was evaluated as another important physico-mechanical parameter to assess the load bearing capacity of CEBs for applications in building construction. The CSE was determined as the ratio between the compressive strength and bulk density of CEBs. The aim is to maximize the resistance (strength) at the same time minimize the weight (density) of material in order to improve the load-bearing capacity.

The stabilization with CCR remarkably improved the CSE which increased 4 times, i.e. from 609 Pa.m^3/kg (J/kg) for unstabilized (0 % CCR) to 2530-3050 J/kg for 10-25 % CCR-stabilized CEBs (Table 4.1a). This implies that the CEBs stabilized with high content of CCR (25 %) can bear more loads given that they are lighter than CEBs stabilized with low content of CCR (10 %), while both have the comparable resistance.

The stabilization with CCR:RHA further increased (0.5 times) the bearing capacity of CEBs, from a CSE of 2902 J/kg with 20:0 % CCR:RHA to a maximum of 4462 J/kg with 16:4 % CCR:RHA (Table 4.1b). This suggests that CEBs stabilized with 16:4 % CCR:RHA are not only the optimum design regarding the compressive strength, but also the load-bearing capacity. In fact, the CSE of CEBs stabilized with 16:4 % CCR:RHA is even greater than the CSE (3547 J/kg) of CEBs stabilized with 8 % cement. Moreover, the CSE of optimum design (16:4 % CCR:RHA) is even higher than CSE deduced from the literature, such as 3040 J/kg for CEBs stabilized with 8 % cement (Bogas et al. 2018), 4290 J/kg with 8 % cement and 2450 J/kg with 10 % geopolymer (Sore et al. 2018). Additionally, this design has better CSE than 4320 J/kg for earth hypercompacted at 100 MPa (Bruno et al. 2015).

By contrast, the incorporation of 0-1.2 % fiber not only decreased the compressive strength, but also the carrying capacity of stabilized CEBs. The CSE decreased from 2528 J/kg with 0 % fiber to 2170 J/kg with 1.2 % fiber (Table 4.1c). Thus, this confirms the usefulness of fiber reinforced CEBs in non-load bearing applications.

Table 4.1. Summary of the physico-mechanical and thermal properties of CEBs stabilized with (a) CCR, (b) CCR:RHA and (c) 10 % CCR containing fibers: average values and coefficient of variations on three (03) specimens*

a

Binder/ fiber content (%)		Compressive strength (MPa)				CWS *	Bulk density, ρ (Kg/m^3)		Total porosity, TP (%)		CSE * ($Pa.m^3/kg$ = J/kg)	Thermal							
												effusivity, E ($J/m^2.K.s^{1/2}$)		capacity, Cp (J/kg.K)		conductivity, λ (W/m.K)		diffusivity, a (m^2/s)		penetration depth, δp (m)	
		Dry		Wet																	
CCR	0	1.1	3	ND		ND	1801	1	35	1	609	1291	3	899	1	1.02	6	6.3E-7	10	0.132	5
	5	3.0	3	1.6	6	0.5	1711	1	38	1	1767	1152	1	922	1	0.89	5	5.6E-7	6	0.121	1
	10	4.3	10	2.7	6	0.6	1689	1	38	2	2528	1159	4	916	1	0.84	1	5.4E-7	1	0.122	0
	15	4.6	5	1.9	5	0.4	1573	0	42	1	2901	1084	3	957	0	0.79	4	5.2E-7	2	0.119	3
	20	4.4	7	1.8	7	0.4	1522	1	44	1	2902	1107	1	966	1	0.83	2	5.6E-7	1	0.124	1
	25	4.5	3	1.7	4	0.4	1477	1	45	1	3053	1010	4	997	1	0.69	6	4.7E-7	2	0.114	1

b

CCR: RHA	20:0	4.4	7	1.8	7	0.4	1522	1	44	1	2902	1107	1	966	1	0.83	2	5.6E-7	1	0.124	1
	18:2	6.4	4	2.4	4	0.4	1578	1	41	0	4045	1042	1	942	1	0.73	1	4.9E-7	1	0.116	0
	16:4	7.0	3	2.7	6	0.4	1575	1	40	1	4462	974	3	939	2	0.64	8	4.1E-7	0	0.106	0
	14:6	6.8	6	2.3	4	0.3	1577	1	30	1	4293	1009	1	933	2	0.69	0	4.7E-7	2	0.114	1
	12:8	6.0	5	1.9	9	0.3	1555	2	39	0	3827	1081	1	880	1	0.86	3	6.3E-7	4	0.131	2
CEM	8	6.2	4	3.1	3	0.5	1781	8	37	1	3547	1231	3	844	6	1.01	7	6.8E-7	10	0.136	5

c

Fiber	0	4.3	10	2.7	6	0.6	1689	1	38	0	2528	1159	4	916	1	0.84	1	5.4E-7	1	0.122	0
	0.2	3.7	7	1.4	6	0.4	1658	0	39	0	2242	1080	4	908	4	0.76	4	5.0E-7	1	0.117	0
	0.4	3.7	7	1.3	3	0.4	1645	1	40	1	2224	1055	3	812	3	0.83	3	6.1E-7	2	0.131	2
	0.8	3.7	7	1.2	9	0.3	1616	1	40	1	2316	983	2	885	0	0.66	3	4.6E-7	1	0.112	1
	1.2	3.5	2	1.3	22	0.4	1612	0	40	0	2170	953	3	915	2	0.63	3	4.2E-7	2	0.108	1

*CWS: coefficient of water strength, CSE: coefficient of structural efficiency, coefficient of variations: percentage ratio of standard deviation and average values, CEM: cement ND: not determined.

4.4. Hygro-thermal properties of stabilized CEBs

4.4.1. Thermal effusivity and specific thermal capacity

The thermal properties of CEBs were also improved by the stabilization with CCR, CCR:RHA or fibers. Specifically, the average thermal effusivity decreased in the range of 1290 to 1010 J/m^2.K.s$^{1/2}$, measured for CEBs stabilized with 0 to 25 % CCR (Table 4.1a). It further evolved in the range of 1110 to 970 J/m^2.K.s$^{1/2}$ for CEBs stabilized with CCR:RHA, reaching the minimum value with 16:4 % CCR:RHA (Table 4.1b). The values of the thermal effusivity of CEBs stabilized with CCR and CCR:RHA are lower than 1231 J/m^2.K.s$^{1/2}$ for CEBs stabilized with 8 % cement. Furthermore, the incorporation of 0-1.2 % fiber decreased the thermal effusivity of stabilized CEBs in the range of 1160 to 950 J/m^2.K.s$^{1/2}$ (Table 4.1c).

The specific thermal capacity measured on CEBs stabilized with 0-25 % CCR increased in the range of 890 to 1000 J/kg.K (Table 4.1a). It evolved in the range of 970 and 880 J/kg.K for CEBs stabilized with CCR:RHA, reaching the maximum with 20:0 % CCR:RHA (Table 4.1b). These values are higher than the thermal capacity of 844 J/kg.K for CEBs stabilized with 8 % cement. The thermal capacity of CEBs containing 0-1.2 % fiber evolved in the range 915 and 810 J/kg.K, reaching the maximum with 1.2 % fiber (Table 4.1c). Table 4.1 further shows that both the thermal effusivity and capacity record the same range of variations (CV < 4). Appendix I shows that that the stabilization effect of at least 15 % CCR is statistically significant on both thermal effusivity and capacity.

The thermal effusivity tends to decrease, and particularly shows linear correlations, with the bulk density for CEBs stabilized with CCR or containing fibers (Figure 4.12a&c). Similar evolution was previously observed on unstabilized and geopolymer-stabilized CEBs (Mansour et al. 2016, Sore et al. 2018). Nevertheless, the evolution of the thermal capacity does not show particular tendency with the bulk density, except for CCR-stabilized CEBs (Figure 4.12a). Moreover, the evolution of the thermal effusivity of CEBs containing plant fiber recorded higher slope (Figure 4.12c) than CEBs containing CCR alone (Figure 4.12a), with respect to the same range of bulk density. This can be explained by the featured effect of the CCR (increase of porosity) and plant fiber which decreases the thermal effusivity (Figure 4.12a&c) and increases the thermal capacity (Figure 4.12a) of CEBs.

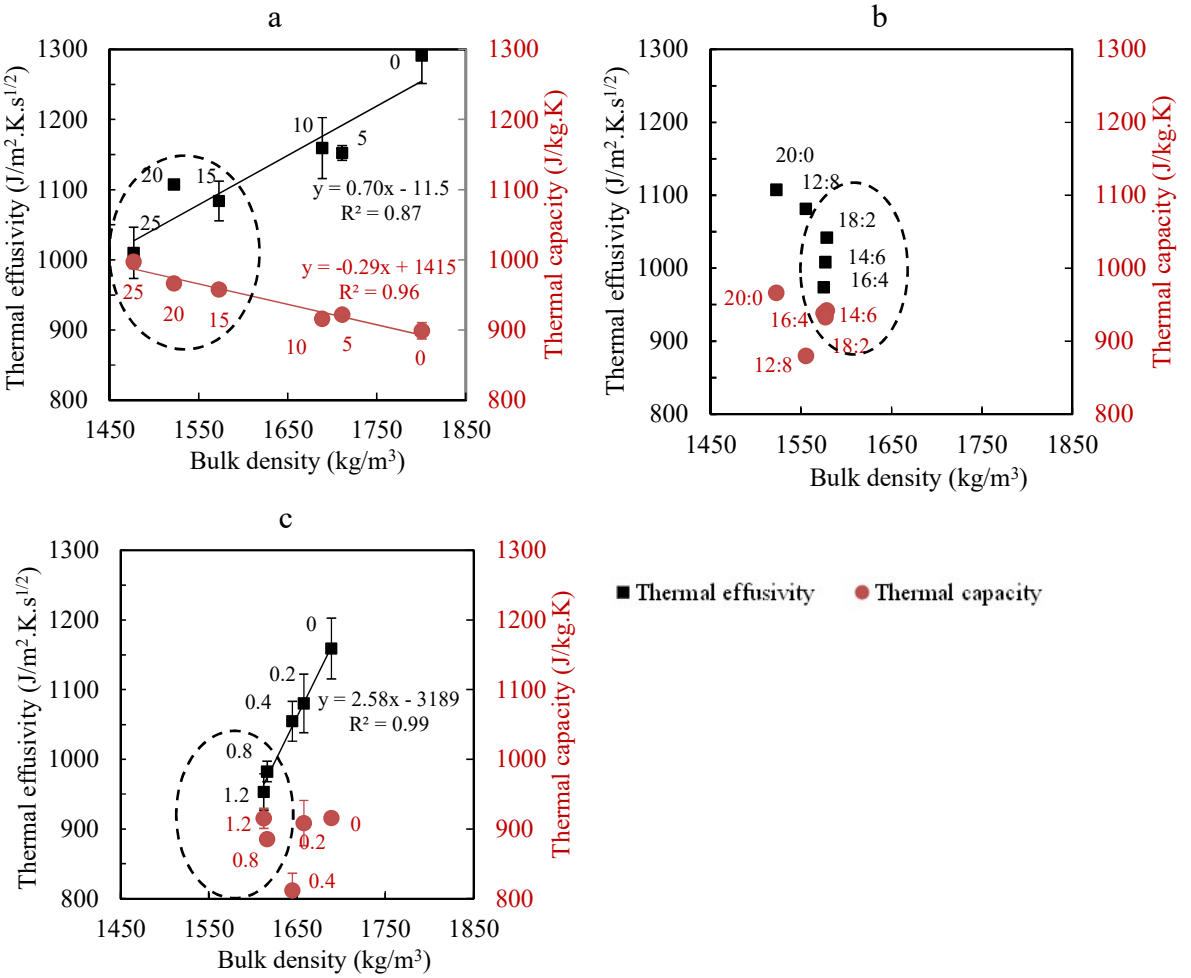

Figure 4.12. Evolution of the thermal effusivity and specific capacity with respect to the bulk density of CEBs stabilized with (a) CCR, (b) CCR:RHA, and (c) 10 % CCR and fibers. Indices represent the content of stabilizer

Ideal building materials for application in facing wall masonry in warm regions should have the lowest thermal effusivity, i.e. the lowest ability to absorb heat from the surrounding and/or the highest specific thermal capacity, i.e. the highest capacity to store the absorbed heat (Félix 2011). This would translate in low thermal conductivity and diffusivity, thus high thermal inertia. Figure 4.12 presents the possibility to design CEBs respectively to minimize and maximize (areas in the circles) the thermal effusivity and capacity with respect to the bulk density. It suggests that CEBs stabilized with 15-25 % CCR (Figure 4.12a), or 14:6-18:2 % CCR:RHA (Figure 4.12b), or containing 0.8-1.2 % fiber (Figure 4.12c) would be better designs for thermal applications in warm climatic context, like in Burkina Faso.

4.4.2. Thermal conductivity and thermal diffusivity

The average thermal conductivity decreased from 1.02 to 0.69 W/m.K for CEBs stabilized with 0 to 25 % CCR (Table 4.1a). The CEBs stabilized with CCR:RHA recorded a minimum value of thermal conductivity of 0.64 W/m.K with 16:4 % CCR:RHA from 0.83 W/m.K with 20:0 %

CCR:RHA. These values are lower than the thermal conductivity of 1.01 W/m.K reached with 8 % cement (Table 4.1b). The thermal conductivity of CEBs containing 0-1.2 % fibers evolved in the range of 0.84 and 0.63 W/m.K (Table 4.1c).

The thermal diffusivity of CEBs similarly decreased from 6.3E-7 to 4.7E-7 m²/s with 0 to 25 % CCR (Table 4.1a). It reached the minimum value of 4.1E-7 m²/s with 16:4 % CCR:RHA from 5.6E-7 m²/s with 20:0 % CCR:RHA, which is also lower than 6.8E-7 m²/s for CEBs stabilized with 8 % cement (Table 4.1b). The thermal diffusivity of CEBs containing fibers evolved in the range of 6.1E-7 m²/s to 4.2E-7 m²/s, reaching the minimum with 1.2 % fibers (Table 4.1c). Table 4.1 further presents the average values of the thermal conductivity and diffusivity along with their coefficients of variations which are in same range of variation (CV<10). Appendix I also shows that the effect of stabilization with CCR is statistically significant on the thermal properties of CEBs.

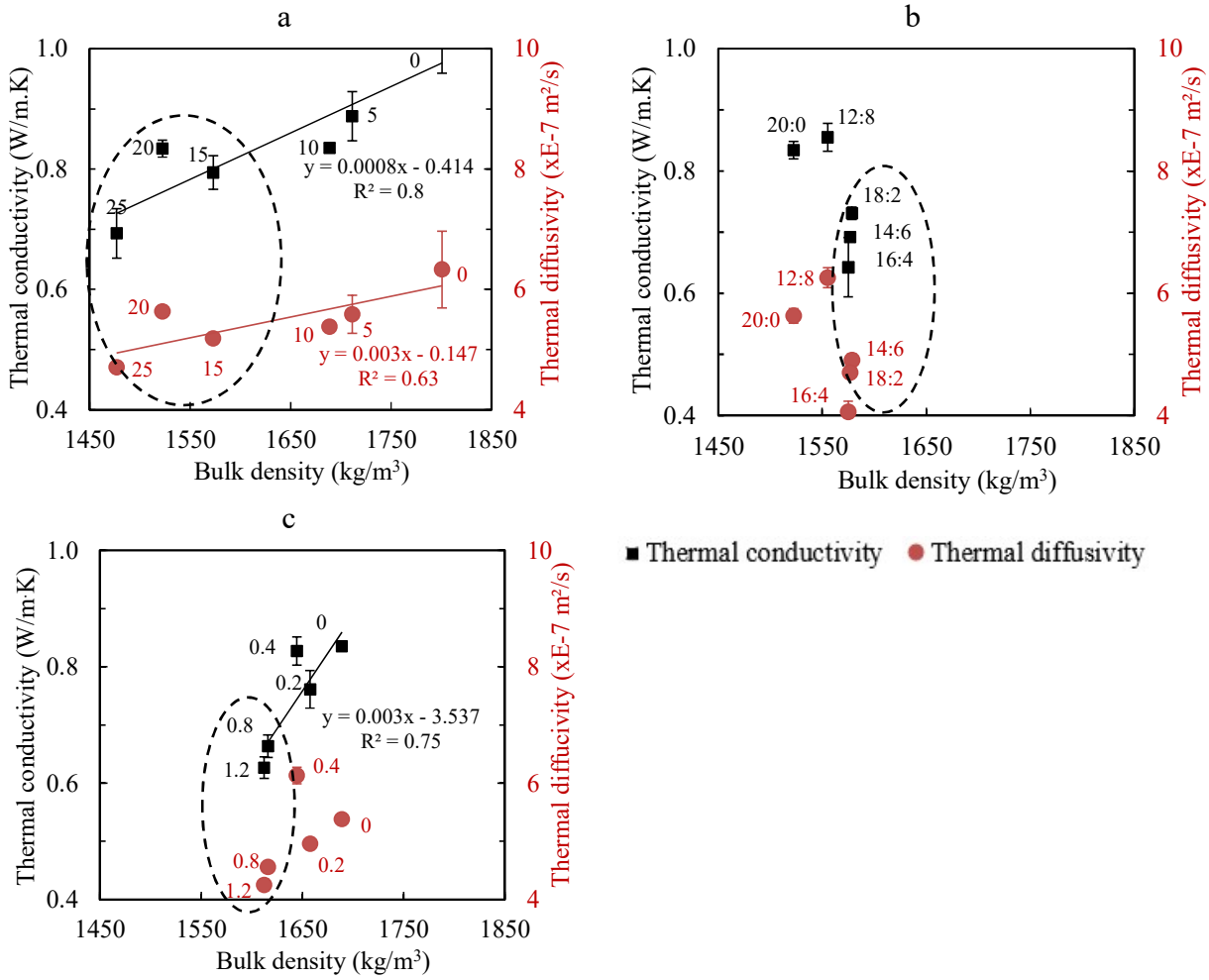

Figure 4.13. Evolution of the thermal conductivity and thermal diffusivity with respect to the bulk density of CEBs stabilized with (a) CCR, (b) CCR:RHA and (c) 10 % CCR containing fibers. Indices represent the content of stabilizer.

Figure 4.13 similarly presents the possibility to minimize (in circles) the thermal conductivity and diffusivity of CEBs with respect to the bulk density, for achieving thermal performances in warm regions.

In the present study, the thermal conductivity of CEBs stabilized with CCR or CCR:RHA reached the values lower or comparable to the values reported in the literature for unstabilized CEBs of similar bulk density (§1.7.3). Similar observation can be made on the thermal diffusivity (Sore et al. 2018, Mansour et al. 2016). Moreover, it was reported that the thermal conductivity and diffusivity of unstabilized CEBs decreased with the bulk density (Mansour et al. 2016), which was also the case for stabilized CEBs in the present study. This may suggest that stabilization is not the direct factor affecting the thermal properties of CEBs, rather the evolution of the resulting bulk density. Note that the stabilization with the CCR (0-25 %) decreased the bulk density (1800-1480 kg/m^3), increasing the total porosity (35-45 %), which decreased the thermal conductivity and diffusivity.

This can partly explain why the values of the thermal conductivity and diffusivity in the present study are lower than the values in the literature, particularly, given that the air (in the pores) has lower values (0.03 W/m.K and 2.2E-7 m^2/s, respectively)[2]. Therefore, it can be deduced that the type of earthen materials and stabilizer possibly influence the thermal properties through the evolution of the bulk density (porosity) resulting from the chemical stabilization and compression of CEBs. Another explanation of this difference can be related to the variability in equipment and methods of measurement. Additionally, the decrease of the values of the thermal conductivity and diffusivity for CEBs containing fibers can be related to the lower value for vegetables fibers. This points out that stabilized CEBs can be engineered during production to control their thermal properties, without compromising the mechanical performances.

4.4.3. Thermal efficiency

The thermal efficiency was assessed on the basis of the evolution of thermal penetration depth into the CEBs, relating the thermal properties of materials for a period of 24 hours. The depth evolved in the range of 0.13 to 0.11 m for CEBs stabilized with 0 to 25 % CCR (Table 4.1a). It reached the minimum value of 0.106 m for CEBs stabilized with 14:6 % CCR:RHA from

[2] https://www.engineeringtoolbox.com/dry-air-properties-d_973.html (Jan. 15, 2020).

0.126 m with 20:0 % CCR:RHA, compared to 0.136 m with 8 % cement (Table 4.1b). The depth evolved in the range of 0.13 to 0.10 m for CEBs containing 0 to 1.2 % fiber (Table 4.1c).

On the one hand, this shows that the heat flux may not cross through the total thickness (0.14 m) of CEBs after period of 24 hours. On the hand, this parameter can be used as basis to design/select the appropriate size of the wall masonry (thickness of CEBs) which would have efficient thermal performance. For comparison, the thermal penetration depth was deduced from the values of thermal diffusivity reported in the literature. It suggested that the thickness should be in the range of 0.09-0.11 m or 0.12 m for CEBs stabilized with 0-10 % geopolymer or 8 % cement (Sore 2017) and 0.14-0.19 m for unstabilized CEBs with bulk density of 1600-2200 kg/m^3 (Mansour et al. 2016).

In fact, a simulation study (Moussa et al. 2019) evidenced the thermal and energy efficiency of a building (wall) constructed using CCR-stabilized CEBs produced with the clay material (Pabre) compared to hollow cement blocks (HCB)-building. The CCR-CEBs-building allows to achieve lesser warm discomfort (400 hours) than HCB-building, only using natural ventilation systems. Moreover, if an air-conditioner is used to keep the average temperature at 28 °C in both buildings, the CCR-CEBs-building allows to save 310 000 CFA francs (535 USD) per year compared to HCB-building on electricity consumption for operation. Furthermore, the CEBs in the present study (stabilized with by-products) are thermally efficient in a sense that the thermal conductivity and specific capacity are respectively lower than 1 W/m.K and higher than 920 J/kg.K, as of the specification of the Brazilian standard for blocks and tiles (de Castro Ferreira and de Carvalho Ulhôa 2016).

4.4.4. Effect of water content on the thermal properties

The thermal properties of CEBs stabilized with CCR and CCR:RHA increased with respect to the content of liquid water (Figure 4.14 & Figure 4.15). The evolution of thermal properties (τ) can tentatively be assimilated to a linear correlation, $\tau=axwc+b$, increasing at different rates (a) with respect to the water content (wc), from the initial values in dry state (b). Although not reported, the experimental results showed that this correlation is no more valuable beyond 15 % water content. Similar observation was previously made by Meukam (Meukam et al. 2004).

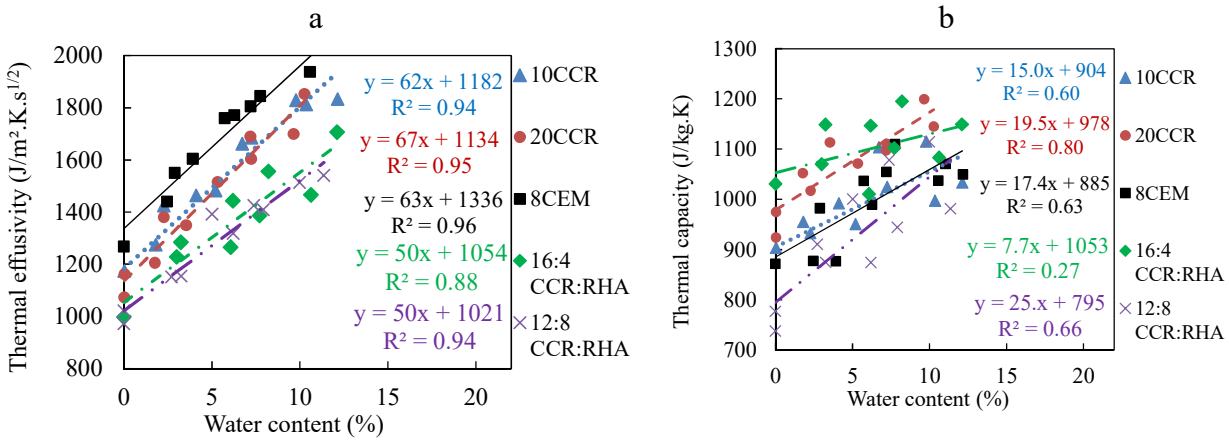

Figure 4.14. Evolution of the thermal (a) effusivity and (b) capacity of CEBs with water content

The thermal effusivity increased in the range of 1000 to 2000 J/m².K.s$^{1/2}$, at an estimate rate, a, of 50-70 J/(m².K.s$^{1/2}$.%) for water content in the range of 0-10 % (Figure 4.14a). The thermal capacity evolved in the range of 800 to 1200 J/kg.K, at rate of 15-25 J/(kg.K.%), except 7.7 J/(kg.K.%) with 16:4 % CCR:RHA (Figure 4.14b). The thermal conductivity increased in the range of 0.6 to 2 W/m.K, at rate of 0.05-0.08 W/(m.K.%) (Figure 4.15a). The thermal diffusivity evolved in the range of 4E-7 to 10E-7 m²/s, without showing reasonable correlations with the water content (Figure 4.15b).

This increase can be related to the higher value of thermal effusivity (1588 J/m².K.s$^{1/2}$), capacity (4180 J/kg.K) and conductivity (0.6 W/m.K) for liquid water compared to the values for air (6 J/m².K.s$^{1/2}$, 1004 J/kg.K, 0.03 W/m.K, respectively) in the pores of CEBs (Thermtest 2020). The water acts as bridge for thermal conduction and/or diffusion. This suggests that the thermal properties of CEBs can be estimated at various water content knowing the thermal properties in dry state.

The thermal conductivity of CEBs stabilized with by-product binders evolved with water content similarly to the few studies reported in the literature; they showed that the rate of increase is around 0.06 W/(m.K.%) (§1.7.3). Bogas et al. (2018) also claimed that the thermal conductivity of water saturated CEBs (water content of 13-16 %) was 2-2.4 times higher than that of dry CEBs. In the present study, the thermal conductivity reached values 2 times higher than that of dry CEBs before saturation (water content of <15 %). This suggests that the more the CEBs absorb water, the higher the thermal conductivity increases. Otherwise, no other studies reported on the effect of water content on the thermal properties of CEBs. Therefore, it is essential to assess the hygrothermal properties of CEB in order to better exploit their potential for hygrothermal regulation in buildings.

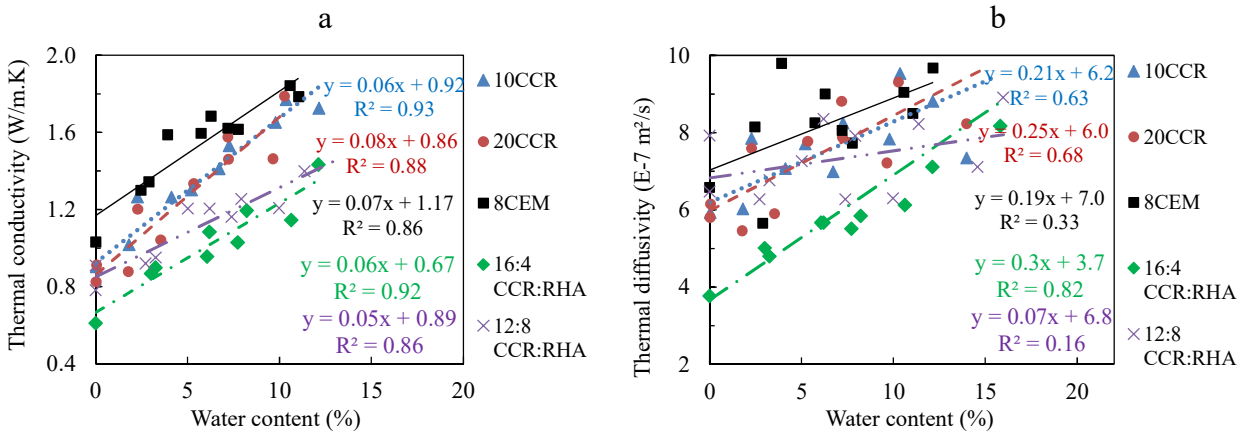

Figure 4.15. Evolution of the thermal (a) conductivity and (b) diffusivity of CEBs with water content

4.4.5. Water vapor sorption behaviors

Following up the understanding of the hygrothermal performances of CEBs, Figure 4.16 presents the sorption behavior of stabilized CEBs. It shows that the equilibrium moisture content (EMC) adsorbed by CEBs increases with relative humidity (RH: 7 to 95 %) of the environment (20±2 °C). The isotherms were fitted very well (R^2>0.99) with the GAB model describing the evolution of EMC of the stabilized CEBs with the Ψ. The isotherms of all CEBs have similar shape, type III, according to the classification of BET (Brunauer-Emmet-Teller) models (Pavlík et al. 2012).

Some studies previously reported the isotherms of same shape for CEBs (Kabre et al. 2019, Zhang et al. 2018, El Fgaier et al. 2016). Although, type II isotherm is usually the most common for porous building materials (Hansen 1986), included some earthen materials (Saidi et al. 2018). The type III isotherm is reported for the rare cases of nonporous adsorbents with very small interactions between the adsorbent and adsorbed medium (Pavlík et al. 2012).

The type III isotherms presents only one point of inflection at higher RH (about 80 % in the present study) characteristic of the beginning of the main adsorption mechanism (capillary condensation), with limited adsorption at lower RH (Zhang et al. 2018, McGregor et al. 2014, Pavlík et al. 2012). This suggests that the CEBs in the present study adsorbed water vapor molecules mainly by capillary condensation in the micropore and mesopore. The electrostatic adsorption by van der Waals forces or hydrogen bonds on the surface of the pore does not seem to be the major physical adsorption process (Zhang et al. 2018, Pavlík et al. 2012). This can be related to the low activity/interaction of kaolinite, the main clay mineral in the earthen material from Kamboinse, with the water molecules.

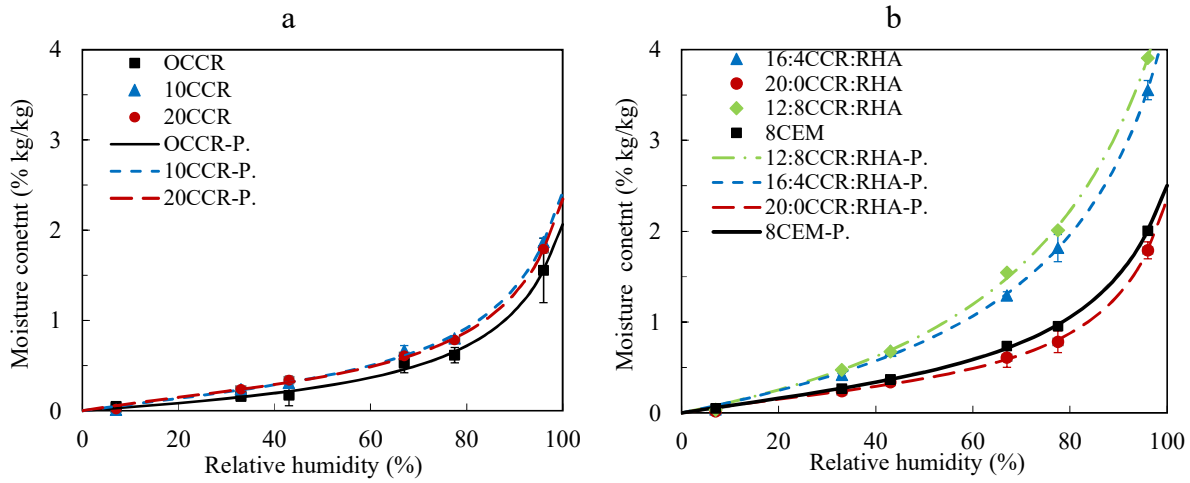

Figure 4.16. Sorption isotherms of CEBs stabilized with (a) CCR and (b) CCR:RHA: fitted with GAB model (P.), R^2 >0.99

CEBs stabilized with 10 and 20 % CCR have similar isotherms as unstabilized CEBs (0 % CCR). They reached the total EMC in the range of 1.6-1.8 % kg/kg, i.e. mass percentage of water vapor adsorbed per mass of CEBs sample (Figure 4.16a). The isotherms of CEBs stabilized with CCR:RHA recorded the highest EMC, in the range of 3.5-3.9 % kg/kg, marking clear difference with respect to the CEBs stabilized with CCR or cement (Figure 4.16b).

Different studies claimed that stabilization, with cement or lime, reduces the moisture sorption/buffering of earthen materials (Saidi et al. 2018, Arrigoni et al. 2017a, McGregor et al. 2014, Morel et al. 2013). By contrast, it is not the case in the present study where the EMC of CCR-stabilized CEBs showed same evolution as the unstabilized CEBs. Similarly, the substitution of the CCR by the RHA resulted in remarkable increase of EMC of CEBs. The reduction of the moisture sorption after stabilization was previous related to the densification of earthen matrix by hydrated cementitious products which blocked the pore spaces and prevented the air from circulating (Saidi et al. 2018). In the present study, it was not the case for the CEBs stabilized with CCR or CCR:RHA which have even higher porosity, thus better moisture sorption capacity than the unstabilized CEBs.

The type of clay is another factor influencing the moisture sorption of earthen materials. The materials containing active clay (high specific surface area) such as montmorillonite would have higher sorption capacity than non-active clay such as kaolinite (El Fgaier et al. 2016, McGregor et al. 2014, Cagnon et al. 2014). Liuzzi et al. (2013) reported high isothermal vapor sorption capacity for lime stabilized bentonite composite compared to other clay-based composite. Nevertheless, the sorption behavior of CEBs in the present study are comparable to that in the literature for kaolinite rich-earthen materials (Arrigoni et al. 2017a).

Therefore, it can be concluded that the stabilization of CEBs using the by-product binders not only improves the mechanical performances but also the hygrothermal performances. It increases the compressive strength and decreases the bulk density (increase the porosity), inducing the decrease of thermal conductivity and diffusivity and increase of moisture sorption capacity. Similarly to the thermal properties, it can be assumed that the sorption of CEBs is indirectly affected by the stabilization through the textural modification (density, porosity). This again gives possibility to control the sorption capacity through the production process. Nevertheless, increasing the total porosity of CEBs may affect the durability. Therefore, further studies should assess the effect on the long term performances such as resistance to abrasion or erodability.

4.5. Summary and conclusions

This chapter discussed the results from the characterizations of chemico-microstructural changes in the mixtures of earth-CCR-RHA and the resulting physico-mechanical and hygro-thermal properties of stabilized CEBs. The chemical interactions took place between the CCR and earthen material, and CCR:RHA which were evidenced by the consumption of portlandite from the CCR by the kaolinite from the earthen material and amorphous silica from the RHA. These interactions were responsible for permanent changes of the mineralogy and microstructure in the cured mixtures. They also improved the physico-mechanical and thermal properties of CEBs, mainly stabilized with at least 10 % CCR or 18:2 to 16:4 % CCR:RHA, such that:

The evolution of the electrical conductivity (EC) and concentration of unconsumed calcium [Ca^{2+}] allows to monitor the curing process and establish linear correlation, such that [Ca^{2+}]=97*EC, in the mix solutions of kaolinitic earthen material, CCR and RHA. The curing process of earthen materials can be monitored by measuring the EC and predicting the unconsumed [Ca^{2+}] and *vice versa*, for selecting the most reactive materials and most appropriate curing conditions.

The curing process of mix solutions containing kaolinitic earthen material and CCR requires at least 45 days at 40±2 °C to reach the optimum maturity of the pozzolanic reaction. The RHA accelerates the curing process in the mix solutions of earth and CCR:RHA to reach the maturity in only 28 days. This implies that CCR:RHA can act like cement for the stabilization of CEBs to reach the optimum compressive strength after only 28 days of curing. The chemical

interactions resulted in the formation of calcium silicate and calcium aluminate hydrates, responsible for the cementation and densification of the microstructure of stabilized CEBs.

The compressive strength of CEBs stabilized with 10 % CCR surpassed the 4 and 2 MPa respectively in dry and wet conditions, as required for the applications in the construction of two-storey buildings. The partial substitution of 20 % CCR by RHA (CCR:RHA) further improved the compressive strength to surpass the 6 MPa with 16:4 % CCR:RHA, required for the applications in three-storey building. However, the CEBs should be protected from the wet environment, using surface or architectural systems, as the wet compressive strength failed to reach the 3 MPa. By contrast, the incorporation of 0-1.2 % Okra bast fiber into the matrix of 10 % CCR-stabilized CEBs decreased the compressive strength from 4.3 to 3.5 MPa. But, this is still above the 2 MPa required for construction of non-load bearing walls.

The bulk density of CEB stabilized with CCR, CCR:RHA or containing okra fibers evolved in the range 1710 to 1550 kg/m^3. This is lower than 1801 kg/m^3 for unstabilized CEBs and 1781 kg/m^3 for CEBs stabilized with 8 % cement. The bulk density was accompanied by the increase of the total porosity in the range of 35 to 45 %.

The structural efficiency of stabilized CEBs was therefore improved, as evidenced by the decrease of bulk density and the increase of compressive strength. The coefficient of structural efficiency (CSE) of CEBs stabilized with CCR increased 4 times (609 to 3050 J/kg). This suggests that the more the CCR content, the better the load-bearing capacity of stabilized CEBs. The CSE further reached the maximum (4462 J/kg) with 16:4 % CCR:RHA; this is not only the optimum design regarding the compressive strength, but also the bearing capacity which is even better than the CSE with 8 % cement (3547 J/kg).

The thermal efficiency of stabilized CEBs was also improved, as evidenced by the decrease of thermal effusivity and increase of thermal capacity. This resulted in the decrease of thermal conductivity from 1.02 W/m.K for unstabilized CEBs to 0.69 W/m.K, 0.64 W/m.K or 0.63 W/m.K respectively for CEBs stabilized with 25 % CCR, 16:4 % CCR:RHA or containing 1.2 % fibers. It is also accompanied by the decrease of thermal diffusivity and thermal penetration depth.

Furthermore, the thermal properties (τ) of stabilized CEBs increased with water content (wc) and can be estimated as τ=axwc+b, knowing the values in dry state (b). The rate (a) was

estimated around 50-70 J/(m².K.$s^{1/2}$.%), 15-25 J/(kg.K.%), 0.04-0.08 W/(m.K.%) respectively for the thermal effusivity, capacity and conductivity.

Moreover, the stabilization with CCR:RHA improved the sorption capacity of CEBs. While the unstabilized CEBs and CCR-stabilized CEBs adsorbed the similar amount of total equilibrium moisture (1.6-1.8 % kg/kg), the CCR:RHA-stabilized CEBs absorbed 3.5-3.9 % kg/kg. This is higher than the absorption of cement-stabilized CEBs. The following chapter (V) assesses the durability of stabilized CEBs in the conditions of usage.

CHAPTER:

V. HYDRIC AND DURABILITY PERFORMANCES OF CEBs STABILIZED WITH BYPRODUCTS

5.0. Hydric and durability performances of CEBs stabilized with by-products

5.1. Introduction

This chapter presents the results from the investigations of hydric behaviors and durability of stabilized CEBs. It specifically aims to answer to the question "*how does the stabilization using by-products affect the durability of CEBs?"* comparing with unstabilized and cement-stabilized CEBs, and specifically referring to the applications in the Sahelian climatic context.

This is achieved by assessing the resistance of stabilized CEBs vis-a-vis water absorption and other indicators of the durability. The water absorption behaviors are assessed of the basis of the rate of absorption by capillary and absorption by total immersion. Among other durability indicators are resistance to abrasion, erodability, wetting-drying cycles as well as the strength of CEBs mainly in saturated conditions. The chapter further proposes recommendations on appropriate usage of stabilized CEBs.

5.2. Water absorption and accessible porosity of stabilized CEBs

5.2.1. Capillary water absorption

The measurement of water uptake by capillary immersion allowed to determine the amount of capillary water absorption, CWA (g/cm²), through the bottom face of stabilized CEBs over the square root of time ($min^{1/2}$). Figure 5.1a-c respectively present the linear correlations between capillary water absorption and square root of time in the range of 1-24 hours for CEBs stabilized with CCR, CCR:RHA and fibers. The slopes of the lines allowed to determine the sorptivity. This coefficient allows to qualitatively evaluate the rate of absorption in the capillary pores: the higher is the coefficient, the bigger is the pore radius (Cassagnabère et al. 2011). The water absorption was not determined for unstabilized CEBs which completely degraded in water.

Table 5.1a shows that the average sorptivity evolved in the range of 0.071-0.084 $g/cm^2.min^{1/2}$ for 5-25 % CEBs stabilized with 5-25 % CCR, reaching the minimum within 10-20 % CCR. For CCR:RHA stabilized CEBs, the sorptivity evolved in 0.056-0.089 $g/cm^2.min^{1/2}$, reaching the minimum within 18:2-16:4 CCR:RHA (Table 5.1b). This is higher than 0.045 $g/cm^2min^{1/2}$ for the CEBs stabilized with 8 % cement. For CEBs containing fibers, the sorptivity evolved in the range of 0.075-0.084 $g/cm^2min^{1/2}$ (Table 5.1c).

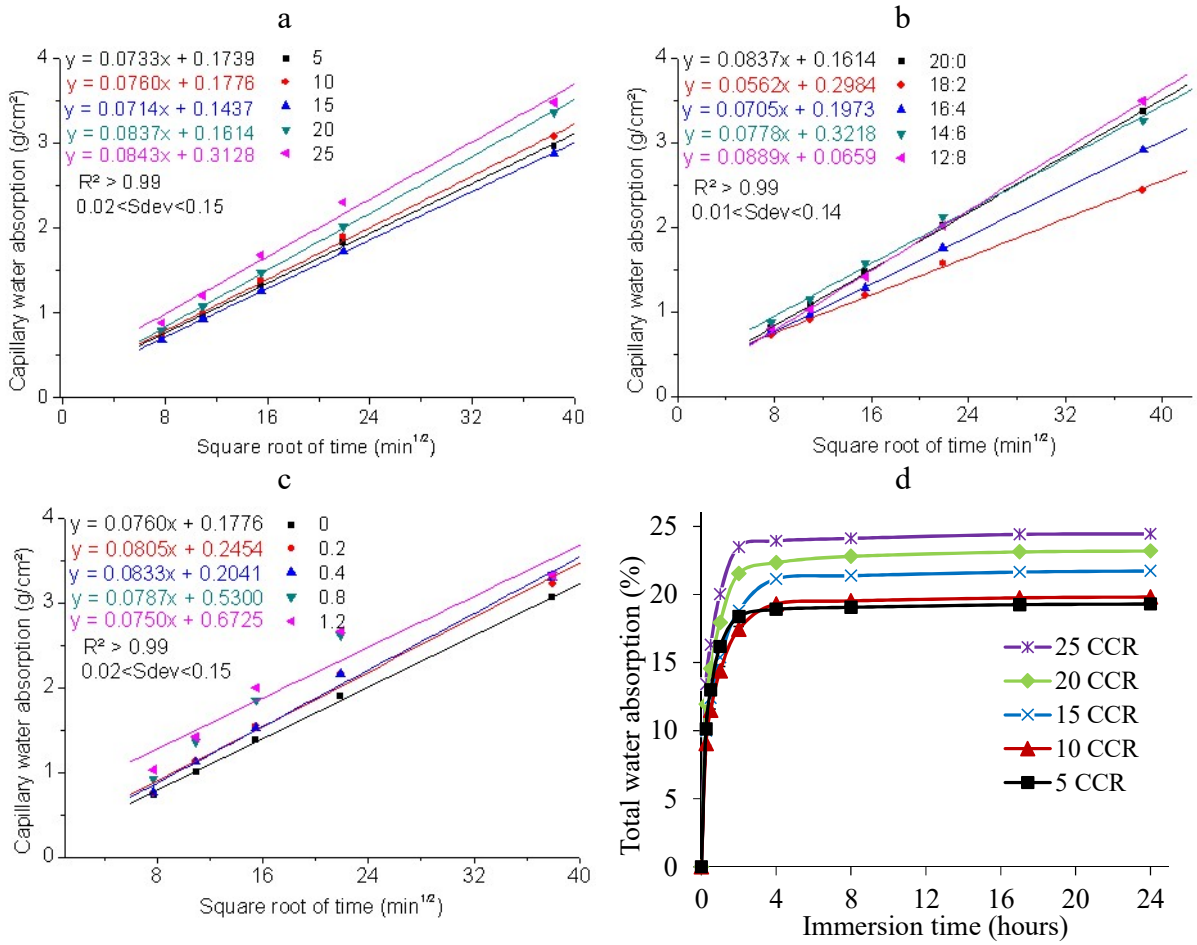

Figure 5.1. Evolution of the water absorption by capillary immersion (1-24 h) of CEBs stabilized with (a) CCR, (b) CCR:RHA and (c) 10 % CCR containing fibers, and (d) by total immersion (0-24 h) typical for CEBs stabilized with the CCR

The evolution of sorptivity suggested that the capillary pores reached the minimum radius (-) for CEBs stabilized with 10-20 % CCR; beyond which it increased (+) (Table 5.1a). CCR:RHA stabilized CEBs recorded the lowest sorptivity, thus the smallest radius (-) of capillary pores with 18:2 % CCR:RHA (Table 5.1b). For CEBs containing fibers, the radius of pores tend to increase, reaching the largest size with 0.4 % fibers (Table 5.1c). Table 5.1 also shows that the stabilization with CCR (>15 %) increased the pore size of CEBs produced at their respective OMC. This can be explained by the increase of the sorptivity with increasing OMC of stabilized CEBs, as observed in a previously study (Morel et al. 2013). Moreover, the decrease of the pore radius with the substitution of CCR by RHA can be explained by better reactivity, forming more cementitious products (§4.2.4), and thus reducing the pore size.

Furthermore, the coefficient of capillary absorption (Cb_{10min}) was determined after 10 minutes of capillary immersion for classification of CEBs. The Cb_{10min} of 5-25 % CCR stabilized CEBs evolved in the range between 9-13 g/cm².min$^{1/2}$, reaching the minimum value with 10-15 % CCR (Table 5.1a). The Cb_{10min} of CCR:RHA stabilized CEBs evolved in the range of

10-12 g/cm²min$^{1/2}$, reaching the minimum within 18:2-14:6 % CCR:RHA, compared to 8.3 g/cm²min$^{1/2}$ for CEBs stabilized with 8 % cement (Table 5.1b). By contrast, the Cb_{10min} of 10 % CCR stabilized CEBs containing 0-1.2 % fibers increased in the range of 10-16 g/cm²min$^{1/2}$ (Table 5.1c). Therefore, all stabilized CEBs have $Cb_{10min} < 20$ g/cm²min$^{1/}$2, and can be classified as CEBs of very low capillary absorption (XP P 13-901 2001).

The Cb_{10min} allows to evaluate the initial rate of water absorption in larger pores, in a sense that CEBs recorded the highest rate in the first minutes of absorption which decreased with time (Bogas et al. 2018). In fact, the Cb_{10min} reported in the present study was much lower than that of CEBs, produced using sandy soil and coarser recycled aggregates, stabilized with 8 % cement (20.8 g/cm²min$^{1/2}$) or 4:4 % cement:lime (29.8 g/cm²min$^{1/2}$) (Bogas et al. 2018). This confirms that finer earthen materials produce CEBs which have smaller pore size, as the finer particles fill in pores left by coarser particles, and thus resulting in high packing density. This was also reported by Mango-Itulamya et al. (2020) who observed that the soil containing higher fraction of clay particles reached lower Cb_{10min} than the soil containing lower fraction of clay.

5.2.2. Total water absorption

Figure 5.1d shows that the evolution of water absorption typically reached the apparent saturation after 2 hours of total immersion for CEBs stabilized with CCR. In fact, the water absorption after 2 hours (Ab_{2h}) and 24 hours (Ab_{24h}: saturation) respectively ranged in 18-24 % and 17-24 % for CEBs stabilized with 5-25 % CCR (Table 5.1a). For CCR:RHA stabilized CEBs, the Ab_{2h} and Ab_{24h} respectively evolved around 17-18 % and 23-24 %, compared to 12 % and 16 % reached by cement stabilized CEBs (Table 5.1b). The Ab_{2h} and Ab_{24h} of CEBs stabilized with 10 % CCR and containing 0-1.2 % fibers respectively increased in the range of 17-21 % and 20-22 % (Table 5.1c). The Ab_{2h} typically represents the content of water in the samples of CEBs during the test of wet compressive strength; the Ab_{24h} represents the total absorption capacity (XP P 13-901 2001).

The ratio Ab_{2h}/Ab_{24h} evolved in the range of 0.87-0.96, 0.74-0.80, and 0.92-0.96 for CEBs stabilized with the CCR, CCR:RHA and those containing fibers (Table 5.1). The smaller ratio for the CEBs stabilized with CCR:RHA can also qualitatively suggest lower rate of water uptake, and thus better wet compressive strength than the CEBs stabilized with CCR alone or fibers. While the Ab_{24h} increased with CCR content, it was quasi-constant during the substitution of CCR by RHA. Nevertheless, the Ab_{24h} for all CEBs was slightly higher than recommended limits (15-20 %) for application in wet conditions (Bogas et al. 2018, Guettala

et al. 2006). Therefore, precaution should be taken if these CEBs are used in wet environment, by applying either surface or architectural protections.

Guettala et al. (2006) observed that water absorption of CEBs decreased (Ab_{24h}: 8.3-7.4 %) with increasing cement content (5-8 %). Similar observation was reported by Masuka et al. (2018), the Ab_{24h} of 16-11 % for CEBs stabilized with 4-10 % cement. By contrast, other binder (lime) may have an opposite effect. Indeed, Bogas et al. (2018) reported the Ab_{24h} of 13.6 and 16.5 % respectively for CEBs stabilized with 8 % cement and 4:4 % cement:lime, using production moisture content of 9.5 and 10 %. Sore (2017) similarly reported the Ab_{24h} in the range of 14-18 % for CEBs stabilized with 10-20 % geopolymer produced using the moisture of 17-22 %, compared to 12 % for 8 % cement-CEBs produced using the moisture of 17 %. This is equivalent to the ratio (Ab_{24h}/ production moisture) in the range of 0.7-0.8 for CEBs stabilized with cement or geopolymer. This ratio is >1 and 0.8 respectively for CEBs stabilized with CCR (lime) or CCR:RHA and cement in the present study.

This shows that the stabilization using cement or alkaline and thermal-activated geopolymer is more effective than lime (CCR) with regards to water absorption. It also shows that the water absorption capacity of CEBs is not only affected by the type and content of stabilizer, but also the type of raw earthen material. The materials requiring high production moisture would produce stabilized CEBs with high porosity, resulting from the evaporation of production moisture, thus high water absorption. Although, other production parameters such as compaction pressure and curing conditions affect the hydric behaviors of stabilized CEBs. Therefore, the final water absorption capacity of CEBs can be controlled by optimization of the initial production conditions (§3.4.1).

5.2.3. Water accessible porosity

Figure 5.2 presents the evolution of water accessible porosity (WAP), after saturation by total immersion, with respect to the total porosity (TP) of stabilized CEBs. Table 5.1 further summarizes the values of the TP and WAP. The WAP is in range of 33-36 % for the CEBs stabilized with 5-25 % CCR, equivalent to 0.88-0.79 (ratio WAP/TP) of the total porosity (Table 5.1a). The WAP slightly increased in the range of 36-38 % for the CEBs stabilized with CCR:RHA, equivalent to 0.89-0.96 of the total porosity. This is higher than the WAP of 29.2 % for the CEBs stabilized with 8 % cement, equivalent to 0.79 of the total porosity (Table 5.1b). For CEBs containing 0-1.2 % fibers, the WAP ranged in 35-36 %, equivalent to 0.89 of the total porosity (Table 5.1c).

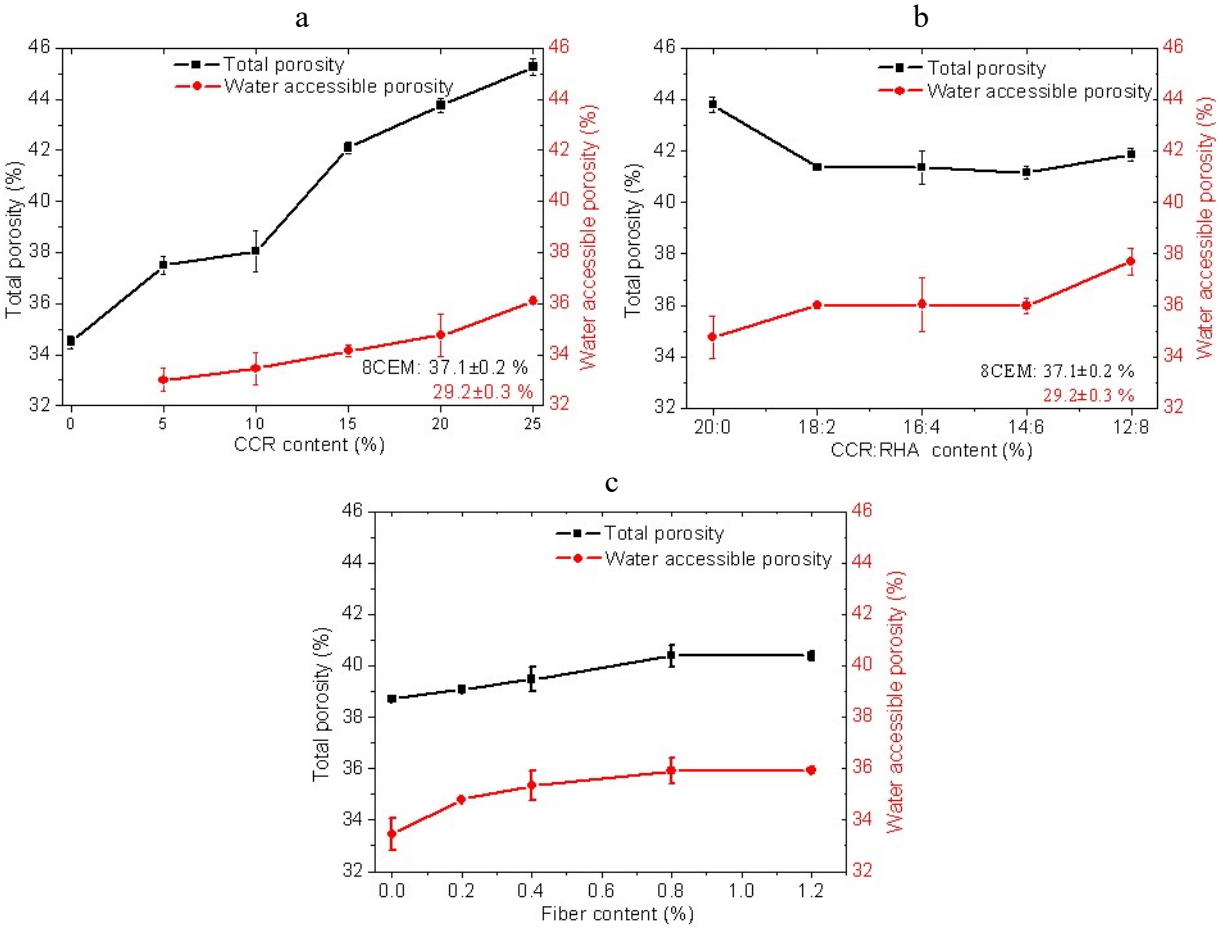

Figure 5.2. Total porosity vs. water accessible porosity of CEBs stabilized with (a) CCR, (b) CCR:RHA and (c) 10 % CCR containing fibers

Bogas et al. (2018) reported the WAP of 25 and 29 % respectively for CEBs stabilized 8 % cement and 4:4 % cement:lime, which was more than 0.80 of the TP. Sore (2017) reported the WAP in the range of 36-38 % for CEBs stabilized with 5-20 % geopolymer, compared to 33 % with 8 % cement. In the present study, the CEBs stabilized with CCR:RHA recorded higher WAP than the CEBs stabilized with CCR alone, but comparable to that of geopolymer-CEBs. This can be related to the production moisture (22 %) for CCR:RHA-CEBs taken equivalent to the moisture for 20 % CCR-CEBs. CEBs stabilized with by-product binders in the present study reached comparable value of WAP as CEBs stabilized with common binders in the literature (Bogas et al. 2018, Sore 2017). Therefore, the WAP, similarly to the Ab_{24h}, can be further reduced by optimizing the production conditions.

While the TP represents the bulk fraction of pores in the CEBs, the WAP represents the fraction which is readily accessible by water, i.e. the interconnected (open) porosity. Figure 5.2a clearly shows that the bulk porosity increased at a relatively higher rate than the interconnected porosity with respect to the CCR content, i.e. decreasing ratio WAP/TP (0.88-0.79) in Table 5.1a.

Figure 5.2b shows a quasi-constant evolution of the porosity around 18:2-14:6 % CCR:RHA, with the ratio WAP/TP of 0.9 (Table 5.1b).

This indicates that the improvement of the durability of stabilized CEBs was achieved around 18:2-14:6 % CCR:RHA. The sorptivity and initial rate of capillary water absorption (Ca_{10min}) reached the minimum values with 15 % CCR, and increased beyond. These parameters also reached the lowest values with 18:2 and 16:4 % CCR:RHA, respectively. Moreover, while the increase of total porosity was beneficial for the structural and thermal efficiency of stabilized CEBs (§4.3.4 and §4.4.3); the WAP should ideally decrease for the improvement of durability. This would turn into the decrease of capillary and total water absorption and possibly the increase of the strength in wet conditions (§4.3.2).

Table 5.1. Hydric properties of CEBs stabilized with (a) CCR, (b) CCR:RHA and (c) 10 % CCR and containing fibers: average values and coefficient of variations

a

Binder/fiber (wt %)		Production moisture (wt %)	Total porosity (TP) (%)		Absorption by capillary immersion (g/cm²min$^{1/2}$)				Absorption by total immersion (%)									
					Sorptivity [a]		Pore radius [b]	Cb_{10min} [c]			Ab_{2h} [d]		Ab_{24h} [e]		Ab_{2h}/ Ab_{24h}	WAP [f]		WAP/TP [g]
CCR	0	17	34.5	1	ND		ND	ND			ND		ND		ND	ND		ND
	5	18	37.5	1	0.073	6	*	10.5	7		18.4	4	19.3	2	0.95	33.0	1	0.88
	10	19	38.1	2	0.076	3	*	10.2	4		17.4	4	19.8	1	0.88	33.4	2	0.88
	15	21	42.1	1	0.071	1	-	9.9	4		18.8	3	21.7	1	0.87	34.2	1	0.81
	20	22	43.8	1	0.084	2	++	12.2	5		21.5	4	23.2	1	0.93	34.8	2	0.79
	25	23	45.3	1	0.084	3	++	12.6	14		23.5	2	24.4	1	0.96	36.1	0	0.80

b

CCR: RHA	20:0	22	43.8	1	0.084	2	++	12.2	5		21.5	4	23.2	1	0.93	34.8	2	0.79
	18:2	22	40.5	0	0.056	2	----	10.9	11		17.5	2	22.8	0	0.77	36.0	0	0.89
	16:4	22	40.4	1	0.071	7	-	10.4	3		18.3	2	22.9	4	0.80	36.0	3	0.89
	14:6	22	39.8	1	0.078	6	+	12.0	8		18.0	3	22.8	1	0.79	36.0	1	0.90
	12:8	22	39.3	0	0.089	1	+++	10.8	3		18.0	5	24.3	2	0.74	37.7	1	0.96
8CEM	8	19	37.1	1	0.045	9	------	8.3	12		12.4	1	16.4	2	0.76	29.2	1	0.79

c

Fibers	0	19	38.1	2	0.076	3	*	10.2	4		17.4	4	19.8	1	0.88	33.4	2	0.88
	0.2	19	39.1	0	0.081	1	+	10.8	4		19.6	2	21.3	2	0.92	34.8	0	0.89
	0.4	19	39.5	1	0.084	1	++	11.4	10		20.3	1	21.6	2	0.94	35.3	2	0.89
	0.8	19	40.4	1	0.079	1	+	13.3	5		21.1	1	22.1	2	0.96	35.9	1	0.89
	1.2	19	40.4	0	0.075	1	*	15.6	15		21.0	2	22.2	1	0.95	35.9	0	0.89

ND: Not determined.

[a] Sorptivity: slope given by linear correlation between coefficient of absorption through the capillary pores and square root of time [R^2>0.99] between 1 and 24 hours (g/cm²min$^{1/2}$) ;

[b] Pore radii: qualitative evaluation of the radius of capillary pore with respect to an arbitrary reference/benchmark sorptivity "*"; "+" and "-" respectively represent relative increase and decrease of the radius. Estimations were made in a margin of 0.005;

[c] Cb_{10min}: coefficient of capillary absorption after 10 min: $Cb_{10min} \leq 20$ g/cm²min$^{1/2}$ for "very low capillary absorption"; $Cb_{10min} \leq 40$ g/cm²min$^{1/2}$ for "low capillary absorption"; conventional estimated according to XP P 13-901 (2001);

[d, e] Ab_{2h}, Ab_{24h}: percentage of water absorbed respectively after 2 and 24 hours of total immersion of CEBs;

[f] WAP: water accessible porosity is the porosity which is freely saturated after 24 h of total immersion in water.

[g] WAP/TP: ratio between the water accessible porosity and total porosity.

5.3. Durability indicators of stabilized CEBs

The stabilization of CEBs with by-products general improved different durability indicators such as the resistance to erodability, abrasion, wetting-drying cycles and compressive, etc. Figure 5.3 shows remarkable improvement of the apparent erodability of stabilized CEBs.

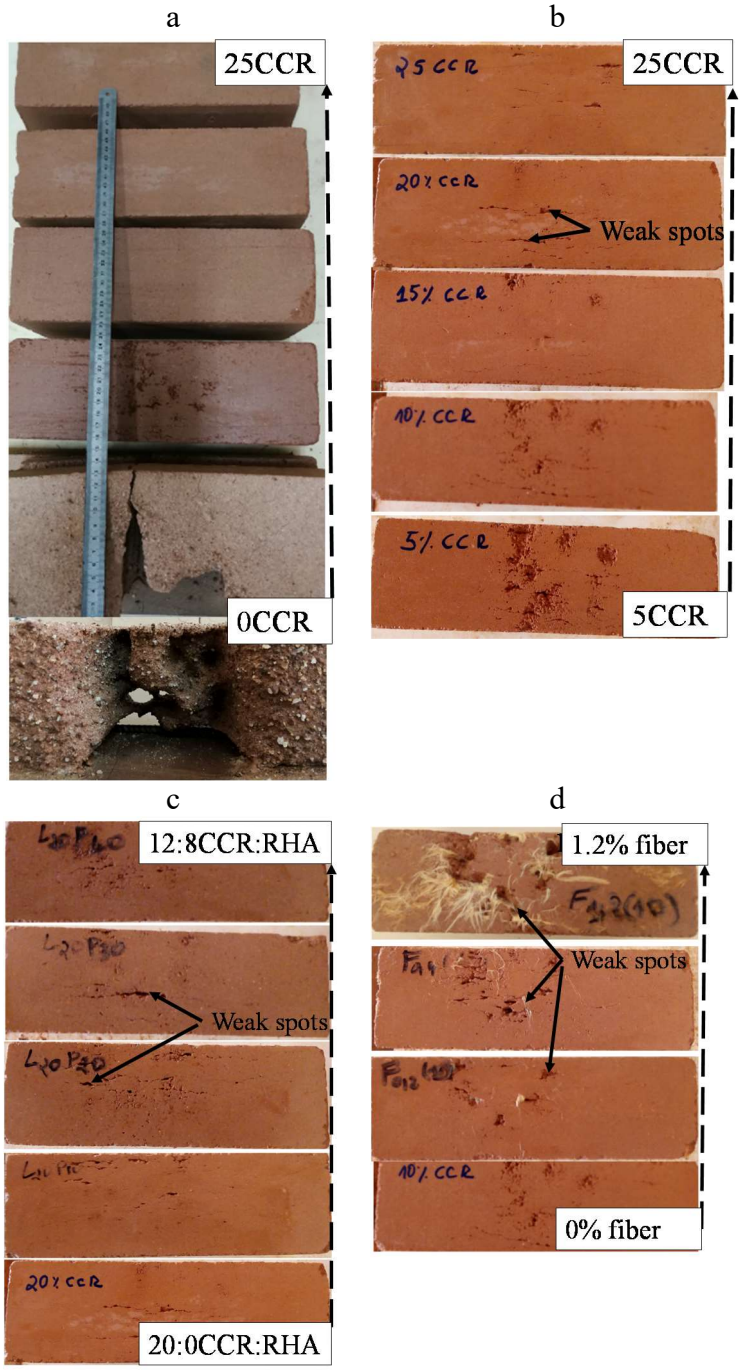

Figure 5.3. Apparent erodability at 50 kPa: (a) unstabilized CEBs vs. CCR stabilized CEBs; and at 500 kPa: CEBs stabilized with (b) CCR, (c) CCR:RHA and (d) 10 % CCR containing fibers

5.3.1. Resistance to water erodability

The resistance to water erodability was tested based on the depth of erosion per hour (DE/hour) and percentage of eroded area, experimentally estimated with respect to the total area of stabilized CEBs exposed to water erosion. The CEBs stabilized with by-products and tested using standardized pressure (50 kPa for 1 hour), by Bulletin 5 Test (NZS 1998), were not eroded. The CEBs successfully passed the test, except unstabilized CEBs which completely degraded in lesser than 15 minutes (Figure 5.3a).

Similar observation was previously made for earth blocks stabilized with 8 % cement or 4:4 % cement:lime (Bogas et al. 2018) or GGBS activated by cement or lime (Seco et al. 2017). The present study presents the results acquired on stabilized CEBs tested using an arbitrary water pressure of 500 kPa for 1 hour. This pressure was deliberately used for assessing the effect of different types and contents of by-product stabilizers on the erodability of CEBs (Figure 5.3b-d). Other studies had previously used modified pressures, such as 300 kPa (Bogas et al. 2018) and 2070-4130 kPa (Obonyo et al. 2010).

The depth of erosion and percentage of eroded area of CEBs stabilized with 5-25 % CCR decreased in the ranges of 7-4 mm/h and 41-3 %, respectively (Table 5.2a). Table 5.2b shows that the depth of erosion and eroded area, respectively, ranged in 5-7 mm/h and 9-27 % for CEB stabilized with 20:0-12:8 % CCR:RHA. This is slightly higher than 3.5 mm/h and 7 % for CEBs stabilized with 8 % cement. The incorporation of 0-1.2 % fibers resulted in depth of erosion and eroded area respectively in the range of 4-7 mm/h and 10-20 % (Table 5.2c).

For the record, the depth of erosion was less than 1 mm/h for CEBs stabilized with 8 % cement or 4:4 % cement:lime tested with water pressure of 300 kPa (Bogas et al. 2018). The depth was 1, 20 and 55 mm/h for CEBs containing 7 % cement, 5:7 % cement:lime and 1 % fiber tested at 4130 kPa, respectively (Obonyo et al. 2010).

Table 5.2 also shows high coefficient of variation (CV up to 100) of the depth of erosion and eroded area which can be related to surface defects constituting the week spots. The weak spots, which suffered aggressive erosion, were observed mainly on the CEBs containing CCR:RHA and fibers (Figure 5.3). In fact, cracks were initially formed on the surface of some stabilized CEBs just after production. Moreover, high fiber content also entangled and resulted in non-homogeneous dispersion, thus forming aggregates of weak spots (Figure 5.3d).

These cracks may have been the origins of continuous and deep fissures; water penetrated through the cracks and induced internal pressure. This not only affected the resistance to surface erosion but also promoted the ingress of water and other agents and may compromise the durability and mechanical resistance of CEBs. Therefore, precautions should be taken to limit surface defects on CEBs or, if needed, apply surface treatment.

Although, the stabilized CEBs were tested using exaggerated water pressure (500 kPa in the present study); they still underwent depth of erosion far below the limit of 120 mm/h recommended for a pressure of 50 kPa. Therefore, they can be classified as no erodable CEBs (NZS 1998). In fact, the spray erosion test can be regarded more like a test of the efficiency of stabilizer than direct durability indicators of CEBs, given its severity (Beckett et al. 2020). However, this shows that the stabilized CEBs can resist erosion very well, even if they are exposed to extremely harsh rainy conditions.

Moreover, the eroded area of CEBs stabilized with at least 10 % CCR in the present study was less than 40 % previously measured in the real conditions for wall masonry made of CEBs stabilized with 8 % lime (Guettala et al. 2006). That study (Guettala et al. 2006) is one of kind, to the best knowledge of the authors, where the masonry was exposed to a real rainfall (120 mm/year) for 4 years in Biskra, Algeria and underwent an erosion depth less than 1 mm.

This suggests that assessing the resistance to erodability only on the basis of the depth of erosion may mislead into over-estimating the depth of erosion resulting from testing the weak spots. Therefore, the depth should be accompanied by the percentage of eroded area for a better interpretation. Nevertheless, there is still need for more studies to couple the analysis of the common durability indicators and percentage of eroded area in order to validate it.

Testing the erodability with water pressure of 500 kPa was equivalent to an average water discharge of 22.4 liter/minute. The knowledge of the total area (diameter of 90 mm) of the sample exposed to the erosion test and time of exposure (1 hour) allowed to estimate the total amount of water (mm) which fell on the sample. Considering the average rainfall of 788 mm/year in Ouagadougou (region Centre of Burkina Faso) allowed to estimate the time, equivalent to 270 years, for exposure to an equivalent amount of rain water used in the present study. It is noteworthy that this is just an indicative comparison, between the water erosion in the lab and rain erosion in real condition, given the differences in impact forces. The (accelerated spray) erosion test in the lab is usually more severe than under normal rainfall conditions (Beckett et al. 2020).

Table 5.2. Durability indicators of CEBs stabilized with (a) CCR, (b) CCR:RHA and (c) 10 % CCR containing fibers: Averages and coefficients of variations

a

Binder/ fiber (%)		Resistance to erodability				Coefficient of abrasion (cm²/g)				Weight loss by abrasion (%)				Dry compressive strength (MPa)			
		DE/hour (mm)		Eroded area (%)		Before W-D		After W-D		Before W-D		After W-D		Before W-D		After W-D	
CCR	0	ND		ND		1	13	ND		2.43	14	ND		1.1	3	ND	
	5	6.7	34	41	37	3	27	1	17	0.5	25	1.78	7	3	3	3.5	5
	10	4.7	31	15	21	12	25	14	14	0.12	27	0.08	39	4.3	10	5.9	8
	15	4.8	7	3	87	16	9	46	0	0.09	10	0.03	0	4.6	5	6.8	6
	20	4.8	12	9	58	20	13	31	0	0.08	12	0.05	0	4.4	7	6.2	6
	25	3.9	16	4	100	27	16	52	17	0.06	18	0.03	16	4.5	3	6.0	16
b																	
CCR: RHA	20:0	5.2	15	9	58	20	13	ND		0.08	12	ND		4.4	7	ND	
	18:2	5.8	31	9	33	27	20	ND		0.06	20	ND		6.4	4	ND	
	16:4	5.3	24	16	4	46	71	ND		0.02	50	ND		7	3	ND	
	14:6	5.3	24	17	43	39	28	ND		0.04	29	ND		6.8	6	ND	
	12:8	7	51	27	61	70	47	ND		0.02	47	ND		6	5	ND	
8CEM		3.5	14	7	63	70	47	ND		0.02	47	ND		6.2	4	ND	
c																	
Fibers	0	4.7	31	15	21	12	25	ND		0.12	27	ND		4.3	10	ND	
	0.2	6.3	12	13	25	14	33	ND		0.1	32	ND		3.7	7	ND	
	0.4	10	17	20	11	14	33	ND		0.11	34	ND		3.7	7	ND	
	0.8	6.5	0	21	28	10	46	ND		0.16	43	ND		3.7	7	ND	
	1.2	7	20	10	56	18	0	ND		0.08	1	ND		3.5	2	ND	

W-D: wetting-drying; DE: depth of erosion; ND: not determined; CV: coefficient of variation.

This can theoretically imply that the CEBs stabilized by the by-products (maximum depth of erosion of 7 mm/h) would undergo a linear erosion rate less than 0.03 mm/year, if exposed to the rainy condition in Ouagadougou. It is noteworthy to mention that the earth practically undergoes a non-linear rate of erosion: it is high at the beginning and decrease over time (Bui et al. 2009). Previous study (Bui et al. 2009) reported an erosion rate of 0.1 mm/year for rammed earth walls stabilized with 5 % hydraulic lime and exposed to natural climatic conditions (average rainfall of 1000 mm/year) for 20 years, in France. Moreover, the erosion rate was 0.25 mm/year, as deduced from Guettala et al. (2006).

Additionally, the erodability of CEBs tested in the standard conditions (NZS 1998) tended to decrease in the range of 1-0.6 mm/min (60-35 mm/h) with increasing fibers content (0-1 %) (Danso et al. 2015). By contrast, the erodability tended to increase with fiber content in the present study. This again suggest that the fiber dominated weak spots may be responsible for the deep erosion in the present study.

5.3.2. Resistance to abrasion

The resistance to abrasion was assessed based on the evolution of the coefficient of abrasion, increasing for high resistant CEBs. The average coefficient of abrasion increased in the range of 1-30 cm^2/g for CEBs stabilized with 0-25 % CCR (Figure 5.4a). The substitution of 20 % CCR by RHA (20:0-12:8 % CCR:RHA) resulted in further increase of the coefficient of abrasion in the range of 20-70 cm^2/g (Figure 5.4b). The CEBs stabilized with CCR:RHA comparatively reached the same average coefficient of abrasion as CEBs stabilized with 8 % cement (70 cm^2/g). The CCR:RHA-CEBs were very hard that they barely lost either 1 or 2 g during the abrasion test, which caused very high fluctuation of the average values and standard deviations of the coefficient of abrasion (Figure 5.4b).

By contrast, the incorporation of 0-1.2 % fibers in the CEBs did not have noticeable effects of the coefficient of abrasion, around 15-20 cm^2/g (Figure 5.4c). However, the coefficient of abrasion for all CEBs stabilized with by-product binder or fibers is far higher than the 7 cm^2/g required for applications in facing wall masonry of three-storey buildings (CDI and CRATerre 1998).

For CEBs steam cured for 24 hours, the coefficient of abrasion also increased (6-10 cm^2/g) with lime content (6-10 %) and reached the maximum (23 cm^2/g) with lime:natural pozzolan (7:3 %)

(Izemmouren et al. 2015). This highlights that coupling the lime-rich stabilizer (CCR) with pozzolan (RHA) yields better resistance to abrasion of CEBs than lime alone.

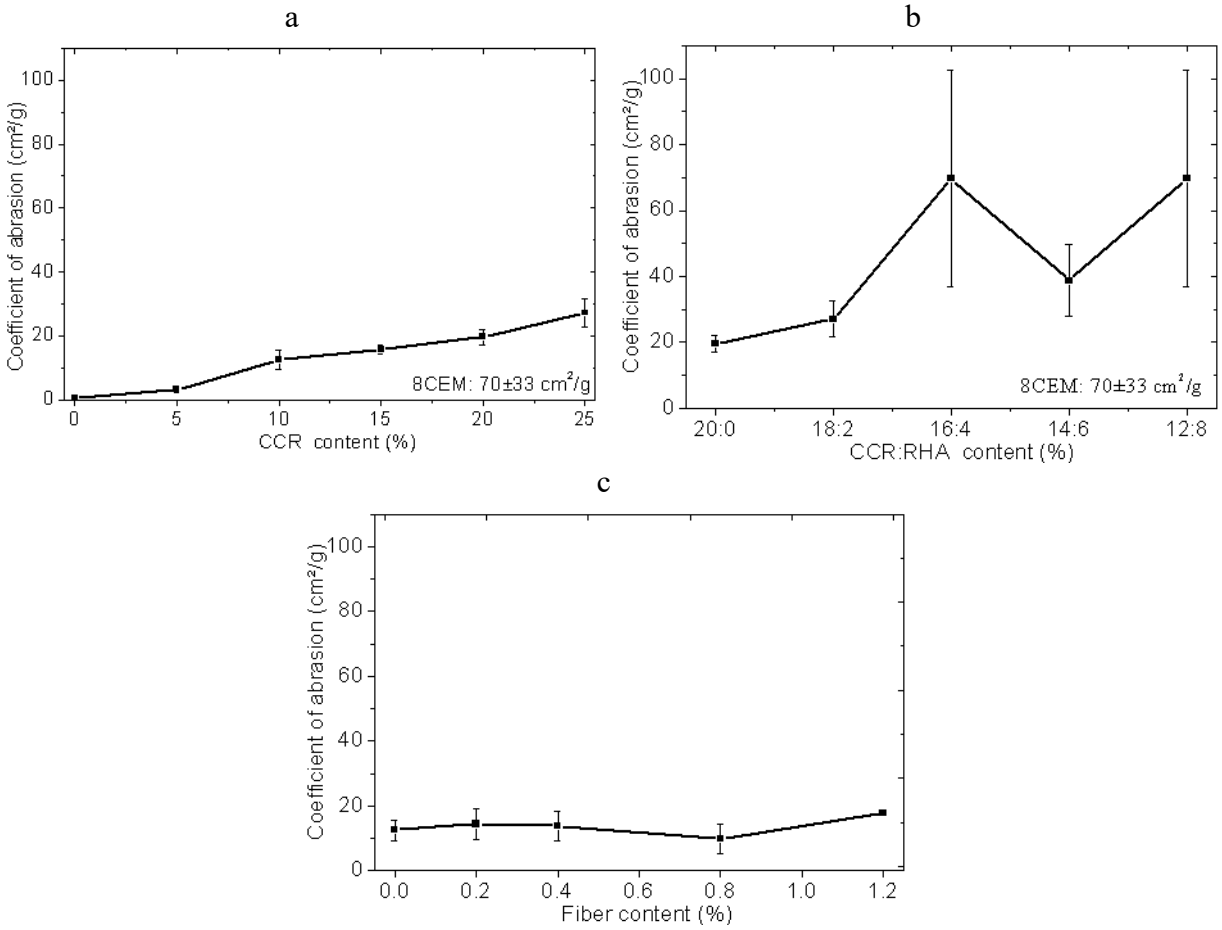

Figure 5.4. Coefficient of abrasion of CEBs stabilized with (a) CCR, (b) CCR:RHA and (c) 10 % CCR containing fibers

Table 5.2 additionally presents the evolution of the average percentage weight loss by abrasion before W-D. The weight loss ranged in 2.43-0.06 %, 0.08-0.02 % and 0.12-0.08 % respectively for the CEBs stabilized with the CCR, CCR:RHA and those containing fibers (Table 5.2a-c). The weight loss was far below the recommended value of 10 %, according to the CRATerre (Ngowi 1997). Table 5.2 also details the average values of the coefficients of abrasion and weight loss, before wetting-drying (W-D), along with the coefficients of variations (CV). It shows that the CV for the coefficient of abrasion is equal or less than 27 for the CCR stabilized CEBs, while it is as high as 71 or 46 for CEBs stabilized with CCR:RHA or containing fibers.

This indicates that the coefficient of abrasion of CEBs containing CCR:RHA and fibers has high variability compared to that of CCR stabilized CEBs. This variability can again be related to the surface defects (weak spots: Figure 5.3c-d) observed on the CEBs containing the CCR:RHA or fibers.

5.3.3. Resistance to wetting-drying cycles

According to the standard D559-03 (ASTM 1989b), the resistance to wetting-drying (W-D) test assesses the weight loss of cement stabilized soil subjected to 12 cycles of W-D. In the present study, it was adapted to test the coefficient of abrasion and compressive strength, because CEBs stabilized with CCR (5-20 %) did not degrade or loss weight over the W-D cycles. Similar observation was reported for earth blocks stabilized with GGBS activated by cement or lime (Seco et al. 2017). However, the test could not be carried out for unstabilized (0 % CCR) CEBs which immediately degraded in contact with water (Figure 5.3a).

Table 5.2a shows that the coefficient of abrasion and compressive strength of CEBs increased with the CCR content, even after the W-D cycles. The coefficient of abrasion and compressive strength respectively evolved in the ranges of 14-52 cm²/g and 5.9-6.8 MPa after W-D, far higher than 12-27 cm²/g and 4.3-4.6 MPa reached before W-D for CEB stabilized 10-25 % CCR (Table 5.2a). This is equivalent to the compressive strength 0.4-0.5 times higher after 12 cycles of W-D than before W-D. It is indeed accompanied by the decrease of the weight loss on abrasion after W-D (0.08-0.03 %) for CEBs stabilized with ≥10 % CCR, which is smaller than the weight loss before W-D (0.12-0.06 %) (Table 5.2a). By contrast, the value of the coefficient of abrasion and compressive strength after W-D was smaller or comparable to the value before W-D for CEBs stabilized with 5 % CCR. This suggests that the CEBs should be stabilized with at least 10 % CCR for keeping the long term performances.

The increase of the coefficient of abrasion and compressive strength is related to the hygro-thermo-activation, during the W-D cycles, of the pozzolanic reaction between the clay material and the excess, previously unreacted, CCR (>10 %). In fact, above 10 %, the CCR could not efficiently react during the curing at ambient temperature (30±5 °C), which resulted in asymptotic evolution of the compressive strength of CCR-stabilized CEBs before W-D cycles. However, the W-D cycles created the favorable conditions of temperature (up to 70 °C) and humidity (up to 100 %) for further pozzolanic reaction to take place. The same phenomenon took place by increasing the curing temperature (40 °C), which resulted in continuous increase of the compressive strength of different clay materials stabilized with up to 20 % CCR (Nshimiyimana et al. 2020a, 2020b). This confirms the previous suggestion (§4.3.1) that CEBs are should be stabilized with lime-rich binders in warm regions such as in Burkina Faso or else, and maintaining the curing humidity relatively high.

The above reveals that the stabilization of CEBs with the CCR (lime-rich stabilizer) is beneficial and further improves the performances with W-D cycles. This is not the case with cement (CEM) stabilization reported in the literature. In fact, Arrigoni et al. (2017b) showed that the compressive strength of earthen material stabilized with CEM and FA improved by 0.4 times after W-D curing compared to standard curing, while that of the earthen materials stabilized with CCR and FA improved by 1.6 times. This is related to better consumption of the calcium hydroxide through the pozzolanic reaction over the W-D cycles. Additionally, the compressive strength of CEBs stabilized with 4 % cement decreased by 0.3 times (Hakimi et al. 1998) and 0.5 times with 8 % cement (Yogananth et al. 2019) respectively after 6 and 12 cycles of W-D, with respect to the initial strength.

5.3.4. Durability indicators versus compressive strength

The compressive strength, in dry or wet conditions, is considered as an indirect indicator of the quality and durability of CEBs (Bogas et al. 2018, CDI and CRATerre 1998). Its improvement can be related to the ability of CEBs to resist attacks of different environmental agents such as water ingress and erosion, dry abrasion, etc. Indeed, the standard ARS 675:1996 (CDI and CRATerre 1998) recommends that *"if the test to establish the water absorption or abrasion are not feasible […], this deficiency can be compensated by increasing the requirements for the dry and/or wet compressive strength by one category"*. The three structural categories of CEBs for application in facing wall masonry were presented in Table 1.5.

In the present study, the evolution of the compressive strength (Rc in MPa) was tentatively correlated with the coefficient of abrasion (Ca in cm²/g) of CEB stabilized with CCR (before W-D) and CCR:RHA (Figure 5.5a). It reached the best fit with an equation $R_c=1.6xC_a^{0.35}$. This suggests that the compressive strength can roughly be predicted from the test of abrasion, and vice versa. It can be useful as a non-destructive abrasion test of the CEBs for preliminary design or quality control in the lab or onsite, contrary to the compressive test which requires high end equipment. Figure 5.5b shows a good agreement between the predicted ($R_c=1.6xC_a^{0.35}$) and measured compressive strength, mainly below the compressive strength of 4 MPa. However, this correlation still needs validation for other type of materials, and also stabilized with classical binders.

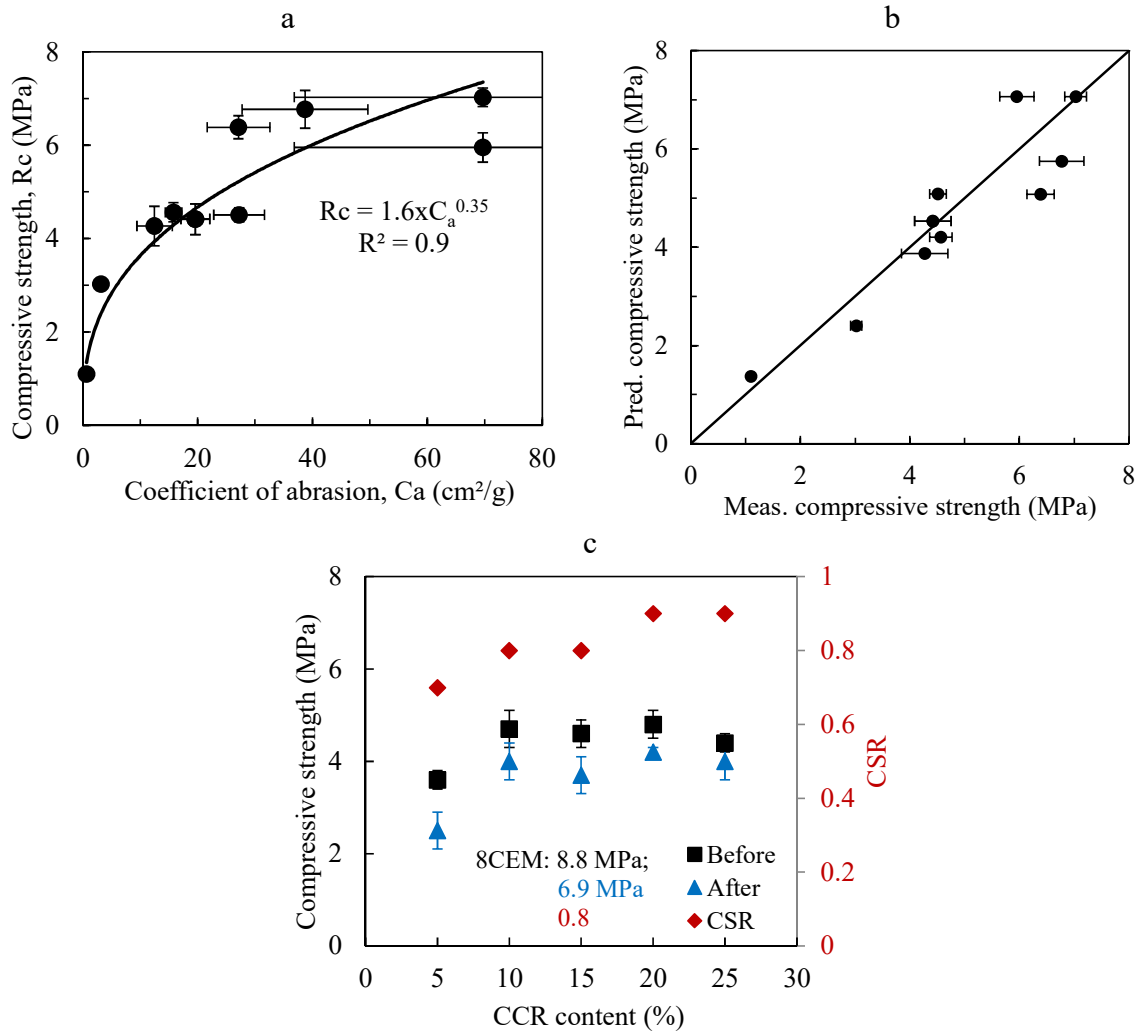

Figure 5.5. Correlation between (a) the coefficient of abrasion and compressive strength, before W-D, (b) predicted (Pred.) versus measured (Meas.) strength, (c) compressive strength before and after saturation (2 h)-drying (40 °C), CSR: coefficient of strength reversibility

The durability of earthen materials is also commonly related to the compressive strength, mainly the ratio between the wet (Rc_{wet}) and dry (Rc_{dry}) strength [5]. This ratio, defined as the coefficient of water strength ($CWS=Rc_{wet}/Rc_{dry}$), evolved in the range of 0.4 and 0.6 for CEBs stabilized with CCR and CCR:RHA. The CWS of at least 0.5 is recommended for CEBs to be considered durable, according to standards XP P 13-901 (2001) and ARS 675:1996 (CDI and CRATerre 1998). However, CWS in the range of 0.3-0.7 can still be acceptable (Bogas et al. 2018, Guettala et al 2006). Therefore, this shows that the CEBs stabilized with the by-products fulfill this criteria.

Moreover, the ratio between the compressive strength ($Rc_{wet-dry}$) of CEBs after soaking in water (2 h) and drying until constant mass (40 °C) and the initial compressive strength (Rc_{dry}) of dry CEBs, after curing, allowed to define the coefficient of strength reversibility ($CSR=Rc_{wet-dry}/Rc_{dry}$). The CSR of CEBs stabilized with 5-25 % CCR ranged in 0.7-0.9

compared to 0.8 for CEBs stabilized with 8 % cement (Figure 5.5c). This suggests that stabilized CEBs would not only resist the degradation and erosion in contact with water but also almost recover the strength after drying.

While the stabilization of CEBs with by-product binders was detrimental on absorption behaviors, it was beneficial on the resistance to erodability, abrasion and wetting-drying cycles. In fact, Bogas et al. (2018) previously suggested that binders have more direct effect on the mechanical and durability properties than on total porosity, thus the water accessible porosity. This confirms that the most challenging indicator of the durability of CEBs is still the resistance to water absorption, which is also a factor of the deterioration of mechanical performances in wet conditions. Nevertheless, the reversibility of the compressive strength and improvement after W-D cycles are promising indicators for the long term performances of CEBs after exposure to environmental conditions.

5.4. Summary and conclusions

This chapter investigated the durability of CEBs stabilized with by-products, mainly referring to applications in the Sahelian climatic context of Ouagadougou, Burkina Faso. Different independent investigations showed that the by-product binders are valuable for the stabilization and improvement of various durability indicators of CEBs. The durability indicators of CEBs reached optimum values with 10 to 15 % CCR or 18:2 to 16:4 % CCR:RHA, such that:

The coefficient of capillary absorption was far below the recommended limit of 20 g/cm².min$^{1/2}$ for very low capillary CEBs. It reached the minimum values of 9.9 g/cm².min$^{1/2}$ with 15 % CCR and 10.4 g/cm².min$^{1/2}$ with 16:4 % CCR:RHA. Nevertheless, the water absorption increased (18-24 %) and exceeded the limits (15-20 %) recommended for usage in wet environment. This affected the water accessible porosity which reached the ratios of 0.96 with respect to the total porosity. The WAP should ideally decrease for the improvement of the durability. This would results in the decrease of capillary and total water absorption and increase of the strength in wet condition.

The resistance to erodability of stabilized CEBs was improved. Stabilized CEBs remained intact when tested at standardized water pressure (50 kPa), while the unstabilized CEBs fully deteriorated in less than 15 minutes. At higher pressure (500 kPa), the stabilized CEBs suffered light erosion. The depth of erosion and percentage of eroded area, respectively, reached 4.8 mm/h and 3 % with 15 % CCR; they respectively reached 5.8 mm/h and 9 % with 18:2 %

CCR:RHA. This is far lower than the recommended value of 120 mm. The lifespan estimated in the Sahelian climatic context exceeds 270 years, equivalent to the linear rate of erosion <0.03 mm/year.

The coefficient of abrasion of stabilized CEBs was far higher than 7 cm²/g required for applications in facing wall masonry. It reached 16 cm²/g with 15 CCR and 16 cm²/g with 16:4 % CCR:RHA. The stabilization with the 10-25 % CCR further increased the resistance to abrasion and compressive strength of CEBs after wetting-drying cycles. This suggests that the stabilization with at least 10 % CCR is required for reaching the long term durability of CEBs.

The correlation ($R_c=1.6xC_a^{0.35}$) was established between the compressive strength (Rc in MPa) and coefficient of abrasion (Ca in cm²/g). This allows to predict the compressive strength from the test of abrasion and vice versa. It can be useful as non-destructive test of CEBs for preliminary design or quality control in the lab or onsite. The correlation established in the present study was established based on one type of (kaolinite-rich) earthen materials and stabilized with by-product binders (CCR and RHA). Therefore, it needs validation for other type of materials, and/or stabilized with common binders (cement, lime).

While stabilized CEBs would not meet the requirement of water absorption for application in wet environment, their performances vis-a-vis other durability indicators are excellent. This clearly confirms that the most challenging indicator of the durability/stability of stabilized CEBs is the water absorption which also remarkably deteriorates the mechanical resistance in wet conditions. Therefore, it is recommendable to take precautions during application of stabilized CEBs, minimizing direct exposure to water by applying either surface or architectural protections.

CONCLUSIONS AND PERSPECTIVES

Conclusions and perspectives

Summary: towards the discussions of major findings

"How to reach the performances required for CEBs using clay earthen materials stabilized with by-products, instead of industrial binders, for load bearing in building wall construction?"

The present study highlighted the current gaps in section 1.10 and answered to the research question through three (03) original chapters (III-V). Each chapter discussed the results and drew the conclusions from a specific objective.

First of all, the review of the literature had recorded a global and exponential increase of the number of research on earth-based materials (adobes, compressed earth blocks, rammed earth) and earth-based construction techniques, in the last two decades. In general, cement and lime-based binders were, and remains, the most common chemical stabilizers. The selection iof these binders is mainly based on the texture and plasticity, and regardless of the reactivity, of earthen materials for stabilization. Although, these binders improve the quality, engineering and durability performances of earthen materials, they are criticized to temper with natural advantages of earthen materials, such as moisture exchange, recyclability and low embodied energy and CO_2, and thus the circularity and environmental sustainability. Moreover, cement stabilized soil fails the durability tests with regards to wetting-drying cycles.

A limited number of studies had previously attempted to stabilize the earthen materials using alternative (from secondary resources) pozzolanic or alkaline-activated binders or incorporation of natural (plant) fibers. In the same framework, the present study attempted to add value to the by-products and clay materials available in Burkina Faso as potential building materials. Moreover, while CEBs are globally regarded as the most accepted modern form of earth-based construction, in the local context of Burkina Faso, most scientific studies were focused on traditional adobe bricks. Therefore, there was necessity to study the suitability of these materials for the production of stabilized CEBs, but also the conditions of the production. This highlights part of review presented in Chapter I.

Through an extensive and diverse experimental program presented in Chapter II, this study was carried out around three (03) specific objectives, which were to:

1. **Identify and characterize the physico-chemical and mineral properties of clay materials and by-products suitable for the production of stabilized CEBs,**
2. **Investigate the effects of by-products on the microstructural, physico-mechanical and hygro-thermal properties of stabilized CEBs, and**
3. **Study the durability performances of stabilized CEBs, and more specifically for structural applications in the Sahelian climatic context of Burkina Faso.**

Firstly, the suitability of different by-products (binders: CCR and RHA or Okra plant fiber) and clay materials (Kamboinse, Pabre, Kossodo, Saaba) was characterized for the production of stabilized CEBs. The physico-chemical and mineral compositions of CCR (mainly hydrated lime), RHA (mainly amorphous silica) and clay materials (kaolinite-rich and sometimes poorly ordered) evidenced their reactivity, and thus their suitability for the production of stabilized CEBs

The content of hydrated lime (43-53 % of portlandite) in CCR is obviously low, compared to the study carried in Brazil (Cardoso et al. 2009), which reported up to 90 % of portlandite. This variability can be due to the handling conditions during the production of (wet) CCR. Prior to the sampling of the CCR used in the present study, BIG (Burkina) left it to dry in open air which was undoubtedly responsible for its carbonation (40 % of total carbonates). Therefore, it is recommendable to control the drying of CCR and the variability of its compositions in time and space. However, the RHA (amorphous and 89 % soluble) is comparable to its counterpart (Muthadhi and Kothandaraman 2010), produced in similar controlled conditions (500 °C for 2 h). Moreover, the values of the tensile strength (346 ±197 MPa) of Okra bast fibers are scattered, in the same fashion, and comparable to their counterpart (Khan et al. 2018). This allows to confirm the potential of Okra, as green fibers, which are only studied since recently (Alam and Khan 2007).

The clay material from Saaba contains the highest fraction of kaolinite clay mineral (up to 80 %). The materials from Saaba, as well as from Kossodo (up to 50 % of kaolinite), reach the (earliest) highest rate of reactivity. This allowed to reach the highest improvement of the compressive strength of CEBs stabilized with 20 % CCR cured at 40 °C for 45 days, compared to unstabilized CEBs: 10 times (0.8 to 8.3 MPa) with Saaba and 3.5 times (1.4 to 6.4 MPa) with Kossodo. However, these materials would not be considerable for the production of CEBs, if

the selection was based on only their particle size distribution and plasticity, which were out of recommended boundaries (Table 1.2 and Figure 1.2).

Pabre has the highest content of quartz mineral (up to 60 %) and the lowest reactivity: the compressive strength improved only 2.6 times (2 to 7.1 MPa) for CEBs stabilized with 20 % CCR. But, it records the highest (fraction of) clay particles (up to 30 %) and cohesion (plasticity), which comply with the recommendations (Table 1.2 and Figure 1.2), and therefore, reached the highest compressive strength (2 MPa) of unstabilized CEBs. Kamboinse records medium fraction of kaolinite (up to 75 %) and reactivity and contains the highest quantity of exploitable material (700 000 m^3). The compressive strength of CEBs from Kamboinse improved 3.3 times (1.1 to 4.7 MPa).

The characteristics of clay materials obviously vary widely, from one site to another and even in the same site, and do not necessary comply with the current recommendations. But, stabilized CEBs produced from all clay materials reached the dry compressive strength which exceeds the 4 MPa required for load-bearing in storey building. Therefore, the clay earthen materials from all (04) studied sites are suitable for the production of CEBs stabilized with lime-rich (CCR) binders. This suitability is regardless the compliance with the texture and plasticity criteria, which can be applied on any type of clay materials, depending on their degree of reactivity.

Moreover, the common trend would be to stabilize the present clay materials with cement, given the predominance of kaolinite clay (Houben and Guillaud 2006). In fact, the clay material from Kossodo is current being used for the production of CEBs stabilized with cement by a local enterprise. Given the wide variability of the characteristics of clay materials, their reactivity should be taken into consideration for appropriate usage as stabilized earthen building materials. This is part of conclusions drawn from chapter III and therefore, the first objective was achieved.

Secondly, the clay material from Kamboinse was considered for further investigations of the effects of stabilization using by-products on the microstructural and macro-engineering properties of stabilized CEBs. The overall properties of stabilized CEBs improved and were influenced by various parameters such as the productions and curing process, the compositions of mix designs and testing conditions.

The stabilized CEBs should be produced at the optimum moisture content (OMC of earth + binder), determined on CEBs by static compression (CDE 2000) and not by the common

Proctor compaction. Not taking into account the moisture demand of binder for the production of stabilized CEBs would be detrimental on the compressive strength of stabilized CEBs. Stabilized CEBs can be cured at the constant production moisture. Curing the CCR-stabilized CEBs at controlled temperature (40 °C) reaches similar compressive strength as curing at ambient temperature of the lab (30±5 °C: Ouagadougou). Therefore, the stabilization of CEBs with lime-rich binder (CCR) is advisable in warm regions. The curing moisture should of course be maintained relatively high, for benefiting from the hygro-thermo-activation of the pozzolanic reaction of lime with clay materials. This confirms the previous observation by Al-Mukhtar et al. (2010a and 2010b), who compared the behavior and mineralogy changes in lime-treated expansive (bentonite-kaolinite-rich) soil at 20°C and 50 °C.

Moreover, the curing process was influenced by the mix design and time. The RHA accelerates the curing in mixtures containing CCR:RHA to reach the earliest and highest rate of pozzolanic reaction and maturity in 28 days, instead of 45 days required for mixtures containing CCR alone. This pozzolanic reaction resulted in the formation of hydrated cementitious products (C-S-H, C-A-H, C-S-A-H), as those from the hydration of cement, and the changes of microstructure in the mixtures of earth-CCR-RHA. It is this reactive component, featured with the physical component from the compaction and densification of particles, which were responsible for more improvement of the performances of CEBs stabilized with CCR:RHA. This was similarly reported for the combination of RHA with cement in mortar or concrete (Muthadhi and Kothanda raman 2010).

The coefficient of structural efficiency of stabilized CEBs was therefore improved: up to 3050 J/kg and 4462 J/kg respectively for CEB stabilized with CCR and CCR:RHA from 609 J/kg for unstabilized CEBs. This was indicated by the increase of the compressive strength and the decrease of the bulk density of CEBs resulting from the stabilization with by-product binders. The decrease of the bulk density was related to the increase of the production moisture of CEBs with the increase of stabilizer (lime-rich CCR) content (Figure 2.2). By contrary, the literature reported the increase of the compressive strength with the bulk density of CEB (Figure 12c), resulting from the increase of compaction pressure (Figure 1.12a) or stabilization with cement (Kerali 2001). The CEBs stabilized with by-product have even higher structural efficiency than the CEBs stabilized with cement in the present study or stabilized with cement, lime or geopolymer or even hypercompacted unstabilized earth in the literature (Bogas et al. 2018, Sore et al. 2018, Bruno et al. 2015).

Therefore, CEBs stabilized with by-product binders can bear load in wall masonry, and thus have structural applications in construction of two or three-storey building (Recommendations for the selection of mix designs). However, precaution should be taken to prevent the direct contact of stabilized CEBs with liquid water, either by surface or architectural protections, as they failed to comply with the required limits of water absorption (Table 1.5).

The thermal efficiency of CEBs was additionally improved by the stabilization with CCR or CCR:RHA, or addition of Okra plant fibers. This was indicated by the decrease of thermal conductivity, diffusivity and effusivity and the increase of thermal capacity related to the decrease of bulk density of CEBs stabilized with by-products (Figure 4.12 & 4.13). By contrary, the increase of density would increase the thermal conductivity (Figure 1.14a). The thermal efficient of CEBs stabilized with by-products was also evidenced by the decrease of thermal penetration depth (Table 4.1). The depth reached lower values than the total thickness (14 cm) of CEBs and the depth deduced for unstabilized CEBs or CEBs stabilized with cement, geopolymer (Mansoure et al. 2016, Bogas et al. 2018, Sore et al. 2018).

More interestingly, the hygro-thermal efficiency was also improved for CEBs stabilized with CCR:RHA, by increasing the water vapor sorption capacity, contrary to cement which decreases the sorption capacity of CEBs (McGregor et al. 2014). At a building scale, the CCR-stabilized CEBs achieves even better efficiency than hollow cement blocks, in terms of thermal comfort and energy cost saving for air conditioning (Moussa et al. 2019). Recommendations for the selection of mix design allows to choose the most thermally efficient stabilized CEBs, also taking into consideration the physico-mechanical requirements for structural applications. This is part of the conclusions drawn from chapter IV; and therefore, the second objective was achieved.

Thirdly, the durability indicators of CEBs were remarkably improved by the stabilization with by-product binders (CCR or CCR:RHA). This was evidenced by the decrease of the depth of erosion and percentage of eroded area, which reached the values compared to those of cement stabilized CEBs. It was also confirmed by the increase of the coefficient of abrasion (Ca) and compressive strength (Rc), in dry and wet conditions, which represent the improvement of hardness and resistance of CEBs.

More interesting, the Ca and Rc increase after 12 cycles of wetting-drying (W-D) for the CCR-stabilized CEBs, showing that CCR-stabilized CEBs would keep the performances over the time, contrary to cement stabilized soil, whose strength decreased after only 6 cycles of

W-D (Hakimi et al. 1998). This is related to more hygro-thermo-activation of the pozzolanic reaction, created by the wetting (100 % humidity)-drying (75 °C) cycles, of the excess unreacted CCR in stabilized CEBs. James and Saraswathy (2020) similarly observed more increase of the compressive strength after 1 cycle of W-D for lateritic soil blocks stabilized with higher content of industrial lime. However, the strength also decreased beyond 1 cycle of W-D, possibly due to the low temperature of drying (ambient air in India) and/or the limited reactivity of lateritic soil. Therefore, this suggests that the susceptibility of stabilized earthen materials to W-D cycles may also depends of the type of earthen material itself, in addition to the type of stabilizer (lime or cement).

By contrary, unstabilized CEBs were immediately deteriorated in contact with liquid water. However, based on the theoretical rate of erosion (0.03 mm/year), the lifespan of stabilized CEBs in the Sahelian context (Ouagadougou) was estimated at more than 270 years. This theoretical evaluation definitely needs to take into consideration the real environmental conditions of durability, as well as the mechanical constraints in building applications. This is part of conclusions drawn from chapter V.

CEBs stabilized with by-products obviously reach excellent structural and thermal performances, and durability indicators. However, stabilized CEBs, from the earthen material of Kamboinse (OMC 17 %), failed to comply with the requirement for water absorption (<15-20 %). They should undergo further treatment for improving the absorption behaviors. Alternatively, one can consider earthen materials which have lower OMC (Kossodo, Pabre) for possibly producing CEBs which have lower water absorption capacity. This suggests that high water absorption remains the challenge for the durability of earthen materials, given that it weaken the stability and mechanical resistance of material.

Main contributions and limitations

The present study contributed towards the applications of by-products, otherwise regarded as wastes, such as the residues from the production of acetylene (calcium carbide residue: CCR), from the agriculture of rice (rice husk ash: RHA) and from the agriculture of Okra (Okra bast fibers), as innovative and efficient stabilizers of clay earthen materials for the production of CEBs.

1. The present study is the first of kind (to the best of our knowledge) to integrate the reactivity among the selection criteria of clay earthen materials for the production of (stabilized) CEBs, not just relying on only the common texture and plasticity criteria. The latter selection criteria would mislead in rejecting the materials which are suitable for the production of stabilized CEBs. Unfortunately, the reactivity criteria was only applied on kaolinite-rich earthen materials, as they are the most predominant in the study area (region of Ouagadougou), but it can also be applied on other materials.
2. A non-standardized test method, by monitoring the electrical conductivity (EC) in mix solutions of clay materials and CCR, was therefore adopted to assess the reactivity of clay materials for the production of stabilized CEBs. However, this test was limited to the usage of a by-product ($Ca(OH)_2$-rich CCR) whose compositions may vary in time and space. This testing approach can be further refined and extrapolated to other types of clay minerals (illite, smectite, etc), and using $Ca(OH)_2$-analytical grade. This can potentially lead towards proposing a standard testing method of the reactivity of clay materials.
3. The monitoring of the EC, as well as the concentration of calcium ions [Ca^{2+}], in the mix solution of earth-CCR-RHA was also applied as a novel and simpler approach toward the assessment of the curing process and chemico-microstructural changes in stabilized earthen materials. The correlation was proposed between the EC and [Ca^{2+}], which however was reported on kaolinite-rich clay materials used in the present study. Therefore, the contribution of calcium and/or other ions needs to be accounted for in the materials which contain other types of (clay) minerals, such as smectite and/or carbonates.
4. The CEBs stabilized with by-product binders (CCR, CCR:RHA) achieve required performances for applications in building construction. This is also comparable to the CEBs stabilized with common industrial binders (cement, lime) reported in the literature. However, the variability of the quality and quantity of the by-products, in time and space, and the effects on the performances of stabilized CEBs need further assessments. This can also be accompanied by the analysis of the recyclability of CEBs incorporated with

by-products and socio-economic and environmental impacts of their usages. This partly constitutes the study carried out by Zoungrana (2020).

5. The study proposed engineering indicators (coefficient of structural and thermal efficiency) which can serve as the basis for the design and selection of the materials for structural applications in the construction of thermally efficient buildings in hot climatic context. The applicability of these indicators is more significant at material scale. At building scale, there is still need to integrate the interactions with others factors such as the effects of joint mortar (or not) in wall masonry, imposed loads (not just the proper weight of CEBs) of other parts of buildings, as well as external loads for the structural stability of the building. There was also need to integrate the hygro-thermal interactions of CEBs (-based buildings) with the environmental conditions and the occupants in order to fully assess the contribution of CEBs-based walls to the improvement of thermal comfort and energy efficiency in buildings. The latter was further elaborated in studies carried out by Hema (2020) and Moussa et al. (2019).
6. A non-destructive abrasive test was carried and used to propose a novel correlation: $Rc=1.6xCa^{0.35}$, between the coefficient of abrasion, Ca (cm^2/g), and the compressive strength, Rc (MPa). This relation can allow to simply estimate the strength of CEBs by a test of abrasion in lab or onsite for mix design or quality control. However, it was proposed from one type of earthen material and stabilized with by-products. Therefore, it needs validation for other type of materials, and also stabilized with classical binders.

The present study consolidated the knowledge from applied clay science, soil mechanics and materials science and engineering for further understanding of the applicability of earthen materials and by-products in building constructions. But of course, the present can be further completed by the assessment of environmental impacts: life cycle analysis, life energy analysis, CO_2 footprint, in order to corroborate the advantages of using non-conventional and secondary materials with respect to industrial materials.

Recommendations for the selection of mix designs and technical implications

The conclusions drawn from chapters III-V, as well as additional analyses in appendices I-II, allowed to establish a matrix for the selection of mix design (Appendix III). This allows to stabilize the earthen material with CCR, CCR:RHA or add fibers, and optimize the properties (performances) of CEBs, depending on the envisaged applications.

Among the CCR stabilizations, which reached the required compressive strength (4 MPa) for the **structural application in two-storey building**:

- ✓ **10-25CCR** reached the highest (best) mechanical and abrasion resistance in dry conditions and erodability resistance for **structural and durability performances.**
- ✓ **10CCR** reached the lowest (best) water absorptions and the highest (best) mechanical resistance in wet conditions: **most appropriate structural performances in wet conditions.**
- ✓ **25CCR** reached the lowest bulk density and highest thermal efficiency, lowest thermal penetration depth: **most appropriate structural and thermal performances.**

Among the CCR:RHA stabilizations, which reached the required compressive strength (6 MPa) for the **structural application in three-storey building**:

- ✓ **18:2-14:6CCR:RHA** reached the highest mechanical resistance in dry and wet conditions, abrasion and erodability resistance for **structural and durability performance.**
- ✓ **16:4-14:6CCR:RHA** also reached the highest thermal efficiency, lowest thermal penetration depth: **excellent structural and thermal performances.**

Okra plant fiber compromised the structural efficient of CCR-stabilized CEBs, but reached the required compressive strength (2 MPa) for **application in one-storey building**:

- ✓ **0.8-1.2 % fiber** reached the highest thermal efficiency, lowest thermal penetration depth: **excellent thermal performances.**

Perspectives for future studies

Future studies should:

- Complete the assessment of the suitability of clay materials from different sites for the production of stabilized CEBs on the basis of the reactivity with $Ca(OH)_2$-analytical grade, engineering and durability properties of CEBs and investigate the correlation with the physico-chemical and mineral compositions of clay materials. This would also allow to confirm the original hypothesis that "*the compliance of the clay material from Kamboinse with the requirements for the production of stabilized CEBs would suggest the compliance of other studies sites*".
- Explore the possibility to reduce the amount of production moisture of highly plastic clay materials and the effect on the water absorption capacity of stabilized CEBs.
- Assess the effects of surface treatments, for controlling the water absorption, on other engineering properties and durability of stabilized CEBs.
- Confirm the rate of pozzolanic reaction of mixtures containing CCR:RHA on the basis of mechanical resistance. Compare the effects of curing time and temperature on the evolution of compressive strength of CEBs stabilized with CCR:RHA versus CCR alone, and cured for 0, 7, 28 and 90 days.
- Investigate the insulating behaviors of stabilized CEBs, containing higher fraction of fibers (up to 20 wt %) and applicability of the law of mixtures. Assess the effects on hygro-thermal, acoustic and other engineering properties and durability. Study the effect of humidity, rather than liquid water, on the thermal properties of stabilized CEBs.
- Investigate the erodability behaviors of stabilized CEBs for further comparison of the depth of erosion and percentage of eroded area, and propose the validation criteria.
- Test the mechanical and durability performances of stabilized CEBs respectively in wall masonry and after exposure to real environmental conditions (Ouagadougou).

Finally, it is fair to conclude that the enhancement of the mechanical, thermal and durability performances of CEBs-based buildings in Burkina Faso, and in Western Africa in general, is possible. This is possible using locally available resources, not expensive and hand on technology. The research goals are achieved, the rest is a question of good will, including the establishment of scientific and technical centers for the promotion of earth-based construction in the region.

References

Abdelmalek, B., Rekia, B., Youcef, B., Lakhdar, B., Fagel, N., 2017. Mineralogical characterization of Neogene clay areas from the Jijel basin for ceramic purposes (NE Algeria -Africa). Appl Clay Sci 136, 176–183. https://doi.org/10.1016/j.clay.2016.11.025.

Alam MS, Khan GM. 2007. Chemical analysis of okra bast fiber (Abelmoschus Esculentus) and its physico-chemical properties. J Text Apparel, Technol Manag. 5:1–9.

Al-Mukhtar M, Lasledj A, Alcover J-F. 2010a. Behaviour and mineralogy changes in lime-treated expansive soil at 20°C. Appl Clay Sci. 50:191–198.

Al-Mukhtar M, Lasledj A, Alcover J-F. 2010b. Behaviour and mineralogy changes in lime-treated expansive soil at 50°C. Appl Clay Sci. 50:199–203.

Al-Mukhtar, Khattab SAA, Alcover J-F. 2012. Micorstructure and geotechnical properties of lime treated expansive soil. Eng Geol. 139–140:17–27.

Arabi M, Wild S. 1986. Microstructural development in cured soil-lime composites. J Mater Sci. 21:497–503.

Arrigoni A, Grillet AC, Pelosato R, Dotelli G, Beckett CTS, Woloszyn M, Ciancio D. 2017a. Reduction of rammed earth's hygroscopic performance under stabilisation: an experimental investigation. Build Environ. 115:358–367.

Arrigoni A, Pelosato R, Dotelli G, Beckett CTS, Ciancio D. 2017b. Weathering's beneficial effect on waste-stabilised rammed earth: a chemical and microstructural investigation. Constr Build Mater. 140:157–166.

Asadi I, Shafigh P, Abu Hassan ZF Bin, Mahyuddin NB. 2018. Thermal conductivity of concrete – A review. J Build Eng. 20:81–93.

Ashour T, Korjenic A, Korjenic S, Wu W. 2015. Thermal conductivity of unfired earth bricks reinforced by agricultural wastes with cement and gypsum. Energy Build. 104:139–146.

ASTM. 1989a. ASTM D 3379-75: Standard test method for tensile strength and Young's modulus for high-modulus single-filamant materials. West Conshohocken, PA.

ASTM. 1989b. ASTM D559-03: Standard test methods for wetting and drying compacted soil-cement mixtures. West Conshohocken, PA.

ASTM. 1994. ASTM C618-12a: Standard specification for coal fly ash and raw or calcined natural pozzolan for use in concrete. West Conshohocken, PA.

ASTM. 1999. ASTM D6276-99a: Standard Test Method for Using pH to Estimate the Soil-Lime Proportion Requirement for Soil Stabilization. West Conshohocken, PA.

ASTM. 2001. ASTM D3822-01: Standard test method for tensile properties of single textile fibers. West Conshohocken, PA.

ASTM. 2003. ASTM C1557-03: Standard test method for tensile and Young's modulus of fibers. West Conshohocken, PA.

Aubert JE, Fabbri A, Morel JC, Maillard P. 2013. An earth block with a compressive strength higher than 45 MPa! Constr Build Mater. 47:366–369.

Bahar R, Benazzoug M, Kenai S. 2004. Performance of compacted cement-stabilised soil. Cem Concr Compos. 26:811–820.

Basha EA, Hashim R, Mahmud HB, Muntohar AS. 2005. Stabilization of residual soil with rice husk ash and cement. Constr Build Mater. 19:448–453.

Beckett CTS, Jaquin PA, Morel J. 2020. Weathering the storm : A framework to assess the resistance of earthen structures to water damage. Constr Build Mater. 242:118098.

Bich, C., Ambroise, J., Péra, J., 2009. Influence of degree of dehydroxylation on the pozzolanic activity of metakaolin. Appl Clay Sci 44, 194–200. https://doi.org/10.1016/j.clay.2009.01.014.

Boffoue MO, Kouadio KC, Kouakou CH. 2015. Influence de la teneur en ciment sur les propriétés thermomécaniques des blocs d'argile comprimée et stabilisée. Afrique Sci. 11:35–43.

Bogas, J.A., Silva, M., Gomes, M. da G., 2018. Unstabilized and stabilized compressed earth blocks with partial incorporation of recycled aggregates of recycled aggregates. Int J Archit Herit 3058, 1–16. https://doi.org/10.1080/15583058.2018.1442891.

Boro D, Florent Kieno P, Ouedraogo E. 2017. Experimental Study of the Thermal and Mechanical Properties of Compressed Earth Blocks Stabilized with Sawdust According to the Rates for the Thermal Insulation of a Building. Int J Constr Eng Manag. 6:103–109.

Boski T, Pessoa J, Pedro P, Thorez J, Dias JMA. 1998. Factors governing abundance of hydrolyzable amino acids in the sediments from the N . W . European Continental Margin (47-50 °N). Prog Oceanogr. 42:145–164.

Bruno AW, Gallipoli D, Perlot C, Mendes J. 2017. Effect of stabilisation on mechanical properties, moisture buffering and water durability of hypercompacted earth. Constr Build Mater. 149:733–740.

Bruno, A. W., Gallipoli, D., Mendes, J., & Salmon, N. 2015. Briques de terre crue : procédure de compactage haute pression et influence sur les propriétés mécaniques. In 33èmes Rencontres de l'AUGC, ISABTP/UPP, 27 au 29 Mai (pp. 1–9). Anglet. https://doi.org/hal-01167676

BSI. 2015. BS EN 771-1: Specification for masonry units. Clay masonry units. London.

Bui Q-B, Morel JC, Venkatarama-Reddy B V., Ghayad W. 2009. Durability of rammed earth walls exposed for 20 years to natural weathering. Build Environ. 44:912–919.

Cagnon H, Aubert JE, Coutand M, Magniont C. 2014. Hygrothermal properties of earth bricks. Energy Build. 80:208–217.

Cardoso FA, Fernandes HC, Pileggi RG, Cincotto MA, John VM. 2009. Carbide lime and industrial hydrated lime characterization. Powder Technol. 195:143–149.

Cassagnabère F, Lachemi M, Mouret M, Escadeillas G. 2011. Caractérisation performantielle d'un liant ternaire à base de ciment, laitier et métakaolin. Can J Civ Eng. 38:837–848.

CDE, CRATerre-EAG, ENTPE. 2000. Compressed earth blocks: testing procedures guide-Technology series N° 16. CDE (ARSO), Brussels-Belgium

CDI&CRATerre. 1998. Compressed Earth Blocks- Standards: Guide technologies series N° 11. Boubekeur S, Houben H, Doat P, D'Ornano S, Douline A, Garnier P, Guillaud H, Joffroy T, Rigassi V, editors. Brussels.

CEN. 2000. EN ISO 12571: Hygrothermal performance of building materials and products - Determination of hygroscopic sorption properties. Brussels.

Chindaprasirt P, Pimraksa K. 2008. A study of fly ash-lime granule unfired brick. Powder Technol. 182:33–41.

Choobbasti AJ, Ghodrat H, Vahdatirad MJ. 2010. Influence of using rice husk ash in soil stabilization method with lime. Front Earth Sci China. 4:471–478.

Ciancio, D., Beckett, C.T.S., Carraro, J.A.H., 2014. Optimum lime content identification for lime-stabilised rammed earth. Constr Build Mater 53, 59–65. https://doi.org/10.1016/j.conbuildmat.2013.11.077

Cid-Falceto J, Mazarron RF, Canas I. 2012. Assessment of compressed earth blocks made in Spain: International durability tests. Constr Build Mater. 37:738–745.

Compaore, A., Ouedraogo, B., Guengane, H., Malbila, E., and Bathiebo, D. J. 2017. Role of Local Building Materials on the Energy Behaviour of Habitats in Ouagadougou. IRA-Inter J Appl Sci, 8(2), 63-73.

Cook HE, Johnson PD, Matti JC, Zemmels I. 1975. Methods of sample preparation and x-ray diffraction data analysis, x-ray mineralogy laboratory. In: Hayes DE, Frakes LA, editors. Init Repts DSDP. Washington: U.S. Govt. Printing Office; p. 999–1007.

Danso H, Martinson DB, Ali M, Williams BJ. 2015a. Physical, mechanical and durability properties of soil building blocks reinforced with natural fibres. Constr Build Mater. 101:797–809.

Danso H, Martinson DB, Ali M, Williams BJ. 2015b. Effect of fibre aspect ratio on mechanical properties of soil building blocks. Constr Build Mater. 83:314–319.

Dao K, Ouedraogo M, Millogo Y, Aubert J-E, Gomina M. 2018. Thermal, hydric and mechanical behaviours of adobes stabilized with cement. Constr Build Mater. 158:84–96.

de Castro Ferreira R, de Carvalho Ulhôa ML. 2016. Mechanical and thermal behaviors of stabilized compressed earth blocks. Cienc y Eng Sci Eng J. 25:125–135.

De Rosa IM, Kenny JM, Maniruzzaman M, Moniruzzaman M, Monti M, Puglia D, Santulli C, Sarasini F. 2011. Effect of chemical treatments on the mechanical and thermal behaviour of okra (Abelmoschus esculentus) fibres. Compos Sci Technol. 71:246–254.

De Rosa IM, Kenny JM, Puglia D, Santulli C, Sarasini F. 2010. Morphological, thermal and mechanical characterization of okra (Abelmoschus esculentus) fibres as potential reinforcement in polymer composites. Compos Sci Technol. 70:116–122.

Delgado, M.C.J., Guerrero, I.C., 2007. The selection of soils for unstabilised earth building: A normative review. Constr Build Mater 21, 237–251. https://doi.org/10.1016/j.conbuildmat.2005.08.006.

Deshmukh P, Bhatt J, Peshwe D, Pathak S. 2012. Determination of silica activity index and XRD, SEM and EDS studies of amorphous SiO2 extracted from Rice Husk Ash. Trans Indian Inst Met. 65:63–70.

Di Sante M, Fratalocchi E, Mazzieri F, Pasqualini E. 2014. Time of reactions in a lime treated clayey soil and influence of curing conditions on its microstructure and behaviour. Appl Clay Sci. 99:100–109.

Diamond, S., White, J.L., Dolch, W.L., 1963. Transformation of Clay Minerals by Calcium Hydroxide Attack, in: Twelfth National Conference on Clays & Clay Minerals. pp. 359–379. https://doi.org/10.1346/CCMN.1963.0120134.

Eades, J.L., Grim, R.E., 1996. A Quick Test to Determine Lime Requirements for Lime Stabilization. Highw Res Rec 3, 61–72.

El Fgaier F, Lafhaj Z, Chapiseau C, Antczak E. 2016. Effect of sorption capacity on thermo-mechanical properties of unfired clay bricks. J Build Eng. 6:86–92.

Elenga RG, Mabiala B, Ahouet L, Goma-Maniongui J, Dirras FF. 2011. Characterization of Clayey Soils from Congo and Physical Properties of Their Compressed Earth Blocks Reinforced with Post-Consumer Plastic Wastes. Geomaterials. 01:88–94.

El-Mahllawy MS, Kandeel AM. 2014. Engineering and mineralogical characteristics of stabilized unfired montmorillonitic clay bricks. HBRC J. 10:82–91.

ETB. 2019. [Engineering toolbox]. Thermal Conductivity of some common Materials and Gases [Internet]. [cited 2019 Sep 19]:1–8. Available from: http://www.engineeringtoolbox.com/thermal-conductivity-d_429.html

Fabbri A, Morel J-C, Gallipoli D. 2018. Assessing the performance of earth building materials: a review of recent developments. RILEM Tech Lett. 3:46–58.

Fagel, N., Boski, T., Likhoshway, L., Oberhaensli, H., 2003. Late Quaternary clay mineral record in Central Lake Baikal (Academician Ridge, Siberia). Palaeogeogr Palaeoclimatol Palaeoecol 193, 159–179. https://doi.org/10.1016/S0031-0182(02)00633-8.

Félix V. 2011. Caractérisation thermique de matériaux isolants légers. Application à des aérogels de faible poids moléculaire. Thèse de doctorat de l'INPLorraine, France.

Földvári, M., 2011. Handbook of the thermogravimetric system of minerals and its use in geological practice, Geological Institute of Hungary. Hungarian Academy of Sciences, Budapest. https://doi.org/10.1556/CEuGeol.56.2013.4.6.

Gecit, J. 2020. Grâce au SNDR II, le Burkina Faso vise l'autosuffisance en riz en 2027. [online]. http://www.commodafrica.com/29-01-2020-grace-au-sndr-ii-le-burkina-faso-vise-lautosuffisance-en-riz-en-2027, accessed 20 July 2020.

Giada G, Caponetto R, Nocera F. 2019. Hygrothermal properties of raw earth materials: A literature review. Sustainability. 11:1–21.

Giroudon M, Laborel-Préneron A, Aubert JE, Magniont C. 2019. Comparison of barley and lavender straws as bioaggregates in earth bricks. Constr Build Mater. 202:254–265.

Guettala A, Abibsi A, Houari H. 2006. Durability study of stabilized earth concrete under both laboratory and climatic conditions exposure. Constr Build Mater. 20:119–127.

Guettala S, Bachar M, Azzouz L. 2016. Properties of the Compressed-Stabilized Earth Brick Containing Cork Granules. J Earth Sci Clim Chang. 7.

Guissou, R., and Ilboudo, F. 2012. Analyse Des Incitations Et Penalisations Pour Le Maïs Au Burkina Faso, SPAAA, FAO, Rome. http://www.fao.org/3/a-at469f.pdf.

Hakimi A, Ouissi H, Kortbi M El, Yamani N. 1998. Un test d'humidification-séchage pour les blocs de terre comprimée et stabilisée au ciment. Mater Struct. 31:20–26.

Hansen KK. 1986. Sorption isotherms - A catalogue. Kgs. Lyngby.

Harichane K, Ghrici M, Kenai S. 2012. Effect of the combination of lime and natural pozzolana on the compaction and strength of soft clayey soils: A preliminary study. Environ Earth Sci. 66:2197–2205.

Heathcote K. 2002. An investigation into the erodability of earthen wall units. Ph.D. theisis of the University of Technology Sydney, Australia.

Hema C. 2020. Optimisation des propriétés thermiques des parois dans les habitations en briques de terre crue au Burkina Faso. Thèse de doctorant de l'Institut 2iE and UCLouvain.

Hema CM, Van Moeseke G, Evrad A, Courard L, Messan A. 2017. Vernacular housing practices in Burkina Faso: Representative models of construction in Ouagadougou and walls hygrothermal efficiency. In: Energy Procedia. Vol. 122. Lausanne: Elsevier; p. 535–540.

Horpibulsuk S, Phetchuay C, Chinkulkijniwat A, Cholaphatsorn A. 2013. Strength development in silty clay stabilized with calcium carbide residue and fly ash. Soils Found. 53:477–486.

Horpibulsuk S, Phetchuay C, Chinkulkijniwat A. 2012. Soil stabilization by calcium carbide residue and fly ash. J Mater Civ Eng. 24:184–193.

Houben, H., Guillaud, H., 2006. CRATerre: Traité de Construction en Terre: L'encyclopédie de la construction en

terre, Vol. I. ed. Editions Parathèses, Marseille.
Hughes E, Valdes-Vasquez R, Elliott JW. 2017. Perceptions of compressed earth block among residential contractors in north carolina: an exploratory evaluation. J Green Build. 12:89–107.
Hwang C, Huynh T. 2015. Investigation into the use of unground rice husk ash to produce eco-friendly construction bricks. Constr Build Mater. 93:335–341.
Hwang CL, Chandra S. 1996. The Use of Rice Husk Ash in Concrete. In: Chandra S, editor. Waste Mater Used Concr Manuf. New Jersey, USA: NoYes Publications; p. 184–234.
INSD. 2015. Tableau de bord démographique. Inst Natl la Stat la démographie, Ouagadougou, Burkina Faso
INSD. 2018. Annuaire statistique 2016. Inst Natl la Stat la démographie, Ouagadougou, Burkina Faso
Izemmouren O, Guettala A, Guettala S. 2015. Mechanical Properties and Durability of Lime and Natural Pozzolana Stabilized Steam-Cured Compressed Earth Block Bricks. Geotech Geol Eng. 33:1321–1333.
James, J., and Saraswathy, R. 2020. Performance of Fly Ash-Lime Stabilized Lateritic Soil Blocks Subjected to Alternate Cycles of Wetting and Drying. Civil and Environmental Engineering, 0(0).
Kabre S, Ouedraogo F, Naon B, Messan A, Benet JC, Zougmore F. 2019. Évaluation des propriétés thermo-hydro-mécaniques des briques en terre compressée (BTC) issues de la carrière de Matourkou, au Burkina Faso. Afrique Sci. 15:12–22.
Kampala A, Horpibulsuk S, Chinkullijniwat A, Shen SL. 2013. Engineering properties of recycled Calcium Carbide Residue stabilized clay as fill and pavement materials. Constr Build Mater. 46:203–210.
Kerali AG. 2000. Destructive Effects of Moisture on the Long-term Durability of Stabilised Soil Blocks. Coventry.
Kerali AG. 2001. Durability of compressed and cement-stabilised building blocks. Ph.D. Thesis University of Warwick, UK.
Khan GMA, Shaheruzzaman M, Rahman MH, Abdur Razzaque SM, Islam MS, Alam MS. 2009. Surface modification of okra bast fiber and its physico-chemical characteristics. Fibers Polym. 10:65–70.
Khan GMA, Yilmaz ND, Yimaz K. 2017. Okra Bast Fiber as Potential Reinforcement of Biocomposites: Can It Be the Flax of the Future? In: Vijay Kumar Thakur, Manju Kumari Thakur MRK, editor. Handb Compos from Renew Mater Funct. John Wiley & Sons, Inc., p. 379–406.
Khan, G. M. A., Yilmaz, N. D., and Yilmaz, K. 2018. Okra Fibers: Potential Material for Green Biocomposites. In: Green Biocomposites: Design and Applications, M. Jawaid, M. S. Salit, and O. Y. Alothman, eds., Springer International Publishing, 261–284.
Kinuthia JM. 2015. The durability of compressed earth-based masonry blocks. In: Pacheco-Torgal F, Lourenço PB, Labrincha JA, et al (eds) Eco-Efficient Masonry Bricks and Blocks-Design, Properties and Durability. Woodhead Publishing, pp 393–421
Labat M, Magniont C, Oudhof N, Aubert JE. 2016. From the experimental characterization of the hygrothermal properties of straw-clay mixtures to the numerical assessment of their buffering potential. Build Environ. 97:69–81.
Laborel-Préneron A, Aubert JE, Magniont C, Tribout C, Bertron A. 2016. Plant aggregates and fibers in earth construction materials : A review. Constr Build Mater. 111:719–734.
Laibi BA. 2018. Comportement hygro-thermo-mécanique de matériaux structuraux pour la construction associant des fibres de kénaf à des terres argileuses. Thèse de doctorat des Universités Caen Normadie & Abomey Calavi.
Latifi N, Vahedifard F, Ghazanfari E, Rashid ASA. 2018. Sustainable usage of calcium carbide residue for stabilization of clays. J Mater Civ Eng. 30:1–10.
Liu Y, Chang CW, Namdar A, She Y, Lin CH, Yuan X, Yang Q. 2019. Stabilization of expansive soil using cementing material from rice husk ash and calcium carbide residue. Constr Build Mater. 221:1–11.
Liuzzi S, Hall MR, Stefanizzi P, Casey SP. 2013. Hygrothermal behaviour and relative humidity buffering of unfired and hydrated lime-stabilised clay composites in a Mediterranean climate. Build Environ. 61:82–92.
Lorentz, B., Shanahan, N., Stetsko, Y.P., Zayed, A., 2018. Characterization of Florida kaolin clays using multiple-technique approach. Appl Clay Sci 161, 326–333. https://doi.org/10.1016/j.clay.2018.05.001.
Mache JR. 2013. Mineralogie et proprietes physico-chimiques des smectites de bana et sabga (cameroun) : Utilisation dans la décoloration d'une huile végétale alimentaire. Thèse Doctorat de l'Université de Liège et de Yaounde 1.
Maïni S. 2010. Compressed stabilized earth blocks and stabilized earth techniques. Auroville Earth Institute (AVEI). India
MAHRH. 2009. Analyse de la compétivité de la filière riz local au Burkina Faso, Ministère de l'agriculture de

l'hydraulique et des ressources halieutiques. www.fao.org/easypol.

Malbila E, Delvoie S, Toguyeni D, Attia, S., Courard, L. 2020. An Experimental Study on the Use of Fonio Straw and Shea Butter Residue for Improving the Thermophysical and Mechanical Properties of Compressed Earth Blocks. J Miner Mater Charact Eng. 8:107–132. https://doi.org/10.4236/jmmce.2020.83008

Malbila E, Toguyeni DYK, Bamogo S, Lawane A, Koulidiati J. 2018. Thermophysical and Mechanical Characterization of Local Stabilized Materials Suitable for Buildings in Dry and Hot Climate. J Mater Sci Surf Eng. 6(2): 767-772.

Mango-Itulamya LA, Collin F, Fagel N. 2020. Improvement of lifetime of compressed earth blocks by adding limestone, sandstone and porphyry aggregates. J Build Eng. 29: 101155. https://doi.org/10.1016/j.jobe.2019.101155

Mansour M Ben, Jelidi A, Cherif AS, Jabrallah S Ben. 2016. Optimizing thermal and mechanical performance of compressed earth blocks (CEB). Constr Build Mater. 104:44–51.

Masuka S, Gwenzi W, Rukuni T. 2018. Development, engineering properties and potential applications of unfired earth bricks reinforced by coal fly ash, lime and wood aggregates. J Build Eng. 18:312–320.

McGregor F, Heath A, Shea A, Lawrence M. 2014. The moisture buffering capacity of unfired clay masonry. Build Environ. 82:599–607.

Mechti, W., Mnif, T., Samet, B., Rouis, M.J., 2012. Effect of the secondary minerals on the pozzolanic activity of calcined clay: case of quartz. IJRRAS 12, 61–71. https://doi.org/10.1684/bdc.2011.1430.

Medvey B, Dobszay G. 2020. Durability of Stabilized Earthen Constructions: A Review. Geotech Geol Eng. 6.

Mehta PK. 1978. Siliceous ashes and hydraulic cements prepared therefrom, US Patent, US4105459 A.

Meukam P, Jannot Y, Noumowe A, Kofane TC. 2004. Thermo physical characteristics of economical building materials. Constr Build Mater. 18:437–443.

Meunier A. 2005. Clays. Berlin: Springer.

Michel F, Courard L. 2014. Particle Size Distribution of Limestone Fillers: Granulometry and Specific Surface Area Investigations. Part Sci Technol. 32:334–340.

Millogo Y, Hajjaji M, Ouedraogo R. 2008. Microstructure and physical properties of lime-clayey adobe bricks. Constr Build Mater. 22:2386–2392.

Minke G. 2006. Building with earth: Design and Technology of a Sustainable Architecture. Basel: Birkhäuser.

Moevus M, Fontaine L, Anger R, Doat P. 2013. Projet Béton d'Argile Environnemental (B.A.E): Rapport scientifique. Grenoble.

Morel JC, Aubert JE, Millogo Y, Hammard E, Fabbri A. 2013. Some observations about the paper "Earth construction: Lessons from the past for future eco-efficient construction" by F. Pacheco-Torgal and S. Jalali. Constr Build Mater. 44:419–421.

Morel JC, Bui Q-B, Hamard E. 2012. Weathering and durability of earthen material and structures. In: Mod earth Build Mater Eng Constr Appl. p. 282–303.

Morel JC, Charef R. 2019. What are the barriers affecting the use of earth as a modern construction material in the context of circular economy? In: IOP Conf Ser Earth Environ Sci. 225. 012053

Mostafa M, Uddin N. 2015. Effect of Banana Fibers on the Compressive and Flexural Strength of Compressed Earth Blocks. Buildings. 5:282–296.

Moussa HS, Nshimiyimana P, Hema C, Zoungrana O, Messan A, Courard L. 2019. Comparative Study of Thermal Comfort Induced from Masonry Made of Stabilized Compressed Earth Block vs Conventional Cementitious Material. J Miner Mater Charact Eng. 07:385–403.

Murmu, A.L., Patel, A., 2018. Towards sustainable bricks production: An overview. Constr Build Mater. https://doi.org/10.1016/j.conbuildmat.2018.01.038.

Mustapha K, Zebaze Kana MG, Soboyejo WO. 2016. Toughening Behavior in Natural Fiber-reinforced Earth-based Composites. MRS Adv. 1:791–797.

Mustapha K. 2015. Mechanical Properties of Natural Fiber-Reinforced Earth-Based Composites. Ph.D. Thesis of the African University of Science and Technology, Abuja, Nigeria.

Muthadhi A, Kothandaraman S. 2010. Optimum production conditions for reactive rice husk ash. Mater Struct. 43:1303–1315.

Nagaraj, H.B., Sravan, M.V., Arun, T.G., Jagadish, K.S., 2014. Role of lime with cement in long-term strength of Compressed Stabilized Earth Blocks. Int J Sustain Built Environ 3, 54–61. https://doi.org/10.1016/j.ijsbe.2014.03.001.

NBR. 1986. NBR 8492: Tijolo maciço de solo-cimento: Determinação da resistência à compressão e da absorção

de água de tijolos maciços de solo-cimento para alvenaria, (in portuguese).
NF P 94-051. 1993. Sols: reconnaissance et essais-Détermination des limites d'Atterberg-Limite de liquidité à la coupelle-Limite de plasticité au rouleau. Saint-Denis La Plaine Cedex: AFNor.
XP P13-901. 2001. Blocs de terre comprimée pour murs et cloisons : Définitions-Spécifications-Méthodes d'essais-Conditions de réception. Saint-Denis La Plaine Cedex. AFNor.
NF P 18-459. 2010. Essai pour béton durci - Essai de porosité et de masse volumique. Saint-Denis La Plaine Cedex. AFNor.
NF EN 1097-6. 2014. Essais pour déterminer les caractéristiques mécaniques et physiques des granulats - Partie 6 : détermination de la masse volumique réelle et du coefficient d'absorption d'eau. Saint-Denis La Plaine Cedex. AFNor.
NF EN ISO 17892-4. 2018. Geotechnical investigation and testing - Laboratory testing of soil - Part 4 : Determination of particle size distribution. Saint-Denis La Plaine Cedex. AFNor.
Ngowi AB. 1997. Improving the traditional earth construc- tion: A case study of Botswana. Constr Build Mater. 11:1–7.
Nkalih Mefire, A., Njoya, A., Fouateu, R.Y., Mache, J.R., Tapon, N.A., Nzeugang, A.N., Chinje, U.M., P.Pilate, P.Flament, Siniapkine, S., Ngono, A., N.Fagel, 2015. Occurrences of kaolin in Koutaba (west Cameroon): Mineralogical and physicochemical characterization for use in ceramic products. Clay Miner 50, 593–606. https://doi.org/10.1180/claymin.2015.050.5.04.
Noolu V, Lal H M, Pillai RJ. 2018. Resilient modulus of clayey subgrade soils treated with calcium carbide residue. Int J Geotech Eng. 1–10.
Noolu, V, Lal H M, and Pillai R. 2019. Multi-scale laboratory investigation on black cotton soils stabilized with calcium carbide residue and fly ash. J Eng Resear 6(4): 1-15 https://doi.org/10.1080/19386362.2018.1512230
Noolu V, Mudavath H, Pillai RJ, Yantrapalli SK. 2019. Permanent deformation behaviour of black cotton soil treated with calcium carbide residue. Constr Build Mater. 223:441–449.
Nshimiyimana P, Fagel N, Messan A, Wetshondo, D O, Courard, L. 2020a. Physico-chemical and mineralogical characterization of clay materials suitable for production of stabilized compressed earth blocks. Constr Build Mater 241:1–13. https://doi.org/10.1016/j.conbuildmat.2020.118097
Nshimiyimana P, Messan A, Zhao Z, Courard L. 2019. Chemico-microstructural changes in earthen building materials containing calcium carbide residue and rice husk ash. Constr Build Mater 216:622–631. https://doi.org/10.1016/j.conbuildmat.2019.05.037
Nshimiyimana P, Miraucourt D, Messan A, Courard L. 2018. Calcium Carbide Residue and Rice Husk Ash for improving the Compressive Strength of Compressed Earth Blocks. MRS Adv 3:2009–2014
Nshimiyimana P, Moussa HS, Messan A, Courard L. 2020b. Effect of production and curing conditions on the performance of stabilized compressed earth blocks: Kaolinite vs quartz-rich earthen material. MRS Adv 1–7. https://doi.org/DOI: 10.1557/adv.2020.155
NZS. 1998. NZS 4298: Materials and workmanship for earth buildings. Wellington.
Obonyo E, Exelbirt J, Baskaran M. 2010. Durability of compressed earth bricks: Assessing erosion resistance using the modified spray testing. Sustainability. 2:3639–3649.
Oti JE, Kinuthia JM, Bai J. 2009a. Compressive strength and microstructural analysis of unfired clay masonry bricks. Eng Geol. 109:230–240.
Oti JE, Kinuthia JM, Bai J. 2009b. Engineering properties of unfired clay masonry bricks. Eng Geol. 107:130-139.
Ouedraogo, M. H., Bougma, L. A., Sawadogo, M., and Sawadogo, N. 2016. Modes de gestion paysanne des semences de gombo (Abelmoschus esculentus L .) au Burkina Faso [Modes of farmers ' management of okra seeds (Abelmoschus esculentus L .) in Burkina Faso]. Inter J Innov Scient Res, 21(1), 69–80. http://www.ijisr.issr-journals.org.
Ouedraogo E, Coulibaly O, Ouedraogo A, Messan A. 2015. Mechanical and Thermophysical Properties of Cement and/or Paper (Cellulose) Stabilized Compressed Clay Bricks. J Mater Eng Struct 2. 2:68–76.
Ouédraogo E, Dianda B, Ky TSM, Ouédraogo A. 2018. Determination of Parameters Influencing Thermal Comfort in a Building. Sci J Energy Eng. 6:42–48.
Ouedraogo KAJ, Aubert JE, Tribout C, Escadeillas G. 2020. Is stabilization of earth bricks using low cement or lime contents relevant? Constr Build Mater. 236:117578.
Ouedraogo M, Dao K, Millogo Y, Aubert JE, Messan A, Seynou M, Zerbo L, Gomina M. 2019. Physical, thermal and mechanical properties of adobes stabilized with fonio (Digitaria exilis) straw. J Build Eng. 23:250–258.
Pacheco-Torgal F, Jalali S. 2012. Earth construction: Lessons from the past for future eco-efficient construction.

Constr Build Mater. 29:512–519.
Pardin CL, Guilherme L, Manhani B. 2002. Influence of the Testing Gage Length on the Strength , Young's Modulus and Weibull Modulus of Carbon Fibres and Glass Fibres. Mater Res. 5:411–420.
Pavía S, Hanley R. 2010. Flexural bond strength of natural hydraulic lime mortar and clay brick. Mater Struct Constr. 43:913–922.
Pavlík Z, Žumár J, Medved I, Černý R. 2012. Water Vapor Adsorption in Porous Building Materials: Experimental Measurement and Theoretical Analysis. Transp Porous Media. 91:939–954.
Payá J, Monzó J, Borrachero M., Mellado A, Ordoñez L. 2001. Determination of amorphous silica in rice husk ash by a rapid analytical method. Cem Concr Res. 31:227–231.
Raheem AA, Bello OA, Makinde OA. 2010. A Comparative Study of Cement and Lime Stabilized Lateritic Interlocking Blocks A Comparative Study of Cement and Lime Stabilized Lateritic Interlocking Blocks . Pacific J Sci Technol. 11:27–34.
Raimondo M, Dondi M, Gardini D, Guarini G, Mazzanti F. 2009. Predicting the initial rate of water absorption in clay bricks. Constr Build Mater. 23:2623–2630.
Reddy BVV, Hubli SR. 2002. Properties of lime stabilised steam-cured blocks for masonry. Mater Struct. 35:293-300.
Reddy BVV, Lal R, Rao KSN. 2007. Optimum soil grading for the soil-cement blocks. J Mater Civ Eng. 19:139-148.
Reeves GM, Sims I, Cripps JC. 2006. Clay Materials Used in Construction. London: Geology Society of London.
RILEM. 2019. 274-TCE [2016-2021]: Testing and characterisation of earth-based building materials and elements.
Saidi M, Cherif AS, Zeghmati B, Sediki E. 2018. Stabilization effects on the thermal conductivity and sorption behavior of earth bricks. Constr Build Mater. 167:566–577.
Saldanha RB, Filho HCS, Mallmann JEC, Consoli NC, Reddy KR. 2018. Physical-mineralogical-chemical characterization of carbide lime: An environment-friendly chemical additive for soil stabilization. J Mater Civ Eng. 30:06018004.
Seco A, Urmeneta P, Prieto E, Marcelino S, García B, Miqueleiz L. 2017. Estimated and real durability of unfired clay bricks: Determining factors and representativeness of the laboratory tests. Constr Build Mater. 131:600-605.
Shubbar AA, Sadique M, Kot P, Atherton W. 2019. Future of clay-based construction materials – A review. Constr Build Mater. 210:172–187.
Siddiqua S, Barreto PNMM. 2018. Chemical stabilization of rammed earth using calcium carbide residue and fly ash. Constr Build Mater. 169:364–371.
Sore OS, Messan A, Prud'homme E, Escadeillas G, Tsobnang F. 2018. Stabilization of compressed earth blocks (CEBs) by geopolymer binder based on local materials from Burkina Faso. Constr Build Mater. 165:333-345.
Sore SO. 2017. Synthèse et caractérisation des liants géopolymères à base des matériaux locaux du Burkina Faso en vue d'une stabilisation des Briques en Terre Comprimées (BTC). Thèse de doctorat d l'Institut 2iE, Ouagadougou, Burkina Faso.
Symington MC, Banks WM, Opukuro DW, Pethrick R a. 2009. Tensile testing of cellulose based natural fibers for structural composite applications. J Compos Mater. 43:1083–1108.
Taallah B, Guettala A, Guettala S, Kriker A. 2014. Mechanical properties and hygroscopicity behavior of compressed earth block filled by date palm fibers. Constr Build Mater. 59:161–168.
Taallah B. 2014. Etude du Comportement Physico-Mecanique du Bloc de Terre Comprimée avec Fibres. Thése Doctorat de l'Universite Mohamed Khider-Biskra, Algeria.
Thermtest. Materials Thermal Properties Database [Internet]. [cited 2020 May 6]. Available from: https://thermtest.com/materials-database
Tironi, A., Trezza, M.A., Scian, A.N., Irassar, E.F., 2012. Kaolinitic calcined clays: Factors affecting its performance as pozzolans. Constr Build Mater 28, 276–281. https://doi.org/10.1016/j.conbuildmat.2011.08.064.
Tiskatine R, Bougdour N, Oaddi R, Gourdo L, Rahib Y, Bouzit S, Bazgaou A, Bouirden L, Aharoune A. 2018. Thermo-physical analysis of low-cost ecological composites for building construction. J Build Eng.
Toguyeni DYK, Lawane A, Zoma F, Khamis G. 2018. Formulation of Compressed Earth Blocks Stabilized With Lime and Hibiscus Sabdariffa Fibres Showcasing Good Thermal and Mechanical Properties. J Mater Sci Surf Eng. 6:817–824.
Tsozué, D., Nzeugang, A.N., Mache, J.R., Loweh, S., Fagel, N., 2017. Mineralogical, physico-chemical and

technological characterization of clays from Maroua (Far-North, Cameroon) for use in ceramic bricks production. J Build Eng 11, 17–24. https://doi.org/10.1016/j.jobe.2017.03.008.

UNESCO, Craterre. 2012. Earthen architecture in today's world. In: Proc UNESCO Int Colloq Conserv World Herit Earthen Archit 17-18 December, Paris-France.

UN-Habitat. 2011. Affordable land and housing in Africa. Volume 3: Majale M, Tipple G, French M, Sietchiping R, editors. Nairobi, Kenya.

Van Damme H, Houben H. 2018. Earth concrete. Stabilization revisited. Cem Concr Res. 114:90–102.

Van Der Linden J, Janssens B, Knapen E. 2019. Potential of contemporary earth architecture for low impact building in Belgium. IOP Conf Ser Earth Environ Sci. 323.

Walker R, Pavía S. 2011. Physical properties and reactivity of pozzolans, and their influence on the properties of lime–pozzolan pastes. Mater Struct. 44:1139–1150.

Walker, P., Stace, T., 1997. Properties of some cement stabilised compressed earth blocks and mortars. Mater Struct Constr 30, 545–551. https://doi.org/10.1007/BF02486398.

Wetshondo OD. 2012. Caractérisation et valorisation des matériaux argileux de la Province de Kinshasa (RD Congo). Thèse de Doctorat de l'Université de Liège, Belgique.

Wyss U. 2005. La construction en « matériaux locaux » état d'un secteur à potentiel multiple. Direction du Développement et de la Coopération Suisse. Ouagadougou, Burkina Faso.

Xu W, Lo TY, Memon SA. 2012. Microstructure and reactivity of rich husk ash. Constr Build Mater. 29:541–547.

Xu Y, Chung DDL. 2000. Cement of high specific heat and high thermal conductivity, obtained by using silane and silica fume as admixtures. Cem Concr Res. 30:1175–1178.

Yogananth Y, Thanushan K, Sangeeth P, Coonghe JG, Sathiparan N. 2019. Comparison of strength and durability properties between earth-cement blocks and cement–sand blocks. Innov Infrastruct Solut. 4:1–9.

Yu Q, Sawayamaa K, Sugitaa S, Shoyaa M, Isojimaa Y. 1999. The reaction between rice husk ash and Ca(OH)2 solution and the nature of its product. Cem Concr Res. 29:37–43.

Yvon J, Lietard O, Cases JM, Delon JF. 1982. Minéralogie des argiles kaoliniques des Charentes. Bull Minéralogie. 105:431–437.

Zhang L, Gustavsen A, Jelle BP, Yang L, Gao T, Wang Y. 2017. Thermal conductivity of cement stabilized earth blocks. Constr Build Mater. 151:504–511.

Zhang L, Yang L, Jelle BP, Wang Y, Gustavsen A. 2018. Hygrothermal properties of compressed earthen bricks. Constr Build Mater. 162:576–583.

Zhu F, Li Z, Dong W, Ou Y (2019) Geotechnical properties and microstructure of lime-stabilized silt clay. Bull Eng Geol Environ 78:2345–2354. https://doi.org/10.1007/s10064-018-1307-5

Zoma F, Kader TDY, Ouedraogo A, Koulidiati J. 2015. Study of Time Lag in a Bioclimatic House Made of Eco Materials. J Mater Sci Eng B. 5:255–262.

Zoungrana O. 2020. Étude socio-anthropologique des conditions de popularisation et de diffusion de construction en BTC au Burkina Faso : Étude de terrain à Ouagadougou. Thèse de doctorant de l'Institut 2iE et Université de Liège.

APPENDIX

Appendix

Appendix I. Analysis of variance: significance of the stabilization effect

The significance of the effect of stabilization/treatment some properties of CEBs was tested by statistical analysis of variance (ANOVA). The analysis was carried out by a non-parametric *Kruskal-Wallis test*, one-way ANOVA on ranks, using XLSTAT 2014.5.03 package incorporated in Microsoft excel 2013. This method allows to compare two or more independent samples, from different treatments, of equal or different sample sizes (k). Like other statistical tests, it assumes the *null hypothesis* (H_0) or the *alternative hypothesis* (Ha). The H_0 is considered when all the samples are from the same population and have the same characteristics, i.e. the effect of treatment is *not significant*. The Ha is considered if the effect of treatment is proven to be *significant*. The risk of error (significance level) related to Ha is defined α=5% and corresponds to the probability of accepting Ha while H_0 is true.

The test consists of determining the Kruskal-Wallis statistic K, asymptomatically distributed following the chi-square with degree of freedom df= k-1. The p-value is estimated by asymptomatic approximation of the statistic K and compared with α for decision making. If the p-value is greater than α, the H_0 is accepted; if the p-value is lesser than α, the H_0 is rejected. The latter case is followed by pair-wise comparison of *samples*, using the *Dunn test* in order to figure out the sample pair(s) which are responsible for the rejection of H_0. Furthermore, the significance level is corrected by *Bonferroni method* for pair-wise comparison of samples.

The tests proved that the treatments have statistically significant effects on some properties of stabilized CEBs, such as the compressive strength, bulk density and thermal properties. Specifically, the effects of treatment with 15CCR or 16:4CCR:RHA was the most significant on the compressive strength (*Appendix 1*). In fact, the pairwise comparison showed the significance of stabilization with 10CCR alone with respect to 0CCR, The 10, 20, 25CCR have the most significant effect on the bulk density (*Appendix 2*). Regarding the thermal properties, the treatment with 15-25CCR had the most significant effects on thermal effusivity and specific capacity, while 5, 15, 25CCR were most significant on the conductivity and diffusivity (Appendix 3).

*Appendix 1. Kruskal-Wallis test: significance of the effect of stabilization on the **compressive strength** of CEB (a) CCR, (b) CCR:RHA*

a

K	14.05	As the computed p-value is lower than the significance level alpha=0.05, one should reject the null hypothesis H0, and accept the alternative hypothesis Ha.
p-value	0.015	
alpha	0.05	The risk to reject the null hypothesis H0 while it is true is lower than 1.53%.

p-values: pairwise comparisons using Dunn's procedure

	0CCR	5CCR	10CCR	**15CCR**	20CCR	25CCR	Groups	
0CCR	1.000	0.491	0.108	**0.003**	0.022	0.006	A	
5CCR	0.491	1.000	0.359	0.022	0.108	0.039	A	B
10CCR	0.108	0.359	1.000	0.169	0.491	0.251	A	B
15CCR	**0.003**	0.022	0.169	1.000	0.491	0.819		**B**
20CCR	0.022	0.108	0.491	0.491	1.000	0.646	A	B
25CCR	0.006	0.039	0.251	0.819	0.646	1.000	A	B

Bonferroni corrected significance level: 0.0033; values in **bold** correspond to significant difference

K	17.28	As the computed p-value is lower than the significance level alpha=0.05, one should reject the null hypothesis H0, and accept the alternative hypothesis Ha.
p-value	< 0.001	
alpha	0.05	The risk to reject the null hypothesis H0 while it is true is lower than 0.01%.

p-values: pairwise comparisons using Dunn's procedure

	0CCR	10CCR	Groups
0CCR	1	**< 0.001**	A
10CCR	**< 0.001**	1	**B**

Bonferroni corrected significance level: 0.05; values in **bold** correspond to significant differences

b

K	11.92	As the computed p-value is lower than the significance level alpha=0.05, one should reject the null hypothesis H0, and accept the alternative hypothesis Ha.
p-value	0.0179	
alpha	0.05	The risk to reject the null hypothesis H0 while it is true is lower than 1.79%.

p-values: pairwise comparisons using Dunn's procedure

	20:0 CCR:RHA	18:2 CCR:RHA	**16:4 CCR:RHA**	14:6 CCR:RHA	12:8 CCR:RHA	Groups	
20:0CCR:RHA	1.000	0.049	**0.003**	0.015	0.411	A	
18:2CCR:RHA	0.049	1.000	0.293	0.648	0.253	A	B
16:4CCR:RHA	**0.003**	0.293	1.000	0.553	0.028		**B**
14:6CCR:RHA	0.015	0.648	0.553	1.000	0.110	A	B
12:8CCR:RHA	0.411	0.253	0.028	0.110	1.000	A	B

Bonferroni corrected significance level: 0.05, values in **bold** correspond to significant differences

*Appendix 2. Kruskal-Wallis test: significance of the effect of stabilization on the **bulk density** of CEB (a) CCR, (b) CCR:RHA*

a

K	31.89	As the computed p-value is lower than the significance level alpha=0.05, one should reject the null hypothesis H0, and accept the alternative hypothesis Ha.
p-value	< 0.001	
alpha	0.05	The risk to reject the null hypothesis H0 while it is true is lower than 0.01%.

p-values: pairwise comparisons using Dunn's procedure

	0CCR	5CCR	**10CCR**	15CCR	**20CCR**	**30CCR**	Groups	
0CCR	1.000	0.283	**< 0.001**	0.059	**< 0.001**	**< 0.001**	**A**	
5CCR	0.283	1.000	0.139	0.521	0.040	0.013	A	B
10CCR	**< 0.001**	0.139	1.000	0.504	0.286	0.095		**B**
15CCR	0.059	0.521	0.504	1.000	0.170	0.065	A	B
20CCR	**< 0.001**	0.040	0.286	0.170	1.000	0.545		**B**
25CCR	**< 0.001**	0.013	0.095	0.065	0.545	1.000		**B**

Bonferroni corrected significance level: 0.0033, values in **bold** correspond to significant differences

b

K	4.23	As the computed p-value is greater than the significance level alpha=0.05, one cannot reject the null hypothesis H0.
p-value	0.3753	
alpha	0.05	The risk to reject the null hypothesis H0 while it is true is 37.53%.

p-values: pairwise comparisons using Dunn's procedure

	20:0 CCR:RHA	18:2 CCR:RHA	16:4 CCR:RHA	14:6 CCR:RHA	12:8 CCR:RHA	Groups
20:0CCR:RHA	1.000	0.144	0.315	0.083	0.083	A
18:2CCR:RHA	0.144	1.000	0.648	0.784	0.784	A
16:4CCR:RHA	0.315	0.648	1.000	0.465	0.465	A
14:6CCR:RHA	0.083	0.784	0.465	1.000	1.000	A
12:8CCR:RHA	0.083	0.784	0.465	1.000	1.000	A

Bonferroni corrected significance level: 0.005

*Appendix 3. Kruskal-Wallis test: effect of stabilization with CCR on the **thermal properties** of CEB: (a) effusivity, (b) capacity*

a

K	57.3	As the computed p-value is lower than the significance level alpha=0.05, one should reject the null hypothesis H0, and accept the alternative hypothesis Ha.
p-value	< 0.001	
alpha	0.05	The risk to reject the null hypothesis H0 while it is true is lower than 0.01%.

p-values: pairwise comparisons using Dunn's procedure

	0CCR	5CCR	10CCR	15CCR	20CCR	25CCR	Groups			
0CCR	1.000	0.005	0.036	**< 0.001**	**<0.001**	**< 0.001**	A			
5CCR	0.005	1.000	0.464	0.019	0.329	**< 0.001**	A	B	C	
10CCR	0.036	0.464	1.000	**0.002**	0.088	**< 0.001**	A		C	
15CCR	**< 0.001**	0.019	**0.002**	1.000	0.169	0.098		**B**		**D**
20CCR	**<0.001**	0.329	0.088	0.169	1.000	**0.002**		**B**	**C**	
25CCR	**< 0.001**	**< 0.001**	**< 0.001**	0.098	**0.002**	1.000				**D**

Bonferroni corrected significance level: 0.0033, values in **bold** correspond to significant differences

b

K	58.19	As the computed p-value is lower than the significance level alpha=0.05, one should reject the null hypothesis H0, and accept the alternative hypothesis Ha.
p-value	< 0.001	
alpha	0.05	The risk to reject the null hypothesis H0 while it is true is lower than 0.01%.

p-values: pairwise comparisons using Dunn's procedure

	0CCR	5CCR	10CCR	15CCR	20CCR	25CCR	Groups		
0CCR	1.000	0.178	0.539	**0.000**	**< 0.001**	**< 0.001**	A		
5CCR	0.178	1.000	0.464	0.017	**0.002**	**< 0.001**	A	B	
10CCR	0.539	0.464	1.000	**0.002**	**0.000**	**< 0.001**	A		
15CCR	**0.000**	0.017	**0.002**	1.000	0.507	0.017		**B**	**C**
20CCR	**< 0.001**	**0.002**	**0.000**	0.507	1.000	0.086			**C**
25CCR	**< 0.001**	**<0. 001**	**< 0.001**	0.017	0.086	1.000			**C**

Bonferroni corrected significance level: 0.0033, values in **bold** correspond to significant differences

*Appendix 4. Kruskal-Wallis test: effect of stabilization with CCR on the **thermal properties** of CEB: (a) conductivity, (b) diffusivity*

a

K	51.66	As the computed p-value is lower than the significance level alpha=0.05, one should reject the null hypothesis H0, and accept the alternative hypothesis Ha.
p-value	<0.001	
alpha	0.05	The risk to reject the null hypothesis H0 while it is true is lower than 0.01%.

p-values: pairwise comparisons using Dunn's procedure

	0CCR	5CCR	10CCR	15CCR	20CCR	25CCR	Groups		
0CCR	1.000	**0.001**	0.048	**< 0.001**	0.004	**< 0.001**	A		
5CCR	**0.001**	1.000	0.201	0.133	0.711	**0.001**		**B**	
10CCR	0.048	0.201	1.000	0.005	0.364	**< 0.001**	A	B	
15CCR	**< 0.001**	0.133	0.005	1.000	0.061	0.065		**B**	**C**
20CCR	0.004	0.711	0.364	0.061	1.000	**0.001**	A	B	
25CCR	**< 0.001**	**0.001**	**< 0.001**	0.065	**0.000**	1.000			**C**

Bonferroni corrected significance level: 0.0033, values in **bold** correspond to significant differences

b

K	44.75	As the computed p-value is lower than the significance level alpha=0.05, one should reject the null hypothesis H0, and accept the alternative hypothesis Ha.
p-value	< 0.001	
alpha	0.05	The risk to reject the null hypothesis H0 while it is true is lower than 0.01%.

p-values: pairwise comparisons using Dunn's procedure

	0CCR	5CCR	10CCR	15CCR	20CCR	25CCR	Groups		
0CCR	1.000	**0.001**	0.076	**< 0.001**	0.108	**< 0.001**	A		
5CCR	**0.001**	1.000	0.110	0.565	0.078	0.008		**B**	**C**
10CCR	0.076	0.110	1.000	0.030	0.868	**< 0.001**	A	B	
15CCR	**< 0.001**	0.565	0.030	1.000	0.019	0.038		**B**	**C**
20CCR	0.108	0.078	0.868	0.019	1.000	**< 0.001**	A	B	
25CCR	**< 0.001**	0.008	**< 0.001**	0.038	**< 0.001**	1.000			**C**

Bonferroni corrected significance level: 0.0033, values in **bold** correspond to significant differences

Appendix II. Principal component analysis: correlation among different properties

This thesis reported the effects of stabilization (treatment) using by-products on various properties of CEBs. The effects were synthetically presented, in different chapters, on the thermophysical and mechanical properties, hydric and durability performances, mainly comparing the stabilization with CCR or CCR:RHA with CEM, in order to draw partial conclusions. However, there is a need to clearly visualize the effects of each stabilizer (observations) on all the studied properties (more than 15 variables: *Appendix 5*), in order to point out their resemblances (correlations). This would require to represent the properties in a space of 15 dimensions, which is normally impossible, but can be approached by principal component analysis (PCA). The PCA allows to summarize, visualize and extract important information from multivariate data. The variables are linearly combined to constitute new variables (principal component), among which few are chosen to visualize the maximum information from the original data. In the present study, the PCA type Pearson (n) was carried out using XLSTAT 2014.5.03 package incorporated in Microsoft excel 2013.

Firstly, analysis considered all the 15 properties for comparing the stabilization effects of CCR and CEM (*Appendix 5*a) or CCR:RHA (*Appendix 5*b). Secondly, only 8 properties, tested in dry conditions, were considered for comparison of unstabilized and stabilized CEBs. Thirdly, the remaining 7 properties, tested in wet conditions, were considered for analyzing the stabilization effect on the water behavior of CEBs.

Appendix 6 summarizes the statistics: minimum, maximum and mean values of different properties of stabilized CEBs. It shows that the stabilization differently affected the properties of CEBs. On the basis of the coefficient of variation (CV), the physical and thermal properties are the least affected with stabilization (CV lesser than 30), while the abrasion and erodability are most affected (CV up to 100). Appendix 7 further presents a correlation matrix established among different properties; it highlights the properties who has high degree of correlations. Moreover, the first (F1) and second (F2) principal component restitute the maximum information, i.e. 91.5 % with CCR (Appendix 8a) and 89.9 % with CCR:RHA (Appendix 8b), and were considered for further analyses. Indeed, various variables present the highest contributions to the constitution of F1 or F2. Appendix 9 & Appendix 10 present the correlations of different properties and stabilizations in the plan made of the two axes (F1 and F2).

For CEBs stabilized with CCR, Appendix 11a shows the correlations with F1: porosity (TP) and hydric properties (positively) and bulk density (ρ), thermal properties and wet compressive strength (Rcwet) (negatively). It also shows correlations with F2: erodability (positively), and abrasion (Cb), dry compressive strength (Rc_{dry}) and thermal capacity (Cap) (negatively). This suggests that these properties reach their highest values toward the directions, positive or negative, of the mostly correlated axis. For instance, the TP reaches the highest values toward the positive end of F1, while the ρ would reach the highest values toward the negative end of F1. This also shows that the TP and ρ are inversely correlated.

The biplot of properties and stabilizers presents the position of different stabilizers with respect to various properties of CEBs (Appendix 11b). On the one hand, it shows that 5, 15, 20, 25CCR have similar effects with respect to F1 (positive side) which is more significant with 25CCR than 5 CCR. On the other hand, 10CCR and 8CEM are at the other side (negative), thus their effects can be compared, CEM of course has more effect (extreme negative) than CCR. The comparison can also be made with respect to F2 where 15-25CCR and 8 CEM seem to have similar effects contrary to 5-10CCR. Regarding F1, 10CCR would reach the highest values of Rcwet, coefficient of abrasion (Cb) and the lowest values of hydric properties. By contrary, 25CCR has the lowest values of thermal properties except Cap, Rcwet and the highest values of hydric properties. Regarding F2, 5CCR and 10 CCR respectively have the highest values of erodability (DE and EA) and $Rc_{dry,}$ and the lowest values of Cap, contrary to 15-25 CCR.

For CEBs stabilized with CCR:RHA, Appendix 11c presents the correlation of different properties with respect to F1and F2. Appendix 11d shows that 18:2 to 16:4 CCR:RHA reach similar effects, particularly medium values of hydric properties: Ca_{10min}, WAP and Ab_{24h} and erodability/abrasion: DE, EA and Cb (center along F1), compared to 12:8 and 20:0 CCR:RHA. It also shows that 16:4 CCR:RHA has the highest values of ρ, Rc_{dry} and Rcwet, and the lowest TP and thermal properties, except Cap (along the F2).

More specially, the PCA carried out on properties tested in dry and wet conditions provided better visualizations of the effects of stabilization in each conditions. Appendix 12a shows that 25CCR reached the lowest ρ and thermal properties, except the Cap (F1) and 10-25 CCR reach highest Rc_{dry} and Cb (F2). Appendix 12b shows that 10CCR reaches the lowest values of hydric properties (F1) and 25CCR reaches the lowest erodability (F2). Appendix 12c shows that 16:4CCR:RHA reaches the highest values of ρ and Rc_{dry} (F1) and the lowest λ and a (F2). Appendix 12d shows that 16:4CCR:RHA also reaches the highest Rcwet and the lowest Ab_{24h} and erodability (F1), while 18:2CCR:RHA reaches the lowest Ca_{10min} and Sorp (F2).

Appendix 5. Summary of observations and variables for CEBs treated with (a) CCR and 8CEM (b) CCR:RHA and 8CEM

a

	ρ	**Rcdry**	Rcwet	**TP**	WAP	Ab24h	Ca10min	Sorp.	**Cb**	DE	EA	**E**	**Cap**	**λ**	**a**
0CCR	**1801**	**1.1**		**34**					**1**			**1285**	**899**	**1.02**	**6.3E-07**
5CCR	**1711**	**3.0**	1.6	**37**	33	19	11	0.075	**3**	6.7	41	**1142**	**918**	**0.83**	**5.3E-07**
10CCR	**1689**	**4.3**	2.7	**38**	33	20	10	0.075	**12**	4.7	15	**1159**	**910**	**0.88**	**5.7E-07**
15CCR	**1573**	**4.6**	1.9	**42**	34	22	10	0.076	**16**	4.8	3	**1084**	**957**	**0.78**	**5.2E-07**
20CCR	**1522**	**4.4**	1.8	**44**	35	23	12	0.084	**20**	4.8	9	**1111**	**966**	**0.85**	**5.8E-07**
25CCR	**1477**	**4.5**	1.7	**45**	36	24	13	0.083	**27**	3.9	4	**1010**	**997**	**0.69**	**4.7E-07**
8CEM	**1781**	**6.2**	3.1	**37**	29	16	8	0.045	**70**	3.5	7	**1231**	**987**	**1.01**	**6.7E-07**

b

20:0CCR:RHA	**1522**	**4.4**	1.8	**44**	35	23	12	0.084	**20**	5.2	9.0	**1111**	**966**	**0.83**	**5.8E-07**
18:2CCR:RHA	**1597**	**6.4**	2.4	**41**	36	23	11	0.056	**27**	5.8	9	**1042**	**942**	**0.73**	**4.9E-07**
16:4CCR:RHA	**1613**	**7.0**	2.7	**40**	36	23	12	0.071	**46**	5.3	16	**974**	**939**	**0.64**	**4.1E-07**
14:6CCR:RHA	**1619**	**6.8**	2.3	**39**	36	23	11	0.078	**39**	5.3	17	**1009**	**933**	**0.69**	**4.7E-07**
12:8CCR:RHA	**1623**	**6.0**	1.9	**39**	38	24	11	0.089	**70**	7	27	**1081**	**880**	**0.86**	**6.3E-07**
8CEM	**1781**	**6.2**	3.1	**37**	29	16	9	0.045	**70**	4	7	**1231**	**844**	**1.01**	**6.8E-07**

ρ:Bulk density, Rcdry: Dry compressive strength, Rcwet: Wet compressive strength, TP: Total porosity, WAP: Water accessible porosity, Ca10min: Coefficient of capillary absorption, Sorp: Sorptivity, DE: Depth of erodability, EA: Eroded area, E: Thermal effusivity, Cap: Thermal capacity, λ: Thermal conductivity, a: Thermal diffusivity

Values in **bold** correspond to the variables which were tested in dry conditions

Appendix 6. Summary statistics: variations of the properties (variables) of CEBs treated (observations) with (a) CCR and 8CEM, (b) CCR:RHA and 8CEM

a

Variables/ properties	Observations/ treatments	Minimum	Maximum	Mean	Std. deviation	Coef. Variation
ρ	6	1477	1781	1625	119	7
Rcdry	6	3.0	6.2	4.5	1.0	23
Rcwet	6	1.6	3.1	2.1	0.6	28
TP	6	37	45	41	4	9
WAP	6	29	36	33	2	7
Ab24h	6	16	24	21	3	14
Ca10min	6	8	13	11	2	15
Sorp.	6	0.045	0.084	0.073	0.014	20
Cb	6	3	70	25	23	95
DE	6	3.5	6.7	4.7	1.1	23
EA	6	2.9	40.8	13.1	14.2	108
E	6	1010	1231	1123	75	7
Cap	6	910	997	956	35	4
λ	6	0.69	1.01	0.84	0.11	13
a	6	4.7E-07	6.7E-07	5.6E-07	6.9E-08	12

b

ρ	5	1522	1623	1595	42	3
Rcdry	5	4.4	7.0	6.1	1.0	17
Rcwet	5	1.8	2.7	2.2	0.4	17
TP	5	39	44	41	2	4
WAP	5	35	38	36	1	3
Ab24h	5	23	24	23	1	3
Ca10min	5	11	12	11	1	5
Sorp.	5	0.056	0.089	0.076	0.013	17
Cb	5	20	70	40	19	48
DE	5	5	7	6	1	13
EA	5	9	27	16	7	47
E	5	974	1111	1043	55	5
Cap	5	880	966	932	32	3
λ	5	0.64	0.86	0.75	0.09	12
a	5	4.1E-07	6.3E-07	5.2E-07	8.8E-08	17

Appendix 7. Correlation matrix (Pearson (n)) for the properties (variables) of CEBs treated (observations) with (a) CCR and 8CEM, (b) CCR:RHA and 8CEM

a

Variables/ properties	ρ	Rcdry	Rcwet	TP	WAP	Ab24h	Ca10min	Sorp.	Cb	DE	EA	E	Cap	λ	a
ρ	**1.00**	0.21	0.67	**-0.98**	**-0.91**	**-0.99**	**-0.87**	-0.80	0.36	0.13	0.46	**0.92**	-0.41	**0.83**	0.72
DCS	0.21	**1.00**	0.76	-0.06	-0.56	-0.35	-0.48	-0.72	**0.94**	**-0.89**	-0.71	0.39	0.66	0.55	0.66
WCS	0.67	0.76	**1.00**	-0.59	-0.78	-0.73	-0.74	**-0.82**	0.73	-0.59	-0.30	0.77	0.06	**0.82**	**0.83**
TP	**-0.98**	-0.06	-0.59	**1.00**	**0.82**	**0.94**	**0.81**	0.69	-0.19	-0.26	-0.56	**-0.88**	0.56	-0.76	-0.62
WAP	**-0.91**	-0.56	-0.78	**0.82**	**1.00**	**0.96**	**0.90**	**0.96**	-0.68	0.18	-0.15	**-0.93**	0.02	**-0.93**	**-0.88**
Ab24h	**-0.99**	-0.35	-0.73	**0.94**	**0.96**	**1.00**	**0.92**	**0.88**	-0.48	-0.02	-0.34	**-0.94**	0.27	**-0.88**	-0.79
Ca10min	**-0.87**	-0.48	-0.74	**0.81**	**0.90**	**0.92**	**1.00**	**0.87**	-0.50	0.13	-0.07	**-0.82**	0.17	-0.78	-0.71
Sorp.	-0.80	-0.72	**-0.82**	0.69	**0.96**	**0.88**	**0.87**	**1.00**	**-0.83**	0.39	0.05	-0.81	-0.20	**-0.84**	**-0.82**
Cb	0.36	**0.94**	0.73	-0.19	-0.68	-0.48	-0.50	**-0.83**	**1.00**	-0.77	-0.47	0.47	0.68	0.61	0.70
DE	0.13	**-0.89**	-0.59	-0.26	0.18	-0.02	0.13	0.39	-0.77	**1.00**	**0.87**	-0.01	-0.74	-0.18	-0.32
EA	0.46	-0.71	-0.30	-0.56	-0.15	-0.34	-0.07	0.05	-0.47	**0.87**	**1.00**	0.27	-0.69	0.09	-0.06
E	**0.92**	0.39	0.77	**-0.88**	**-0.93**	**-0.94**	**-0.82**	-0.81	0.47	-0.01	0.27	**1.00**	-0.29	**0.98**	**0.92**
Cap	-0.41	0.66	0.06	0.56	0.02	0.27	0.17	-0.20	0.68	-0.74	-0.69	-0.29	**1.00**	-0.11	0.05
λ	**0.83**	0.55	**0.82**	-0.76	**-0.93**	**-0.88**	-0.78	**-0.84**	0.61	-0.18	0.09	**0.98**	-0.11	**1.00**	**0.98**
a	0.72	0.66	**0.83**	-0.62	**-0.88**	-0.79	-0.71	**-0.82**	0.70	-0.32	-0.06	**0.92**	0.05	**0.98**	**1.00**

b

ρ	**1.00**	**0.88**	0.47	**-0.99**	0.78	0.15	-0.70	-0.13	0.73	0.45	0.67	-0.65	-0.71	-0.39	-0.30
Rcdry	**0.88**	**1.00**	0.82	-0.82	0.41	-0.31	-0.42	-0.46	0.38	0.01	0.29	**-0.92**	-0.30	-0.78	-0.72
Rcwet	0.47	0.82	**1.00**	-0.37	-0.07	-0.64	0.07	-0.70	-0.05	-0.40	-0.19	**-0.93**	0.20	**-0.94**	**-0.94**
TP	**-0.99**	-0.82	-0.37	**1.00**	-0.84	-0.22	0.79	0.11	-0.75	-0.55	-0.70	0.54	0.77	0.28	0.19
WAP	0.78	0.41	-0.07	-0.84	**1.00**	0.71	-0.75	0.24	**0.93**	**0.90**	**0.89**	-0.08	**-0.99**	0.24	0.32
Ab24h	0.15	-0.31	-0.64	-0.22	0.71	**1.00**	-0.31	0.70	0.75	0.87	0.77	0.55	-0.79	0.79	0.83
Ca10min	-0.70	-0.42	0.07	0.79	-0.75	-0.31	**1.00**	0.15	-0.49	-0.68	-0.49	0.04	0.71	-0.14	-0.21
Sorp.	-0.13	-0.46	-0.70	0.11	0.24	0.70	0.15	**1.00**	0.46	0.31	0.60	0.47	-0.39	0.61	0.65
Cb	0.73	0.38	-0.05	-0.75	**0.93**	0.75	-0.49	0.46	**1.00**	0.78	**0.98**	-0.14	**-0.95**	0.19	0.28
DE	0.45	0.01	-0.40	-0.55	**0.90**	0.87	-0.68	0.31	0.78	**1.00**	0.75	0.34	**-0.91**	0.60	0.66
EA	0.67	0.29	-0.19	-0.70	**0.89**	0.77	-0.49	0.60	**0.98**	0.75	**1.00**	-0.05	**-0.94**	0.27	0.36
E	-0.65	**-0.92**	**-0.93**	0.54	-0.08	0.55	0.04	0.47	-0.14	0.34	-0.05	**1.00**	-0.03	**0.95**	**0.91**
Cap	-0.71	-0.30	0.20	0.77	**-0.99**	-0.79	0.71	-0.39	**-0.95**	**-0.91**	**-0.94**	-0.03	**1.00**	-0.34	-0.43
λ	-0.39	-0.78	**-0.94**	0.28	0.24	0.79	-0.14	0.61	0.19	0.60	0.27	**0.95**	-0.34	**1.00**	**0.99**
a	-0.30	-0.72	**-0.94**	0.19	0.32	0.83	-0.21	0.65	0.28	0.66	0.36	**0.91**	-0.43	**0.99**	**1.00**

*Values in **bold** are different from 0 with a significance level alpha=0.05*

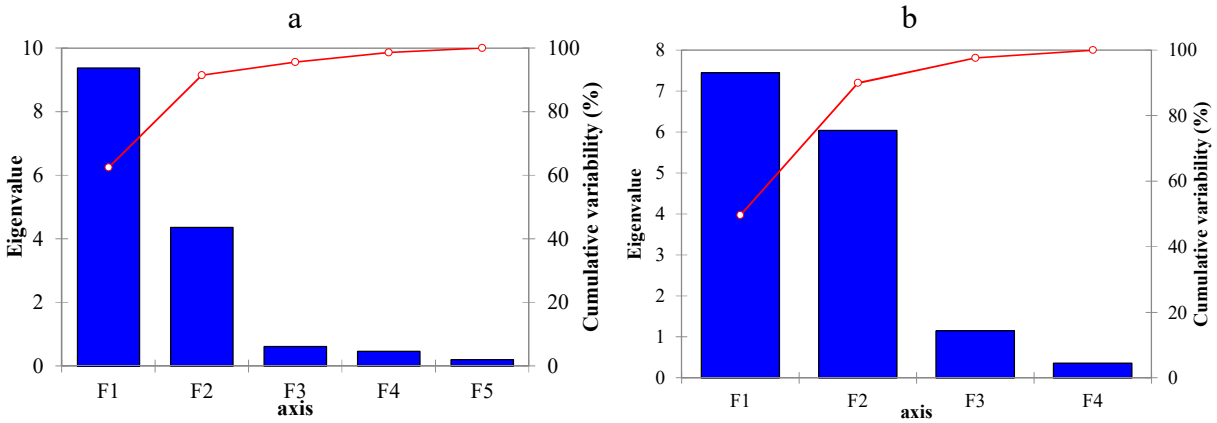

Appendix 8. Scree plot: constitution of the principal component for CEBs stabilized with (a) CCR and (b) CCR:RHA

Appendix 9. Squared cosines of the variables (properties) for CEBs treated (observations) with (a) CCR and 8CEM, (b) CCR:RHA and 8CEM

a

Variables/ properties	F1	F2	F3	F4	F5
ρ	**0.79**	0.19	0.00	0.01	0.01
DCS	0.39	**0.60**	0.00	0.00	0.00
WCS	**0.78**	0.07	0.12	0.00	0.03
TP	**0.65**	0.33	0.00	0.02	0.01
WAP	**0.97**	0.00	0.03	0.00	0.00
Ab24h	**0.89**	0.09	0.01	0.01	0.00
Ca10min	**0.81**	0.02	0.00	0.12	0.06
Sorp.	**0.91**	0.03	0.05	0.02	0.00
Cb	**0.50**	0.43	0.06	0.00	0.01
DE	0.08	**0.85**	0.03	0.01	0.03
EA	0.00	**0.85**	0.10	0.01	0.03
E	**0.88**	0.07	0.01	0.04	0.00
Cap	0.00	**0.81**	0.19	0.00	0.00
λ	**0.90**	0.00	0.01	0.08	0.00
a	**0.84**	0.01	0.01	0.13	0.01

b

ρ	0.35	**0.64**	0.00	0.01
Rcdry	0.02	**0.98**	0.00	0.00
Rcwet	0.13	**0.79**	0.01	0.07
TP	0.44	**0.54**	0.01	0.01
WAP	**0.90**	0.09	0.00	0.01
Ab24h	**0.76**	0.18	0.02	0.04
Ca10min	**0.45**	0.11	0.37	0.07
Sorp.	0.25	0.31	**0.38**	0.07
Cb	**0.83**	0.07	0.09	0.01
DE	**0.88**	0.01	0.06	0.05
EA	**0.85**	0.03	0.12	0.01
E	0.04	**0.90**	0.06	0.00
Cap	**0.97**	0.03	0.00	0.00
λ	0.25	**0.73**	0.03	0.00
a	0.33	**0.65**	0.02	0.00

*Values in **bold** correspond for each variable to the factor for which the squared cosine is the largest*

Appendix 10. Squared cosines of the observations/ treatments for CEBs treated (observations) with (a) CCR and 8CEM, (b) CCR:RHA and 8CEM

a

Observations/ treatments	F1	F2	F3	F4	F5
5CCR	0.01	**0.94**	0.05	0.00	0.00
10CCR	0.20	0.33	**0.44**	0.01	0.04
15CCR	**0.45**	0.08	0.02	0.23	0.22
20CCR	**0.56**	0.09	0.01	0.33	0.01
25CCR	**0.70**	0.26	0.01	0.01	0.02
8CEM	**0.92**	0.07	0.01	0.00	0.00

b

20:0CCR:RHA	0.25	**0.74**	0.01	0.00
18:2CCR:RHA	0.22	0.16	**0.61**	0.01
16:4CCR:RHA	0.16	**0.66**	0.15	0.04
14:6CCR:RHA	0.02	**0.65**	0.01	0.32
12:8CCR:RHA	**0.96**	0.04	0.00	0.00

*Values in **bold** correspond for each observation to the factor for which the squared cosine is the largest*

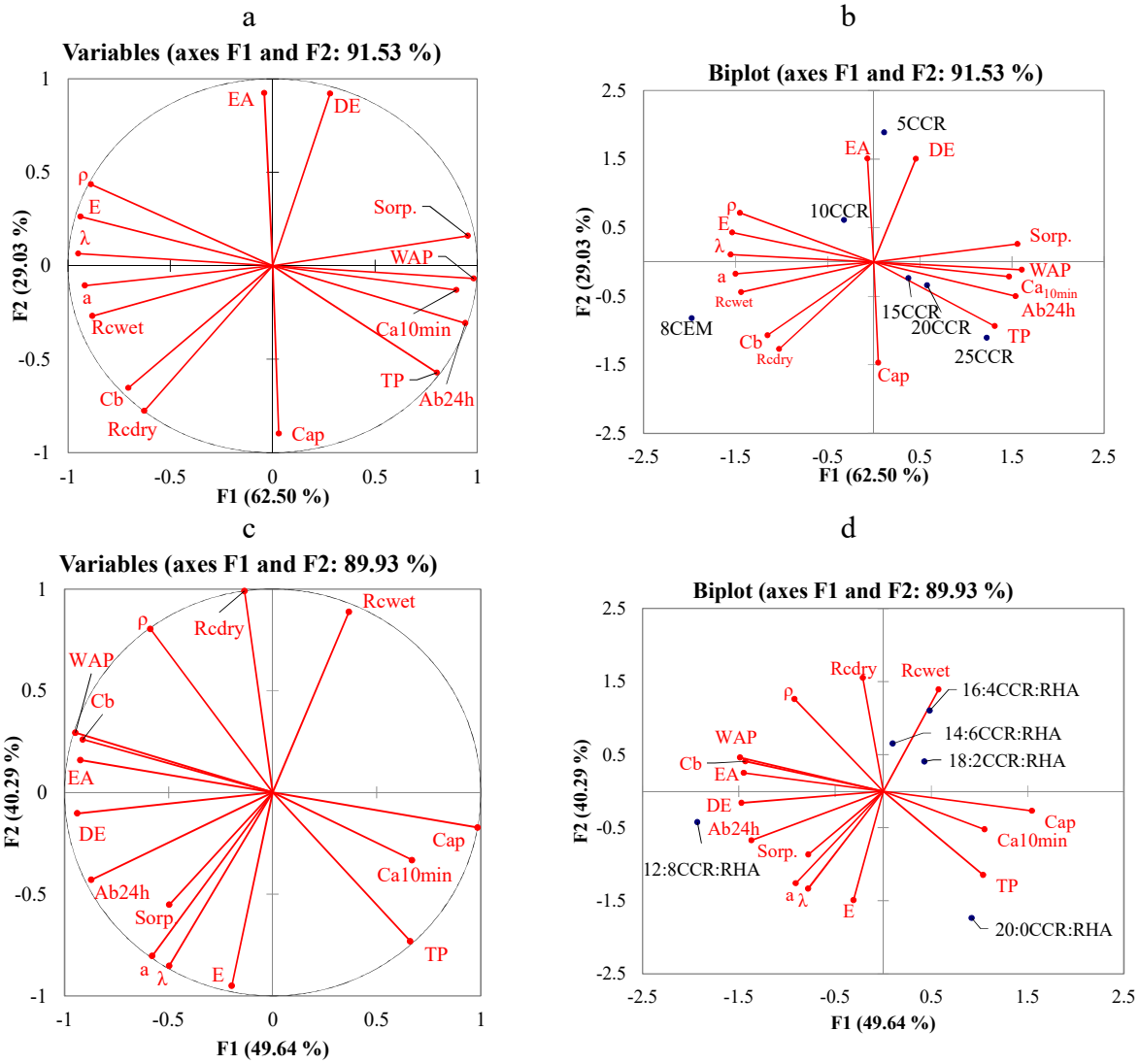

Appendix 11. Projection of properties (left) and observations (right) with respect to the 1st (F1) and 2nd (F2) principal component for CEBs treated with (a)-(b) CCR and (c)-(d) CCR:RHA

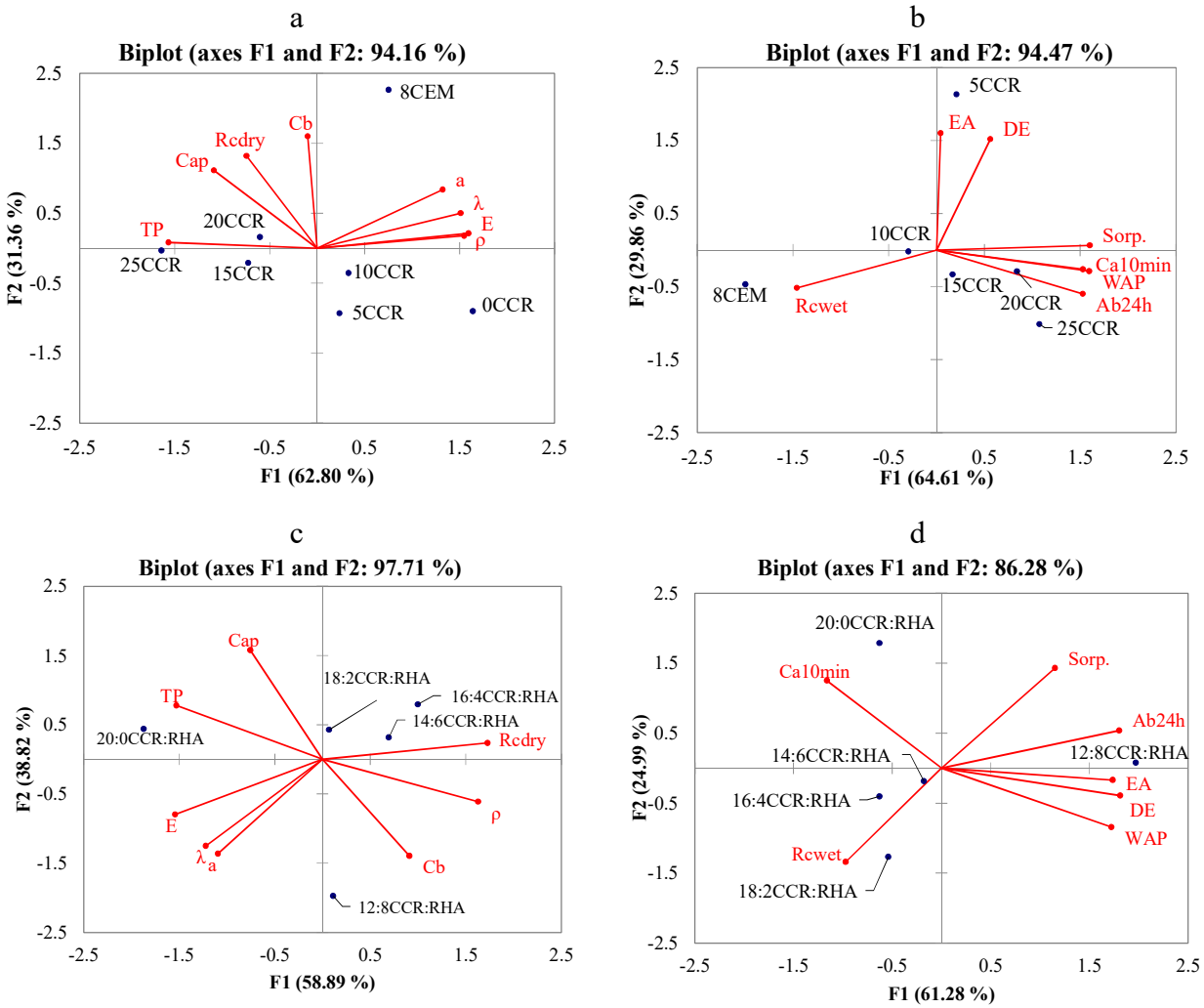

Appendix 12. Projection of variables and observations with respect to F1 and F2 for properties tested in dry (left) and wet (right) conditions: (a)-(b) CCR, (c)-(d) CCR:RHA

Appendix III. Selection of mix design

Appendix 13. Matrix for the selections of mix design (stabilizers added to earth), on the basis of the required properties for stabilized CEBs envisaged for applications in (a) one-storey, (b) two-storey, (c) three-storey building

a

Mix design	Physico-mechanical properties						Thermal properties						Hydric properties					Durability indicators			
	ρ	TP	Rcdry	Rcwet	CSE		E	Cap	λ	a	Depth		WAP	Ab24h	Ca10min	Sorp.		Cb	DE	EA	
(a)																					
10CCR+0fiber	1689	39	4.3	2.7	2528	++++	1159	915.7	0.84	5.4E-07	0.12	-	33	20	10	0.071	-	12	5	15	+
10CCR+0.2fiber	1658	39	3.7	1.4	2242	+++	1080	908.5	0.76	5.0E-07	0.12	-	35	21	11	0.081	+	14	6	13	+
10CCR+0.4fiber	1645	39	3.7	1.3	2224	+++	1055	811.6	0.83	6.1E-07	0.13	*	35	22	11	0.084	++	14	10	20	+
10CCR+0.8fiber	1616	40	3.7	1.2	2316	+++	983	885.3	0.66	4.6E-07	0.11	--	36	22	13	0.079	+	10	7	21	+
10CCR+1.2fiber	1612	40	3.5	1.3	2170	++	953	915.2	0.63	4.2E-07	0.11	--	36	22	16	0.075	*	18	7	10	++
Standards requiremements			>2	>1	The higher, the better (one-storey building)			>920	<1		The lower, the better			<20	<20		The lower, the better	>5	<120		The higher, the better
(b)																					
0CCR	1801	34	1.1		609	-----	1291	899	1.02	6.3E-07	0.13	*						1			*
5CCR	1711	37	3	1.6	1753	*	1152	922	0.83	5.3E-07	0.12	-	33	19	11	0.073	*	3	7	41	*
10CCR	1689	38	4.3	2.7	2546	++++	1159	916	0.88	5.7E-07	0.12	-	33	20	10	0.076	*	12	5	15	+
15CCR	1573	42	4.6	1.9	2924	++++++	1084	957	0.78	5.2E-07	0.12	-	34	22	10	0.071	-	16	5	3	++
20CCR	1522	44	4.4	1.8	2891	++++++	1107	966	0.85	5.8E-07	0.12	-	35	23	12	0.084	++	20	5	9	++
25CCR	1477	45	4.5	1.7	3047	+++++++	1010	997	0.69	4.7E-07	0.11	--	36	24	13	0.084	++	27	4	4	+++
Standards requiremements			>4	>2	The higher, the better (two-storey building)			>920	<1		The lower, the better			<20	<20		The lower, the better	>5	<120		The higher, the better
(c)																					
20:0CCR:RHA	1522	44	4.4	1.8	2890	++++++	1111	966	0.83	5.8E-07	0.12	-	35	23	12	0.084	++	20	5	9	++
18:2CCR:RHA	1597	41	6.4	2.4	3999	++++++++++++	1042	942	0.73	4.9E-07	0.12	-	36	23	11	0.056	----	27	6	9	+++
16:4CCR:RHA	1613	40	7.0	2.7	4357	+++++++++++++++	974	939	0.64	4.1E-07	0.11	--	36	23	12	0.071	--	46	5	16	++++
14:6CCR:RHA	1619	39	6.8	2.3	4181	++++++++++++++	1009	933	0.69	4.7E-07	0.11	--	36	23	11	0.078	+	39	5	17	++++
12:8CCR:RHA	1623	39	6.0	1.9	3667	++++++++++	1081	880	0.86	6.3E-07	0.13	*	38	24	11	0.089	+++	70	7	27	+++++++
8CEM	1781	37	6.2	3.1	3493	+++++++++	1231	844	1.01	6.8E-07	0.14	++	29	16	8	0.045	------	70	4	7	+++++++
Standards requiremements			>6	>3	The higher, the better (two-storey building)			>920	<1		The lower, the better			<20	<20		The lower, the better	>7	<120		The higher, the better

ρ: Bulk density (kg/m^3), TP: Total porosity (%), Rcdry : Dry compressive strength (MPa), Rcwet: Wet compressive strength (MPa), CSE: Coefficient of structural efficiency (J/kg), E: Thermal effusivity (J/m².K.s$^{1/2}$), Cap: Thermal capacity (J/kg.K), λ: Thermal conductivity (W/m.K), a: Thermal diffusivity (m²/s), Depth: Depth of thermal penetration (m), WAP: Water accessible porosity (%), Ab24h: Water absorption in 24 at saturation (%), Ca10min: Coefficient of capillary absorption in 10 min (g/cm²), Sorp: Sorptivity (g/cm².min$^{1/2}$), Cb: Coefficient of abrasion (cm²/g), DE: Depth of erodability (mm), EA: Percentage of Eroded area (%)

	*	Benchmark	+	Increasing with respect to (*)	-	Decreasing with respect to (*)		Acceptable/ considerable	Values do NOT comply with the standard

La terre argileuse reste le matériau de construction le plus couramment utilisé dans le monde entier pour une construction respectueuse de l'environnement. De nos jours, on constate une augmentation spectaculaire de la population et de l'urbanisation, spécifiquement dans les pays en développement. Ainsi, une meilleure connaissance du comportement des matériaux de construction en terre serait une réponse adéquate à son utilisation contemporaine par les populations urbaines et/ou rurales. La présente thèse visait à caractériser la convenance de la terre argileuse de quatre sites: Kamboinsé, Pabré, Kossodo et Saaba, aux alentours de Ouagadougou, Burkina Faso, pour la production de blocs en terre comprimées stabilisées (BTCs). L'étude a consisté également à caractériser un sous-produit industriel: le carbure de calcium résiduel (CCR) de Kossodo et deux sous-produits agricoles: la cendre de balle du riz (RHA) de Bagré et les fibres végétales de gombo de Kaya pour la stabilisation des BTCs. Les caractérisations ont été menées sur les propriétés physico-texturales et chimico-minérales de ces matières premières. Ensuite, l'étude a consisté à tester les propriétés physico-mécaniques, hygro-thermiques et de durabilité des BTCs stabilisées avec les sous-produits pour des applications dans la construction de bâtiments adaptés spécifiquement au contexte climatique Sahélien. Les mélanges ont été produits par addition de 0-25% CCR, 10-25% CCR:RHA (divers ratios) et 0,2-1,2% fibres par rapport à la masse du matériau en terre. Les mélanges ont été utilisés pour produire les solutions et confectionner les BTCs stabilisés (295x140x95 mm^3) par compression statique à l'aide d'une presse manuelle de Terstaram (pression de ~35 bars), et maturés dans diverses conditions pendant 0 à 90 jours. Les résultats montrent que la terre argileuse des sites de Pabré et Kossodo contient respectivement la plus forte fraction de particules argileuses (20-30%) et gravier (40%). La composition minérale est dominée par la kaolinite, le quartz et la goethite. Saaba et Pabré contiennent respectivement la plus forte fraction d'argile kaolinite (60-80%) et quartz (40-60%). Kamboinsé contient la plus grande quantité de gisement exploitable (700 000 m^3), 10-25% des particules argileuses et 40-75% de kaolinite; tandis que Kossodo contient une moyenne fraction de kaolinite (35-50%). Le CCR contient principalement de la portlandite (40-50% de chaux hydratée: $Ca(OH)_2$). La RHA est principalement amorphe, avec une réactivité pouzzolanique. Saaba et Kossodo ont une réactivité pouzzolanique avec le CCR la plus élevée, liée à la teneur et au taux mal cristallisée élevé de kaolinite. Pabré et Kamboinsé ont une réactivité la plus faible. Par rapport aux BTCs non-stabilisés (0% CCR), la résistance à la compression des BTCs stabilisées avec 20% CCR, maturées à 40 ± 2 °C pendant 45 jours, produit avec le matériau argileux de Saaba est améliorée dix-fois (0,8 à 8,3 MPa) comparé à Kamboinsé (1,1 à 4,7 MPa), Pabre (2 à 7,1 MPa) et Kossodo (1,4 à 6,4 MPa). Tous les matériaux argileux sont adéquats pour la production des BTCs stabilisées et atteignant une résistance à la compression requise de 4 MPa. En outre, la stabilisation de matériau de Kamboinsé en utilisant les sous-produits a amélioré l'efficacité structurelle des BTCs maturés dans les conditions ambiantes du labo (35 ± 5 ° C): augmentation de la résistance à la compression et diminution de la densité apparente. Il a également amélioré l'efficacité hygro-thermique: diminution de l'effusivité thermique, de la conductivité et diffusivité et augmentation de la capacité thermique et de la sorption de vapeur d'eau. Les BTCs stabilisés avec au moins 10% CCR ou 18-2 à 16:4% CCR:RHA répondent aux diverses exigences techniques et ont des excellents indicateurs de durabilité pour la construction de bâtiments à deux ou trois étages.